40317

National Library of Canada | Bibliothèque nationale du Canada

CANADIAN THESES ON MICROFICHE | THÈSES CANADIENNES SUR MICROFICHE

UNIVERSITY
OF ALBERTA
4 2 - 1978

NAME OF AUTHOR/*NOM DE L'AUTEUR* MARIOS SOPHOCLEOUS

TITLE OF THESIS/*TITRE DE LA THÈSE* ANALYSIS OF HEAT AND WATER TRANSPORT IN UNSATURATED-SATURATED POROUS MEDIA.

UNIVERSITY/*UNIVERSITÉ* THE UNIVERSITY OF ALBERTA

DEGREE FOR WHICH THESIS WAS PRESENTED/ *GRADE POUR LEQUEL CETTE THÈSE FUT PRÉSENTÉE* PH.D.

YEAR THIS DEGREE CONFERRED/*ANNÉE D'OBTENTION DE CE GRADE* 1978

NAME OF SUPERVISOR/*NOM DU DIRECTEUR DE THÈSE* DR. FRANK W. SCHWARTZ

Permission is hereby granted to the NATIONAL LIBRARY OF CANADA to microfilm this thesis and to lend or sell copies of the film.

The author reserves other publication rights, and neither the thesis nor extensive extracts from it may be printed or otherwise reproduced without the author's written permission.

L'autorisation est, par la présente, accordée à la BIBLIOTHÈQUE NATIONALE DU CANADA de microfilmer cette thèse et de prêter ou de vendre des exemplaires du film.

L'auteur se réserve les autres droits de publication; ni la thèse ni de longs extraits de celle-ci ne doivent être imprimés ou autrement reproduits sans l'autorisation écrite de l'auteur.

DATED/*DATÉ* Aug. 21, 1978 SIGNED/*SIGNÉ* [signature]

PERMANENT ADDRESS/*RÉSIDENCE FIXÉ* c/o DR. FRANK W. SCHWARTZ
DEPT. OF GEOLOGY
THE UNIV. OF ALBERTA
EDMONTON, ALBERTA, CANADA T6G2E1

NL-91 (3-74)

National Library of Canada

Cataloguing Branch
Canadian Theses Division

Ottawa, Canada
K1A 0N4

Bibliothèque nationale du Canada

Direction du catalogage
Division des thèses canadiennes

NOTICE

The quality of this microfiche is heavily dependent upon the quality of the original thesis submitted for microfilming. Every effort has been made to ensure the highest quality of reproduction possible.

If pages are missing, contact the university which granted the degree.

Some pages may have indistinct print especially if the original pages were typed with a poor typewriter ribbon or if the university sent us a poor photocopy.

Previously copyrighted materials (journal articles, published tests, etc.) are not filmed.

Reproduction in full or in part of this film is governed by the Canadian Copyright Act, R.S.C. 1970, c. C-30. Please read the authorization forms which accompany this thesis.

THIS DISSERTATION
HAS BEEN MICROFILMED
EXACTLY AS RECEIVED

AVIS

La qualité de cette microfiche dépend grandement de la qualité de la thèse soumise au microfilmage. Nous avons tout fait pour assurer une qualité supérieure de reproduction.

S'il manque des pages, veuillez communiquer avec l'université qui a conféré le grade.

La qualité d'impression de certaines pages peut laisser à désirer, surtout si les pages originales ont été dactylographiées à l'aide d'un ruban usé ou si l'université nous a fait parvenir une photocopie de mauvaise qualité.

Les documents qui font déjà l'objet d'un droit d'auteur (articles de revue, examens publiés, etc.) ne sont pas microfilmés.

La reproduction, même partielle, de ce microfilm est soumise à la Loi canadienne sur le droit d'auteur, SRC 1970, c. C-30. Veuillez prendre connaissance des formules d'autorisation qui accompagnent cette thèse.

LA THÈSE A ÉTÉ
MICROFILMÉE TELLE QUE
NOUS L'AVONS REÇUE

THE UNIVERSITY OF ALBERTA

ANALYSIS OF HEAT AND WATER TRANSPORT IN UNSATURATED-SATURATED POROUS MEDIA

by

MARIOS A. SOPHOCLEOUS

(C)

A THESIS

SUBMITTED TO THE FACULTY OF GRADUATE STUDIES AND RESEARCH

IN PARTIAL FULFILMENT OF THE REQUIREMENTS FOR THE DEGREE

OF DOCTOR OF PHILOSOPHY

DEPARTMENT OF GEOLOGY

EDMONTON, ALBERTA

FALL, 1978

THE UNIVERSITY OF ALBERTA

FACULTY OF GRADUATE STUDIES AND RESEARCH

The undersigned certify that they have read, and recommend to the Faculty of Graduate Studies and Research, for acceptance, a thesis entitled ANALYSIS OF HEAT AND WATER TRANSPORT IN UNSATURATED-SATURATED POROUS MEDIA submitted by MARIOS A. SOPHOCLEOUS in partial fulfilment of the requirements for the degree of DOCTOR OF PHILOSOPHY IN GEOLOGY

Frank W. Schwartz
Supervisor

Nathaniel W. Rutter

D. G. Miller

H. A. K. Charlesworth

R. William T. Nelson
External Examiner

DATE June 27, 1978

TABLE OF CONTENTS

Page

ABSTRACT viii

ACKNOWLEDGMENTS xi

LIST OF TABLES xiii

LIST OF FIGURES xv

LIST OF SYMBOLS xviii

Chapter

1. STATEMENT OF THE PROBLEM 1

2. THEORETICAL DEVELOPMENT 16

2.1 Introduction

2.2 Assumptions

2.3 Vapor Transport

2.4 Liquid Transport

2.5 Total Water Transport

2.6 Transient Flow Equations

2.7 Heat Transport

2.8 Proposed Field-oriented Methodology for Transport Coefficients

3. FIELD AND LABORATORY STUDIES 43

3.1 Introduction

3.2 Preliminary Considerations

3.3 Location and Surficial Geology of the Study Area

3.4 The Field Sites

3.5 Weather Observations

3.6 Measurement of Basic Parameters and Equipment Required for the Present Study

3.6.1 Soil Types

3.6.2 Hydraulic Potential

3.6.2.1 Piezometers

3.6.2.2 Tensiometers

3.6.2.3 Soil Psychrometers

3.6.3 Water Table and Water Content

3.6.4 Water Characteristic Curves

3.6.5 Hydraulic Conductivity

3.6.5.1 Saturated Hydraulic Conductivity

3.6.5.2 Unsaturated Hydraulic Conductivity

3.6.6 Density and Porosity

3.6.7 Temperature

3.6.8 Thermal Conductivity

3.6.9 Heat Capacity

3.6.10 Heat and Water Fluxes

3.6.10.1 Heat Flux

3.6.10.2 Water Flux

3.7 Experimental Results and Discussion

3.7.1 Soil Types and Analyses

3.7.2 Hydraulic Head

3.7.3 Water Contents

3.7.4 Temperature and Potential Evaporation

3.7.5 Characteristic Curves

3.7.6 Hydraulic Conductivity

3.7.7 Thermal Conductivity and Heat Capacity

3.8 Evaluation of Field and Laboratory Studies

4. MODEL STUDIES 120

4.1 Introduction

4.2 The Mathematical Model

4.3 The Numerical Approach

4.4 Numerical Solution

4.5 Solution of Linear Algebraic Systems and Convergence Requirements

4.6 Solution of Non-linear Algebraic Systems

4.7 Computer Simulation Program

4.8 Program Verification

4.9 Results and Discussion

5. CONCLUDING COMMENTS AND RECOMMENDATIONS 179

REFERENCES 186

APPENDIX A TEMPERATURE AND POTENTIAL EVAPORATION DISTRIBUTIONS 212

APPENDIX B WATER CHARACTERISTIC CURVES - SITE 2 216

APPENDIX C HYDRAULIC PROPERTIES OF POROUS MATERIALS FROM THE TABER SITES 220

APPENDIX D DERIVATION OF THE FINITE DIFFERENCE EQUATIONS OF THE ONE-DIMENSIONAL COUPLED NON-ISOTHERMAL FLOW USING A CRANK-NICHOLSON APPROXIMATION METHOD 235

APPENDIX E DOCUMENTED COMPUTER PROGRAMS 240

E.1 Introduction

E.3 Subroutines

E.3 List of Variables

E.4 Program Listing

E.5 Sample Input data and Output Results

ABSTRACT

It is possible to model mathematically the simultaneous transport of heat and water in liquid and vapor phases in unsaturated-saturated porous media. The theoretical development of the model is an adaptation and extension of the Philip and de Vries' non-isothermal model based on the more general pressure head approach. A methodology for subsurface coupled heat and water transport suitable for field applications is proposed. This methodology involves calculation of ratios of transport parameters in combination with a detailed heat flux equation, the introduction of a new approach for the calculation of liquid thermal diffusion coefficients and the extension of the Philip and de Vries-type theory to saturated regions.

A general and versatile one-dimensional computer simulation program for modeling coupled non-isothermal transport is developed based on a unified unsaturated-saturated approach. Temperature, pressure head and water content, as well as all relevant transport coefficients and fluxes of head and fluid components are predicted by the model. This model is successfully verified with field and complementary laboratory data collected for this purpose. A variety of field and laboratory methods and instrumentation was used to collect this array of data. The

equipment for thermal conductivity measurements was redesigned to meet the requirements of this study. An error analysis is used to identify the data causing the greatest amount of error.

The influence of coupling on diurnal subsurface moisture and heat transfer can be evaluated by comparing the transient non-isothermal numerical solutions to the heat and water transport problem under varying top boundary conditions. The results confirm that coupling does not appreciably influence the temperature field but does affect the evaporation and subsurface moisture fluxes. Thus, depending on the direction of the temperature and pressure head gradients, the evaporation and subsurface water fluxes may have been overestimated or underestimated significantly using an isothermal model. The analysis of transport coefficients indicated that thermally induced moisture movement becomes dominant at very low water contents. It is suggested that for long term simulations under extended drying conditions, the coupled non-isothermal model should be preferred in studying the long range seasonal influences on water transport. The non-isothermal theory can be applied to calculate evaporation from dry land surfaces. Simulation results show a very interesting cyclical evaporation pattern.

The theoretical and field analysis pointed out difficulties and deficiencies of non-isothermal models, such

as the calculation of flow enhancement factors and liquid thermal diffusion coefficients, the field performance of thermocouple psychormeters and others. Areas of hydrogeological interest of such models, such as the subsurface waste heat disposal, thermal influences on the migration of radionucleides and other environmental and hydrological problems are pointed out.

ACKNOWLEDGMENTS

I wish to express my appreciation to my academic advisor Dr F. W. Schwartz for his continued encouragement, support and useful comments. His constructive criticism contributed to the improvement of this thesis.

I also wish to express my appreciation to Dr J. G. Van Schaik, formerly of Canada Agriculture, Lethbridge Research Station, for his continued support and fruitful discussions during the planning and execution of this research.

I am thankful to Dr D. C. Mackay, head of the Soil Science Section of that Research Station, for his cooperation with this research. Messrs. D. P. Graham and W. Holstein of the Soil Physics Laboratory and Mr D. B. Bligh of the Machine Shop provided able assistance in technical aspects of this work. Mr G. E. Grisak formerly of the Groundwater section of the Department of the Environment, Lethbridge, kindly provided that Department's drilling rig for use at the field sites.

I would like to thank my wife Thelma for her continued encouragement, and her assistance with typing and editing the manuscript.

Funds for this study were provided by Canada Agriculture and the National Research Council of Canada. I

also received financial support from the Department of Geology of The University of Alberta and the I. W. Killam Memorial Scholarship Fund.

LIST OF TABLES

Table		Page
1-1	Philip and de Vries model	9
1-2	Non-equilibrium thermodynamics model	11
2-1	Present model	39
3-1	Measured thermal conductivity of air-dry 20/30 mesh Ottawa sand	74
3-2	Typical values of parameters required for the estimation of damping depths for the diurnal temperature variation at the sites	94
3-3	Saturated hydraulic conductivity analyses	103
3-4	Maximum error analysis for heat flux parameters at Site 2	118
4-1	Conditions for case simulation runs	154
4-2	Sample output information from simulation runs ..	155
4-3	Comparison of evaporation fluxes calculated using the coupled and uncoupled equations for Runs 1 and 2. Soil temperatures decreasing with depth ..	156
4-4	Comparison of moisture fluxes calculated using the coupled and uncoupled equations for Runs 1 and 2. Soil temperatures decreasing with depth ..	157
4-5	Comparison of evaporation fluxes calculated using the coupled and uncoupled equations for Runs 1 and 2. Soil temperatures increasing with depth ..	158
4-6	Comparison of moisture fluxes calculated using the coupled and uncoupled equations for Runs 1 and 2. Soil temperatures increasing with depth ..	159
4-7	Comparison of evaporation fluxes calculated using the coupled and uncoupled equations for Run 3 ...	163
4-8	Comparison of moisture fluxes calculated using the coupled and uncoupled equations for Run 3 ...	164
4-9	Comparison of $D_{T\ell}$ values computed using the presently proposed model and Philip and de Vries's for Run 1	166

4-10 Comparison of conductive and convective heat flux components for Run 3 169

LIST OF FIGURES

Figure		Page
3-1	Location of study area	46
3-2	Meteorology of study area	48
3-3	Site instrumentation diagram	50
3-4	Psychrometer calibration curves	56
3-5	Neutron calibration curve	58
3-6	Thermal conductivity probe	68
3-7	Thermal conductivity probe insertion and recovery apparatus	70
3-8	Field equipment for thermal conductivity measurements	72
3-9	Typical calibration curves for thermal conductivity measurements	73
3-10	Physical properties of Site 1	81
3-11	Soil texture triangle for the study area	82
3-12	Physical properties of Site 2	84
3-13	Time distribution of piezometric water levels	85
3-14	Time distribution of hydraulic head at Site 1	87
3-15	Time distribution of hydraulic head at Site 2	88
3-16	Time-depth distribution of water contents at Site 1	91
3-17	Time-depth distribution of water contents at Site 2	92
3-18	Time-depth distribution of temperature at Site 2	95
3-19	Water characteristic curve for Site 1	96
3-20	Water characteristic curve for Site 2 (0-45 cm)	98
3-21	Field water characteristic curve for Site 2	

(45-180 cm) 99

3-22 Overall characteristic curve for Site 2 100

3-23 Hysteresis loop 101

3-24 $K_r(\psi)$ relationship for Site 2 (0-20 cm) 104

3-25 $K(\theta)$ relationship for Site 2 (0-20 cm) 105

3-26 Field-determined $K(\theta)$ curve for Site 2 107

3-27 Field-determined thermal conductivity 109

3-28 $\lambda(\theta)$ relationship for Site 2 110

3-29 $C(\theta)$ relationship for Site 2 111

4-1 One-dimensional coupled transient mathematical model 125

4-2 Space-time discretization network 126

4-3 Numerical algorithm 134

4-4 Harmonic mean hydraulic conductivity of adjacent layers 136

4-5 Time distribution of temperature for the conduction problem 147

4-6 Comparison of observed and simulated temperature distributions 148

4-7 Comparison of observed and simulated moisture distributions 149

4-8 Initial conditions for case simulation runs 152

4-9 Upper boundary time distribution of temperature for case simulation runs 153

4-10 Total water (hydraulic) conductivity function $K_\psi(\theta)$ 161

4-11 Thermal diffusivity function $D_T(\theta)$ 162

4-12 $D_L(\theta)$ coefficient function 171

4-13 Time distribution of evaporation flux and temperatures at various depths 173

4-14 Time distribution of heat fluxes at various depths 174

4-15 Time distribution of pressure head in the vicinity of the water table 175

4-16 Cyclic evaporation distribution 177

4-17 Pressure head distribution during infiltration . 178

A-1 Time-depth distribution of temperature at Site 1 213

A-2 Potential evaporation fluxes, air temperatures and wind speeds at the Taber sites during August 11-12/76 214

A-3 Potential evaporation fluxes, air temperatures and wind speeds at the Taber sites during August 13-14/76 215

B-1 Laboratory-determined water characteristic curves for Site 2 217

B-2 Comparison of laboratory and field-determined water characteristic data for Site 2 218

B-3 Vapor equilibration experiments using acid solutions for Site 2 (0-20 cm) 219

C-1 $\psi(\theta)$ relationship for Site 1 (0-30 cm) 221

C-2 $S_e(\psi)$ relationship for Site 1 (0-30 cm) 222

C-3 $K_r(\psi)$ relationship for Site 1 (0-30 cm) 223

C-4 $K(\theta)$ relationship for Site 1 (0-30 cm) 224

C-5 $\psi(\theta)$ relationship for Site 1 (90-150 cm) 225

C-6 $S_e(\psi)$ relationship for Site 1 (90-150 cm) 226

C-7 $K_r(\psi)$ relationship for Site 1 (90-150 cm) 227

C-8 $K(\theta)$ relationship for Site 1 (90-150 cm) 228

C-9 $\psi(S_w)$ relationship for Site 2 (0-20 cm) 229

C-10 $S_e(\psi)$ relationship for Site 2 (0-20 cm) 230

C-11 $\psi(S_w)$ relationship for Site 2 (150-200 cm) ... 231

C-12 $S_e(\psi)$ relationship for Site 2 (150-200 cm) ... 232

C-13 $K_r(\psi)$ relationship for Site 2 (150-200 cm) ... 233

C-14 $K(\theta)$ relationship for Site 2 (150-200 cm) 234

LIST OF SYMBOLS[1]

Upper case Roman letters

A, D, E, F, G, H, H', L, M and U represent various matrices and vectors in the finite difference formulation.

A_i, B_i, C_i, $\overline{A}_i$, $\overline{B}_i$, $\overline{C}_i$, A_i', B_i', C_i', $\overline{A}_i'$, $\overline{B}_i'$, $\overline{C}_i'$, X_i, and Y_i are abbreviations associated with equations (4-4).

C	volumetric heat capacity of a moist porous medium (cal cm^{-3} C^{-1})
C_{wm}	volumetric heat capacity of mineral matter (cal cm^{-3} C^{-1})
C_o	volumetric heat capacity of organic matter (cal cm^{-3} C^{-1})
C_w	volumetric heat capacity of water (cal cm^{-3} C^{-1}) ;
C_w	specific water capacity (cm^{-1})
%C	percentage of clay
D	diffusion coefficient in moist soil of a gas insoluble in water (cm^2 sec^{-1})
D	damping depth (cm)
D	diameter of piezometer (cm)
D_a	molecular diffusion coefficient of water vapor in air (cm^2 sec^{-1})
D_L	coefficient for heat transport by pressure head gradients (cal cm^{-2} sec^{-1})
D_o	diffusion coefficient in air of a gas insoluble in water (cm^2 sec^{-1})
D_s	diffusion coefficient in dry soil of a gas insoluble in water (cm^2 sec^{-1})
D_θ	isothermal water diffusivity

[1] Additional symbols associated with the computer simulation program are included in Appendix E.

	($cm^2\ sec^{-1}$)
$D_{\theta l}$, $D_{\theta v}$	liquid and vapor components of D_θ , respectively ($cm^2\ sec^{-1}$)
D_T	thermal water diffusivity ($cm^2\ sec^{-1}\ C^{-1}$)
D_{Tl} , D_{Tv}	liquid and vapor components of D_T , respectively ($cm^2\ sec^{-1}\ C^{-1}$)
D_v	diffusion coefficient of water vapor in a porous medium ($cm^2\ sec^{-1}$)
E	voltage input (V)
E_a	absolute error
EV or E	evaporation flux or rate ($cm\ sec^{-1}$)
F	generalized storage coefficient - C_w in the unsaturated domain, S_s in the saturated zone (cm^{-1})
F	a measured quantity in error analysis
GHP	guarded hot plate
H	total heat content of a unit of volume of moist porous medium ($cal\ cm^{-3}$)
I	rate of irrigation application ($cm\ sec^{-1}$)
I	electric current (A)
J	time step index
J'	mechanical equivalent of heat (cal)
K or $K_{\psi l}$	liquid hydraulic conductivity ($cm\ sec^{-1}$)
K_ψ	total water hydraulic conductivity ($cm\ sec^{-1}$)
$K_{\psi v}$	vapor component of K_ψ ($cm\ sec^{-1}$)
K_r	relative hydraulic conductivity (dimensionless)
K_{sat}	saturated hydraulic conductivity ($cm\ sec^{-1}$)

L	intake length of piezometer (cm)
L	total length of subsurface profile studied (cm)
L'	latent heat of vaporization of water (cal gm^{-1})
L_{wq} , L_{qw} , L_{ww} , L_{qq}	phenomenological coefficients
M	molecular weight of water vapor (gm $mole^{-1}$)
N	total number of items
%OM	percentage of orgamic matter
P	total gas pressure (cm H_2O or atm)
P_o	standard atmospheric pressure (atm)
Q	heat input to the thermal conductivity probe per unit length (cal cm^{-1} sec^{-1} or w cm^{-1})
R	universal gas constant (erg $mole^{-1}$ K^{-1})
R	radius of piezometer (cm)
R	rate of effective precipitation (cm sec^{-1})
R, R'	resistance and resistance per cm of the heating element, respectively (Ω , Ω cm^{-1})
S	shape factor (cm)
S	slope of the temperature curve in thermal conductivity measurements (C)
S_e	effective saturation (dimensionless)
S_r	residual saturation (dimensionless)
S_s	specific storage (cm^{-1})
S_w	water saturation (dimensionless)
%S	percentage of sand
T	temperature or absolute temperature (C or K)

T'	basic time lag (sec)
T_o, T_{ref}	arbitrary reference temperature (C)
V	microscopic vector fluid velocity (cm sec^{-1})
W	heat of wetting (cal gm^{-1})

Lower case Roman letters

a	volumetric air content (dimensionless)
b, b'	column vectors of known quantities in finite difference formulation
c	specific heat capacity of the porous medium (cal gm^{-1} C^{-1})
c_ℓ	specific heat of liquid water (cal gm^{-1} C^{-1})
c_v	specific heat of water vapor (cal gm^{-1} C^{-1})
c_{mm} or c_s	specific heat of mineral matter (cal gm^{-1} C^{-1})
c_o	specific heat of organic matter (cal gm^{-1} C^{-1})
f	pore geometry factor
g	acceleration of gravity (cm sec^{-2})
h	soil relative humidity (dimensionless)
i	unit vector in the positive z direction
k	intrinsic permeability (cm^2)
p	point fluid pressure (dyne cm^{-2})
p_v	water vapor pressure (cm H_2O)
p_v^s	saturated water vapor pressure (cm H_2O)
q_w	total water flux density (gm cm^{-2} sec^{-1})
q_ℓ, q_v	liquid and vapor components of q_w

	respectively (gm cm^{-2} sec^{-1})
q_h	total heat flux (cal cm^{-2} sec^{-1})
q_{cd} , q_{cv}	conductive and convective components of q_h , respectively (cal cm^{-2} sec^{-1})
r^{-1}	mean curvature of the water-air interface (cm^{-1})
r	$\Delta t / \Delta z^2$
t	time (sec)
x	column vector of unknown variables in finite difference formulation
x_i	input data
x_{mm}	volumetric mineral matter fraction
x_o	volumetric organic matter fraction
y	distance from the water table to the water level in the piezometer (cm)
z	depth
w	bottom boundary water flux (cm sec^{-1})
Greek letters	
α	tortuosity (dimensionless)
α	thermal diffusivity (cm^2 sec^{-1})
α'	organic matter fraction by weight
γ	temperature coefficient of surface tension (C^{-1})
Δ	difference operator
Δx_i	error operator on input x_i
ϵ	small positive number
ζ	ratio of average temperature gradient in air-filled pores to the overall temperature gradient (dimensionless)
η	exponent in equation (3-8)
θ	volumetric water content

	(dimensionless)
θ_ℓ , θ_v	volumetric liquid and vapor components of θ, respectively
θ_x	volumetric moisture content at which liquid continuity first occurs in the porous medium
λ	apparent thermal conductivity (cal cm^{-1} sec^{-1} C^{-1})
λ'	pore size distribution index
λ^*	thermal conductivity not including convection of fluids (cal cm^{-1} sec^{-1} C^{-1})
μ	water viscosity (gm cm^{-1} sec^{-1} or poise)
ν	mass flow factor (dimensionless)
ξ	liquid-assisted vapor enhancement factor (dimensionless)
π	3.14 (constant)
ρ or ρ_ℓ	liquid water density (gm cm^{-3})
ρ_b	bulk density (gm cm^{-3})
ρ_m or ρ_s	particle density (gm cm^{-3})
ρ_o	organic matter density (gm cm^{-3})
ρ_v	water vapor density (gm cm^{-3})
$\rho(\cdot)$	spectral radius
σ	water-air interfacial tension (dyne cm^{-1})
Σ	summation sign
ϕ	porosity
Φ_v	viscous dissipation function (sec^{-2})
Φ	hydraulic potential (cm H_2O)
Ψ	hydraulic head (cm H_2O)
Ψ_b	air entry or bubbling pressure (cm H_2O)

ω	radial frequency (rad sec^{-1})
ω	relaxation factor

Other notation

∇	gradient operator
D/Dt	substantial time derivative
i, j	space and time indices when subscripts and superscripts, respectively
$O(\ )$	order of ( )
$\sim$	approximately equal to
$-$	mean value when superscript
$=$	tensor quantity when superscript
$\lvert\ \rvert$	absolute value

CHAPTER 1

STATEMENT OF THE PROBLEM

In recent years, there has been considerable and varied research interest in problems relating to the simultaneous transfer of heat and mass in flow systems. Although this progress is visible in a broad range of scientific disciplines (Whitaker, 1977; Rossen and Hayakawa, 1977; de Vries, 1975; Guymon and Luthin, 1974; Klute, 1973, Harlan, 1973; Nielsen et al., 1972; Keey, 1972; Fulford, 1969), there is little evidence that this work is making an impact on hydrogeological research (Stallman, 1964,1967). However there are a number of practical problems that would be of interest to the hydrogeologist concerned with thermal influences on the subsurface flow regime, for example, the migration of radionucleides away from subsurface waste management sites in dry desert regions; hydrothermal convection in porous media; subsurface waste heat disposal; evaporation from land surfaces; seasonal fluctuations of the water table in cold environments; natural and artificial recharge problems; systems for land treatment of waste water involving a surface soil saturation followed by evaporative drying; underground storage of cryogenic fluids and heat storage in aquifers; laying of pipelines in cold regions and other frost problems; and generally the subsurface hydrology

of arid, semiarid, as well as cold regions.

Although problems involving the simultaneous water and heat transport have been studied extensively, many aspects are not yet well understood. The fact that different transfer mechanisms operate simultaneously, and often in opposite directions, poses serious difficulties in the development of a suitable mathematical framework and analytical methodologies.

Let us now examine some of the reasons why the problem of the simultaneous movement of water and heat is so complex. Transfer of liquid occurs mainly as a result of gravity, external pressure forces, capillary forces, sorption forces and electrical forces (de Vries, 1965; Nerpin and Globus, 1969). Transfer of vapor is governed by several mechanisms, for example, vapor diffusion under the influence of vapor concentration differences and flow under the influence of external pressure, gravity and friction at the liquid-vapor interfaces. Heat is transported by conduction, radiation and convection (including sensible heat transfer by liquid and vapor movement, as well as latent heat transfer by vapor movement). The complicated internal geometry of the porous media adds further complexities to the liquid-vapor-heat transfer. In addition to these difficulties, it should be noted that even basic quantities such as the soil water potential or the hydraulic and thermal conductivities as functions of moisture content

and temperature are not easy to measure.

In the past, particular mechanisms of moisture and heat transfer in porous media have been emphasized while others have been totally ignored (Harmathy, 1969; Young, 1969; Whitney and Porterfield, 1968; King, 1969; Matthes and Bowen, 1963; Wiegand and Taylor, 1961; Cary, 1961). In most cases, this tendency to emphasize only some of the mechanisms has been adequate for particular situations. However, continued reliance on simplified analyses has led to contradictions and difficulties in generalizing to other cases (Fulford, 1969).

In general, the movement of water and heat in porous media may be analysed using three levels of analysis: molecular, microscopic and macroscopic. For the molecular level of analysis, one develops transport theories based on the movement of molecules. Statistical mechanical concepts might be used to overcome the difficulty of discontinuous media. At the microscopic level, one may utilize the continuous medium approach and examine the detailed behavior of fluids within the pores. An example of this approach is the application of the Navier-Stokes equation to the problem of finding the detailed fluid velocity pattern within the pores. The difficulty of this approach is in the complexity of the boundary conditions between the phases present. This difficulty may be circumvented by using a macroscopic level of analysis in which one replaces microscopic variables by

their volume averages. These averages are taken over an elementary volume large enough to contain a representative assortment of pores, but also small enough to maintain approximately constant values of macroscopic variables within the element (Klute, 1969). Therefore, at this level of analysis, overall macroscopic values of physical properties of a representative volume element are introduced, such as hydraulic and thermal conductivies, diffusivities and volumetric heat capacities, among others. A study of the connection between the description of the transport processes on the microscopic and macroscopic levels provides further insight into the transport processes, especially with respect to the calculation of the macroscopic transport coefficients from appropriate microscopic or molecular aspects of the porous media.

Two main macroscopic models generally form the basis for predicting water and temperature distributions in porous media: the mechanistic model of Philip and de Vries (1957), based on diffusion and heat flow theory, which has been adapted for porous media; and the phenomenological approach based on irreversible thermodynamics (deGroot and Mazur, 1962; Prigogine, 1967; Fitts, 1962; Katchalsky and Curran, 1965; Hanley, 1969). In both these macroscopic theories, the principal problem is to express the microscopic phenomena of flow in proper macroscopic terms, insuring that those mechanisms of primary importance are included while those of secondary importance are neglected. This evaluation

of the relative significance of the mechanisms tends to be arbitrary depending on the interests and objectives of the researcher. Because the transfer mechanisms are not yet completely understood, more complex models -- which are presumably more correct in some details -- may not necessarily be more correct overall (Gupta and Churchill, 1973).

The paper published by Philip and de Vries (1957) consolidating most of the previous knowledge on the influence of temperature gradients on moisture movement laid the groundwork for a better understanding of simultaneous heat and water movement in the soil. The "simple" vapor diffusion theory based on the modified Fick's equation for porous media, predicted the vapor flux density as

$$q_v = -fD_{\alpha v} \nabla \rho_v = -D_v \nabla \rho_v \qquad (1\text{-}1)$$

where

q_v is the vapor flux density (gm/cm²/sec)

$f = \alpha a$ is a pore geometry factor (dimensionless)

α is a tortuosity factor for diffusion of gases in porous media (dimensionless)

$a = \phi - \theta$ is the volumetric air content of the medium (cm³ air/cm³ soil)

ϕ is the porosity of the porous medium (dimensionless)

θ is the volumetric water content of the medium (cm³ water/cm³ soil)

D_α is the molecular diffusion coefficient of water

vapor in air (cm^2/sec)

v is a mass-flow factor arising from differences in boundary conditions governing air and vapor components (dimensionless)

ρ_v is the density of water vapor (gm/cm^3)

$D_v = fD_a v$ is the diffusion coefficient of water vapor in the porous medium (cm^2/sec)

The transport of water vapor in soils under isothermal and solute-free conditions has been studied experimentally by Jackson (1964a, b, c, 1965) and Rose (1963a, b) who found that (1-1) describes isothermal water vapor transport in a satisfactory manner.

However (1-1), while adequate in isothermal conditions, underestimated the vapor flux significantly under temperature gradients, so that the ratio of the observed vapor flux to the value predicted by the simple diffusion theory ranged from about 4 to 18 (Philip and de Vries, 1957). Moreover, the above equation predicted a maximum vapor transfer at a much lower moisture content than the observed one.

The Philip and de Vries theory, in short, attempts to reconcile those discrepancies by taking into account the following two factors which were previously neglected. At low moisture content, the liquid phase is not continuous but is confined to small "islands" in the necks of the pores

between solid particles. Water vapor, however, does not necessarily flow around these water-filled necks, as was assumed in the simple diffusion theory. It can condense on one side of these "islands", move in the liquid phase through the liquid wedge and evaporate from the other side. These "islands" therefore act effectively in shortening the actual path length for vapor diffusion. Thus, the entire pore volume -- not just the air-filled porosity -- is effective in vapor transfer as a series-parallel process of flow through regions of vapor and liquid. This liquid-assisted vapor transfer at low moisture contents was confirmed experimentally under isothermal conditions by Rose (1963a, b, 1965). Such liquid-vapor interaction, therefore, is not restricted to temperature induced diffusion as Philip and de Vries suggested.

The second factor considered was the temperature gradient across air-filled pores within the porous medium. It was found that this gradient is several times greater than the average gradient across the porous medium as a whole, because of the lower thermal conductivity of the air. According to Philip and de Vries, the ratio of the temperature gradient in the air-filled pores to the overall temperature gradient may be as large as 3.2 for dry sand or higher (Woodside and Kuzmak, 1958). This represents a large increase in the thermally induced vapor flow because of the non-linear dependance of vapor pressure on temperature. This ratio can be measured according to the method of de Vries

(1963) when certain assumptions are made about the shape of the soil particles and their thermal conductivities.

Taking into account the above factors in the vapor flux equation, Philip and de Vries developed an approximate analysis which generally provides satisfactory agreement with the experimental observations. In order to describe thermally induced liquid movement, Philip and de Vries modified Darcy's equation by incorporating the temperature dependence of surface tension and its effect on matric potential. Table 1-1 summarizes the equations and parameters of the Philip and de Vries model (Philip and de Vries, 1957; de Vries, 1958; de Vries and Peck, 1958b; de Vries, 1975).

Some of the shortcomings of this analysis are that the temperature coefficient of the matric potential is greater than that of the surface tension of pure water considered by Philip and de Vries (Wilkinson and Klute, 1962; Cary, 1966; Jury and Miller, 1974); and that the Philip - de Vries model predicts zero thermally induced water flux in a saturated system, which has been shown not to be the case (Taylor and Cary, 1960; Corey and Kemper, 1961; Cary, 1966). From a practical viewpoint, the determination of the numerous soil and water parameters appearing in the equations of Table 1-1 makes the applicability of that model difficult.

Due to the fact that all transfer of heat and moisture occurs under non-equilibrium conditions,the concepts of the theory of non-equilibrium thermodynamics may be applied to

TABLE 1-1

Philip and de Vries Model*

(1-2)	$q_v/\rho = -D_{\theta v}\nabla\theta - D_{Tv}\nabla T$	vapor	Flux Equations
(1-3)	$q_l/\rho = -D_{\theta l}\nabla\theta - D_{Tl}\nabla T - Ki$	liquid	
(1-4)	$q_w/\rho = -D_{\theta}\nabla\theta - D_{T}\nabla T - Ki$	water	
(1-5)	$q_h = -\lambda\nabla T - \rho L' D_{\theta v}\nabla\theta$	heat	
(1-6)	$\partial\theta/\partial t = \nabla(D_{\theta}\nabla\theta) + \nabla(D_T\nabla T) + \partial K/\partial z$	water	Transient Flow Equations
(1-7)	$C\partial T/\partial t = \nabla(\lambda\nabla T) + \rho L'\nabla(D_{\theta v}\nabla\theta)$	heat	
(1-8)	$D_{\theta v} = f D_a \nu (Mg/RT) p_v^s \partial h/\partial\theta$	vapor moisture diffusivity	Transport Coefficients
(1-9)	$D_{Tv} = \zeta f D_a \nu (Mg/RT) h\, dp_v^s/dT$	thermal vapor diffusivity	
(1-10)	$D_{\theta l} = K(\partial\psi/\partial\theta)_T$	liquid moisture diffusivity	
(1-11)	$D_{Tl} = \gamma\psi K$	thermal liquid diffusivity	
(1-12)	$D_{\theta} = D_{\theta v} + D_{\theta l}$	isothermal moisture diffusivity	
(1-13)	$D_T = D_{Tv} + D_{Tl}$	thermal moisture diffusivity	

* See List of Symbols for the definitions of the various terms involved.

porous media (Groenevelt and Bolt, 1969; Kay and Groenevelt, 1974; Groenevelt and Kay, 1974). Such an approach was first attempted for porous solids by Luikov (1966) and Taylor and Cary (1960). For a system in which the simultaneous flow of heat and water only are considered, the appropriate fluxes may be written in a form similar to those derived by Philip and de Vries (Table 1-2). Jury (1973) presented a derivation and a comparison of such equations with those of Philip and de Vries.

The non-equilibrium thermodynamics approach is more general than the Philip and de Vries's one because it does not invoke any models or mechanisms and can be easily extended to include other influencing factors, such as osmotic or concentration gradients, among others. Certain theorems and restrictions allow the use of the Onsager reciprocity relation which states that

$$L_{wq} = L_{qw} \qquad (1\text{-}18)$$

thus reducing the number of the unknown phenomenological coefficients (Table 1-2) by one. Cary (1963,1964), among others, has demonstrated the validity of the Onsager relation in soils. The main problem with this phenomenological approach is that it does not provide insight into the transport coefficients, which makes their calculation difficult. Other limitations include the following: the domain for which the equations apply must be very close to equilibrium for the Onsager reciprocal relations to be valid. The condition for linear

TABLE 1-2

Non-equilibrium Thermodynamics Model*

(1-14)	$q_w = -L_{ww}\nabla\phi - L_{wq}\nabla(\ln T)$	water	Flux Equations
(1-15)	$q_h = -L_{qw}\nabla\phi - L_{qq}\nabla(\ln T)$	heat	
(1-16)	$\partial\theta/\partial t = \nabla(L_{ww}\nabla\phi) + \nabla(L_{wq}\nabla(\ln T))$	water	Transient Flow Equations
(1-17)	$C\partial T/\partial t = \nabla(L_{qw}\nabla\phi) + \nabla(L_{qq}\nabla(\ln T))$	heat	

* See List of Symbols for the definitions of the various terms involved.

phenomenological relations inherent in the general theory implies constant coefficients, a situation which does not correspond to real porous media flow conditions. Although in recent years significant progress has been made with regard to far-from-equilibrium thermodynamics (Glansdorff and Prigogine, 1971; Prigogine and Nicolis, 1977), such progress has not yet reached the area of flow through porous media.

The similarity of the equations in Tables 1-1 and 1-2 has prompted a comparison of the two previously discussed approaches by several researchers (Gee, 1966; Dirksen and Miller, 1966; Hadas, 1968; Cassel et al., 1969). However, these scientists were not able to demonstrate any clearcut advantage of one method over the other in approximating the observed data.

Analytical solutions of the non-linear transient equations (1-6) and (1-7) or (1-16) and (1-17) of Tables 1-1 and 1-2, respectively, are not available, unless it is assumed that the transport coefficients appearing in those equations are constant. This assumption is the basis for the analytical solutions presented by Crank (1956), de Vries and Peck (1958), Luikov and Michailov (1965), Husain et al. (1971). However, the transport coefficients -- like conductivities and diffusivities, which represent the thermophysical properties of porous media -- are not constant but depend on moisture content and temperature

(Klute, 1973). Therefore, numerical methods are the appropriate means for solving these non-linear equations.

The numerical approach, however, is limited by the lack of satisfactory measurements of porous media properties under non-isothermal conditions, which are needed for model descriptions (Fulford, 1969; Wooding and Morel-Seytoux, 1976; Whitaker, 1977). Therefore, the difficulty in comparing theoretical and model results with experimental data is the major obstacle to carrying out numerical calculations on coupled systems.

Experimental investigations of simultaneous water and heat transport have been almost exclusively carried out in the laboratory (Stallman, 1967; Jackson et al., 1975). Little or no emphasis has been placed on investigating field situations. The hot and dry surface layers of bare soils are one example where temperature effects on water transfer are very pronounced because of the predominance of moisture transport in the vapor phase. Also, in deeper layers of the ground, seasonal climatic trends may create persistent temperature gradients which can transport water in a vertical direction.

However, few investigations -- based primarily on the Philip and de Vries theory -- have been carried out in the field. Investigations of the non-isothermal water flux of the upper 15 cm of a bare soil (Rose, 1968a, b, c) showed that the thermally induced vapor flux was of comparable

magnitude to the liquid flux and was oscillatory in direction and magnitude. A field and modeling study of heat transfer in bare soils (Wierenga and deWit, 1970) showed close agreement between predicted and observed soil temperatures for a wet soil. A study of the simultaneous water and heat fluxes within the top 10 cm of a field soil (Jackson et al., 1974, 1975) showed that the Philip and de Vries theory best predicts the soil water flux under diurnal conditions at intermediate water contents.

At present, a wide discrepancy seems to exist between the 'field-scale' approach of the hydrogeologists and the 'local scale' approach of the soil physicists. The hydrogeologists' approach has been largely empirical and crudely averaging, while the more physically based "micro" approach of soil physicists has so far not been successful in describing the field condition and its associated heterogeneity (Swartzendruber and Hillel, 1973). These two approaches are parallel lines of attack that have not converged. If both approaches moved towards a common scale of system characterization, the above mentioned discrepancy might cease to exist.

In order to reconcile these approaches, I propose the development of a theory which will treat the subsurface flow domain as an integrated entity, rather than as a series of isolated or loosely connected local systems. Several scientists (Childs, 1960; Stallman, 1964, 1967; Freeze,

1969a; Klute, 1969; van Bavel, 1969; Vachaud et al., 1975) have argued for an integrated approach to the problem of ground water recharge and discharge. In emphasizing the division of Hydrology into surface and groundwater Hydrology, hydrogeologists have tended to forget that events at the surface and underground waters are connected -- not just as a matter of geologic continuity -- but in a real sense, in that there is continuous movement of water from one domain into the other. This connecting link constitutes the unsaturated zone.

Accordingly, the following main objectives are set forth for this thesis:

to develop and apply a methodology for subsurface coupled heat and water transport suitable for field applications;

to develop and test a general computer simulation model for the simultaneous water and heat movement in unsaturated-saturated subsurface domains based on an adaptation of the Philip and de Vries model;

to evaluate the influence of coupling on diurnal subsurface moisture and heat transfer, and to use the coupled flow equations to calculate evaporation from dry land surfaces.

CHAPTER 2

THEORETICAL DEVELOPMENT

2.1 Introduction

In this chapter, the equations for water and heat transport in porous media are derived. These will be used in Chapter 4 for the development of a general digital simulation model of non-isothermal transport in porous media. The following presentation is based on the transport phenomena viewpoint and is concerned with the fluxes of mass, momentum and energy which describe the macroscopic equations of change for porous media. These quantities can be determined from basic principles of physics listed below (Bird et al., 1960):

Continuity equation $\partial\rho/\partial t + \nabla(\rho V) = 0$

(Conservation of mass equation) (2-1)

Momentum equation $\rho\, DV/Dt = \rho g - \nabla p + \mu\nabla^2 V$ (2-2)

Thermal energy eqn. $\rho c\, DT/Dt = -\nabla q_{cd} - T(\partial p/\partial T)_\rho \nabla V + \mu\Phi_V$ (2-3)

where

ρ is the mass density (gm/cm^3)

V is the microscopic vector flow velocity (cm/sec)

μ is the dynamic viscosity (poise)

p is the point fluid pressure (dyne/cm^2)

c is the specific heat capacity (cal/gm/C)

q_{cd} is the conductive heat flux (cal/cm²/sec)

Φ_v is the viscous dissipation function (sec^{-2})

D/Dt is the substantial time derivative

and all other quantities are as defined previously. A detailed derivation of the simultaneous heat, mass and momentum transfer in porous media from basic principles has recently been given by Whitaker (1977). However, for reasons of simplicity and brevity, a less rigorous approach in deriving the required equations will be followed here.

Before proceeding, it is essential to examine the parameters of interest in this study and the assumptions made in deriving appropriate equations, which are necessary for the determination of these parameters. Pressure potential or pressure head of interstitial water and temperature of the porous medium, as functions of space and time, are the main quantities sought in the present development. The pressure potential of interstitial water is the fraction of its energy per unit quantity of water that results from a pressure that is different from the reference pressure of one standard atmosphere. If a unit weight is taken as the unit quantity of water, then the pressure potential has the unit of length (cm) and is often called pressure head ψ (see also p. 26). The pressure head of interstitial water is positive in saturated porous media, zero at the water table and negative in unsaturated media. This negative pressure potential is also known as matric or capillary potential (Rose, 1966, Corey et al., 1967).

2.2 Assumptions

The following are the major assumptions and approximations underlying the derivation of the coupled non-isothermal equations of water and heat transfer in porous media to be presented in this chapter:

1) the system is comprised of a non-deformable and chemically inert matrix with liquid water and its vapor in the voids among the grains;
2) liquid flow can be described by a Darcy-type equation, which implies -- among other things -- that the flow is laminar;
3) all flow parameters are unique functions, so that hysteresis is avoided;
4) solute effects are negligible; no water composition variable or electrochemical effects are considered;
5) the liquid water and its vapor are in a continuous local phase equilibrium in the pores;
6) the macroscopic heat flux equation as presented by de Vries (1958) with negligible heat transfer by air convection, radiation and viscous generation of heat (2-55) is considered to be a valid approximation of porous media heat flux;
7) the soil relative humidity is independent of temperature at constant water content;
8) air pressure remains constant and air effects (entrapped air, solution of soil air) are negligible.

When the above assumptions are applied to porous media, they generally present no serious limitations (de Vries and Peck, 1958). Probably the most serious exception is assumption 3) above, which removes hysteresis from consideration. It is well-known that relationships such as the water characteristic function (ψ vs θ) and to a smaller degree the hydraulic conductivity function (K vs θ or K vs ψ) exhibit hysteretic behavior, especially for the near-surface domain. However, as Philip (1955) pointed out, hysteresis does not in itself invalidate the use of subsurface water flow equations, as long as the water characteristic relation adopted is appropriate to the phenomenon under study. In order to sidestep the problem, scientists considered monotonically drying or wetting flow problems and avoided materials which exhibit pronounced hysteretic behavior, such as swelling soils and others. In other cases a mean wetting-drying characteristic curve was shown to be satisfactory under field conditions (Watson et al., 1975). Rose (1971) concluded that variations caused by hysteresis, though real, are likely to be negligible in relatively dry soils and therefore it should be possible to ignore hysteresis in practice without serious errors. Royer and Vachaud (1975), however, concluded that hysteresis was too important to be neglected in their field study.

Although problems involving hysteresis have been solved numerically, assuming that the hysteretic functions were known in sufficient detail (Whisler and Klute, 1965; Rubin,

1967; Ibrahim and Brutsaert, 1968; Freeze, 1969a, 1971), the complexity of the developed theoretical techniques for handling hysteretic phenomena quantitatively, and the uncertainties associated with them make the applicability of such techniques difficult (Poulovassilis, 1962; Topp and Miller, 1966; Topp, 1969, 1971; Poulovassilis and Childs, 1971). Considerable research is still required in the area of hysteresis, so that the techniques developed recently can be simplified and effectively used in the hysteretic behavior of field soils (Watson et al., 1975; Klute, 1973). Also evaluations of the errors introduced both by neglect of hysteresis and by the use of approximate treatments are required.

In the following sections, the constitutive relationships between fluxes and appropriate gradients for vapor and liquid, as well as for heat transport, are developed. Transport parameters or coefficients are defined and/or briefly discussed. Subsequently the transient water and heat flow equations are derived by invoking conservation principles. As will be pointed out, the equations developed are more general than those usually found in the literature, in that they are valid for both unsaturated and saturated domains, as well as for non-homogeneous porous media. Finally, a field-oriented methodology is developed for estimating the various transport coefficients involved in coupled, non-isothermal equations.

2.3 Vapor Transport

By making the following assumptions

1) the water vapor behaves as an ideal gas, which means that the vapor density ρ_v (gm/cm^3) is related to the vapor pressure p_v (cm H_2O) by the ideal gas law (2-4), and

$$\rho_v = (M/RT) \rho g p_v \qquad (2\text{-}4)$$

where

M is the molecular weight of water vapor (gm/mole)

R is the universal gas constant (erg/mole/K)

T is temperature (K)

ρ is the liquid water density (gm/cm^3)

g is the acceleration of gravity (cm/sec^2)

2) the total gas pressure P is constant throughout the porous medium,

a modified Fickian type expression to describe vapor flux (q_v) in porous media can be written as follows (van Bavel, 1952; Rollins et al., 1954; de Vries, 1975):

$$q_v/\rho = -fD_a \nu (Mg/RT) \nabla p_v \qquad (2\text{-}5)$$

where $\nu = P/(P-p_v)$ is the mass flow factor which is always close to unity; f is a pore geometry factor (dimensionless), and D_a is the molecular diffusion coefficient of water vapor in air (cm^2/sec).

The molecular diffusion coefficient D_a of water vapor in air is a function of temperature and total gas pressure and may be expressed as (Kruger et al., 1970)

$$D_a = c\,(P_o/P)\,(T/T_o)^n \qquad (2\text{-}6)$$

where P_o is the standard atmospheric pressure (1 atm); P is the total gas pressure (atm); T and T_o are absolute (Kelvin) temperatures; T_o = 273.15 K; c=0.217 cm²/sec and n=1.88. (2-6) is an empirical relationship based on both isothermal and non-isothermal experimental data and on theoretical considerations (de Vries and Kruger, 1967).

The pore geometry factor f is a modification designed to account for the effects of the increase of the diffusion path length that results from the presence of the solid matrix and the effects that result from the presence of the liquid phase enhancing flow (see p. 7). Philip and de Vries (1957) expressed f as follows:

$$f = \alpha\phi \qquad \text{for } \theta \leq \theta_x \qquad (2\text{-}7a)$$

$$f = \alpha(a + x\theta) \qquad \text{for } \theta > \theta_x \qquad (2\text{-}7b)$$

where α is tortuosity (dimensionless), usually approximated by the constant value 0.66 (Penman, 1940); ϕ is porosity (dimensionless) and θ_x is the moisture content at which liquid continuity first occurs in the porous medium. This latter quantity is approximated here by the moisture content corresponding to the matric potential of one bar of the characteristic curve (ψ vs θ). In equation (2-7b), x is a function of moisture content. It is approximated as $x \rightarrow a/a_x$ (Philip and de Vries, 1957), where $a = \phi - \theta$ (air content) and $a_x = \phi - \theta_x$; tends to unity when liquid continuity no longer exists and to zero near saturation.

The pore geometry factor for a gas insoluble in water may also be represented as (Currie, 1960, 1961; Rose, 1968a, b)

$$f = (D/D_s)\ (D_s/D_o) \qquad (2\text{-}8)$$

where D is the diffusion coefficient in moist soil of a gas insoluble in water (cm^2/sec); D_o and D_s are diffusion coefficients of the same gas in air and dry soil respectively (cm^2/sec). The ratio (D/D_s) accounts for the reduction of diffusion by the presence of water, and (D_s/D_o) accounts for the tortuosity or the presence of soil matrix.

In order to express the vapor flux (2-5) in terms of variables of interest, such as T and θ or ψ , the thermodynamic relationship expressed in equation (2-9) is used (Edlefsen and Anderson, 1943). It is based on the assumption that a continuous equilibrium exists between vapor and liquid contents per unit volume

$$\rho_v = \rho_v^s h = \rho_v^s \exp[(Mg/RT)\psi] \qquad (2\text{-}9)$$

where ρ_v^s is the saturated water vapor pressure ($cm\ H_2O$) and h is the soil relative humidity (dimensionless). On the basis of arguments presented by Philip and de Vries (1957), it can be shown that the relative humidity h is mainly a function of moisture content, and that the saturation vapor pressure ρ_v^s is a function of temperature only. Thus, the vapor pressure can be expressed as

$$\rho_v(\theta, T) = \rho_v^s(T)\ h(\theta) \qquad (2\text{-}10)$$

Applying the chain rule of differentiation to $\nabla \rho_v$ in (2-5)

and making use of (2-10), the following relationship is obtained:

$$\nabla p_v = p_v^s \, (\partial h/\partial\theta) \nabla\theta + h \, (dp_v^s/dT) \, (\nabla T)_a \qquad (2\text{-}11)$$

where $(\nabla T)_a$ represents the average temperature gradient across air-filled pores in the porous medium. This gradient, as is mentioned in Chapter 1 (p. 7), may be several times larger than the overall macroscopic gradient ∇T, so that

$$(\nabla T)_a = \zeta \nabla T \qquad (2\text{-}12)$$

where $\zeta \geq 1$. As indicated by Philip and de Vries (1957) and Rose (1968a, b), typical values of ζ range from 1.3 to 3.0 for most soil materials.

In order to replace the $\partial h/\partial\theta$ gradient in (2-11) by a pressure head gradient, (2-9) is differentiated with respect to θ to give

$$\partial h/\partial\theta = (Mg/RT) \, h \, \partial\psi/\partial\theta \qquad (2\text{-}13)$$

so that (2-11) becomes

$$\nabla p_v = p_v^s \, (Mg/RT) \, h \, \partial\psi/\partial\theta \, \nabla\theta + h \, (dp_v^s/dT) \, \{(\nabla T)_a/\nabla T\} \, \nabla T \qquad (2\text{-}14)$$

or

$$\nabla p_v = p_v^s \, (Mg/RT) \, h \nabla\psi + \zeta \, h \, (dp_v^s/dT) \nabla T \qquad (2\text{-}15)$$

Substituting (2-15) in (2-5) yields the vapor flux in terms of the unknowns ψ and T

$$q_v/\rho = -fD_a \nu (Mg/RT)^2 p_v^s \, h \nabla\psi - \zeta f D_a \nu (Mg/RT) \, h (dp_v^s/dT) \nabla T \qquad (2\text{-}16)$$

By defining the following generalized parameters:

$$K_{\psi v} = fD_a \nu (Mg/RT)^2 p_v^s \, h \qquad (2\text{-}17)$$

where $K_{\psi v}$ (cm/sec) is the vapor conductivity; and

$$D_{Tv} = \zeta f D_a \nu (Mg/RT) \, h \, dp_v^s/dT \qquad (2\text{-}18)$$

where D_{Tv} ($cm^2/sec/C$) is the thermal vapor diffusivity,

the vapor flux, can be more simply written as

$$q_v/\rho = -K_{\psi_v} \nabla\psi - D_{T_v} \nabla T \qquad (2\text{-}19)$$

For the saturated zone, the vapor flux becomes zero.

2.4 Liquid Transport

The starting point for the theoretical formulation of liquid transport is the momentum principle -- expressed by the Navier-Stokes equation (Schlichting, 1968; Le Méhauté, 1976) -- which describes the isothermal flow of a Newtonian incompressible fluid with constant viscosity

$$\underbrace{\rho\, DV/Dt}_{\text{Inertial Forces}^1} = \underbrace{\rho g \quad -\nabla p \quad +\mu\nabla^2 V}_{\text{gravity pressure friction}\ \text{Applied Forces}} \qquad (2\text{-}20)$$

Because the boundary conditions in porous media are extremely complex (the microscopic flow velocity V equals zero at the surface of every grain), the above equation must be transformed to a more useful form. Consequently, instead of dealing with microscopically varying values of velocity and pressure, only the mean values need to be considered. Also by making the following approximations:

1) for a porous medium the inertial forces are negligible, which is the case with a steady, laminar flow; and

2) the viscous (friction) forces are proportional to the

---

[1] These forces characterise the natural resistance of matter to any change in its state of motion.

mean velocity of the fluid flowing through a porous medium, which is an empirical approximation;

the Navier-Stokes equation (2-20) reduces to

$$0 = \rho g - \nabla\bar{p} + (\mu/k)\bar{V} = \rho(g - \nabla\bar{p}/\rho) + (\mu/k)\bar{V} \qquad (2\text{-}21)$$

where $\bar{V}$ is the macroscopic (mean) vector flow velocity and $\bar{p}$ is the mean fluid pressure. Both of these quantities are the outcome of smoothing the actual microscopic distribution of velocity and pressure over a volume larger than that of the individual pores. Solving (2-21) for $\bar{V}$ one obtains:

$$\bar{V} = -(k\rho/\mu)\left[-\nabla\bar{p}/\rho + g \right] = -(k\rho/\mu)\nabla\Phi' =$$

$$-(k\rho g/\mu)\nabla\Phi = -K\nabla\Phi = -K\nabla(\psi + z) \qquad (2\text{-}22)$$

where $\Phi' = g\Phi = g[(\bar{p}/\rho g) + z] = g(\psi + z)$ (2-23)

Φ is the total (hydraulic) potential corresponding to the hydraulic head (cm);

k is the intrinsic permeability (cm^2) of the porous medium; and

z is the elevation (cm), here taken as positive in the upward direction.

(2-22) is the Darcy equation (Hubbert,1956) for the steady isothermal solute-free flow of water in isotropic saturated porous media with constant hydraulic conductivity K. By expressing that equation in the following form, the macroscopic flow velocity for an anisotropic medium is defined as

$$\bar{V} = q_l/\rho = -\bar{\bar{K}}\nabla\Phi \qquad (2\text{-}24)$$

where $\bar{\bar{K}}$ is the hydraulic conductivity tensor.

In summary, provided that the inertial terms are

negligible, as is generally the case with porous media, the macroscopic mean flow velocity is directly proportional to the macroscopic mean potential gradient. This represents the hydrodynamic element in Darcy's equation. Implicit in this equation is the statistical requirement that the medium must be "sufficiently homogeneous" on the scale of the averaging volume -- the so-called "Darcy scale" -- for local mean quantities, such as $\overline{v}$ and $\overline{p}$ or Φ, to exist (Philip, 1970).

Darcy's equation can be applied to unsaturated porous media (Richards, 1931; Childs and Collis-George, 1950) when the hydraulic conductivity K is allowed to vary as a function of the matric potential ψ or the volumetric moisture content θ. This change is due to the fact that the unsaturated hydraulic conductivity decreases very rapidly as the porous media water content decreases from its saturation value and as the pressure head becomes negative. Thus, for unsaturated media, (2-22) is expressed as

$$q_\ell/\rho = -K(\psi)\nabla\Phi = -K(\theta)\nabla\Phi \qquad (2\text{-}25)$$

Assuming the coordinate z to be positive in a downward direction, the hydraulic head becomes

$$\Phi = \psi - z \qquad (2\text{-}26)$$

so that (2-25) is written as

$$q_\ell/\rho = -K(\psi)\nabla[\psi(\theta,T)-z] = -K\nabla\psi + Ki \qquad (2\text{-}27)$$

where both K and ψ are functions of moisture content and temperature, and i is a unit vector in the positive z direction.

In order to generalize Darcy's equation (2-22 and 2-27) to take into account non-isothermal conditions, (2-27) is expanded using the chain rule of differentiation

$$q_\ell/\rho = -K\,\partial\psi/\partial\theta\,\nabla\theta - K\,\partial\psi/\partial T\,\nabla T + Ki \qquad (2\text{-}28)$$

or

$$q_\ell/\rho = -D_{\theta\ell}\,\nabla\theta - D_{T\ell}\,\nabla T + Ki \qquad (2\text{-}29)$$

where the following generalized diffusivities are introduced:

$D_{\theta\ell} = K\,(\partial\psi/\partial\theta)_T$ -- liquid moisture diffusivity (cm^2/sec) (2-30)

$D_{T\ell} = K\,(\partial\psi/\partial T)_\theta$ -- liquid thermal diffusivity ($cm^2/sec/C$) (2-31)

In employing the diffusivity concepts mentioned above, it should be stressed that although vapor transport through porous media is mainly carried out by true diffusion, the process of liquid movement is not achieved by diffusion but by viscous flow. The term "diffusivity" arose in order to set the transport equation in a form analogous to the equations of diffusion and heat conduction. For equations of this form, numerous mathematical solutions are available (Crank, 1956; Carslaw and Jaeger, 1959). However, the main problem in applying the liquid moisture diffusivity concept to real situations is that such a concept is restricted to homogeneous unsaturated porous media (Kirkham and Powers, 1972). Therefore, in this work, (2-28) and (2-29) are written as functions of ψ and T

$$q_\ell/\rho = -K_{\psi\ell}\,\nabla\psi - D_{T\ell}\,\nabla T + Ki \qquad (2\text{-}32a)$$

where $K_{\psi\ell} = K$ (2-32b)

Thus, (2-32a) is more general than (2-29) because it is applicable to both saturated and unsaturated porous media and valid for heterogeneous conditions.

In order to estimate the liquid thermal diffusivity $D_{T\ell}$ (2-31) Philip and de Vries (1957) argued that in the range of dominant liquid transfer, the negative pressure potential ψ is determined by capillarity and thus the equation of capillarity holds

$$\psi = (2/r)\,\sigma \qquad (2\text{-}33)$$

where σ is the water-air interfacial tension (dyne/cm); $1/r$ is the mean curvature of the water-air interface (cm^{-1}). Hence,

$$\partial\psi/\partial T|_{\theta} = (2/r)\ d\sigma/dT = (\psi/\sigma)\ d\sigma/dT = (d\ln\sigma/dT)\psi = \gamma\psi \qquad (2\text{-}34)$$

where $\gamma = d\ln\sigma/dT$ is the temperature coefficient of surface tension, which is reasonably constant in the range of 10 to 30 C. Thus, the following simple surface tension model was used by Philip and de Vries (1957) and numerous subsequent investigators (Gee, 1966; Rose, 1968a, b, c; Cassel et al., 1969; Fritton et al., 1970) to estimate $D_{T\ell}$:

$$D_{T\ell} = \gamma\psi K \qquad (2\text{-}35)$$

However, there are problems with this simple formulation. Measured values of $\partial\psi/\partial T$ were consistently higher than the calculated estimates from the above equation (Wilkinson and Klute, 1962; Cary, 1966; Jury and Miller, 1974). The explanation for the differences is that several other mechanisms, besides the previously mentioned surface tension

model, also contribute to liquid flow in the presence of temperature gradients (Cary, 1966).

In order to circumvent this difficulty, I propose an alternative formulation which gives a better approximation to measured data. Invoking assumptions 5) and 7) listed previously in this chapter (see also 2-9 and 2-10), the following relation can be deduced by differentiation:

$$\partial\psi/\partial T = (R/Mg)\ \ln h \qquad (2\text{-}36)$$

so that

$$D_{T\ell} = K\ (R/Mg)\ |\ln h| \qquad (2\text{-}37)$$

Both the above described model (2-37) and the surface tension model for estimating $D_{T\ell}$, however, suffer from the limitation that they are not applicable to saturated conditions. Taylor and Cary (1960), reported several instances of thermally induced flow in saturated porous media.

2.5 Total Water Transport

In order to obtain the combined liquid and vapor flux or total water flux q_w/ρ , both liquid (2-32) and vapor (2-19) flux components are added algebraically as follows:

$$q_w/\rho = q_\ell/\rho + q_v/\rho = -K_\psi \nabla\psi - D_T \nabla T + Ki \qquad (2\text{-}38)$$

where

$K_\psi = K_{\psi_v} + K_{\psi\ell}$ -- total hydraulic conductivity (cm/sec) (2-38)

$D_T = D_{Tv} + D_{T\ell}$ -- thermal water diffusivity (cm^2/sec/C) (2-40)

The total non-isothermal water flux (2-38) is governed by

Darcy's equation plus terms included to account for vapor flux and thermally driven liquid and vapor. This constitutive relation was termed "the general Darcy law" by Guymon and Luthin (1974).

2.6 Transient Flow Equations

Both vapor and liquid flux equations discussed previously describe only steady flow processes in which the flux and potential gradient at each point remain constant with time. In order to extend the flow processes to transient or unsteady conditions -- in which the flux and potential gradient vary with time -- the principle of conservation of mass, expressed by the continuity equation (Cooper, 1966; De Wiest, 1966; Eagleson,1970) is introduced in (2-41) as:

$$\partial(\rho\phi S_w)/\partial t + \nabla(\rho\bar{V}) = 0 \qquad (2\text{-}41)$$

where S_w is the volumetric degree of saturation ($0 \le S_w \le 1$). By combining (2-41) with the previously derived flux equations, the transient flow equations result. Substituting Darcy's equation (2-22) into (2-41) yields

$$\partial(\rho\phi S_w)/\partial t = \nabla[\ \rho K \nabla(\psi+z)\ ] \qquad (2\text{-}42)$$

Expanding the left-hand-side of (2-42) and substituting in it the mathematical definitions of water and formation compressibilities (Jacob, 1950; De Wiest, 1966; Cooper, 1966; Cooley,1971), one obtains (2-43)

$$[\underbrace{\partial\theta/\partial\psi + (\theta/\phi)\, S_s}_{F}\ ]\ \partial\psi/\partial t = \nabla K\,[\nabla\ (\psi+z)\ ] \qquad (2\text{-}43)$$

where S_s is the specific storage coefficient (cm^{-1}) and

$$F = \partial\theta/\partial\psi + (\theta/\phi)\ S_s \qquad (2\text{-}44)$$

is a generalized storage coefficient (cm^{-1}). It is assumed that the spatial variations in ρ are negligible due to the slight compressibility of water.

(2-43) is the transient isothermal flow equation which applies to both saturated and unsaturated porous media. For saturated media, (2-43) reduces to the elastic storage equation

$$S_s\ \partial\psi/\partial t = \nabla K[\ \nabla\ (\psi+z)\ ] \qquad (2\text{-}45)$$

For unsaturated media, (2-43) reduces to Richards' equation

$$C_w\ \partial\psi/\partial t = \nabla K[\ \nabla\ (\psi+z)\ ] \qquad (2\text{-}46)$$

where $C_w = \partial\theta/\partial\psi$ (2-47)

is the specific water capacity (cm^{-1}).

By applying the continuity principle to the non-isothermal vapor (2-19), liquid (2-29) and total water flux (2-38), the following differential equations are obtained:

$$\partial\theta_v/\partial t = -\nabla(q_v/\rho) + E = \nabla(K_{\psi_v}\nabla\psi + D_{T_v}\nabla T) + E \qquad (2\text{-}48)$$

$$\partial\theta_l/\partial t = -\nabla(q_l/\rho) - E = \nabla(K_{\psi_l}\nabla\psi + D_{T_l}\nabla T - Ki) - E \qquad (2\text{-}49)$$

$$\partial\theta/\partial t = -\nabla(q_w/\rho) = \nabla(K_\psi\nabla\psi + D_T\nabla T - Ki) \qquad (2\text{-}50)$$

The possibility of water transfer from the liquid to the vapor phase and vice versa is accounted for by the source-sink (evaporation-condensation) term E in (2-48) and (2-49) (de Vries, 1958).

Assuming that liquid and vapor phases are always in

equilibrium -- which is shown to be a valid assumption (Novak and Coulman, 1974) -- the following relation holds (de Vries, 1958) for any small region of porous medium:

$$\theta_v = (\phi-\theta_\ell)\,\rho_w/\rho = (\phi-\theta_\ell)\,(\rho_v^s/\rho)\,h = (\phi-\theta_\ell)\,(\rho_v^s/\rho)\,\exp[(Mg/RT)\psi] \qquad (2\text{-}51)$$

Differentiating the above relationship with respect to time by means of the chain rule and substituting the result together with the relation $\theta = \theta_\ell + \theta_v$ in (2-50), one obtains the general non-isothermal transient flow equation

$$\begin{aligned}\partial\theta/\partial t &= \partial\theta_\ell/\partial t + \partial\theta_v/\partial t = \\ &[\,1+(\rho_v^s/\rho)\exp\{Mg/RT\}\,(\phi-\theta_\ell)\,(Mg/RT)\,\partial\psi/\partial\theta\,]\,\partial\theta_\ell/\partial t \\ &+[\,(\rho_v^s/\rho)\exp\{Mg\psi/RT\}\,(\phi-\theta_\ell)\,(1/\rho_v^s\,\partial\rho_v^s/\partial T - Mg\psi/RT^2)\,]\,\partial T/\partial t \\ &= \nabla(K_\psi\nabla\psi + D_T\nabla T - Ki) \qquad (2\text{-}52)\end{aligned}$$

or

$$\partial\theta/\partial t = (1+A)\,\partial\theta/\partial t + (B-G)\,\partial T/\partial t = \nabla(K_\psi\nabla\psi + D_T\nabla T - Ki) \qquad (2\text{-}53)$$

where

$$A = (\rho_v^s/\rho)\exp[Mg\psi/RT]\,(\phi-\theta_\ell)\,(Mg/RT)\,\partial\psi/\partial\theta_\ell$$

$$B = (\rho_v^s/\rho)\exp[Mg\psi/RT]\,(\phi-\theta_\ell)\,(1/\rho_v^s)\,\partial\rho_v^s/\partial T$$

$$G = (\rho_v^s/\rho)\exp[Mg\psi/RT]\,(\phi-\theta_\ell)\,(Mg/RT^2)\,\psi$$

However, many terms in the above equation are negligibly small compared to dominant terms in that equation. Thus term A in the equation above is of the order of $10^{-12}\,(\phi-\theta_\ell)\,\partial\psi/\partial\theta$ (cm^{-1}), term B is of the order of $10^{-7}\,(\phi-\theta_\ell)$ (C^{-1}), and term G is of the order of $10^{-14}\,(\phi-\theta_\ell)$ ($cm^{-1}\,C^{-1}$). Therefore, for moisture contents above extreme dryness, terms A, B, and G can be neglected; so that the above equation becomes identical to (2-50).

In order to express (2-48), (2-49) and (2-50) in terms of one dependent variable (ψ), the concept of the generalized storage coefficient (2-44) is invoked. For instance (2-50) becomes

$$F\,\partial\psi/\partial t = \nabla(K_\psi\nabla\psi + D_T\nabla T - Ki) \qquad (2\text{-}54)$$

The above relationship constitutes the general, non-isothermal transient flow equation for both saturated and unsaturated porous media.

2.7 Heat Transport

The heat flux q_h through porous media may be expressed as follows:

$$q_h = q_{cd} + q_{\ell h} + q_{sv} + q_{s\ell} \qquad (2\text{-}55)$$

where

$$q_{cd} = -\lambda^*\nabla T \qquad (2\text{-}55a)$$

$$q_{\ell h} = L'(T_o)\,q_v \qquad (2\text{-}55b)$$

$$q_{sv} = c_v(T-T_o)\,q_v \qquad (2\text{-}55c)$$

$$q_{s\ell} = c_\ell(T-T_o)\,q_\ell \qquad (2\text{-}55d)$$

q_{cd} is the conductive (Fourier) heat flux; λ^* is the thermal conductivity of the porous medium (cal/cm/sec/C) in the hypothetical case where no liquid or vapor movement occurs;

$q_{\ell h}$ is the latent heat flux by vapor movement; $L'(T_o)$ is the latent heat of vaporization of water at the arbitrary reference temperature T_o;

q_{sv} and $q_{s\ell}$ are convective sensible heat fluxes transported by the moving vapor and liquid respectively; c_v and

c_ℓ are the specific heats of water vapor (at constant pressure) and liquid water, respectively.

The separation of q_h into these component parts is discussed by de Vries (1958), who recognized the approximate character of (2-55). The approximate nature of that relationship stems from the fact that while all processes of heat transfer were assumed to take place uniformly throughout the porous medium (notice the additive structure of 2-55), they in fact do not. Furthermore, it is assumed that heat transfer by air convection and radiation is negligible, which is usually the case (de Vries, 1958).

Identifying the heat of vaporization per unit mass at temperature T by

$$L'(T) = L'(T_o) + c_v (T-T_o) - c_\ell (T-T_o) \qquad (2\text{-}56)$$

in (2-55), the following relation is obtained:

$$q_h = -\lambda^* \nabla T + L'(T)\, q_v + c_\ell\, q_w (T-T_o) \qquad (2\text{-}57)$$

or, by replacing the water vapor flux q_v above by (2-19), one obtains

$$q_h = -\lambda \nabla T - \rho L'(T)\, K_{\psi v} \nabla \psi + c_\ell\, q_w \Delta T \qquad (2\text{-}58)$$

where

$$\lambda = \lambda^* + \rho L'(T)\, D_{Tv} \qquad (2\text{-}59)$$

λ is the thermal conductivity of a porous medium including the effect of heat transfer by vapor movement under the influence of temperature gradients. Experimentally, it is this quantity which is measured and not λ^* because when a temperature

gradient is imposed across a porous medium, fluid motion will certainly occur;

ΔT is the difference in temperature between the cross-sections in question.

In terms of θ, (2-59) becomes

$$q_h = -\lambda \nabla T - \rho L'(T)\, D_{\theta v} \nabla \theta + c_\ell q_w \Delta T \qquad (2\text{-}60)$$

At saturation, the second term of the right-hand side of (2-58) and (2-60) becomes zero, so that the saturated heat flux equation becomes

$$q_h = -\lambda \nabla T + c_\ell q_w \Delta T \qquad (2\text{-}61)$$

In order to derive the transient heat flow equation, the principle of heat conservation is used in a manner similar to the one used in deriving the water flow equations. The equation for the conservation of heat, in the absence of sources or sinks, may be expressed as

$$\partial H/\partial t = -\nabla q_h \qquad (2\text{-}62)$$

where H is the total heat content of a unit volume of moist porous medium (cal/cm^3). The total heat content term may be broken down into the following constituents:

$$H = H_d + H_{\ell v} + H_v + H_\ell + H_w \qquad (2\text{-}63)$$

where

$$H_d = c_d (T - T_o) \qquad (2\text{-}63a)$$

$$H_{\ell v} = L'(T_o)\, \rho \theta_v \qquad (2\text{-}63b)$$

$$H_v = c_v \rho \theta_v (T - T_o) \qquad (2\text{-}63c)$$

$$H_\ell = c_\ell \rho \theta_\ell (T - T_o) \qquad (2\text{-}63d)$$

$$H_w = -\rho \int_o^{\theta} W \, d\theta \qquad (2\text{-}63e)$$

$$W = (RT/Jh)\,\partial h/\partial T \qquad (2\text{-}63f)$$

H_d is the heat content of the dry porous medium; $H_{\ell v}$ the latent heat of the vapor; H_v and H_ℓ the heat contents of vapor and liquid water, respectively; and H_w is the heat of wetting. (2-63f)-- representing the differential heat of wetting W -- is obtained according to thermodynamic theory (Edlefsen and Anderson, 1943); J in that equation is the mechanical equivalent of heat. By grouping the heat capacity terms from (2-63a, c and d), the following total heat capacity of a moist porous medium may be defined

$$C = c_d + c_v \rho \theta_v + c_\ell \rho \theta_\ell \qquad (2\text{-}64)$$

Combining (2-55) and (2-63) in the heat conservation equation (2-62) and making use of definitions (2-56) and (2-64), one obtains

$$C\,\partial T/\partial t + L'(T)\,(\rho\,\partial\theta_w/\partial t + \nabla q_v) - \rho W\,\partial\theta_\ell/\partial t = \nabla(\lambda^*\nabla T) - c_v q_v \nabla T - c_\ell q_\ell \nabla T \qquad (2\text{-}65)$$

where the continuity equation, as indicated by the first two terms of (2-50) is used as well. By combining the last two terms of the right-hand side of (2-65), the following general transient heat flow equation is obtained

$$C\,\partial T/\partial t + L'(T)\,(\rho\,\partial\theta_w/\partial t + \nabla q_v) - \rho W\,\partial\theta_\ell/\partial t = \nabla(\lambda^*\nabla T) - c_\ell q_w \nabla T \qquad (2\text{-}66)$$

The term $\rho W\,\partial\theta_\ell/\partial t$ representing the heat content change due to liberation of the heat of wetting is a small quantity, especially for porous media with a small clay fraction and, therefore, can be neglected. The $\partial\theta_v/\partial t$ term may also be neglected due to its negligibly small magnitude. Finally

replacing q_v in the above equation by (2-19), one obtains the reduced transient heat flow equation

$$C\,\partial T/\partial t = \nabla(\lambda\nabla T) + \rho L'(T)\,\nabla(K_{\psi_v}\nabla\psi) - c_\ell\, q_w \nabla T \qquad (2\text{-}67)$$

At saturation, the second term of the right-hand side of the above equation becomes zero and (2-67) reduces to

$$C\,\partial T/\partial t = \nabla(\lambda\nabla T) - c_\ell\, q_w \nabla T \qquad (2\text{-}68)$$

Table 2-1 summarizes the final forms of the developed equations and transport coefficients.

The derived flow equations (2-54) and (2-67) form a system of coupled partial differential equations which, in principle, may be solved in order to predict the evolution of a given flow system subject to appropriate boundary and initial conditions. However, the flow equations are non-linear; that is, the various transport parameters appearing in (2-54) and (2-67) are functions of the dependent variables ψ (or θ) and T; this fact makes the solution of the above equations very difficult. Chapter 4 contains a more complete elaboration of this problem and a discussion of methods that may be utilized to solve the flow equations.

2.8 Proposed Field-oriented Methodology for Transport Coefficients

As mentioned in Chapter 1, the coupled non-isothermal flow equations have not been adequately tested by application to field problems. Accordingly, field data --

TABLE 2-1

Present Model

(2-19)	q_v/ρ	$= -K_{\psi v} \nabla\psi - D_{Tv} \nabla T$	vapor	Flux Equations
(2-32)	q_l/ρ	$= -K_{\psi l} \nabla\psi - D_{Tl} \nabla T + Ki$	liquid	
(2-38)	q_w/ρ	$= -K_{\psi} \nabla\psi - D_T \nabla T + Ki$	water	
(2-58)	q_h	$= -\lambda \nabla T - \rho L' K_{\psi v} \nabla\psi + c_l q_w \Delta T$	heat	
(2-54)	$F\, \partial\psi/\partial t$	$= \nabla(K_{\psi} \nabla\psi) + \nabla(D_T \nabla T) - \partial K/\partial z$	water	Transient Flow Equations
(2-67)	$C\, \partial T/\partial t$	$= \nabla(\lambda \nabla T) + \rho L' \nabla(K_{\psi v} \nabla\psi) - c_l q_w \nabla T$	heat	
(2-17)	$K_{\psi v}$	$= f D_a \nu (Mg/RT)^2 p_v^s h$		
(2-32b)	$K_{\psi l}$	$= K$		
(2-18)	D_{Tv}	$= \zeta f D \nu (Mg/RT) h\, dp_v^s/dT$		Transport Coefficients
(2-37)	D_{Tl}	$= K (R/Mg) \ln h$		
(2-39)	K_{ψ}	$= K_{\psi v} + K_{\psi l}$		
(2-40)	D_T	$= D_{Tv} + D_{Tl}$		
(2-44)	F	$= \partial\theta/\partial\psi + (\theta/\phi) S_s$	generalized storage coefficient	

necessary to develop relevant models -- are extremely scarce. One of the major difficulties in applications of such models to field situations is the calculation of transport coefficients because they constitute difficult-to-measure physical properties of the porous and fluid media. In this section I will develop simplified procedures for estimating the transport parameters for a unified unsaturated-saturated profile without sacrificing accuracy in relation to the analytical relations of Table 2-1. Next, the heat and water transport equations will be considered in one-dimensional form. Formulations based on both pressure head ψ and water content θ as the dependent variables will be put forward.

By introducing a new quantity D^* defined as

$$D^* = D_{\theta v} / D_{Tv} \tag{2-69}$$

and substituting from Table 1-1 the analytical expressions for D_{Tv} and $D_{\theta v}$, the following expression results:

$$D^* = (p_v^s \, \partial h/\partial\theta) / (\zeta h \, dp_v^s/dT) \tag{2-70}$$

The advantages of using the above expression over the expressions for the transport coefficients $D_{\theta v}$ and D_{Tv} are clearly evident. Simply stated, using the D^* definition, one avoids the following terms common in the analytical formulas of $D_{\theta v}$ and D_{Tv} : f (or $f(a)$ and ξ if Rose's 1968a, b formulation is used), D_a, ν , Mg/RT , thus eliminating the uncertainties associated with their direct calculation. With the exception of ζ , which may be approximated from

literature data or simply as indicated in Chapter 4 (p. 141), the evaluation of D^* may not be difficult in the field, provided that the soil psychrometers used for measuring soil relative humidity (h) function properly.

I suggest further that the measurement of heat flux, thermal conductivity and water flux can be achieved under field conditions as described in Chapter 3, together with moisture, temperature and pressure potential measurements. Thus, after measuring the above quantities appearing in (2-60), the only unknown remaining in the equation is the coefficient $D_{\theta v}$, which may be calculated as

$$D_{\theta v} = [\ -q_h - \lambda(\partial T/\partial z) + c_\ell q_w \Delta T\ ] / [\rho L'\ \partial\theta/\partial z\ ] \qquad (2\text{-}71)$$

$K_{\psi v}$ can be obtained by multiplying $D_{\theta v}$ by the specific water capacity C_w (2-47). Having thus estimated D^* and $D_{\theta v}$, it is obvious that D_{Tv} can be estimated from the definition of D^* (2-69).

In view of the uncertainties regarding the Philip and de Vries' (1957) surface tension model for $D_{T\ell}$, I propose an alternative formulation (2-37). The unsaturated hydraulic conductivity may be calculated from the non-isothermal expression of the water flux, once the latter is known for each layer in the profile.

As for the saturated region, the water flux may be calculated from the heat flux equation (2-61) as follows:

$$q_\ell = [\ q_h + \lambda \partial T/\partial z\ ] / (c_\ell \Delta T) \qquad (2\text{-}72)$$

Once the saturated water flux is known, the liquid thermal

diffusivity $D_{T\ell}$ may be calculated from the non-isothermal liquid flux equation (2-32) as

$$D_{T\ell} = (-K\,\partial\psi/\partial z - q_\ell/\rho + Ki)/(\partial T/\partial z) \qquad (2\text{-}73)$$

where the saturated K may be measured by piezometric methods (Chapter 3).

This proposed methodology may be used to establish and solve non-isothermal equations for field systems. Although a discussion on the accuracy and limitations of this approach is presented later (Chapter 3), it is important to remember that this methodology depends mainly on the accuracy of tne estimation of the water fluxes and, particularly, of the heat fluxes.

CHAPTER 3

FIELD AND LABORATORY STUDIES

3.1 Introduction

A general lack of adequate data on the simultaneous heat and water transfer in porous media has severely limited field testing of the non-isothermal theories and modeling of coupled systems. For this reason, the significance of thermally induced flow, especially under field conditions, has not yet been definitely assessed. At the time I designed the set of field experiments for this study in early 1974, there were no comprehensive field experiments on non-isothermal flow reported in the literature. Only a few aspects of the problem had been considered. Rose (1968a, b) worked with non-isothermal water flux only; whereas, Wierenga and de Wit (1970) worked with the heat flux only. In recent years, there has been evidence of a more complete treatment of the coupled aspects of the problem. Jackson et al. (1974, 1975) investigated heat and water fluxes under field conditions. However, their work concentrated only on the top 10 cm of the soil, and several relevant quantities in the non-isothermal flow equations were not directly measured in their experiments.

Thus, an important objective of this research was to design a field experiment to measure directly the relevant physical quantities that would enable me to implement the methodology for non-isothermal studies under field conditions that I proposed in Chapter 2 (Section 2.8). This program of field studies will be supported by appropriate laboratory studies.

3.2 Preliminary Considerations

A major problem with the field measurement approach was the selection of a suitable field site. At the outset, it appeared that the following criteria would have to be met:

1) surficial materials at the site should be of uniform texture with clay contents less than 20-25%;
2) the area should be characterized by a shallow water table;
3) the area should be easily accessible and close to the base station. It would be preferable to have a meteorological station located a reasonably short distance from the field site.

The reasons for establishing the first criterion are to avoid the complications that would arise from hydraulic and thermal heterogeneities, serious swelling and hysteretic effects which occur in clay-rich soils. The criterion of shallow water table is a practical one, designed to facilitate the installation of instrumentation and reduce

costs. Proximity to the base station will, in general, assist the field operation; while, the presence of a nearby meteorological station will provide the researcher with a suitable set of data readily available.

3.3 Location and Surficial Geology of the Study Area

A field site meeting most of the criteria mentioned above was selected near Taber, Alberta (Lsd.11-Sec.13-Twp.10- Rg.17-W4M), approximately 50 km east of the Canada Agriculture Lethbridge Research Station, Lethbridge, Alberta (Fig. 3-1). The study area is part of a large terrace above the escarpment of the Oldman River (Fig. 3-1) It is entirely underlain by glacial till. This unit ranges in thickness from several centimeters to more than nine meters. In the immediate vicinity of the study area, this till unit is found at a depth of approximately 5.5 meters. Two types of material overlie the till: (a) alluvial sand and gravel and (b) aeolian sand. In the study area, the deposits overlying the till consist of sandy material that is classified texturally as sandy loam to sand. Some discontinuous thin silt or clay loam lenses are interbedded with the sand.

The water table depth is variable, ranging from 2 to 3 meters below the surface of the study area. In general, the lack of potholes indicates good internal drainage.

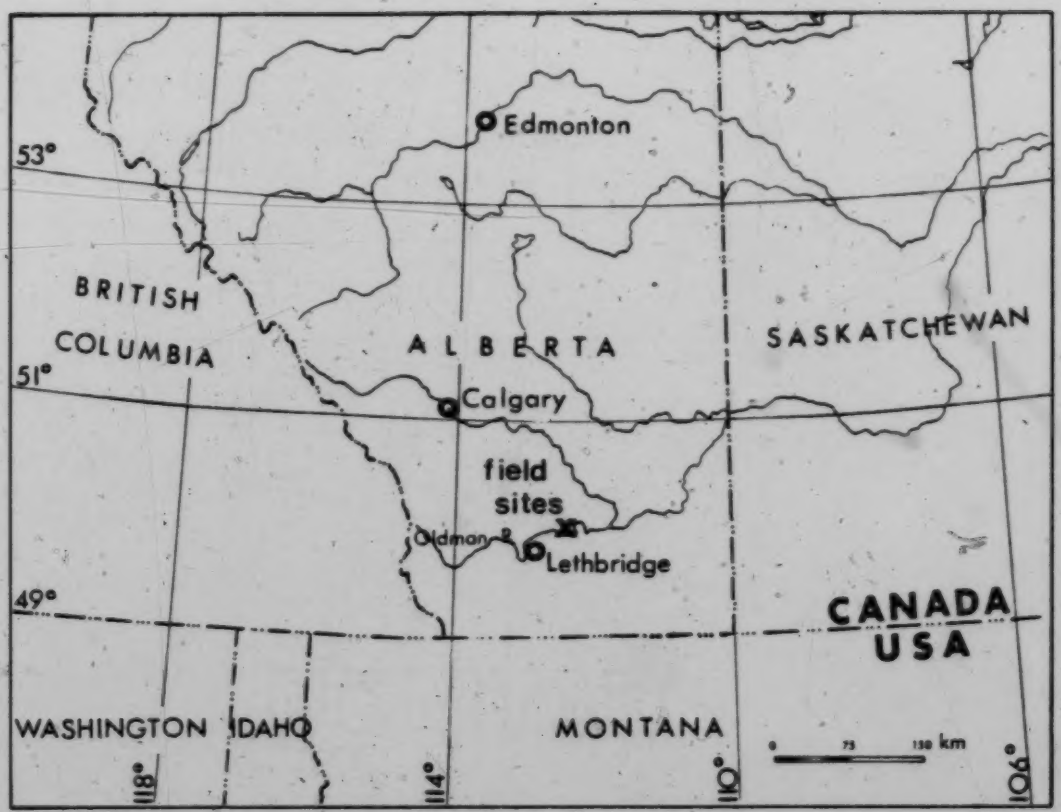

Figure 3-1. Location of study area

3.4 The Field Sites

Two sites, which were located approximately 150 meters apart, were selected for detailed study. An area approximately 9x9 meters square around each site was fenced to protect them from cattle grazing nearby.

None of the two sites was, however, entirely satisfactory. The extreme sandiness of one of the sites (Site 1) severely restricted the range of field-measured hydraulic head distribution and limited the effectiveness of laboratory support data on the range of water characteristic and hydraulic conductivity functions. The second site (Site 2), although having the more favorable sandy loam textures, was characterized by a relatively high degree of heterogeneity of the subsurface profile. In analysing the field data, however, more emphasis was placed on data from the second site.

3.5 Weather Observations

The Taber area is generally characterized by hot and dry summers and cold winters (Fig. 3-2). A small weather station is located approximately five kilometers from the field sites.

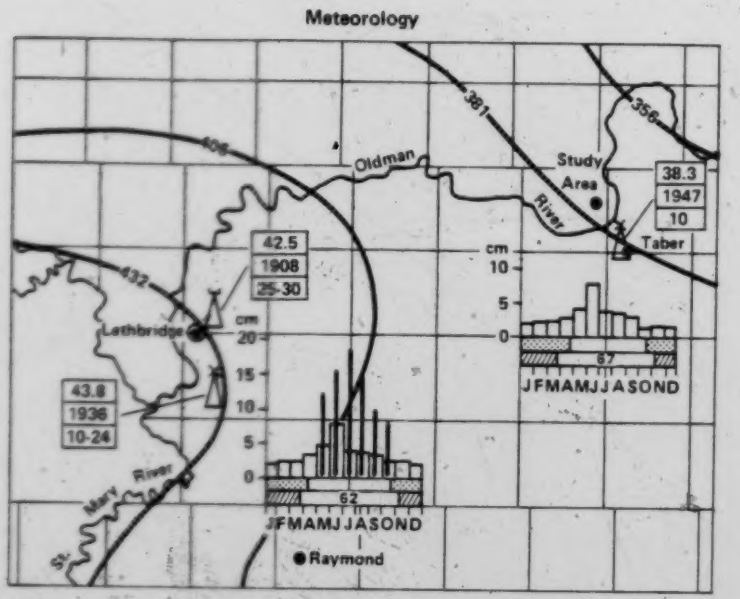

Legend

Isohyet, mean annual precipitation in cm 380

Meteorological station .....

Standard rain gauge only .....

Precipitation data:

Mean annual precipitation in cm 43.8

Year of commencement of observations 1936

Number of years of record averaged to determine the mean annual precipitation figure 10-24

Mean monthly potential evapotranspiration* .....

Mean monthly precipitation .....

Period when surface is usually snow covered .....

Period with mean daily temperature below freezing (0° C) .....

Figure indicates percentage of mean annual precipitation falling as rain

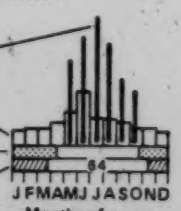

Sources of data:

Climatic Maps of Alberta (Longley, 1968); Monthly Record of Meteorological Observations (Meteorological Branch, Canada Department of Transport); and Provisional Evaporation Maps of Canada, Department of Transport Circular 4531 (Bruce and Weiseman, 1967).

*Evapotranspiration estimates are based on the Provisional Evaporation Maps of Canada.

(from: Tokarsky, 1974)

Figure 3-2. Meteorology of study area

3.6 Measurement of Basic Parameters and Equipment Required for the Present Study

In the following paragraphs, a brief description of the parameters required for coupled non-isothermal field studies will be presented ; for instance, types of materials, hydraulic potential, water content, water characteristic functions, hydraulic conductivity, density and porosity, temperature, thermal conductivity, heat capacity and water and heat fluxes. Also the equipment and methods of installation used to measure the above mentioned parameters will be briefly described.

Hydrometeorological equipment at the study area consisted of a hygrothermograph placed in an instrument shelter, a Gen atmometer and a standard rain gauge. This instrumentation was installed at Site 1. Each of the two sites was equipped with the instrumentation depicted diagrammatically in Fig. 3-3. Three piezometers were installed at Site 1 (1a, 1b and 1c) and two at Site 2 (2a and 2b) in June 1975. The rest of the instrumentation was installed during June 1976. All lead wires protruding from the ground surface were protected by passing them through rubber tubes, the outer ends of which were covered by plastic bags. For the collection of field data daily or weekly visits to the sites were made at irregular intervals during the summer-early fall 1976 measurement period, hereafter referred to as the 1976 measurement period.

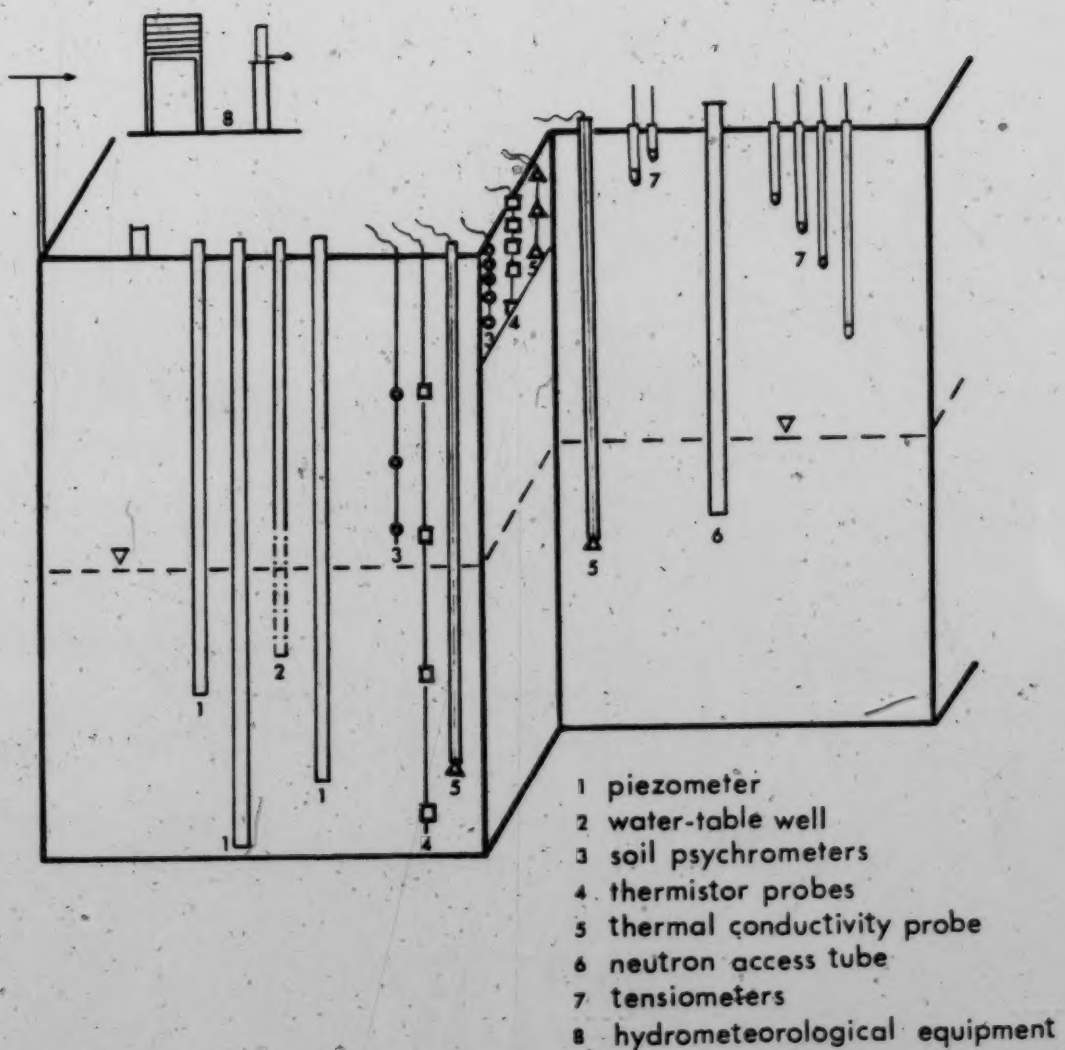

Figure 3-3. Site instrumentation diagram

3.6.1 Soil Types

Both sites were sampled during the summers of 1975 and 1976 using a Stirling auger drill and a hollow-stem auger. Depth intervals of approximately 30 cm -- with a finer spacing for the upper layers of the profile -- were sampled down to 485 cm depth. Soil texture was determined in the laboratory using the hydrometer method (Day, 1965).

3.6.2 Hydraulic Potential

3.6.2.1 Piezometers

Piezometers were installed in order to measure saturated hydraulic potentials at the sites. They were constructed from 3.8 cm I. D. PVC pipe. The lower 30 cm of each pipe were hacksaw slotted and wrapped with fiberglass tape to form an intake, and the lower end of the pipe was capped. The piezometers were emplaced by lowering them inside of the 15 cm hollow-stem auger after the center-bit was removed. A mixture of sand from the hole and pea gravel was poured around the outside of the PVC pipe to cover the slotted interval. The hole was then filled with the excavated material and the surface around the protruding end of the pipe was sealed with bentonite. The upper end of the piezometer was capped using a PVC fitting with a small hole drilled in it for pressure equalization.

Two piezometers (1d and 2d) were neither slotted nor

capped at the lower end but a stainless steel screen of approximately 1 mm mesh was attached to the lower end of the tube. The purpose of this type of instrumentation was to enable calculation of predominantly vertical hydraulic conductivities, as will be discussed later (Sections 3.6.5 and 3.7.6).

Piezometers were installed at the following approximate depths: 565 (1b), 435 (1d), 405 (1c) and 350 (1a) cm at Site 1 and 475 (2b), 440 (2d) and 390 (2a) cm at Site 2. After installation, the piezometers were developed by repeated bailing.

3.6.2.2 Tensiometers

Although the pressure potential or head is positive compared to atmospheric pressure under saturated conditions, it is negative under unsaturated conditions. This negative pressure head is due to capillary and adsorptive forces which attract and bind water in the soil and thus lower its potential energy below that of bulk water (Hillel, 1971). Tensiometers (Richards, 1949, 1965; Klute and Gardner, 1962) are used to measure negative pressure head up to approximately -0.8 bar, which is the air-entry or bubbling pressure of the tensiometer porous cup.

All tensiometers were tested in the laboratory prior to installation in the field and the porous cup conductance and response time constant for most of them were determined

according to the procedures outlined in Danielson (1956). The average response time constant was approximately 2 minutes. Scales directly reading in cm H_2O were attached to each mercury manometer tensiometer and adjusted for the zero reading.

For field installation, a hole was made in the soil to the appropriate depth using an approximately 2.5 cm I. D. King tube. Before inserting the tensiometer, a handful of loose soil from the hole and a small amount of water was poured into the hole to insure water continuity betwen the tensiometer cup and the soil. The tensiometer was inserted into the hole with a twisting downward motion and the soil surface around the tensiometer was sealed with a small amount of bentonite. Tensiometers were installed in duplicate at both sites to depths of approximately 30, 60, 90, 120 and 180 cm in a semicircle around the neutron access tube (Section 3.6.3). After installation, all tensiometers in each nest were filled with deaerated distilled water and the mercury pot was filled.

In order to minimize the influence of temperature on the operation of the tensiometers, the first reading of the field instruments was taken as early in the morning as possible before the sun had warmed the tensiometers to a temperature different from that of the soil.

3.6.2.3 Soil Psychrometers

Because the upper limit of the tensiometer range is about -0.8 atmospheres, soil psychrometers are used to measure water potential at higher tensions or suctions. Soil psychrometers are thermocouple psychrometers which measure the relative vapor pressure or relative humidity of the water vapor in a system (Brown and van Haveren, 1972). Soil water potential may be inferred from measurements of relative humidity h using the thermodynamic relation (Rose, 1966)

$$\psi = (RT/Mg) \ln h \qquad (3\text{-}1)$$

Because the vapor pressure depends on both the matric (or negative pressure head) and osmotic components of the soil water potential, psychrometers measure both components while tensiometers only measure the matric component of soil water potential.

The psychrometers used for this study were of the Peltier type. They were constructed following procedures outlined in Wiebe et al. (1971) and Lopushinsky and Klock (1970), except that ready-made Chromel-Constantan (0.025 mm in diameter from Omega Engineering Inc.) thermocouple junctions were used. The thermocouple junction was protected by a cup-shaped ceramic bulb, constructed using methods described by Lopushinsky and Klock (1970). These ceramic bulbs were checked for their air-entry value by means of a hanging water column. The ceramic cup was considered

satisfactory if the air-entry value was in the range of at least 200 cm H_2O. Prior to the insertion of the porous cup, thermocouple junctions were cleaned carefully using an ultrasonic device. All soil psychrometers were calibrated under controlled temperature conditions with KCL salt solutions for which the vapor pressure was known. Fig. 3-4 shows two of the calibration curves obtained. A number of ready-made Wescor Inc. psychrometers were also used.

For field installation, a trench approximately 90 cm deep was dug at each site (Fig.3-3) and two or three soil psychrometers were emplaced in the side walls of the trench at chosen depths. The copper lead wires were laid horizontally in the trench for a short distance before being brought to the ground surface. At depths greater than 90 cm, the psychrometers were taped in pairs on a wooden dowel at the appropriate depths and the dowel was inserted in an augered hole. Psychrometers were installed at depths ranging from approximately 1 cm to 240 cm. The field recording apparatus consisted of a battery operated Keithley 150B microvolt ammeter, a milliamperemeter and an HP field chart recorder (Moseley 7100B).

3.6.3 Water Table and Water Content

Water table wells were constructed by slotting PVC pipe throughout most of its length, wrapping it with fiberglass and emplacing it in boreholes. The volumetric water content

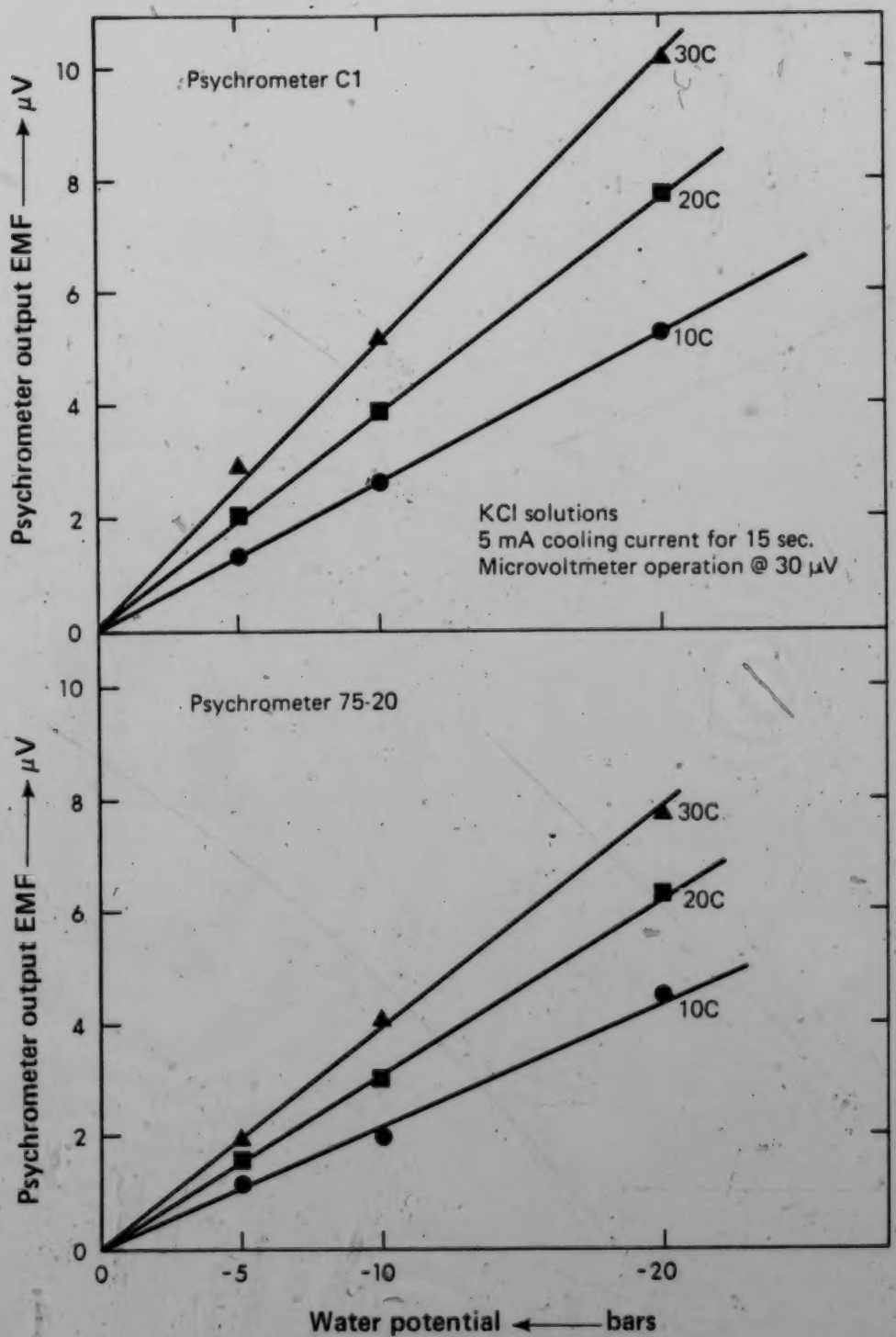

Figure 3-4. Psychrometer calibration curves

from a depth of approximately 20 cm below the ground surface down to the water table was measured using the neutron scattering method (Gardner, 1965; Long and French, 1967). At each site, an aluminum access tube, approximately 4 meters long, 4.0 cm I. D. and sealed at its bottom, was inserted in an augered hole. A Nuclear-Chicago model 5810 neutron depth probe in conjunction with a portable scaler model 5920 was used to take three one-minute counts for each 15 or 30 cm depth interval. Standard counts were taken before and after water content measurements. The ratio of the average count to the average standard count was used in a linear regression equation provided by the manufacturer to estimate the water content on a volumetric basis.

Prior to field use, the neutron probe was calibrated using a sand with a composition similar to that at the field sites. This sand was passed through a 2 mm sieve and was packed in layers to an average density of 1.5 gm/cm^3 in a 0.22 m^3 drum. By sampling the sand for moisture content using a small hand auger, and comparing the average water content of two samples for each depth with that obtained using the neutron probe, the calibration curve of Fig. 3-5 was obtained. The linear regression equation was used to obtain a best fit to the measured data.

3.6.4 Water Characteristic Curves

The relation between water content and pressure head

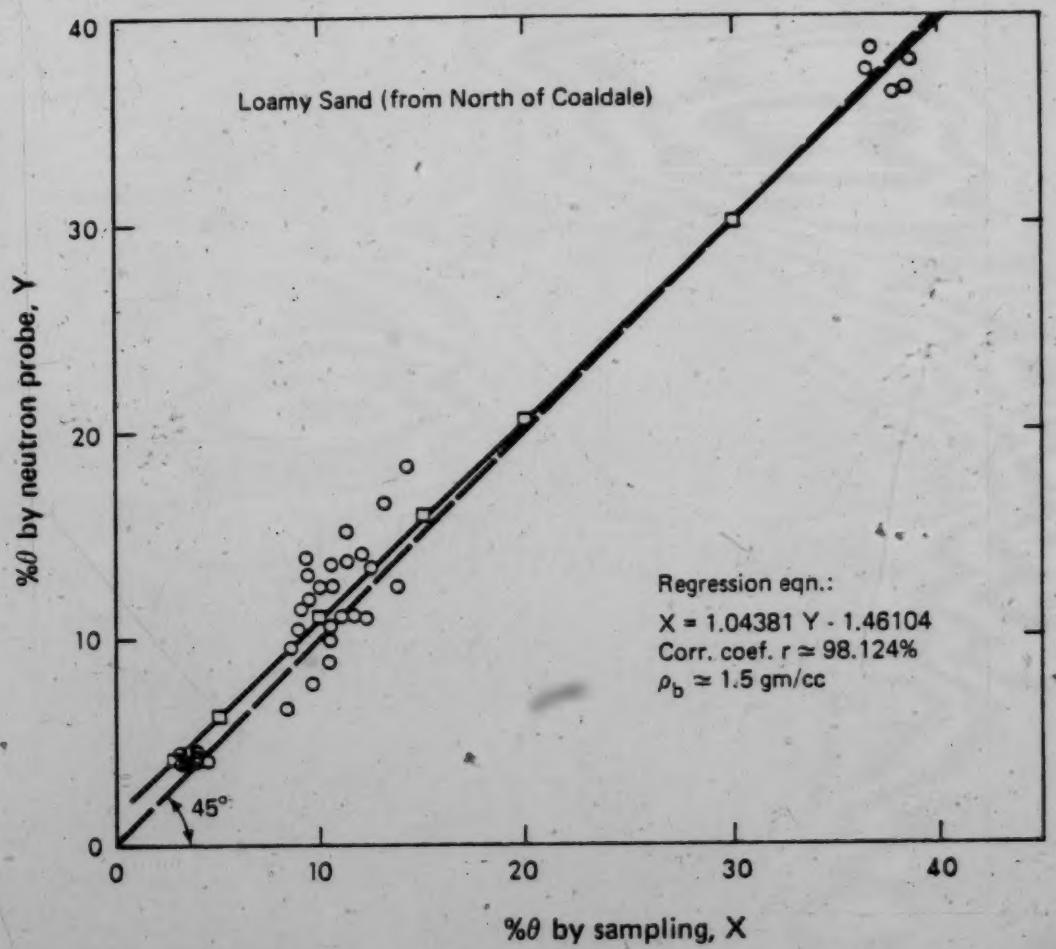

Figure 3-5. Neutron calibration curve

(water characteristic curve) at each site was obtained from simultaneous field measurements using the neutron probe and the tensiometers. However, due to the limited range of water contents and pressure heads observed during the measurement period, characteristic curves were determined in the laboratory in order to check the field results and to extend the range of measurements.

Four separate methods were utilized for testing the soil samples in the laboratory in order to obtain water characteristic curves over a sufficiently wide range of tensions. For tensions above 15 bars, vapor equilibration techniques involving saturated H_2SO_4 solutions were employed (Danielson, 1956). For measurements in the 1 to 15 bar tension range, a procedure described by Richards (1954, 1965) involving a pressure membrane apparatus was used. For the tension range of 100 to 1,000 mb, pressure cookers with ceramic porous plates were utilized (Richards, 1954, 1965). A saturation-capillary pressure (or pressure head) experiment (Laliberte et al., 1966) was employed to measure the water characteristic function for tensions less than 100 mb. Data from gravimetric moisture determinations were converted to volumetric moisture contents by multiplying by the bulk density of the soil samples.

3.6.5 Hydraulic Conductivity

3.6.5.1 Saturated Hydraulic Conductivity

The saturated hydraulic conductivity was measured in the field using the piezometer method (Kirkham, 1955; Hvorslev, 1951). When the inlet section of a piezometer is constructed by slotting the casing, hydraulic conductivity is measured essentially in a horizontal direction while with only the end of the casing available as an intake, hudraulic conductivity is determined in a predominantly vertical direction.

The hydraulic conductivity is determined by the use of the following formula based on Darcy's equation (Kirkham, 1945)

$$K = [\pi R^2 \ln(y_1/y_2)]/[S(t_2-t_1)] \qquad (3\text{-}2)$$

or, using Hvorslev's (1951) definition of basic time lag T',

$$K = \pi R^2/(ST') \qquad (3\text{-}3)$$

where R is the radius of the piezometer;

y_1 is the distance from the water table to the water level in the piezometer at time t_1;

y_2 is the distance from the water table to the water level in the piezometer at time t_2;

S is a shape factor with dimensions of length which depends on the geometry of the intake of the piezometer.

Values of the shape factor for different configurations of

the piezometer intake are given by Luthin and Kirkham (1949), Hvorslev (1951), Youngs (1968), among others. For the slotted piezometers used in this study, the shape factor is given as (Hvorslev, 1951)

$$S = 2\pi L/[\ln\{L/D + \sqrt{1+(L/D)^2}\}] \qquad (3\text{-}4)$$

(where L and D are the length and diameter of the piezometer intake respectively), or as a graph relating S/D vs L/D (Luthin and Kirkham, 1949; Al-Dhahir and Morgenstern, 1969), or as a table of values presented by Youngs (1968). For the open end piezometer, Hvoslev (1951) proposed

$$S = 2.75D \qquad (3\text{-}5a)$$

while Luthin and Kirkham (1949) suggested

$$S = 2.45D \qquad (3\text{-}5b)$$

The latter relation is preferred by Maasland (1957) because the first one (3-5a) is based on small tank experiments.

Saturated hydraulic conductivity of disturbed 1 mm sieve samples was also determined in the laboratory using the constant head method (Klute, 1965).

3.6.5.2 Unsaturated Hydraulic Conductivity

Unsaturated hydraulic conductivity over a range of water contents was determined in the laboratory using the methods of Brooks and Corey (1964) and Laliberte et al. (1966). It was shown (Brust et al., 1968; Klute, 1972) that these methods agree better with field measured conductivities than others.

Briefly, the determination procedure was as follows. An average characteristic (desaturation) curve (ψ vs S_w or θ) obtained from three soil samples was derived and the relationship between hydraulic conductivity and pressure head was determined. The methods and equipment employed were those described in Brooks and Corey (1964), Anat et al. (1965), Laliberte et al. (1966), van Schaik and Laliberte (1968) and van Schaik and Graham (1969). From the desaturation curve, the residual saturation S_r was determined by a trial and error procedure (Brooks and Corey, 1964). The effective saturation S_e, defined by Brooks and Corey (1964) as

$$S_e = (S_w - S_r)/(1-S_r) \qquad (3\text{-}6)$$

is linear for S_e less than approximately 0.8 when plotted versus on a log-log paper. The slope of this straight line portion is called the pore-size distribution index λ' (Brooks and Corey, 1964). The intercept of the straight line at $S_e=1.0$ is called the bubbling or air entry pressure ψ_b, which corresponds very closely to the minimum pressure head at which air begins to enter a saturated porous medium and the gas phase first becomes continuous. The relative hydraulic conductivity K_r ($=K/K_{sat}$) may then be calculated as

$$K_r = S_e^{(2+3\lambda')/\lambda'} \qquad (3\text{-}7)$$

or

$$K_r = (\psi_b/\psi)^{\eta} \qquad \text{for } \psi<\psi_b \qquad (3\text{-}8)$$

where $\eta = 2+3\lambda'$.

Accordingly, by combining the experimental desaturation data with the calculated value of residual saturation, the relationship between ψ and θ from saturation to residual saturation is obtained. When the experimentally determined K_r vs ψ relationship is plotted on a log-log paper, a straight line results for $\psi<\psi_b$, as is implied by (3-8) above. This line has a slope of $-\eta$ and intercepts the ψ-axis at the air-entry pressure ψ_b, where K_r =1.0. This straight line may be extrapolated to higher absolute values of ψ. Thus, by combining this K_r vs ψ relation with the ψ vs θ relationship for the same soil, the hydraulic conductivity as a function of water content from residual saturation to saturation is obtained.

The unsaturated hydraulic conductivity may also be determined in the field using a water balance equation as described by Rose et al. (1965) and others.

$$q_w/\rho = R + I - E - \int_0^z \partial\theta/\partial t \, dz \qquad (3-9)$$

where R is the rate of precipitation (actually "effective" precipitation);

I is the rate of irrigation application;

E is the evaporation rate.

Once the unsaturated water flux q_w/ρ is known (Section 3.6.10.2), the isothermal and non-isothermal expression for q_w/ρ (2-38) in one-dimensional form may be used to calculate K. Thus, using the non-isothermal water flux equation (2-38) in combination with (2-37), the unsaturated hydraulic conductivity may be calculated as

follows

$$|K| = \frac{q_w/\rho + K_{\psi_v}\,\partial\psi/\partial z + D_{T_v}\,\partial T/\partial z}{-\partial\psi/\partial z - (R/Mg)\,|\ln h|\,\partial T/\partial z + 1} \qquad (3\text{-}10)$$

or, using the much simpler isothermal water flux equation (2-22)

$$|K| = (q_w/\rho)/(-\partial\psi/\partial z) + 1) \qquad (3\text{-}11)$$

The procedures for calculating hydraulic conductivity proposed by Brooks and Corey (1964) using (3-7) or (3-8), or those developed by Childs and Collis-George (1950), Marshall (1958) and Millington and Quirk (1959, 1960) using the water characteristic function become field methods if the water characteristic is determined by field measurements. Although these methods may be adequate for wet soils which satisfy the capillary model of flow, they are not satisfactory for drier soils. In this case, adsorptive forces become dominant and the above capillary tension-based models may not be adequate (Gardner, 1974). These computational methods for obtaining the hydraulic conductivity function are most successful when applied to soils possessing a narrow range of pore size distributions (Nielsen et al., 1972). For well-aggregated soils, where considerable amounts of water are relatively immobile in intra-aggregate pores (residual saturation), better results are obtained if the water-filled pore space S_w is replaced by an effective water-filled pore space $(S_w - S_r)$, as was done in the method of Brooks and Corey (1964).

3.6.6 Density and Porosity

Bulk density was calculated from cores of known volume obtained in the field to depths of approximately 90 cm. Alternatively, a Cs-gamma density probe (Model P205) was also used to measure bulk densities at various depths.

Particle densities were determined using the pycnometer method (Blake, 1965). Once bulk and particle density is known, porosity ϕ can be determined from the following relationship:

$$\phi = 1 - (\rho_b / \rho_s) \qquad (3\text{-}12)$$

where ρ_b is bulk density and

ρ_s is particle density.

3.6.7 Temperature

Soil temperatures were measured in the field using general purpose rugged thermistor probes of the series 400 (Fisher Catalogue No. 15-176-22) in combination with a YSI Telethermometer model 42. All thermistor probes were calibrated in the laboratory with mercury thermometers. The average thermistor temperature deviated less than 0.11 C from the mercury thermometer temperature in the range of 0 to 30 C. For field installation, the same procedure as for the soil psychrometers was used. Thermistors were emplaced at depths of approximately 1, 2.5, 5, 10, 30, 60, 120, 250, 370 and 500 cm at both study sites.

Air temperatures were measured using a hygrothermograph which provided continuous temperature and air humidity recordings over weekly periods. The hygrothermograph, which was also checked for accuracy in the laboratory, was placed in an instrument shelter approximately 1.3 meters above the ground surface.

3.6.8 Thermal Conductivity

The thermal conductivity of the subsurface profile at the field sites was measured using thermal conductivity probes (Blackwell, 1954; Jaeger, 1956; Carslaw and Jaeger, 1959; de Vries and Peck, 1958a). The following formula is applied for such determinations

$$\lambda = [\, Q \ln(t_2/t_1) \,]/[\, 4\pi(T_2-T_1) \,] \qquad (3\text{-}13)$$

where λ is the thermal conductivity of the porous medium (cal/cm/sec/C);

$Q=I^2R'$ is the heat produced per unit time and unit length of the probe heating element; I is the current and R' is the resistance per centimeter of the heat source;

(T_2-T_1) is the temperature rise (or drop) during the time interval (t_2-t_1).

The thermal conductivity probes used for this study were similar to those described by Slusarchuk and Foulger

(1973).[1] The following modifications were employed. One bead thermistor (GB35L1-Fenwal Electronics, "Thermistor Manual") was potted in a hole in the wall of a 4.85 mm OD plastic tube. Teflon-coated constantan wire (of 0.127 mm diameter plus 3 mil teflon wall) was wound tightly in a bifilar manner around the plastic tube using a lathe to form a heating element approximately 33 cm long. The four lead wires (2 thermistor leads and 2 constantan leads) were connected to a four-wire coaxial cable. A stainless steel ring, 3.8 cm in diameter, with a groove near its perimeter and small protruding rods from two opposite sides, was attached near the top of the 8.0 mm O.D. stainless steel tube. A plastic cap was then glued into the groove of the ring to seal and protect the lead wire-coaxial cable junctions. An arch-shaped thin stainless steel rod was attached to the ring. A long steel wire was connected to the arch for recovery purposes (Fig. 3-6). The probes were checked for leaks by inserting them for several days in a long pipe filled with water.

In order to insert and recover the probes at depths below the water table, a device was designed (Fig. 3-7) to fit and lock on the two protruding rods of the ring mentioned above. This device was connected to steel rods

---

[1]Details on the operation and construction of thermal conductivity probes may also be found in Wechsler (1966); Janse and Borel (1965); Jackson and Taylor (1965); Beck et al. (1971), Fritton et al. (1974), among others.

Figure 3-6. Thermal conductivity probe

which fit together to facilitate installation in boreholes of any desired depth. Aluminum conduit tubes, approximately 5 cm in diameter, were inserted in drilled holes at depths of approximately 305 and 340 cm in Site 1, and 375 cm and 440 cm in Site 2. The conductivity probes were emplaced into the soil at the bottom of the conduit tubes by using the device described above. At shallower depths of approximately 6, 30 and 60 cm the probes were simply inserted horizontally into the walls of the trench dug at each site. In all cases, only the heating curve was considered. The duration of each experiment in the field was approximately 12 minutes.

Prior to field installation, the thermal conductivity probes were calibrated in the laboratory using air-dry and water-saturated 20/30 mesh Ottawa sand (ASTM designation C-190). A 12 V battery in combination with an EICO converter and a Lamda voltage regulator was used (Fig. 3-8) to provide a constant voltage source of 40 V in the field and laboratory experiments. A digital multimeter was used to monitor the change of the resistance of the heater element with time. A typical calibration curve is shown in Fig. 3-9, where the thermal conductivity of the dry Ottawa sand calculated at three different times is shown in order to indicate the variation of thermal conductivity measurements. (The thermistor resistance versus temperature curve was plotted using the manufacturer's data). A random check of the thermistor resistance and the temperature indicated by a mercury thermometer showed a satisfactory agreement with the

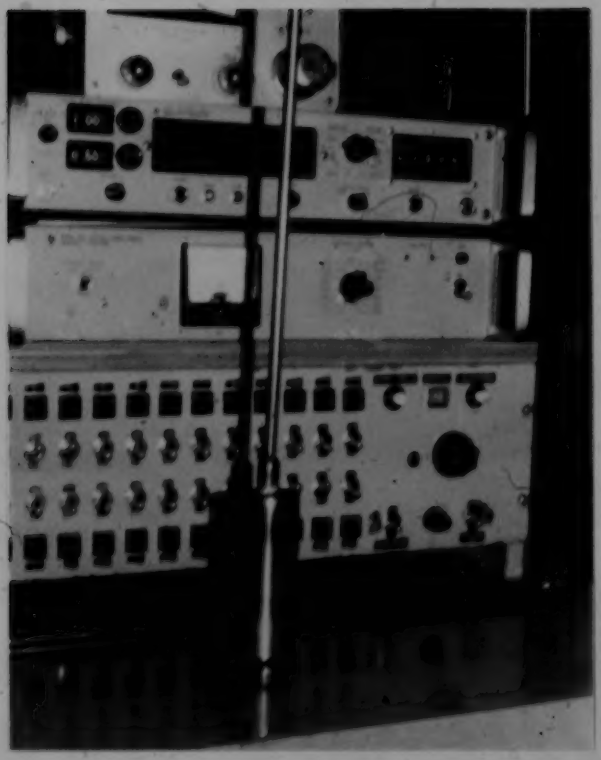

Figure 3-7. Thermal conductivity probe insertion and recovery apparatus

plotted curve. Comparison of the mean value of thermal conductivity for the coarse-grained dry Ottawa sand obtained from five probes (λ=7.214X10^{-4} cal/cm/sec/C) by Slusarchuk and Foulger (1973) as well as of their guarded hot plate value (7.262X10^{-4} cal/cm/sec/C) -- which was treated as their thermal conductivity standard -- with the mean value {(7.114±0.168)X10^{-4} cal/cm/sec/C} obtained from our ten probes under the same conditions, showed a satisfactory correspondence (Table 3-1). For calibration purposes, the ratios of our air-dry and saturated Ottawa sand thermal conductivities for each probe to those of Slusarchuk and Foulger (1973) using the guarded hot plate apparatus were joined by straight lines, assuming a linear relationship between thermal conductivity and water content. Therefore, at intermediate water contents between air dryness and saturation, the calculated thermal conductivity may be divided by the above mentioned ratio at the appropriate water content to give a standardized thermal conductivity value.

Several empirical (Kersten, 1949) and semi-empirical equations (de Vries, 1963) have been developed for calculating λ. However, as van Rooyen and Winterkorn (1957) indicated, none of those equations was able to give consistently dependable results. The thermal conductivity probe method avoids all problems involved with a theoretical calculation of thermal conductivity (Kimball et al., 1976, Hadas, 1977).

Figure 3-8. Field equipment for thermal conductivity measurements

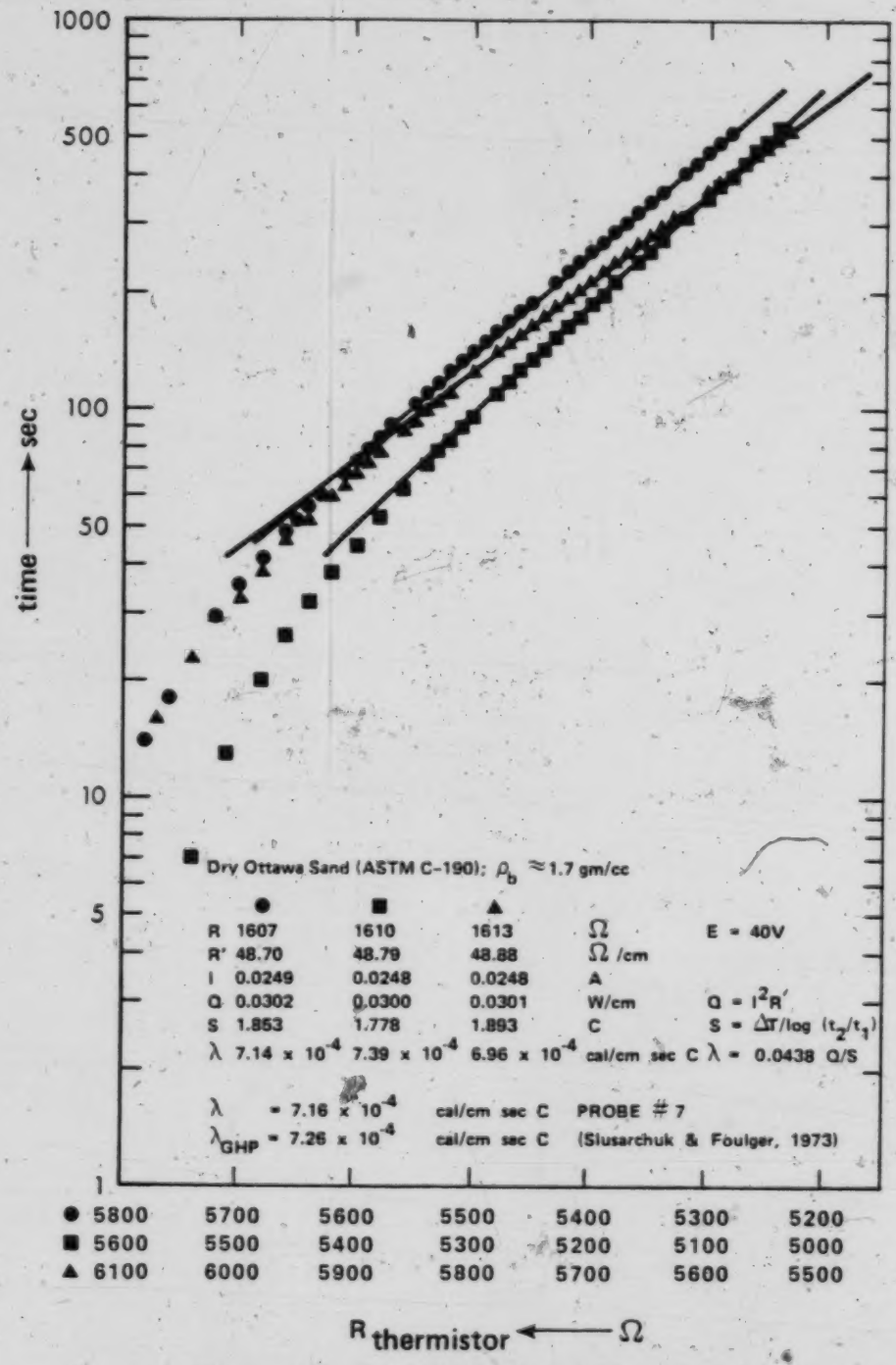

Figure 3-9. Typical calibration curves for thermal conductivity measurements

TABLE 3-1

Measured thermal conductivity of air-dry 20/30 mesh Ottawa sand

Probe	Thermal Conductivity* $\lambda \times 10^{-4}$ (cal/cm sec C)	Ratio of measured λ to the std value obtained using the GHP**
1	7.137	0.983
2	8.197	1.129
3	6.303	0.868
4	7.150	0.985
5	6.910	0.951
6	6.433	0.886
7	7.163	0.986
8	7.320	1.008
9	7.032	0.968
10	7.497	1.032
Mean λ	7.114×10^{-4}	
Standard error of mean, S_m***	1.679×10^{-5}	

*Each entry represents an average of 3 to 4 determinations.

**Guarded hot plate: $\lambda_{GHP} = 7.262 \times 10^{-4}$ cal/cm sec C (Slusarchuk and Foulger, 1973)

***$S_m = s/\sqrt{N}$, where s is the standard deviation.

3.6.9 Heat capacity

The volumetric heat capacity of a soil (de Vries, 1963) can be found by adding the heat capacities of the mineral matter (C_{mm}), the organic matter (C_o), the water (C_w) and the air constituents in a unit volume of porous medium. The heat capacity of air is very small and can be neglected. Thus, the volumetric heat capacity of a soil is given as

$$C = x_{mm}C_{mm} + x_oC_o + \theta C_w \qquad (3\text{-}14)$$

where C is the volumetric heat capacity (cal/cm³/C) of a moist porous medium and x_{mm}, x_o are the volumetric fractions of mineral matter and organic matter respectively, and θ is the volumetric water content. de Vries (1963) gives the following average values of heat capacities: C_{mm}=0.46 cal/cm³/C and C_o =0.60 cal/cm³/C . The volumetric heat capacity of water is unity. Therefore, the above equation becomes

$$C = 0.46x_{mm} + 0.60x_o + \theta \qquad (3\text{-}15)$$

for each volume increment of the subsurface profile. Notice that for non-deformable soils and for negligible heat of wetting (Stigter, 1969) the volumetric heat capacity is a linear function of the volumetric water content.

The organic matter content on a weight basis for each 30 cm depth increment (with a finer spacing in the first 30 cm) was determined in the laboratory using a variant of the Walkley and Black (1934) wet oxidation method (Piper, 1950; Richards, 1954).

In order to obtain the volumetric percentages of organic and mineral fractions of the various soil layers, an average organic matter density of 1.3 gm/cm³ (de Vries, 1963) was assumed. The average mineral particle density was found to be 2.64 gm/cm³ in the top 60 cm of the profile. This value was assigned to the entire subsurface profile. Using these density values together with the field-measured bulk densities, the organic and mineral matter fractions x_o and x_{mm} were calculated as follows:

$$x_o = \alpha' (\rho_b/\rho_s) \qquad (3\text{-}16)$$

$$x_{mm} = (1-\alpha') \rho_b/\rho_s \qquad (3\text{-}17)$$

where α' is the organic matter fraction by weight, measured experimentally. Values of x_o and x_{mm} at each depth in the profile remain constant for non-deformable media. However, because the volumetric water percentage θ varies in time, the volumetric heat capacity (3-14) varies as a function of time.

3.6.10 Heat and Water Fluxes

3.6.10.1 Heat Flux

The heat fluxes at different depths in the subsurface profile were computed by the temperature integral or calorimetric method (Portman, 1954; Lettau and Davidson, 1957; Tanner, 1963; Kimball and Jackson, 1975). In this method, the heat flux is calculated from the change of the heat content or storage in the subsurface profile over a

given time interval. The equation for the heat flux computation can be derived from the heat balance equation (2-62), which in one-dimensional form is

$$C\ \partial T/\partial t = -\partial q_h/\partial z \qquad (3\text{-}18)$$

Multiplying both sides of (3-18) by dz and integrating from depth z to depth z+dz results in

$$q_h|_z = q_h|_{z+dz} + \int_z^{z+dz} C\ \partial T/\partial t\ dz \qquad (3\text{-}19)$$

The term under the integral represents the change in heat content per unit time. Equation (3-19) is applied by dividing the subsurface profile into N layers of thickness Δz_i. Accordingly, it is possible to discretize (3-19) in the following manner:

$$q_h|_i = q_h|_{i+1} + C_i \Delta z_i \Delta T_i/\Delta t \qquad (3\text{-}20)$$

Due to the fact that the heat content of all soil layers (C_i) can be determined, the heat flux at any depth in the subsurface profile can be computed if the heat flux at any one particular depth can be estimated. Generally, this reference depth is taken to be at least 100 cm (Kimball and Jackson, 1975). In the present study, the reference depth has been chosen below the water table depth, where the heat flux can be calculated from the thermal conductivity and the temperature gradient with reasonable accuracy.

The heat flux meter approach (Lettau and Davidson, 1957; Philip, 1961; Fuchs and Tanner, 1968) might appear to be an attractive alternative to the above procedure, especially if the thermal conductivity of the meter and the porous medium are the same. Unfortunately this approach can

only determine heat flow by conduction because the meter is impervious to liquid and gas. Therefore, heat transfer by water liquid and vapor movement cannot be determined. The same limitation is apparent with the null-alignment method (Kimball and Jackson, 1975), where null points in the temperature gradient are used to provide zero heat fluxes at known depths in the profile.

3.6.10.2 Water Flux

The total water flux in the unsaturated zone can be measured in the same way as the heat flux; that is, by accounting for the change of water content in the subsurface profile over a given time interval. If a one-dimensional water balance is employed, the following difference equation is obtained in a manner analogous to (3-20):

$$q_w/\varrho|_i = q_w/\varrho|_{i+1} + \Delta z_i (\Delta\theta_i/\Delta t) \qquad (3\text{-}21)$$

Once the water flux at a particular depth is known, the water fluxes along the whole profile can be easily calculated using the above equation (Richards et al., 1956; Rose et al., 1965; Rose and Krishnan, 1967; van Bavel et al., 1968; Flocker et al., 1968; Hillel et al., 1972; Nielsen et al., 1973). However, a reference water flux at a certain depth may not be easy to determine. The major problem with this approach is that the hydraulic conductivity function must be determined. The procedure I have adopted is the following: (1) sample soil from any layer of the subsurface profile and determine the hydraulic

conductivity-water content function in the laboratory; (2) use the non-isothermal flux equation (2-38) in one-dimensional form to calculate the water flux at the bottom of this layer, the K function being known. Other relevant parameters, such as the depth distribution of hydraulic head, are already known.

The procedure followed by Nielsen et al., 1964, 1973; Davidson et al., 1969, among others -- which involves covering the ground surface with plastic sheets and assuming zero water flux (no evaporation) at the surface -- may not be appropriate under conditions not near saturation. Suppression of evaporation will increase the subsurface temperature regime and change the water vapor flux contribution to total water flow. The method used by Rose (1968c) for calculating bare soil evaporation by application of the principle of water conservation (3-9) in a volume of surface soil, in combination with the non-isothermal water flux equation (2-38) in one-dimensional form, may be preferable. Application at the field sites of the method proposed by Brutsaert (1975) for calculating evaporative fluxes based on non-dimensionless parameters (similarity concepts) resulted in unacceptably high evaporative fluxes. Therefore, this approach was not taken further. With regard to the saturated water flux, this may be calculated from the heat flux equation as suggested in (2-72). (An evaluation of such a method is presented in section 3.8).

The potential evaporative flux from a saturated surface was measured at the field sites using a Gen atmometer (Mukammal, 1961). This atmometer consists of a flat black porous plate (Bellani plate), 7.5 cm in diameter, kept moist by distilled water held in a tube which is connected to a supply reservoir.

3.7 Experimental Results and Discussion

3.7.1 Soil Types and Analyses

Site 1 is comprised of uniform medium sand (Figs. 3-10 and 3-11) of an average particle density of 2.6542 gm/cm^3. Underlying the sand is a clay loam till found at depths below approximately 5.5 m. However, an isolated clay loam lens was sampled at a 430-460 cm depth interval. The variation with depth of other physical properties of the Site 1 sand is indicated in Fig. 3-10. Although the textural profile is nearly uniform, the saturated hydraulic conductivity is variable (Fig. 3-10). This situation is probably due to differences in the compaction state of the porous material, as well as to experimental errors.

Site 2 has a more complicated geological setting than Site 1. The subsurface units are texturally variable both laterally and vertically, with sandy loam predominating (Fig. 3-11). Fig. 3-12 shows the variation with depth of soil textures, as well as other physical properties of a

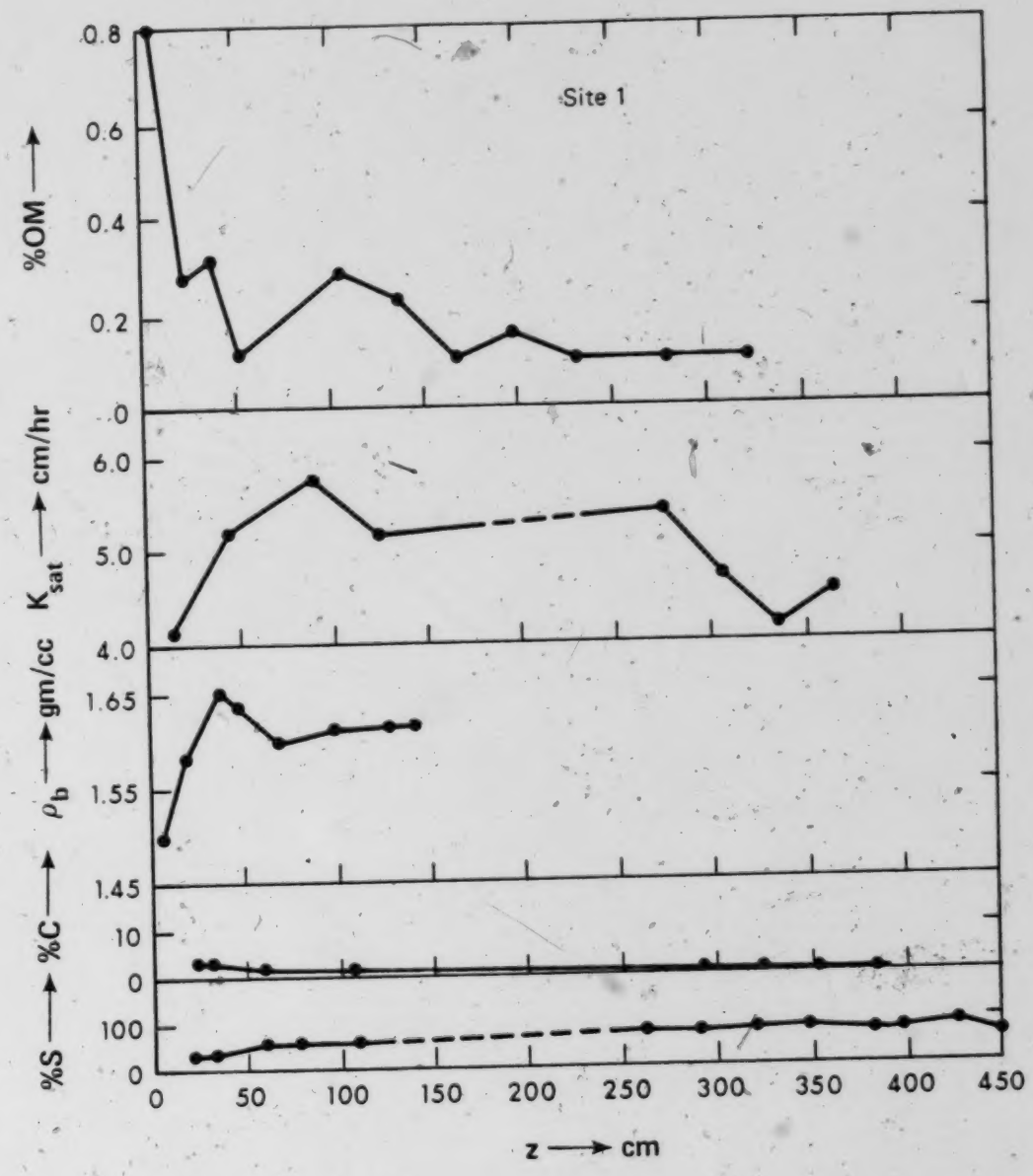

Figure 3-10. Physical properties of Site 1

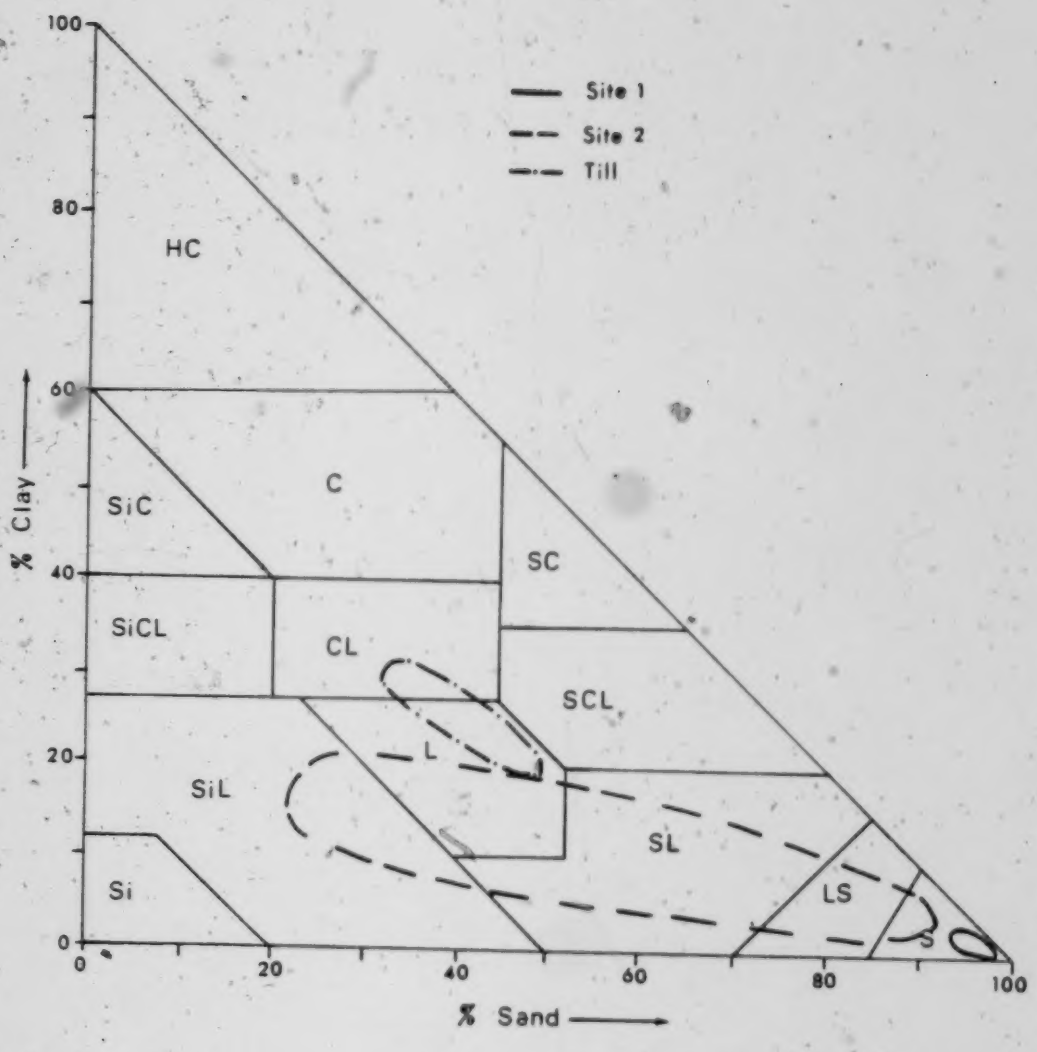

Figure 3-11. Soil texture triangle for the study area

sampled borehole at Site 2. A correlation between percentage of sand and saturated hydraulic conductivity is apparent (Fig. 3-12). The average particle density of the top 30 cm of the soil was 2.6281 gm/cm^3.

3.7.2 Hydraulic Head

The hydraulic head values at the Taber sites, determined from the piezometers, showed a relatively small fluctuation during the 1975-1976 measurement period (Fig. 3-13). Because of the relatively high hydraulic conductivity of the porous materials of the sites, the recovery rate of each piezometer after removal of water from them was relatively rapid, ranging from a few minutes to several hours depending on where the piezometer was terminated. Therefore, it was not necessary to correct head measurements for the effects of time-lag (Hvorslev, 1951; Freeze, 1969b).

The time distribution of hydraulic head as indicated by tensiometers and piezometers at Site 1, as well as the water table fluctuations during a nineteen-hour measurement period, are shown in Fig. 3-14. The advantage of such prolonged measurements is that the diurnal changes of several physical parameters can be studied in detail to assess their significance. From Fig. 3-14 it can be deduced that the direction of flow was generally downwards. However, the direction of flow was not always constant depending on whether water was infiltrating after a rainfall or was

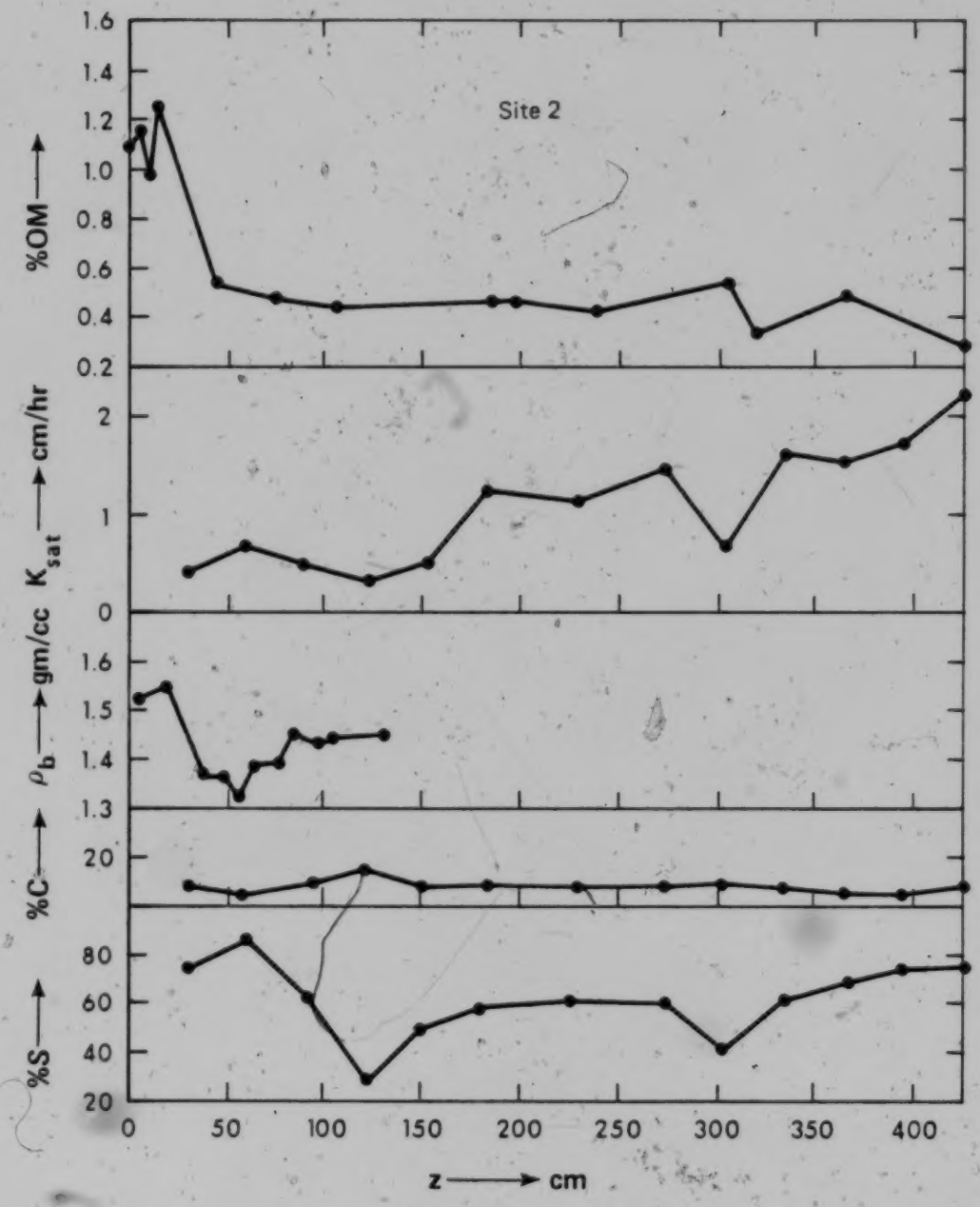

Figure 3-12. Physical properties of Site 2

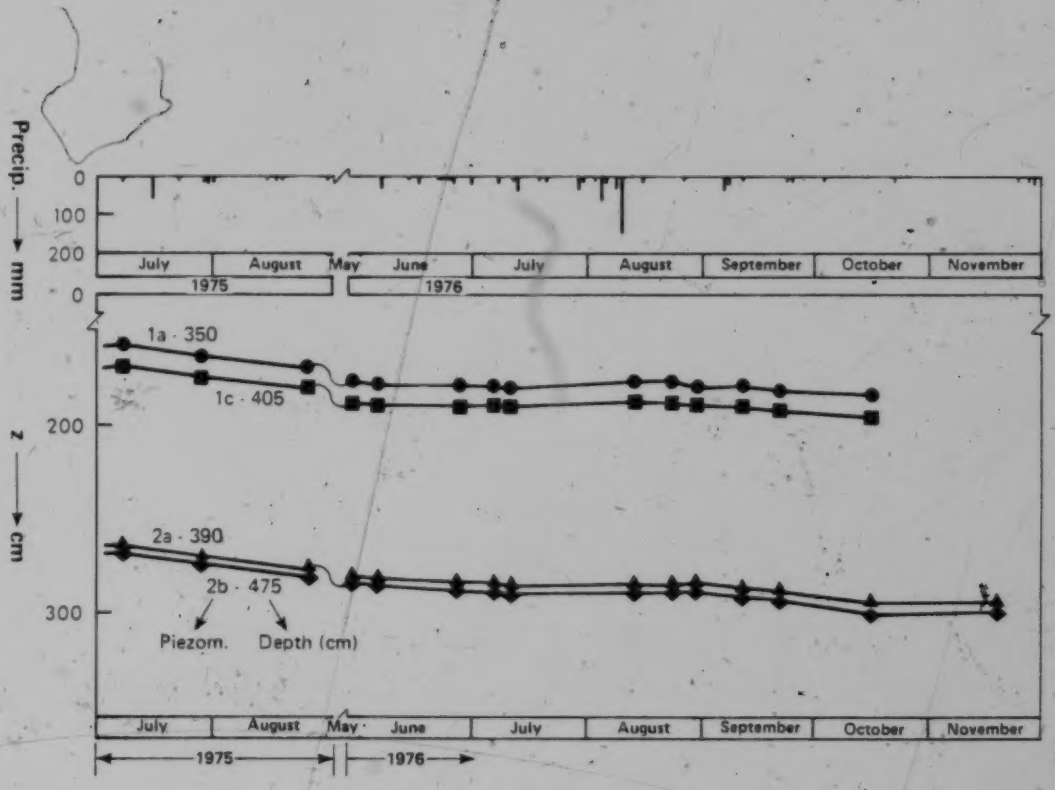

Figure 3-13. Time distribution of piezometric water levels

evaporating during an extended drying period. For example, the period of measurements depicted in Fig. 3-14 (August 11-12, 1976) followed a period of significant rainfall (Fig. 3-13) and water was still percolating downward. However, toward the end of the measurement period, the hydraulic head gradient between tensiometer 6 and piezometer 1a was reversed, indicating the completion of the percolation process and a return to evaporation-controlled upward flow. The piezometric head distribution indicated downward water flow at shallow depths superimposed on a deeper upward water flow condition (Fig. 3-14). This saturated flow pattern was consistent throughout the 1976 measurement period.

The hydraulic head distribution at Site 2 was more complicated and variable than at Site 1. The significant degree of heterogeneity of the subsurface profile of Site 2 contributed to this hydraulic head pattern. Fig. 3-15 presents a twenty-four-hour measurement of hydraulic head, where a reversal of hydraulic head gradient between tensiometers 4 and 6 is observed twice during that measurement period. However, the observed hydraulic head distribution in the saturated zone with an upward water flow pattern at shallow depths superimposed on a deeper downward water flow pattern was consistent throughout the 1976 measurement period.

Despite the care taken in constructing and calibrating the soil psychrometers, their performance in the field was

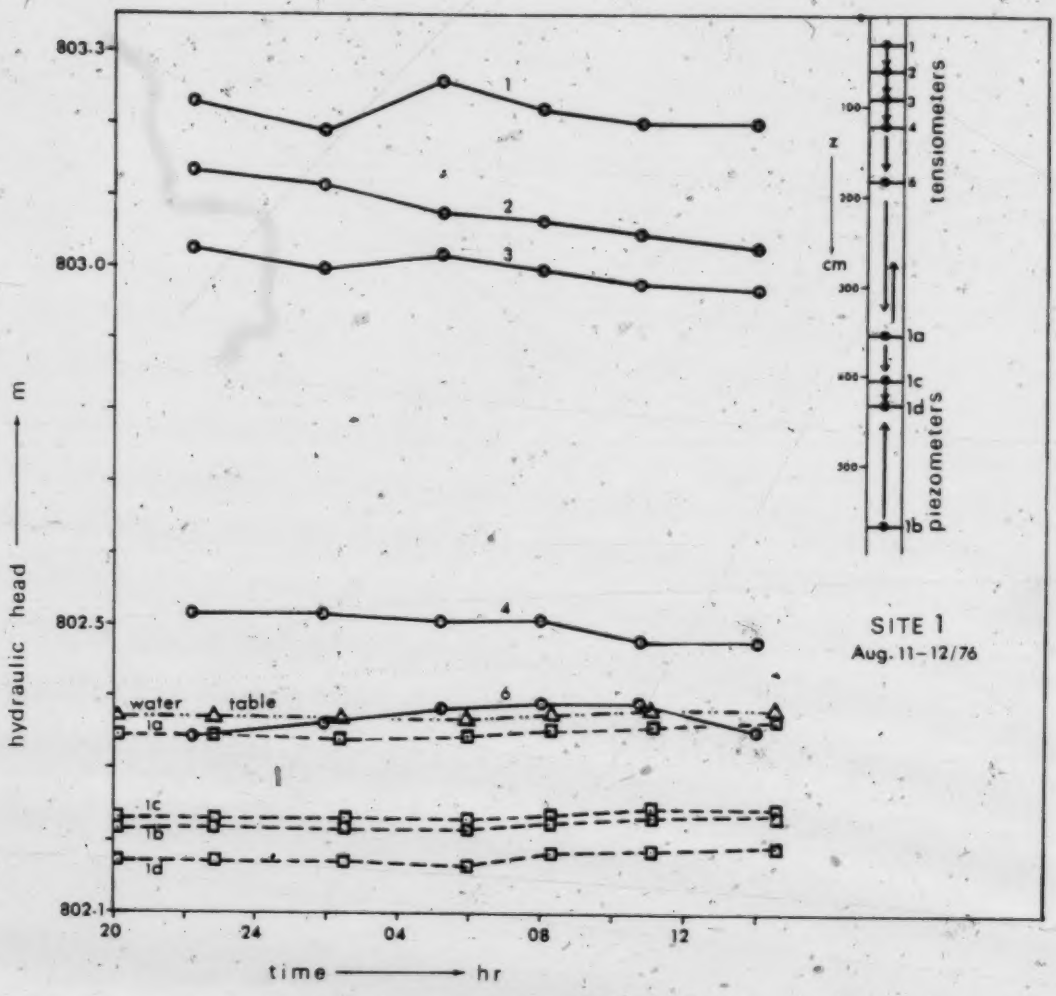

Figure 3-14. Time distribution of hydraulic head at Site 1

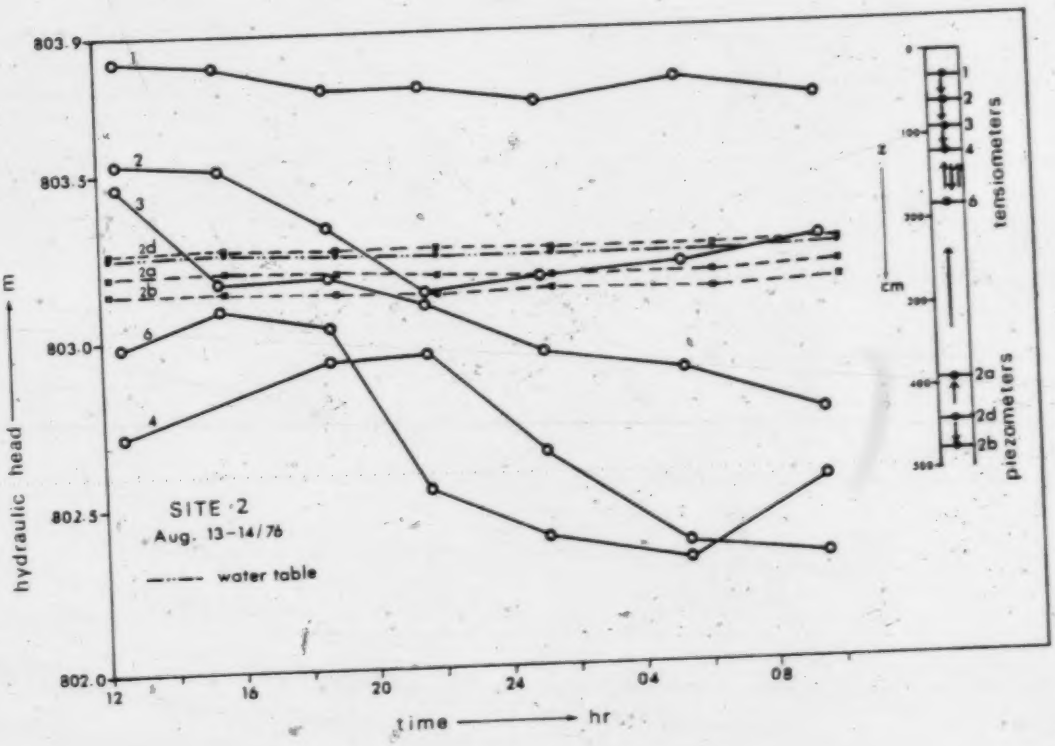

Figure 3-15. Time distribution of hydraulic head at Site 2

not satisfactory. Normally, soil psychrometers are most useful for dry soils with tensions above one atmosphere because of the higher resolution of the psychrometer output. However, after installation, an extended wet period followed with soil water tensions usually in the tensiometer range. This situation reduced the effectiveness of psychrometric measurements. Although occasional good psychrometer readings were obtained, they were not consistent. In addition, the calibration of the psychrometers left in the field probably changed with time as a result of corrosion of the psychrometer wire (Wiebe et al., 1971). It was considered impractical to remove and recalibrate the psychrometers during the course of the field measurement period. The procedure of encasing thermocouple psychrometers in perforated stainless steel tubes (Moore and Caldwell, 1972) would have facilitated removal, recalibration and reinsertion in the field.

3.7.3 Water Contents

A typical distribution of water contents at Site 1 -- obtained by using the neutron probe -- is shown in Fig. 3-16. Due to the very uniform grain size of the sand, the water content distribution indicated in that figure is a smooth curve. In contrast, the distribution of moisture with depth at Site 2 is complicated (Fig. 3-17). The presence of lower hydraulic conductivity layers, such as the silty loam (SiL) or loam (L) layer in between the predominantly sandy

loam (SL) layers, produces the observed moisture "bulges" just above those low conductivity layers. This water content distribution with depth was persistent throughout the 1976 measurement period.

3.7.4 Temperature and Potential Evaporation

The variation of soil temperature with time and depth at Site 2 for a diurnal period is shown in Fig. 3-18 together with the air temperatures at the site. A similar graph for Site 1 is shown in Appendix A. A dissipation of the amplitude of the temperature wave with depth is particularly evident. Assuming nearly harmonic temperature-time distribution, the damping depth D -- that is the depth at which the amplitude of a fluctuation is diminished by a factor of 1/e or 0.37 times the amplitude of the surface temperature -- is given by the formula (van Wijk and de Vries, 1963)

$$D = (2\lambda/C\omega)^{1/2} \qquad (3\text{-}22)$$

where ω is the radial frequency and equals 2π times the frequency of the temperature variation. Thus, for the diurnal variation, ω equals $2\pi/86{,}400$ or 7.27×10^{-5} sec^{-1}. Therefore, considering the near-average values indicated in Table 3-2, which represent the top 60 cm of the subsurface profile for the month of August 1976, the damping depths for the diurnal temperature variation for Sites 1 and 2 are 14.9 and 9.3 cm respectively. Correlated with a smaller damping depth is a more rapid decrease of the temperature amplitude

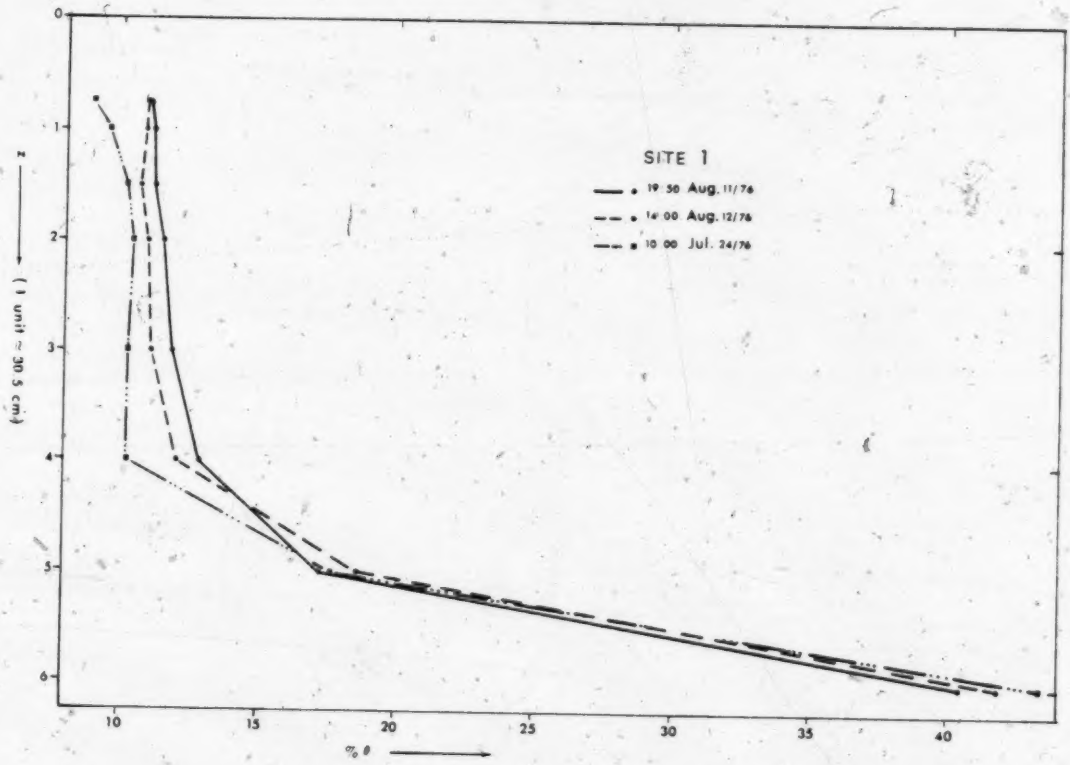

Figure 3-16. Time-depth distribution of water contents at Site 1

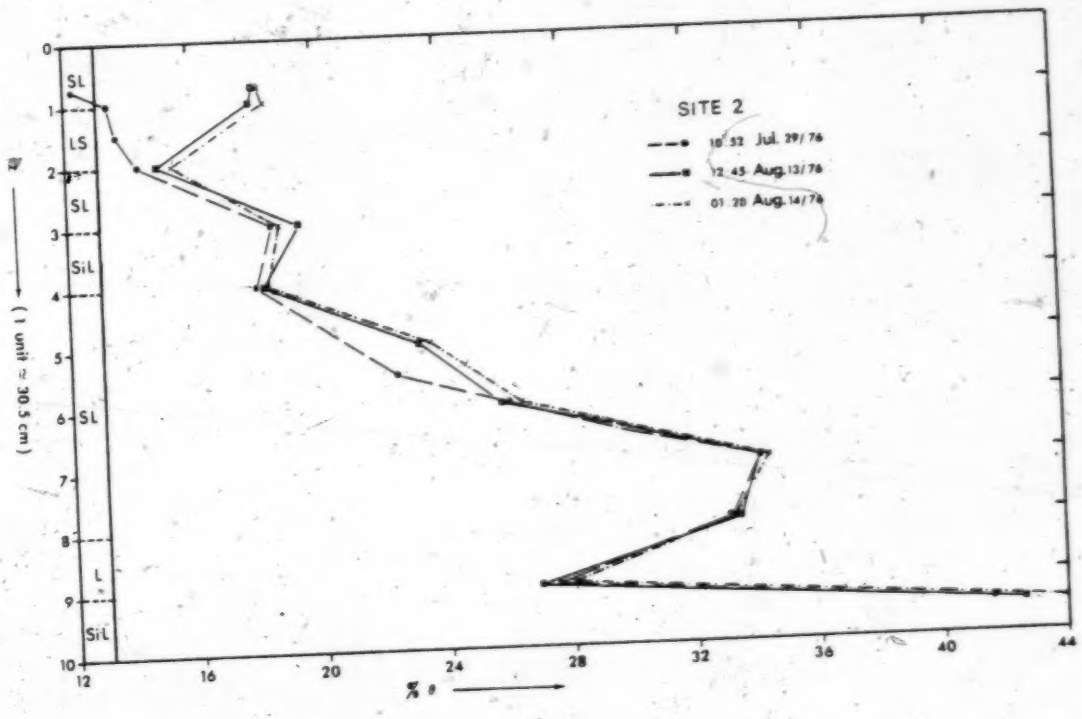

Figure 3-17. Time-depth distribution of water contents at Site 2

(Figs. 3-18 and A-1) as shown by van Wijk and de Vries (1963).

The cumulative potential evaporation as indicated by the Gen atmometer at the Taber sites during two diurnal periods in August 1976 are shown in Figs. A-2 and A-3 of Appendix A. The air temperatures and wind speeds -- as indicated by a portable anemometer -- are also shown on those figures. A correlation between air temperature and wind speed on the one hand and potential evaporation on the other are apparent from those figures.

3.7.5 Characteristic Curves

The water characteristic curve obtained from field measurements during the 1976 measurement period for Site 1 is shown in Fig. 3-19 together with laboratory-determined values. Despite the appreciable scatter of data, a satisfactory agreement between field and laboratory data is observed.

The field water characteristic relationship for Site 2 obtained during the same period indicated two distinct characteristic curves, one for the uppermost 45 cm and another for the 45 to 180 cm depth interval (Figs. 3-20 and 3-21). All field tensiometer data were carefully scrutinized to reject the data from tensiometers which had air-bubbles in the manometer tube, too much air in the tensiometer air trap, or had been serviced a short time before the

TABLE 3-2

Typical values of parameters required for the estimation of damping depths for the diurnal temperature variation at the sites

Site	θ	$\%x_o$	x_{mm}	C (CGS units)	λ
1	.16	.37	.601	.389	3.155×10^{-3}
2	.11	.86	.604	.443	1.385×10^{-3}

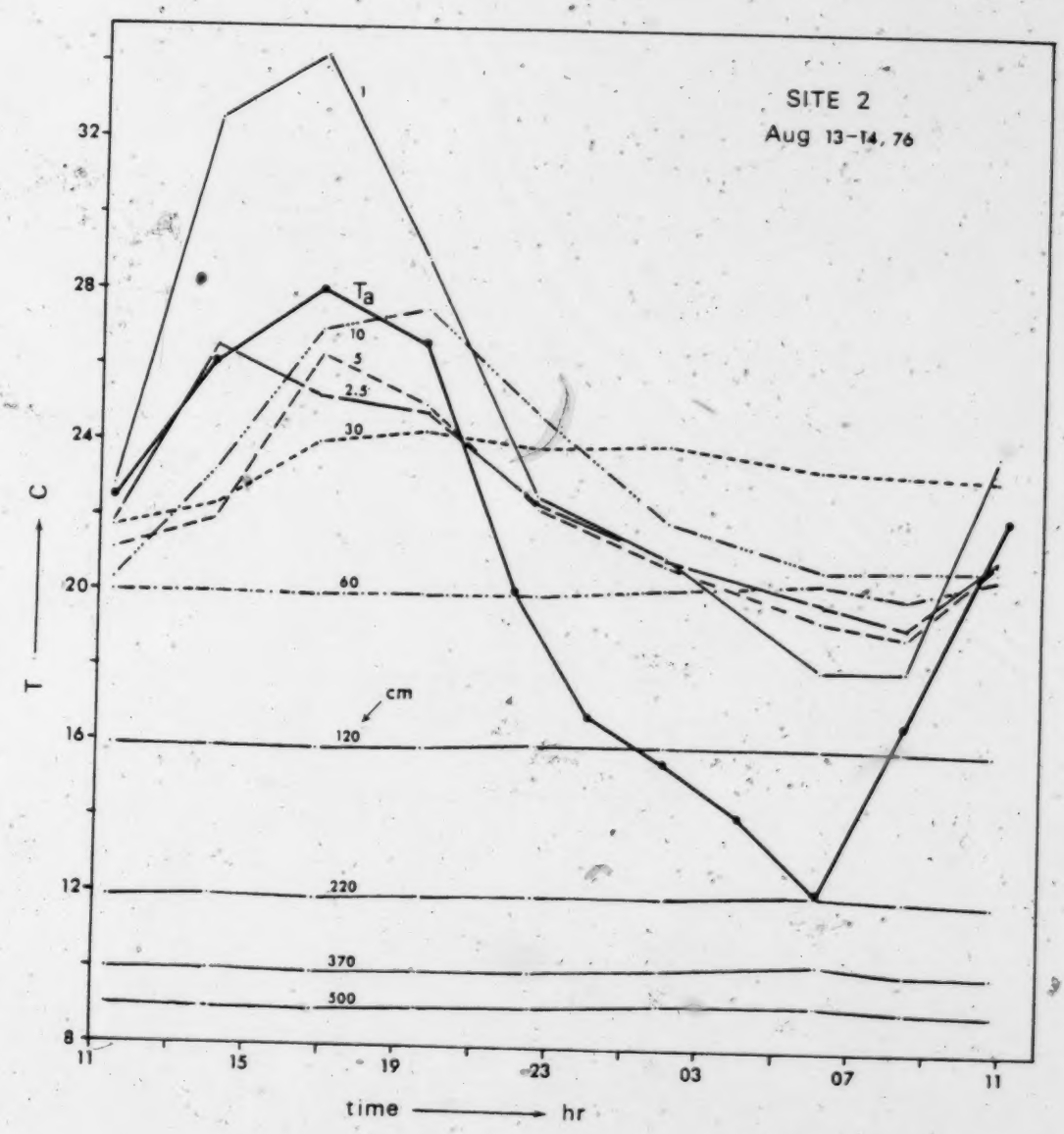

Figure 3-18. Time-depth distribution of temperature at Site 2

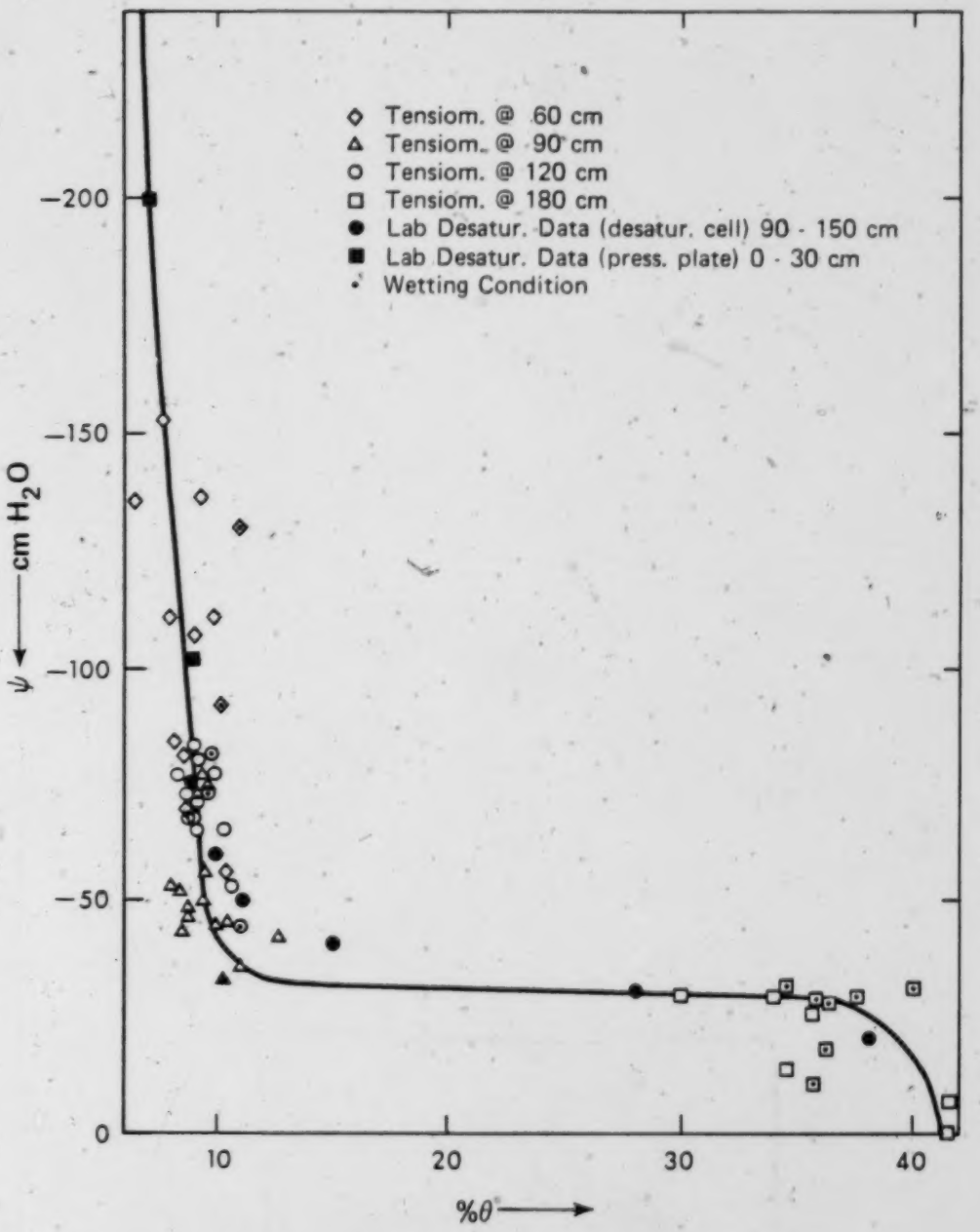

Figure 3-19. Water characteristic curve for Site 1

measurement. The data were classified in Figs. 3-20 and 3-21 according to whether the soil was wetting or drying during the period of measurement. The data scatter around the mean characteristic curve (Fig. 3-21) is approximately ± 1.5% volumetric moisture. This indicates that field hysteresis was probably not important. The overall composite characteristic curve for Site 2 obtained from vapor equilibration techniques, pressure membrane and pressure plate apparatuses, and desaturation cells is shown in Fig. 3-22 together with field-measured data. The reader should refer to Appendix B for further laboratory data and their comparison with field-observed water characteristic values.

The relation between pressure head and water content in unsaturated soils is not generally a unique and single-valued one. Here, a laboratory experiment was used to assess the major wetting and drying curves of the uppermost ~20 cm of the soil at Site 2. The results of this experiment are shown in Fig. 3-23. A significant degree of hysteresis, approximately twice that inferred for the top 180 cm of Site 2 (Fig. 3-21), was observed for that soil.

3.7.6 Hydraulic Conductivity

The saturated hydraulic conductivity K_{sat} of soils below the water table was calculated in the field using the Hvorslev (1951) method. Table 3-3 shows the results of these analyses which represent averages of approximately three

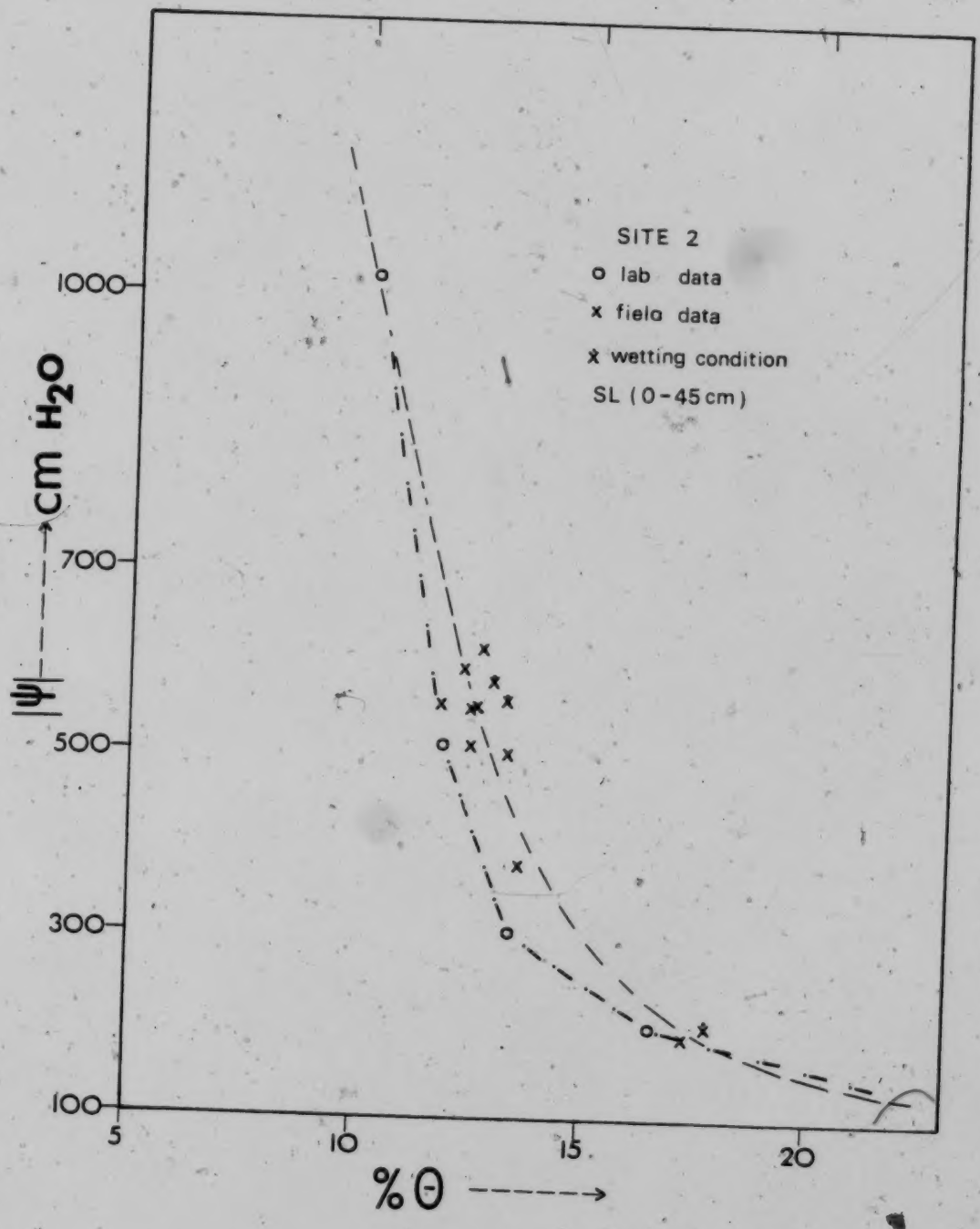

Figure 3-20. Water characteristic curve for Site 2 (0-45 cm)

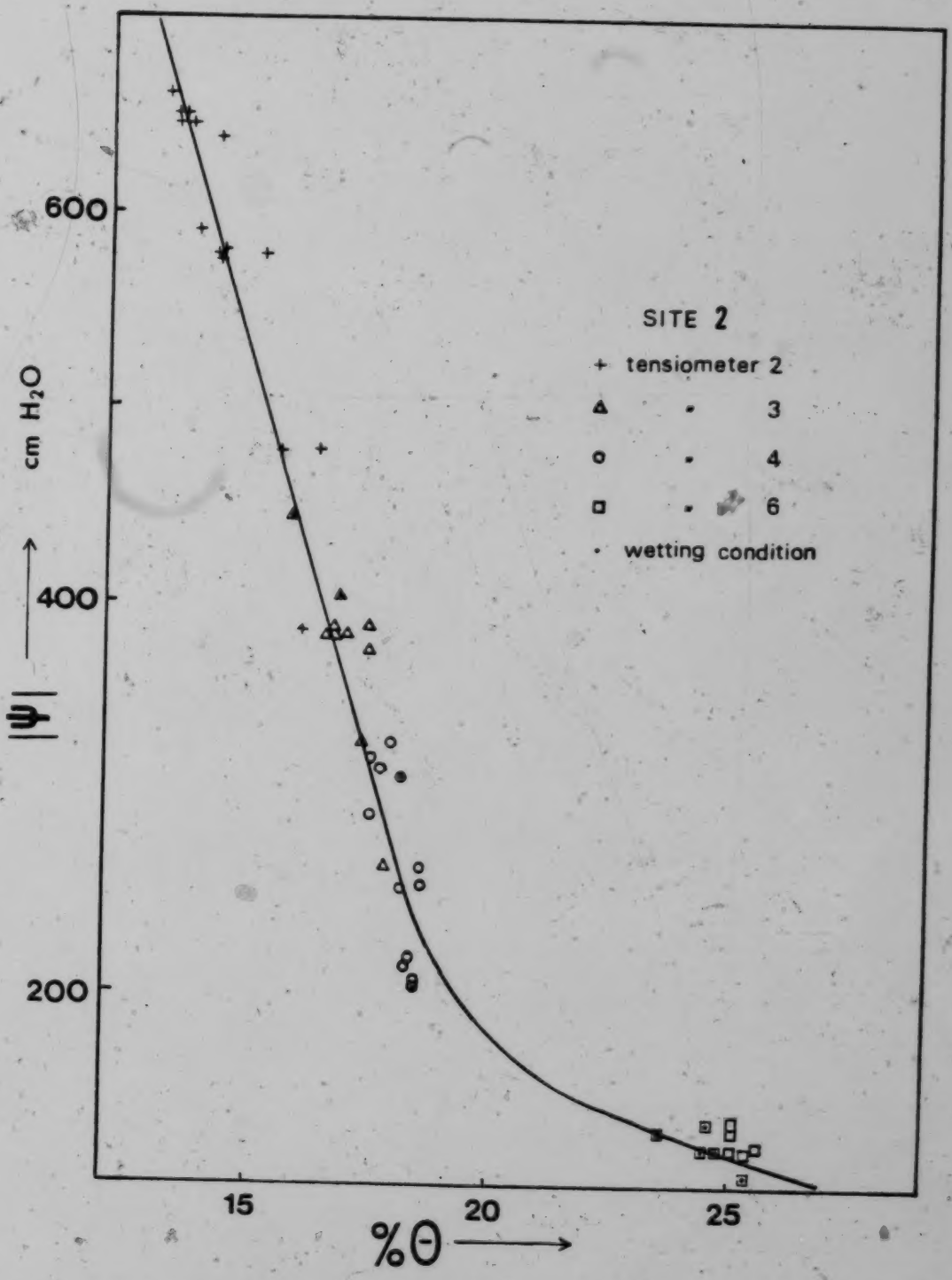

Figure 3-21. Field water characteristic curve for Site 2 (45-180 cm)

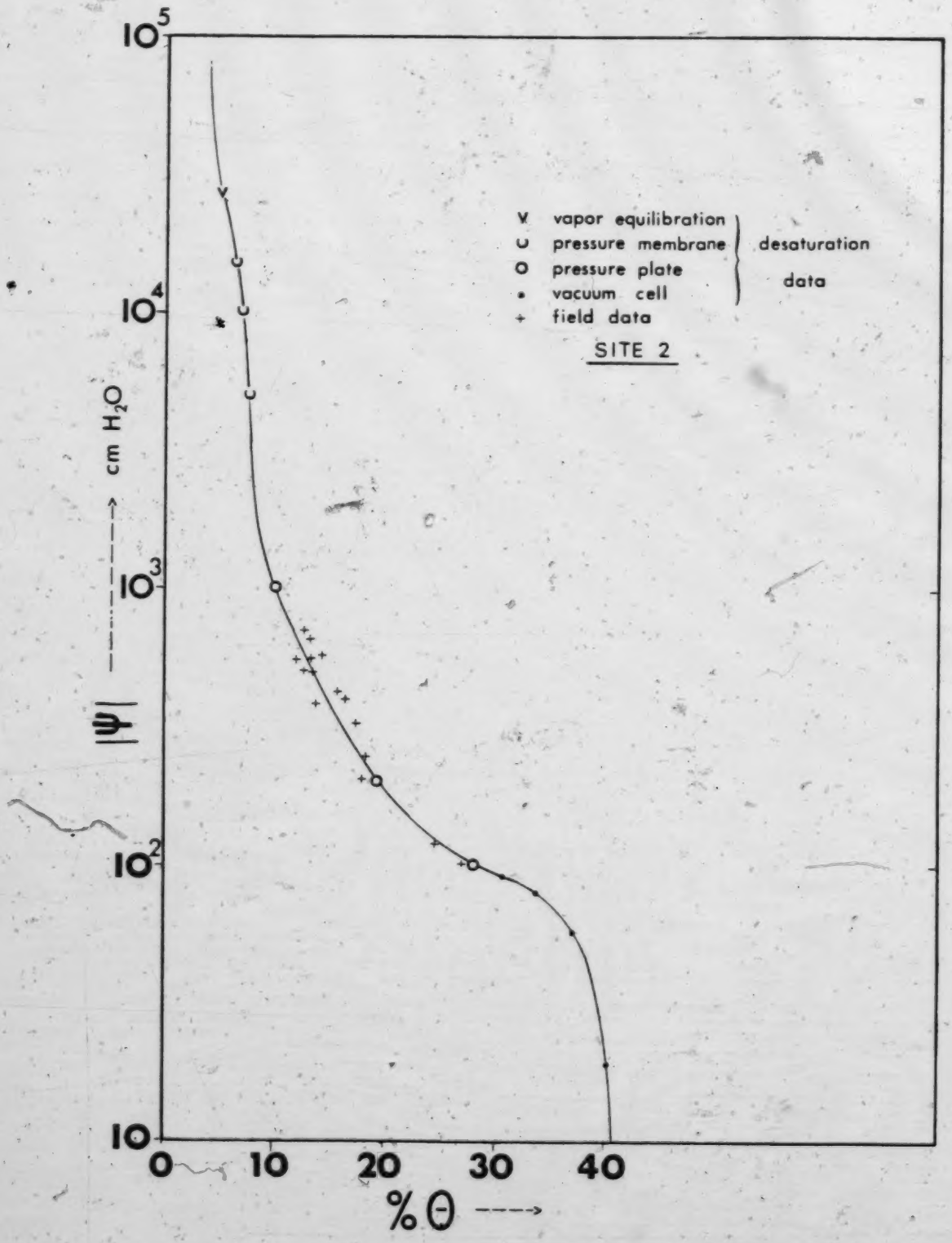

Figure 3-22. Overall characteristic curve for Site 2

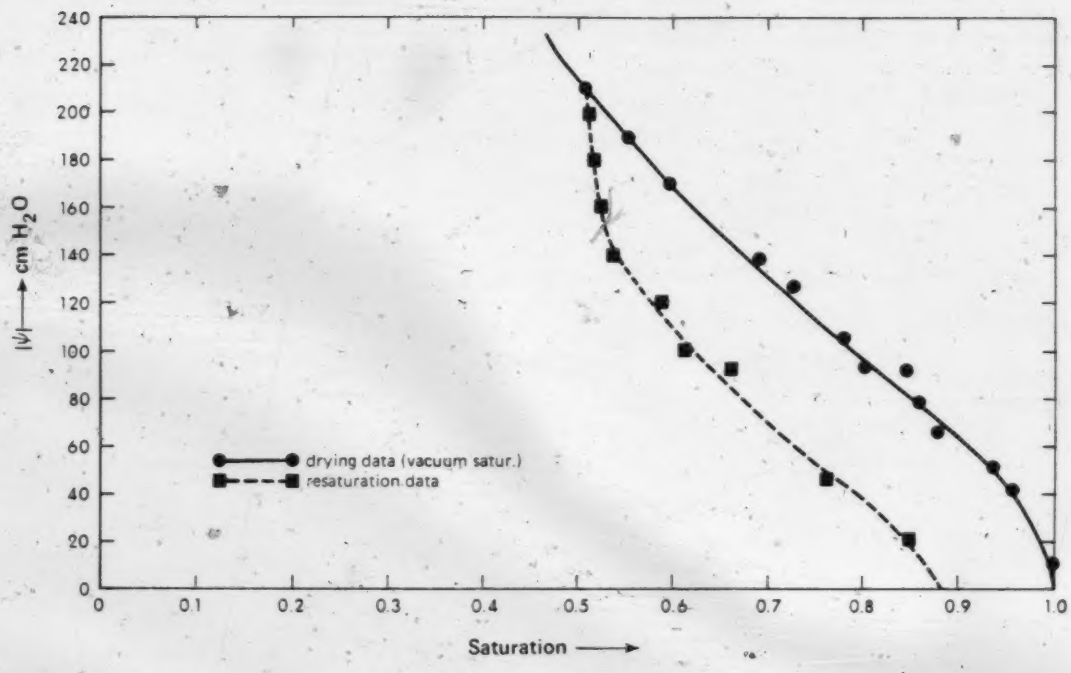

Figure 3-23. Hysteresis loop

tests together with K_{sat} values determined in the laboratory using the constant head method. In general, the agreement between field and laboratory values of hydraulic conductivity and their correlation with soil texture falls within the expected range of reliability for such measurements.

The results of the laboratory hydraulic conductivity measurements are presented in two sets of curves for each site. Each set consists of the following four relationships: (ψ vs S_w or θ), (S_e vs ψ), (K_r vs ψ) and (K vs θ). Only the $K_r(\psi)$ and $K(\theta)$ relationships for the top 20 cm of Site 2 are shown here (Figs. 3-24 and 3-25) as the latter is used as an input relationship in the simulation study to be presented in Chapter 4. (The rest of these relationships are shown in Appendix C). The laboratory hydraulic conductivity measurements are characterized by their limited range of water content or pressure head values over which the hydraulic conductivity can be determined. The extension of measured hydraulic conductivity values to lower water contents or higher absolute values of pressure head is of dubious validity, especially when the extrapolation is well beyond the measured data. Although the above mentioned method of hydraulic conductivity measurement provides a satisfactory tool for extending the hydraulic conductivity values through the linear portion of the $K_r(\psi)$ relationship, caution should always be exercised in interpreting and quantifying such extrapolated results.

TABLE 3-3

Saturated hydraulic conductivity analyses

Site and Piezometer	Depth (cm)	Apparent K, cm/sec Horizontal	Vertical	Lab K_{sat} (cm/sec)	Soil Texture
1a	350	1.1×10^{-4}		1.2×10^{-3}	S
1c	400	6.0×10^{-4}			L-CL
1d	430		9.7×10^{-4}		S
1b	565	1.4×10^{-6}			CL*
2a	390	3.5×10^{-4}		4.7×10^{-4}	LS
2d	440		2.4×10^{-4}	5.4×10^{-4}	SL
2b	475	2.9×10^{-5}			SL-L

*Till

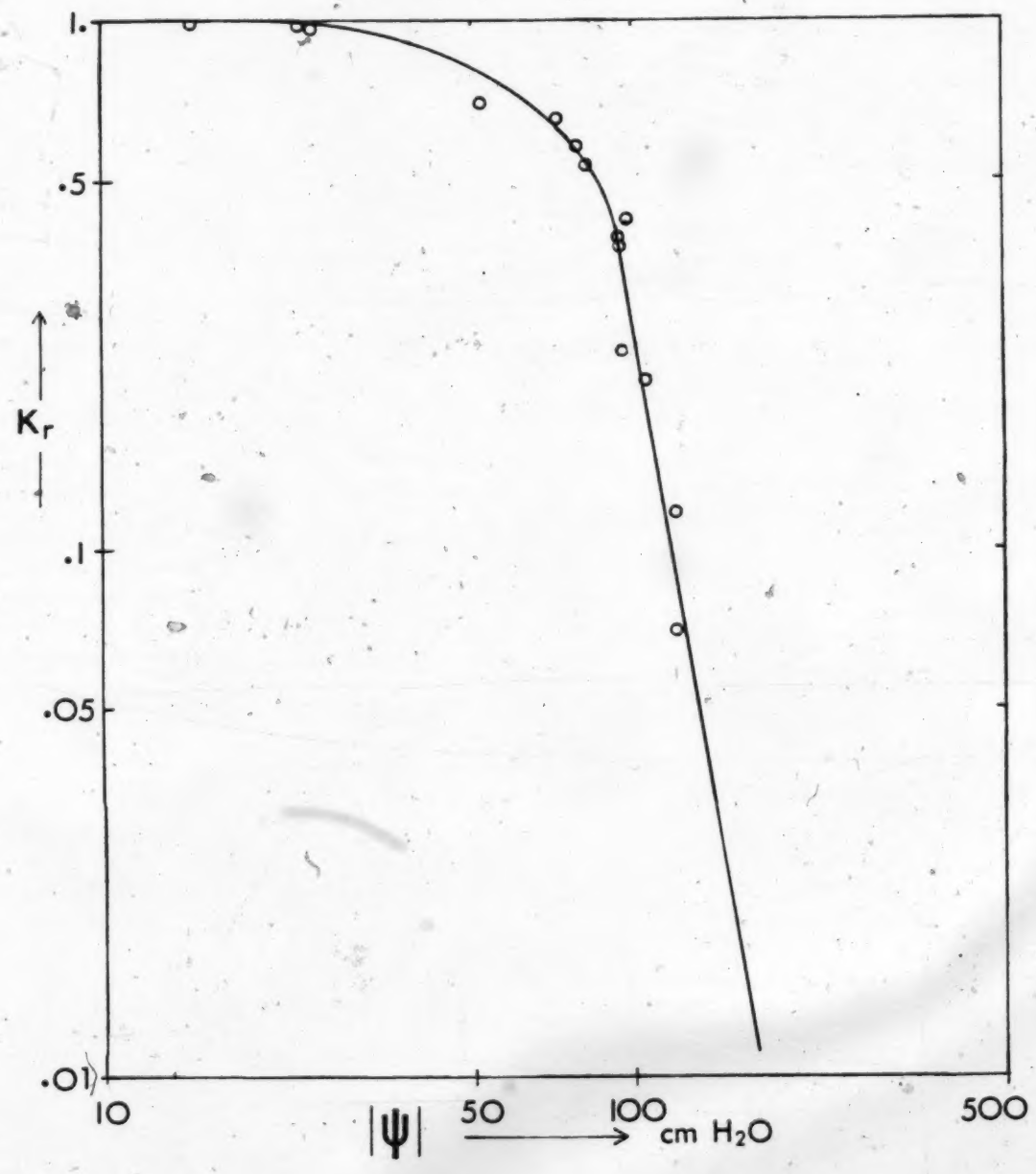

Figure 3-24. K_r (ψ) relationship for Site 2 (0-20 cm)

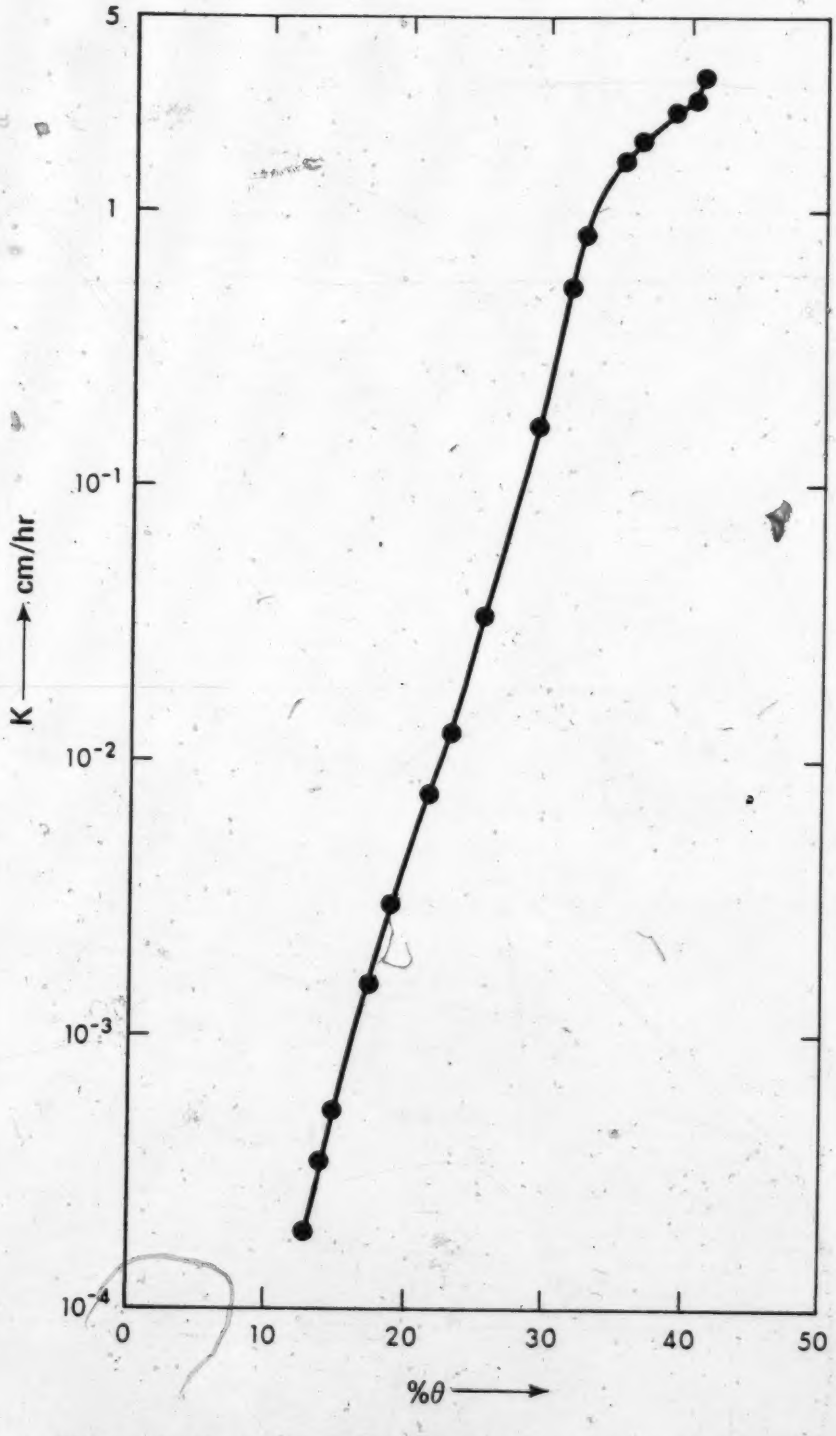

Figure 3-25. K (θ) relationship for Site 2 (0-20 cm)

The porosity value used in the hydraulic conductivity experiments was calculated from (3-12) using field- and laboratory-measured values of bulk and particle density of the upper soil layers of the sites. It was assumed that the calculated value of 41% porosity was representative of the field condition and was constant. Measurements of water contents at saturation near the water table using the neutron probe confirmed the representativeness of such a porosity value. This assumption with regard to the porosity distribution -- although used extensively in subsurface water modeling studies -- is probably an oversimplification. However, a lack of field data prevented the more detailed description of porosity variation.

An attempt to calculate the unsaturated hydraulic conductivity by field methods was made using graphically smoothed data from Site 2. Because of the relatively high water contents (15 to 25% by volume) at Site 2 below a depth of a few centimeters, and because measurement errors would probably be reduced, the isothermal field method based on (3-11) was utilized with the reference flux calculated as described in Section 3.6.10.2. The agreement between field measured and laboratory determined hydraulic conductivity values was found to be satisfactory (Fig. 3-26).

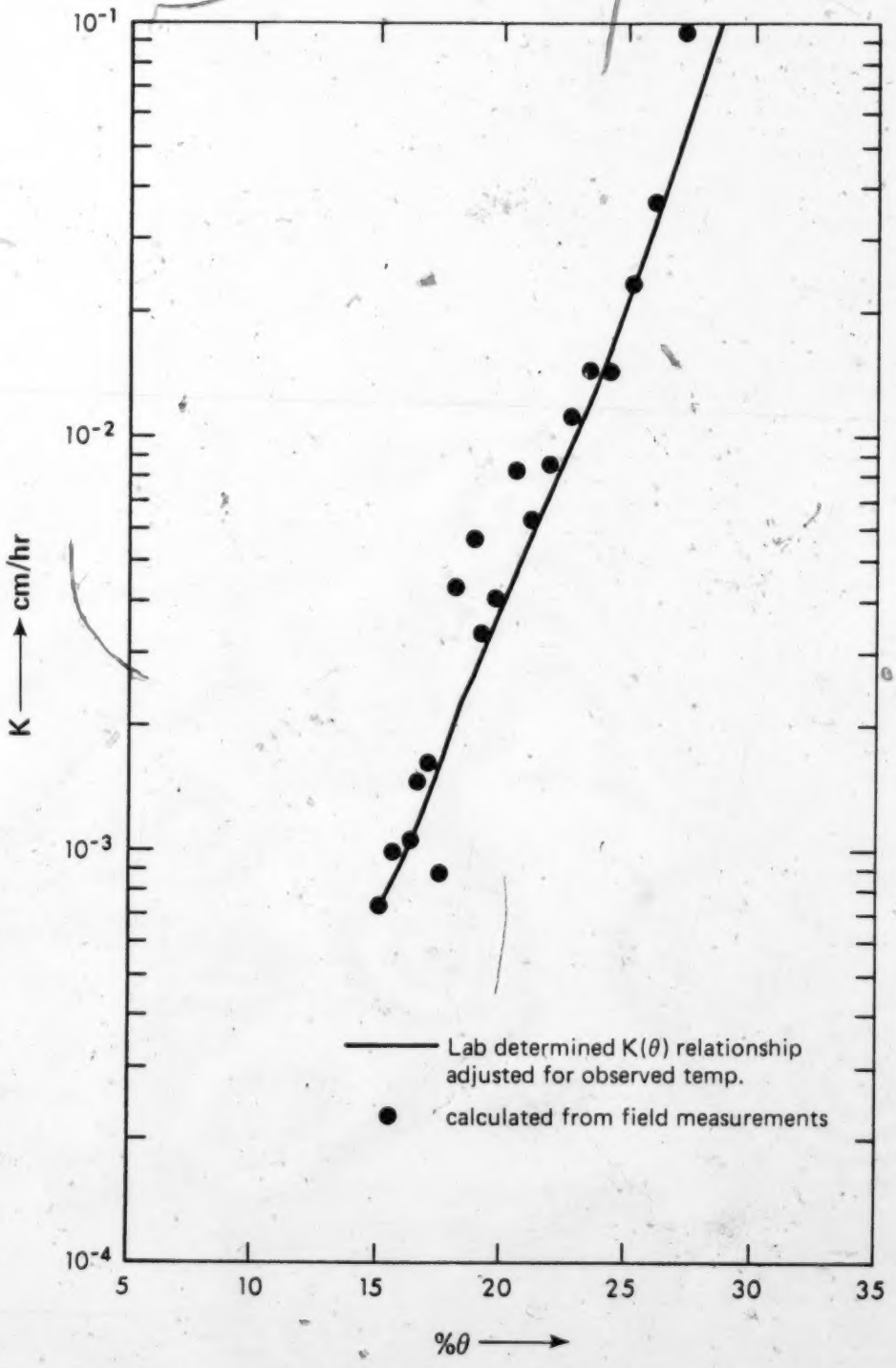

Figure 3-26. Field-determined K (θ) curve for Site 2

3.7.7 Thermal Conductivity and Heat Capacity

Figure (3-27) shows a typical field curve obtained during the month of July 1976 from Site 1 using the thermal conductivity probe. The value of thermal conductivity calculated from these data is also indicated. The points on such graphs asymptotically approach a straight line somewhere between 100 and 200 seconds after the start of the test. The early time deviation is due to initial lag effects (Wechsler, 1966) mainly attributable to the effects of probe diameter and conductivity, and contact resistance between the test medium and the probe.

Assuming that the entire subsurface profile is homogeneous with respect to thermal conductivity, a relationship between thermal conductivity and water content $\lambda(\theta)$ is represented in Fig. 3-28 by a hand-drawn line passing through the points. The limited range of water contents over which the thermal conductivities were determined in the field, as well as thermal conductivity heterogeneities, prevented a better definition of the $\lambda(\theta)$ relationship.

The volumetric heat capacity $C(\theta)$ function, calculated from the procedure outlined in Section 3.6.9, is shown in Fig. 3-29. The deviations from non-linearity observed in that figure are due to the variation in bulk density and organic matter content (Fig. 3-12).

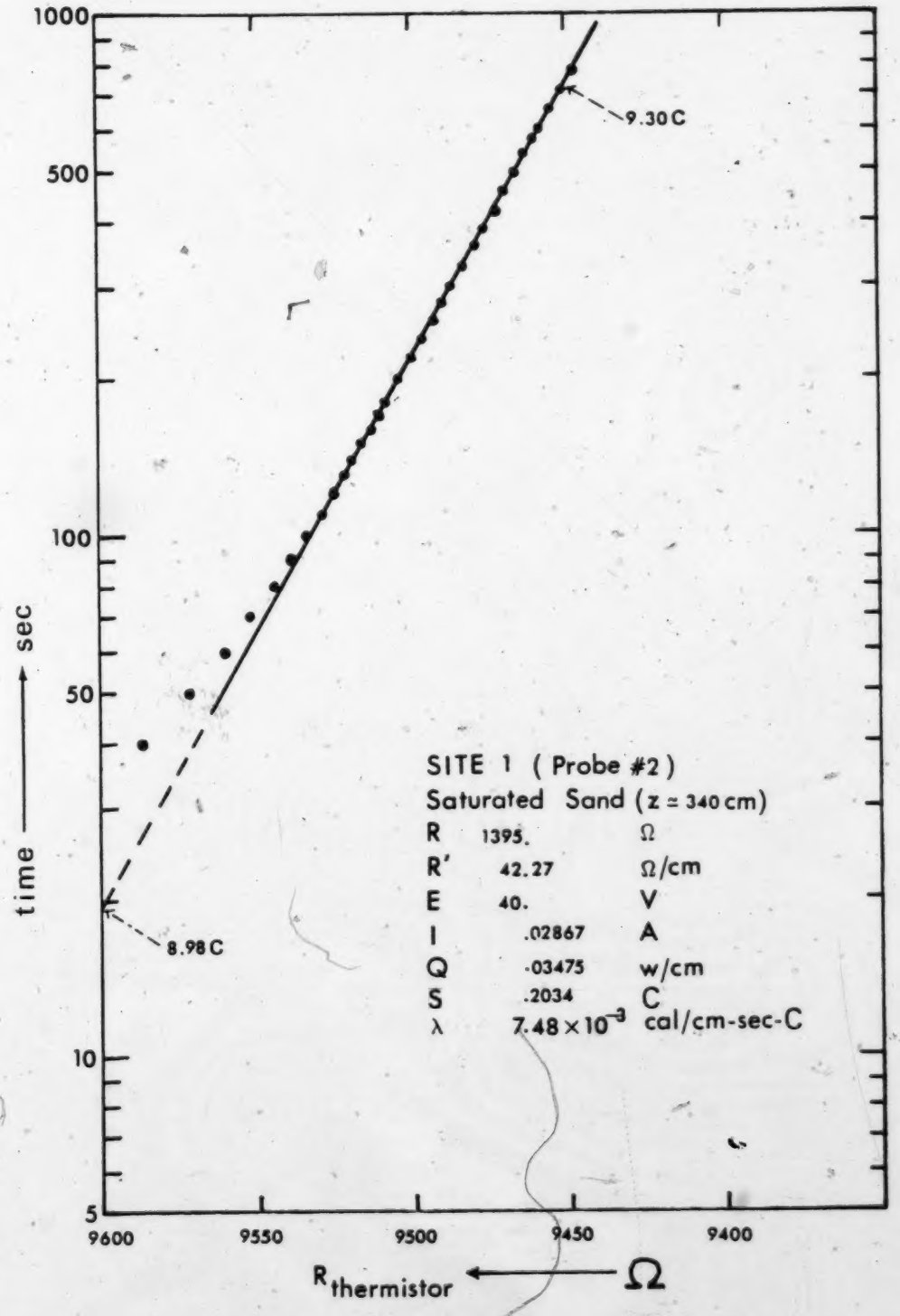

Figure 3-27. Field-determined thermal conductivity

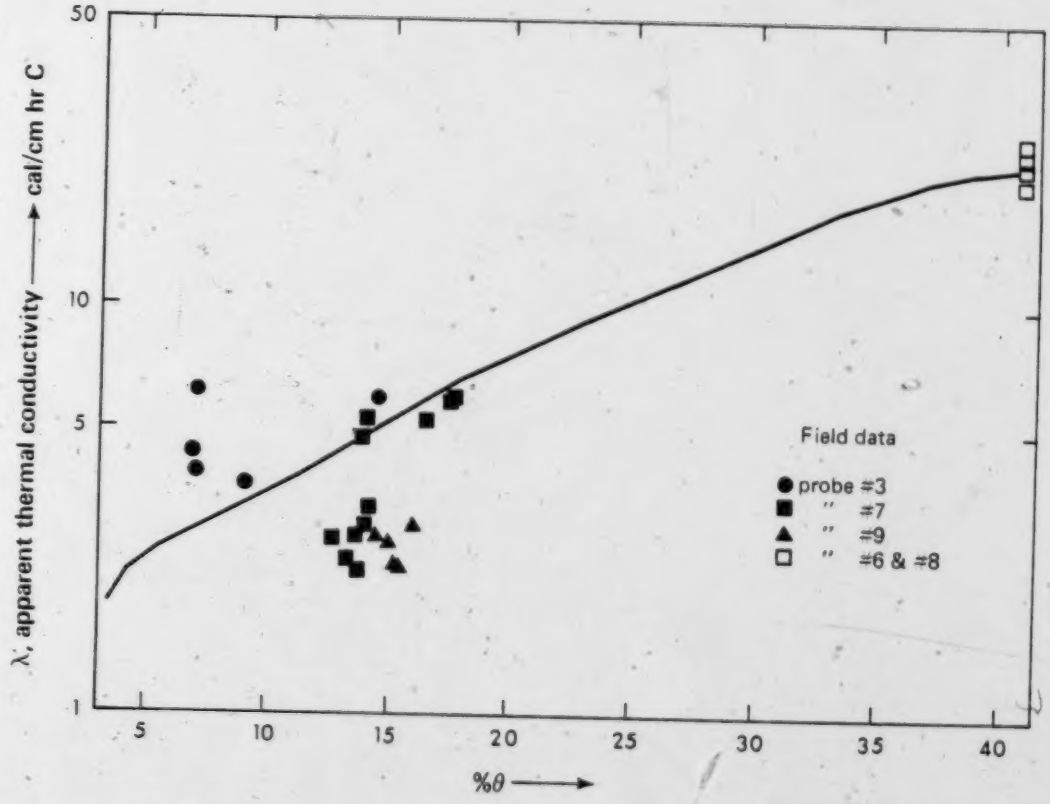

Figure 3-28. λ (θ) relationship for Site 2

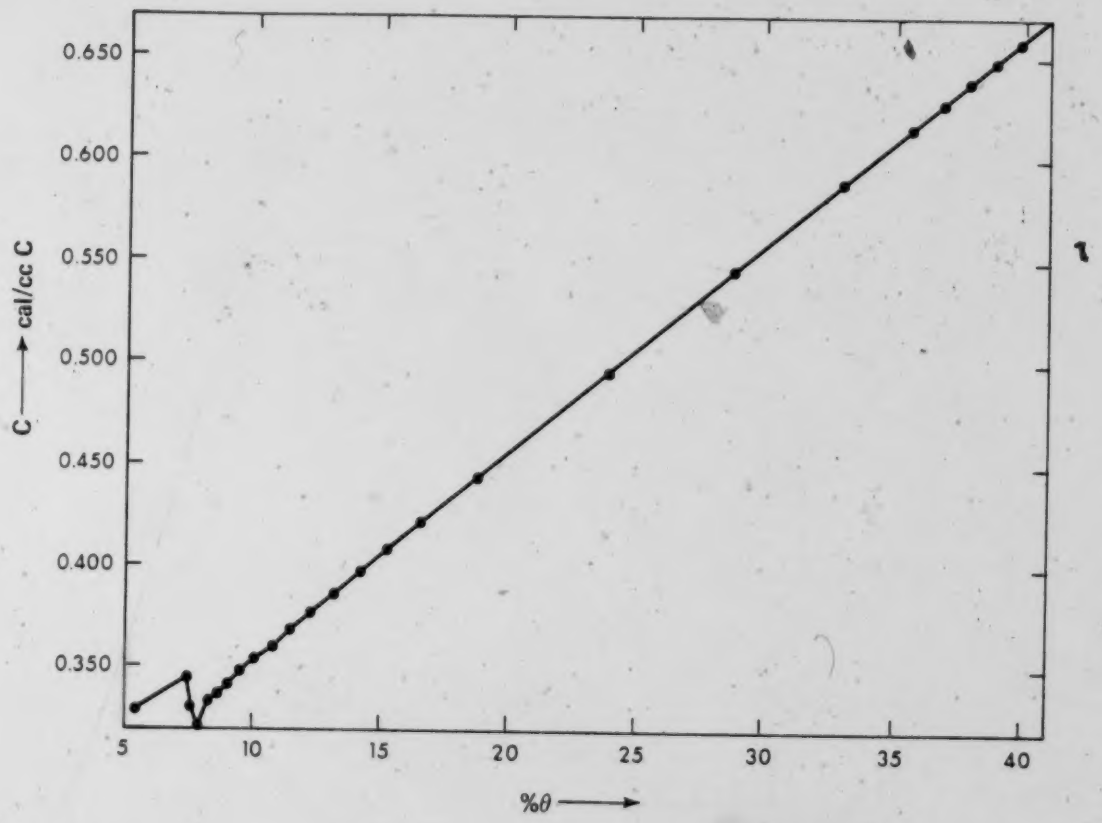

Figure 3-29. C (θ) relationship for Site 2

3.8 Evaluation of Field and Laboratory Studies

Reliable field measurements can be achieved by using properly designed and calibrated field instrumentation in combination with careful field installation involving minimum soil disturbance and appropriate spacing. However, even if appropriate precautions are taken, the field researcher is faced with many difficulties in assuring the long-term accuracy of the instrumentation. For example, in the case of the mercury tensiometers, the problems of maintaining the associated manometer completely full of liquid under partial vacuum, time lag and temperature influences on tensiometer performance cause appreciable difficulties in obtaining accurate measurements of matric potentials over a long period of time. Other problems with tensiometers relate to difficulties in maintaining constant physical contact with the soil, especially with windy conditions; disruptions caused by repeated servicing; and plant roots which tend to grow around the base of the tensiometer.

As mentioned earlier, the field use of soil psychrometers was not satisfactory. This result is typical of problems reported by other workers (Maclean, 1974; Mayo, 1976). Thus, few successful field measurements with soil psychrometers are reported in the literature (Enfield and Hsieh, 1971; Merril and Rawlins, 1972; Moore and Caldwell, 1972; Wheeler et al., 1972). The major shortcomings of this

instrumentation are related to the delicacy of the psychrometric measurements themselves and the frequent recalibration of field psychrometers necessary for accurate measurements.

The variation of water content and temperature is usually very small under normal conditions and it is often not possible to measure these changes. Only when the magnitude of the changes are large, such as in the upper soil zone and capillary fringe, can these changes be measured with reasonable accuracy. Difficulties in measuring small temperature and moisture gradients also influence tne accuracy of derived data which are functions of these variables. Thus, the possibility of accurately specifying the heat flux and particularly the water flux at some location in the subsurface profile is not great. In addition, the small magnitude of several parameters involved in the calculation of the subsurface flow regime and especially of the thermal diffusion coefficients, coupling coefficients and conductivity coefficients add to the difficulties in applying flow theories.

The methodology proposed in Section 2-8 would appear to make the field endeavor easier. However, the small magnitude of relevant quantities often poses serious error problems. For example, I found that calculating the saturated water flux from the heat flux equation (2-61), as was suggested by Stallman (1963) and Bredehoeft and Papadopoulos (1965), was

not a satisfactory measure of water flux if compared with the value obtained from a Darcy-type expression. This apparent discrepancy is probably due to the very small magnitude of the convective term in (2-61), which, in association with small errors in measurements of the various quantities involved in that equation, makes this procedure questionable for field situations.

The field methodology depends strongly on the accurate determination of water and especially of the heat fluxes in the subsurface profile (Taylor and Cary, 1965). However, relatively small errors in the calculation of heat and water fluxes propagate and amplify in subsequent transport coefficient calculations. For example, let HF be the ratio of the heat flux calculated using the temperature integral method (Section 3.6.10.1) over the heat flux calculated using (2-58) or (2-60). Also let DC be the ratio of the water vapor diffusion coefficient $D_{\theta v}$ -- (2-71) neglecting the convective term -- estimated using the heat flux calculated by the temperature integral method over the diffusion coefficient calculated using the heat flux equation (2-58) or (2-60). I found that for the surface 120 cm of Site 2 soils, a ratio of heat fluxes HF ranging from 1.0 to 1.8 resulted in a ratio of water vapor diffusion coefficients DC ranging from 1 to over 30. This discrepancy is caused in part by error propagation involved in (2-71), which requires that two nearly equal numbers be subtracted (provided the temperature gradient is negative) and the

difference divided by a small number.

Similarly, let WF be the ratio of the water flux obtained by using a water balance equation (Section 3.6.10.2) over the water flux calculated using the non-isothermal water flux equation (2-38). Also, let HC be the ratio of the hydraulic conductivity calculated using the proposed field procedure (Section 3.6.5.2) -- with the water flux calculated from a water balance equation -- over the hydraulic conductivity calculated using the same field procedure but with the water flux calculated by (2-38). I found that for the upper 120 cm of Site 2 soils, a WF ratio ranging from 1 to 10 resulted in an HC ratio ranging from 1.1 to over 17.

Because of the problems originating from measurement errors, field heterogeneities, replacement of some field data by laboratory data and inadequacies in the model expressions of the various transport parameters -- as opposed to actually measured quantities -- the proposed field methodology was not carried any further with the data presented here. Ideally, however, with the availability of better field equipment, better installed and calibrated, this methodology will prove to be of practical significance in environments where temperature gradients are very pronounced.

In order to determine the magnitude of the uncertainty involved in every experimental measurement, an error

analysis similar to the ones performed by Gardner (1965), Hanks and Jacobs (1971), Fritton (1974), Flühler et al. (1976), among others, has been carried out. Let a measured quantity F be a function of several independent variables x_i representing measured input data, that is $F = f(x_1, x_2, \ldots, x_n)$ and that these input data are in error by $\pm\Delta x_1, \pm\Delta x_2, \ldots, \pm\Delta x_n$, respectively. These errors will cause an error ΔF in the computed result F. Expanding the function f in a Taylor series and neglecting all higher order terms, as the Δx_i's will all be small quantities, one obtains (Doebelin, 1975)

$$f(x_1 \pm \Delta x_1, x_2 \pm \Delta x_2, \ldots, x_n \pm \Delta x_n) =$$
$$f(x_1, x_2, \ldots, x_n) + \Delta x_1 \partial f/\partial x_1$$
$$+\Delta x_2 \partial f/\partial x_2 + \ldots + \Delta x_n \partial f/\partial x_n \qquad (3\text{-}23)$$

The absolute error E_a is given by

$$E_a = \Delta F = |\Delta x_1 \partial f/\partial x_1| + |\Delta x_2 \partial f/\partial x_2| + \ldots + |\Delta x_n \partial f/\partial x_n| \qquad (3\text{-}24)$$

where the absolute value signs are used to avoid possible reduction of the total error by negative signs of partial derivatives associated with positive Δx_i's, or vice versa. Thus, the actual error ΔF will never exceed E_a as long as the Δx_i's do not exceed their estimated values. The form of (3-24) is useful because it indicates which variables (x_i's) exert the strongest influence on the accuracy of the overall result. The maximum error approach is different from the standard error approach (Beers, 1957; Lyon, 1970), in which a statistical average of the errors Δx_i's liable to be present -- usually the root-mean-square errors -- is

estimated.

In order to illustrate the practical usefulness of this technique, approximate measures of the uncertainty in the various parameters involved in calculating the heat flux (3-20) in a general manner, as related to the present field measurements, are obtained using the maximum error approach outlined above. The results of this analysis are detailed in Table 3-4. For error analysis it is necessary to arrive at an estimate of error (Δx_i) for each of the variables. These error estimates could be standard deviations, 95% confidence intervals, ranges or other measures of error. The maximum absolute error estimates used here (column (4) of Table 3-4) were based on the instrumentation and experiments used for this study. The error estimates of specific heats c_s, c_o and density of organic matter ρ_o are based on data given by de Vries (1963). The variable x_i exerting the greatest influence on the accuracy of the overall result is indicated by an arrow in column (6) of the table for each of the four example calculations shown there.

It should be noted that for this analysis no errors were assigned to the problem of measuring true field conditions caused by instrumentation emplacement and the resulting disturbance of the soil, field heterogeneities, annual heat wave influences (Hanks and Tanner, 1972), data smoothing, departure of reality from theory, and possibly other factors. Because the computed errors depend on the

TABLE 3-4*

Maximum error analysis for heat flux parameters at site 2

(1) Equation & magnitude of F	(2) x_i	(3) Magnitude of x_i		(4) Approx. max. abs. error Δx_i	(5) $\left(\partial F/\partial x_i\right)\Delta x_i$	(6) Contrib. to abs. error of term x_i	(7) Total abs. error	(8) Total relative error (in %)
(eqn. 3-14)	c_s	0.86 cal/g/C		0.02	$\left[\frac{1-a'}{\rho_s}\rho_b\right]\Delta c_s$	0.0107		
	c_o	0.48 cal/g/C		0.02	$\left[\frac{a'}{\rho_o}\rho_b\right]\Delta c_o$	0.00012		
$C = c_s\frac{1-a'}{\rho_s}\rho_b + c_o\frac{a'}{\rho_o}\rho_b + \theta$	a'	0.0055		0.0007	$\left[\frac{c_o\rho_b}{\rho_o} - \frac{c_s\rho_b}{\rho_s}\right]\Delta a'$	0.00030		
	ρ_b	1.42	g/cm^3	0.1	$\left[\frac{c_s(1-a')}{\rho_s} + \frac{c_o a'}{\rho_o}\right]\Delta\rho_b$	0.0164	0.038	9.3
	ρ_s	2.64	g/cm^3	0.01	$\left[-\frac{c_s(1-a')}{\rho_s^2}\right]\Delta\rho_s$	0.00061		
	ρ_o	1.3	g/cm^3	0.01	$\left[-\frac{c_o a'}{\rho_o^2}\right]\Delta\rho_o$	0.000019		
C=0.4103 $\frac{cal}{cm^3 C}$	θ	0.1767		0.01	$\Delta\theta$	0.01		
(eqn. 3-13)	I	0.0249	A	0.0005	$\left[\frac{(.0438)2IR'\log(t_2/t_1)}{(T_2-T_1)}\right]\Delta I$	0.000048		
	R	49.58	Ω/cm	0.5	$\left[\frac{(.0438)\ I^2\log\ (t_2/t_1)}{(T_2-T_1)}\right]\Delta R$	0.000017		
$\lambda = \frac{.0438\ I^2R'}{T_2-T_1}\log\frac{t_2}{t_1}$	T_2	19.9	C	0.01	$\left[-\frac{(.0438)\ I^2R'\log\ (t_2/t_1)}{(T_2-T_1)^2}\right]\Delta T_2$	0.000057	1.99x10^{-4}	11.7
	T_1	19.0	C	0.01	$\left[\frac{(.0438)\ I^2R'\log\ (t_2/t_1)}{(T_2-T_1)^2}\right]\Delta T_1$	0.000057		
	t	600.0	sec	negligible				
λ= 1.705x10^{-3} cal/ cm sec C	t	29.0	sec	negligible				
$Q' = \bar{C}\frac{\Delta T}{\Delta z} + \bar{C}\frac{\Delta z}{\Delta t}$	$\bar{C}$	0.4104	$\frac{cal}{cm^3 C}$	0.038	$\left[\frac{i+1}{i}(\Delta T/\Delta t)\Delta z\right]\Delta\bar{C}$	0.0116		
	ΔT	0.1	C	0.05	$\left[\frac{i+1}{i}\bar{C}(\Delta z/\Delta t)\right]\Delta(\Delta T)$	0.0616		
	Δz	12.0	cm	0.25	$\left[\frac{i+1}{i}\bar{C}(\Delta T/\Delta t)\right]\Delta(\Delta z)$	0.0026	0.0756	61.4
	Δt	4.0	hr	0.02	$\left[\frac{i+1}{i}\bar{C}(\Delta T/\Delta t^2)\right]\Delta(\Delta t)$	0.00005		
Q' = 0.1231 $\frac{cal}{cm^2 hr}$								
$q = -\lambda\frac{T_{i+1}-T_i}{\Delta z}$	λ	6.138	$\frac{cal}{cm\ hr\ C}$	0.716	$\left[-\frac{T_{i+1}-T_i}{\Delta z}\right]\Delta\lambda$	0.0477		
	T_i	20.0	C	0.05	$\left[\frac{\lambda}{\Delta z}\right]\Delta T_i$	0.0256		
	T_{i+1}	19.2	C	0.05	$\left[-\frac{\lambda}{\Delta z}\right]\Delta T_{i+1}$	0.0256	0.107	26.1
	z	12.0	cm	0.25	$\lambda\left[\frac{T_{i+1}-T_i}{(\Delta z)^2}\right]\Delta(\Delta z)$	0.0085		
q = 0.4092 $\frac{cal}{cm^2 hr}$								

*Data from a depth of 40 cm from Site 2 during the August 13-14, 1974 measurement period

magnitude of the variables involved in the error analysis, representative data from some depth (60 cm in the examples shown in Table 3-4), where the time change in various physical properties is not very pronounced, were arbitrarily chosen. The purpose of this exercise is not to present a precise and detailed error analysis but to get a general feeling of the approximate maximum errors involved in this type of field calculation.

One should not be discouraged by the error analysis shown above because any other field method would most likely result in similar, if not greater, uncertainties (Flühler et al., 1976). The maximum error analysis can be used as a criterion for selecting the best field method from others available. Such a selection was done, for example, by Hanks and Jacobs (1971) who showed that the calorimetric (or temperature integral) method for estimating soil heat flux resulted in a smaller relative error than the heat flux meter approach or the combination of heat flux meter and calorimetric method.

CHAPTER 4

MODEL STUDIES

4.1 Introduction

The purpose of this chapter is to apply the theoretical and experimental results of the previous chapters to model the simultaneous transport of water and heat in the subsurface. This modeling effort is not simply designed to reproduce flow mechanisms but is an integral part of the study of these mechanisms. It provides the vehicle for better understanding of the flow processes involved; it establishes the framework in which to collect the field data; it is the device to test the adequacy of any existing theories through sensitivity analysis and it provides the means for prediction of non-isothermal flow processes and thus for their control.

4.2. The Mathematical Model

The first step in a quantitative modeling effort of the simultaneous heat and mass transfer in porous media is the development of a mathematical model. Such a model consists of the system of coupled, non-linear, second-order, parabolic partial differential equations developed in

Chapter 2 (2-54 and 2-67) and presented below in one-dimensional form:

$$F\,\partial\psi/\partial t = \partial(K_\psi\,\partial\psi/\partial z)/\partial z + \partial(D_T\,\partial T/\partial z)/\partial z - \partial K/\partial z \qquad (4\text{-}1a)$$

$$C\,\partial T/\partial t = \partial(\lambda\,\partial T/\partial z)/\partial z + \partial(D_L\,\partial\psi/\partial z)/\partial z - c_\ell\, q_w \partial T/\partial z \qquad (4\text{-}1b)$$

where

$$F = \partial\theta/\partial\psi \text{ in the unsaturated zone}$$

$$= S_s \text{ in the saturated zone}$$

$$K_\psi = K + K_{\psi v}$$

$$D_T = D_{T\ell} + D_{Tv}$$

$$C = 0.46x_{mm} + 0.60x_o + \theta$$

$$D_L = L' K_{\psi v} \qquad (4\text{-}1c)$$

$$q_w/\rho = -K_\psi\,\partial\psi/\partial z - D_T \partial T/\partial z + Ki \qquad (4\text{-}1d)$$

Because the flow of heat and water is treated as a coupled phenomenon, it is necessary to specify initial and boundary conditions at the same boundaries for both equations (4-1a,b). Therefore, I used the following type of initial and boundary conditions associated with (4-1a,b).

Initial Conditions $T(z,t) = T(z)$ @ $t=0$, $z\epsilon(0,L)$ (4-2a)

$\psi(z,t) = \psi(z)$ @ $t=0$, $z\epsilon(0,L)$ (4-2b)

Top Boundary Conditions $T(0,t) = T(t)$ @ $t>0$, $z=0$ (4-3a)

$$q_w/\rho\,(0,t) = \pm\, E(t) \qquad (4\text{-}3b)$$

specified evaporation or infiltration rate

Bottom Boundary Conditions $\partial T/\partial z|_{z=L} = 0 \qquad (4\text{-}3c)$

$$q_w/\rho\,(L,t) = \pm\, w(t) \qquad (4\text{-}3d)$$

specified water flux entering or leaving the system

The solution of (4-1a,b), with the initial and boundary conditions (4-2) and (4-3) respectively, form a mathematical basis for describing the spatial and temporal distribution of temperature and pressure head, as well as all relevant fluxes and transport coefficients in porous media. The form of the present mathematical model is more general than the one used by Philip and de Vries (1957) in that the pressure head is used as the dependent variable instead of the volumetric water content θ. Because ψ is a continuous function of position and time, its values are identical on both sides of an internal boundary separating two different types of porous media, which is not the case with θ-values. For this reason, the ψ-based equations are applicable to layered and heterogeneous porous media, parts of which are completely saturated, while the θ-based approach is limited to homogeneous and unsaturated porous media (Corey, 1977). However, one disadvantage of the ψ-based approach, which is avoided in the θ-based formulation, is the strong non-linearity of F in (4-1a), especially in the vicinity of

very sharp wetting fronts.

4.3 The Numerical Approach

The complexity of the system of coupled non-linear partial differential equations (2-54) and (2-67) suggests that analytical solutions are not possible. Numerical techniques provide the most practical means for obtaining a solution to the (4-1) system of partial differential equations. Because the direction of heat and moisture flow is predominantly unidirectional, I chose to solve the one-dimensional form of the coupled equations. Besides reducing the complications of the modeling effort, the one-dimensional form also reduces the amount of experimental data required and thus the uncertainty associated with their calculation. The latter situation holds especially with regard to determining transport coefficients for non-homogeneous porous media. However, once a one-dimensional solution to the relevant system of partial differential equations is established, the extension to two or three dimensional situations should be feasible.

The system of equations (4-1) may be solved using a variety of numerical methods, the most common of which are the finite-difference (Forsythe and Wasow, 1960; Richtmyer and Morton, 1967; Smith, 1969; Mitchell, 1969; von Rosenberg, 1969; Remson et al., 1971) and finite element methods (Zienkiewicz, 1971; Desai and Abel, 1972; Sagerlind,

1976; Pinder and Gray, 1977). Although the recently popular finite element methods are more advantageous for two- or three-dimensional problems, especially if complex geometries are involved, at present they show little or no advantage over the better known finite difference techniques for non-linear transient one-dimensional problems (Emery and Carson, 1971; Mercer and Faust, 1976).

The finite difference approach was followed here. The derivatives in the coupled equations (4-1) and in the corresponding initial and boundary conditions (4-2) and (4-3) were replaced by finite difference approximations at discrete points of the solution domain. The resulting system of non-linear algebraic equations are solved for ψ and T. The water characteristic input function was utilized to obtain the corresponding θ values. Figure 4-1 shows a schematic diagram of the one-dimensional model chosen to represent continuous water and heat flow from the ground surface to a point beneath the water table. The subsurface profile is discretized using the equidistant finite difference nodes shown in Fig. 4-1.

4.4 Numerical Solution

Although explicit methods for solving finite difference equations are simple and straightforward, the severe restrictions on mesh size and time increments that are sometimes necessary make this method rather unsuitable for

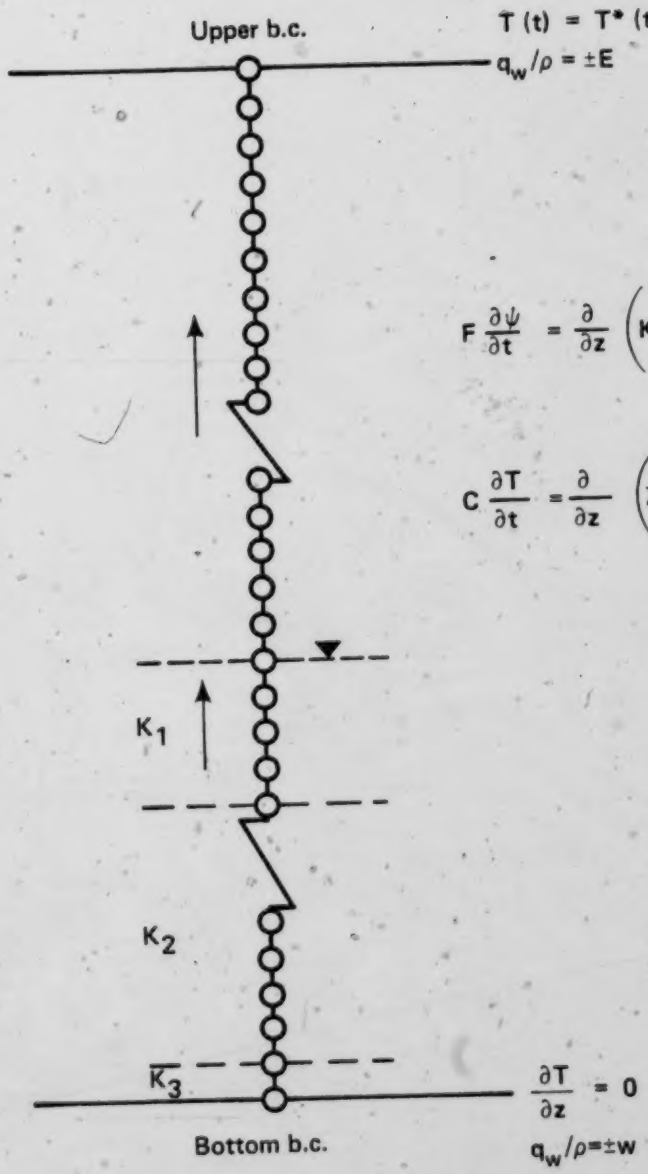

$$F\frac{\partial \psi}{\partial t} = \frac{\partial}{\partial z}\left(K\psi\frac{\partial \psi}{\partial z} + D_T\frac{\partial T}{\partial z} - K\right)$$

$$C\frac{\partial T}{\partial t} = \frac{\partial}{\partial z}\left(\lambda\frac{\partial T}{\partial z} + D_L\frac{\partial \psi}{\partial z}\right) - c_1 q_w\frac{\partial T}{\partial z}$$

Figure 4-1. One-dimensional coupled transient mathematical model

practical applications. Thus, I have adopted an implicit method which is less restrictive but numerically more complicated because it involves the solution of a system of algebraic equations at each time step. Specifically, a form of the Crank-Nicholson implicit method (Richtmyer and Morton, 1967) was followed (Appendix D). This implicit scheme converges with a smaller discretization error, $O\{(\Delta t)^2 + (\Delta z)^2\}$, compared to the error $O\{(\Delta t) + (\Delta z)^2\}$ of the backward-difference implicit method. The resulting set of simultaneous non-linear algebraic equations using the space-time network of Fig. 4-2 is as follows

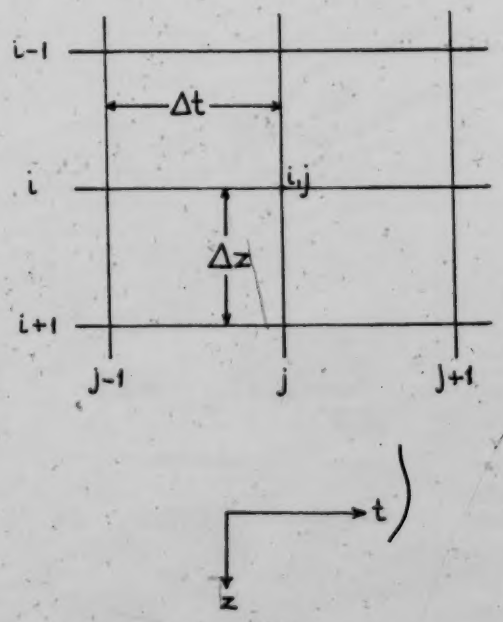

Figure 4-2

$$-A_i \psi_{i-1}^{j} + B_i \psi_i^{j} - C_i \psi_{i+1}^{j} - \bar{A}_i T_{i-1}^{j} + \bar{B}_i T_i^{j} - \bar{C}_i T_{i+1}^{j} = H_i \quad (4\text{-}4a)$$

$$-A_i' T_{i-1}^{j} + B_i' T_i^{j} - C_i' T_{i+1}^{j} - \bar{A}_i' \psi_{i-1}^{j} + \bar{B}_i' \psi_i^{j} - \bar{C}_i' \psi_{i+1}^{j} = H_i' \quad (4\text{-}4b)$$

where

$$A_i = K_{\psi_{i-1/2}}^{j-1/2} \quad (4\text{-}4c)$$

$$B_i = 2F_i^{j-1/2}/r + K_{\psi_{i+1/2}}^{j-1/2} + K_{\psi_{i-1/2}}^{j-1/2} \quad (4\text{-}4d)$$

$$C_i = K_{\psi_{i+1/2}}^{j-1/2} \quad (4\text{-}4e)$$

$$r = \Delta t / (\Delta z)^2 \quad (4\text{-}4F)$$

$$\bar{A}_i = D_{T_{i-1/2}}^{j-1/2} \quad (4\text{-}4G)$$

$$\bar{B}_i = D_{T_{i+1/2}}^{j-1/2} + D_{T_{i-1/2}}^{j-1/2} \quad (4\text{-}4H)$$

$$\bar{C}_i = D_{T_{i+1/2}}^{j-1/2} \quad (4\text{-}4I)$$

$$H_i = K_{\psi_{i+1/2}}^{j-1/2} (\psi_{i+1}^{j-1} - \psi_i^{j-1}) + K_{\psi_{i-1/2}}^{j-1/2} (\psi_{i-1}^{j-1} - \psi_i^{j-1}) + D_{T_{i+1/2}}^{j-1/2} (T_{i+1}^{j-1} - T_i^{j-1}) + D_{T_{i-1/2}}^{j-1/2} (T_{i-1}^{j-1} - T_i^{j-1}) + (K_{i-1/2}^{j-1/2} - K_{i+1/2}^{j-1/2}) 2\Delta z + (2F_i^{j-1/2}/r) \quad (4\text{-}4J)$$

$$A_i' = \lambda_{i-1/2}^{j-1/2} + c_{l_i}^{j-1/2} q_{w_i}^{j-1/2} \Delta z/2 \quad (4\text{-}4K)$$

$$B_i' = 2C_i^{j-1/2}/r + \lambda_{i+1/2}^{j-1/2} + \lambda_{i-1/2}^{j-1/2} \quad (4\text{-}4L)$$

$$C_i' = \lambda_{i+1/2}^{j-1/2} - c_{l_i}^{j-1/2} q_{w_i}^{j-1/2} \Delta z/2 \quad (4\text{-}4M)$$

$$\bar{A}_i' = D_{L\,i-1/2}^{j-1/2} \quad (4\text{-}4N)$$

$$\bar{B}_i' = D_{L\,i+1/2}^{j-1/2} + D_{L\,i-1/2}^{j-1/2} \quad (4\text{-}4O)$$

$$\bar{C}_i' = D_{L\,i+1/2}^{j-1/2} \quad (4\text{-}4P)$$

$$H' = \lambda_{i+1/2}^{j-1/2} (T_{i+1}^{j-1} - T_i^{j-1}) + \lambda_{i-1/2}^{j-1/2} (T_{i-1}^{j-1} - T_i^{j}) + D_{L\,i+1/2}^{j-1/2} (\psi_{i+1}^{j-1} - \psi_i^{j-1}) + D_{L\,i-1/2}^{j-1/2} (\psi_{i-1}^{j-1} - \psi_i^{j-1}) + c_{l_i}^{j-1/2} q_{w_i}^{j-1/2} \Delta z (T_{i-1}^{j-1} - T_{i+1}^{j-1})/2 + (2C_i^{j-1/2}/r) T_i^{j-1} \quad (4\text{-}4Q)$$

$$X_{i+1/2}^{j-1/2} = (X_i^{j-1} + X_{i+1}^{j-1} + X_{i+1}^{j} + X_i^{j})/4 \quad (4\text{-}4R)$$

$$X_{i-1/2}^{j-1/2} = (X_i^{j} + X_{i-1}^{j} + X_{i-1}^{j-1} + X_i^{j-1})/4 \quad (4\text{-}4S)$$

$$Y_i^{j-1/2} = (Y_i^{j-1} - Y_i^j)/2 \qquad (4\text{-}4T)$$

(The reader is referred to Appendix D for the forms that (4-4) take at the top and bottom boundaries of the solution domain.)

The system of equations (4-4) may be represented in matrix form as follows, where brackets indicate square matrices and braces denote column matrices:

$$[G]\{\psi\} + [F]\{T\} = \{H\}$$
$$[E]\{\psi\} + [D]\{T\} = \{H'\} \qquad (4\text{-}5a)$$

or

$$\begin{bmatrix} G & F \\ E & D \end{bmatrix} \begin{Bmatrix} \psi \\ T \end{Bmatrix} = \begin{Bmatrix} H \\ H' \end{Bmatrix} \qquad (4\text{-}5b)$$

Each of the matrices G, F, E, D above represents a tridiagonal, diagonally dominant square matrix. Thus the system (4-5) has the following form

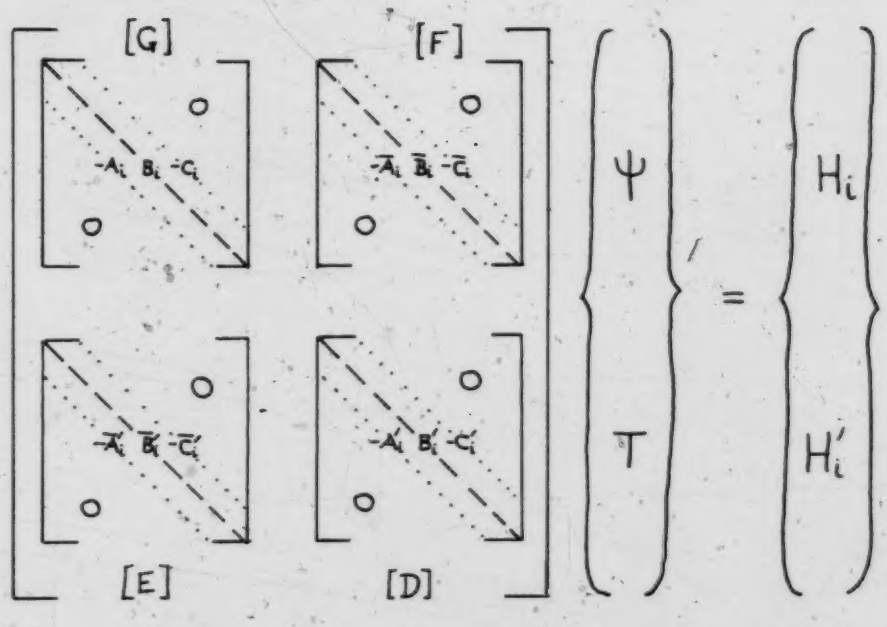

(4-5c)

This system of algebraic equations is non-linear because the coefficient matrices G, F, E, D depend on values of ψ_i^j and T_i^j, which are unknown at the time the solution to (4-4) or (4-5) is sought. In order to remove this non-linearity, an iteration process was used in which initial estimates of the ψ_i^j and T_i^j values at each point in the solution domain were made and subsequently used to determine those coefficient matrices.

4.5. Solution of Linear Algebraic Systems and Convergence Requirements

At this point let us briefly examine systems of linear algebraic equations of the form

$$[A]\{x\} = \{b\} \qquad (4\text{-}6)$$

where [A] is an nxn constant matrix;

{x} is a column vector of unknown variables; and

{b} is a constant column vector.

Such a system may be obtained, for example, from linearization of (4-5b) by assuming the coefficient matrices to be constant. Numerical methods for solving linear systems, such as (4-6), may be divided into two types (Forsythe and Moler, 1967; Conte and de Boor, 1972): direct and iterative. The direct methods, exemplified by the Gaussian elimination method, will yield the exact solution for any non-singular system of equations in a finite number of arithmetic operations in the absence of round-off or other computation errors. However, errors arising from round-off, instability and loss of significance may lead to poor or useless results. The iterative methods, on the other hand, start with an initial approximation and may converge to the solution of the system of equations, by applying a suitable algorithm. The iterative methods, although approximate even if the process converges, are marked by their simplicity and relative insensitivity to the growth of round-off errors. Many systems of equations arising in practice result, after discretization, in coefficient matrices that are sparse; that is, they contain a high proportion of zeros. For example, (4-5c) is such a sparse system. Iterative methods, if they work, are ideally suited for the solution of sparse matrices, especially if their order is very large; elimination methods usually produce a triangular system that is no longer sparse (Dorn and

McCracken, 1972).

The matrix A may be partitioned into three separate matrices

$$A = L+D+U \tag{4-7}$$

where

L is a strictly lower triangular matrix whose entries are the entries of A below the main diagonal;

D is a diagonal matrix consisting of the diagonal entries of A; and

U is a strictly upper diagonal matrix whose entries are the entries of A above the main diagonal.

(4-6) may now be written as

$$[L+D+U]\{x\} = \{b\} \tag{4-8}$$

which gives rise to the following well-known Jacobi (4-9), Gauss-Seidel (4-10) and successive over-relaxation (4-11) iterative schemes for the solution of systems of linear equations (Varga, 1962)

$$x^{i+1} = D^{-1}[b-(L+U)x^i] \tag{4-9}$$

$$x^{i+1} = (L+D)^{-1}[b-Ux^i] \tag{4-10}$$

$$x^{i+1} = (\omega L+D)^{-1}[\omega b+\{(1-\omega)D-\omega U\}x^i] \tag{4-11}$$

where ω is a relaxation factor which lies between 1 and 2, and i is an iteration index. Note that (4-11) reduces to (4-10) when $\omega = 1$. The matrices $M = -D^{-1}(L+U)$ from (4-9), $M = -(L+D)^{-1}U$ from (4-10) and $M = (\omega L+D)^{-1}\{(1-\omega)D-\omega U\}$ from (4-11) are defined as the Jacobi, Gauss-Seidel and successive over-relaxation iteration matrices, respectively. Using the above definitions of the iteration matrices, each

of the previous three iterative methods (4-9 to 4-11) have the general linear form

$$x^{i+1} = Mx^i + b' \qquad (4\text{-}12)$$

A necessary and sufficient condition for convergence of such a linear iterative scheme is that the spectral radius of the iteration matrix M -- $\rho(M)$ -- that is, the largest eigenvalue in absolute value of the iteration matrix M, be less than unity (Varga, 1962). By Gerschgorin's theorem (Varga, 1962; Conte and de Boor, 1972), the spectral radius of the iteration matrix M is less than unity if $|a_{ii}| > \sum_{\substack{j=1 \\ j \neq i}}^{n} |a_{ij}|$ for all i = 1, 2, ... , n, where a_{ii} are the diagonal entries of matrix A; that is, if the matrix A is a diagonally dominant matrix.

4.6 Solution of Non-linear Algebraic Systems

There are no completely general methods for solving arbitrary systems of non-linear equations. Existence and/or uniqueness of such solutions is a largely unanswered question (Rall, 1973). In addition to the complexity of the programming required, there is no guarantee of convergence of the iterations. However, the fact that a system of partial differential equations may be non-linear does not preclude its solution by one of the basic methods presented above in relation to linear algebraic systems. The aim of any finite difference representation is to approximate the non-linear partial differential equation by an algebraic equation which is linear in its unknowns. Remson et al.

(1971) describe some linearization methods for several non-linear problems in subsurface hydrology. Although predictive-corrective schemes (Douglas and Jones, 1963) or three-level schemes (Lees, 1966; Mitchell, 1969) are effective linearization methods, a Picard-type iteration (Remson et al., 1971; Whisler and Klute, 1965) was used here with the objective of keeping the numerical solution scheme as simple as possible. This simplicity criterion is also the reason for using a uniform grid throughout the studied profile. The linearization scheme used -- together with the main steps of the numerical procedure -- are indicated in the following block diagram (Fig. 4-3).

Attempts to solve the system of equations (4-5) directly using matrix inversion techniques failed because the matrices $[D - EG^{-1}F]$ or $[G - FD^{-1}E]$ -- resulting from solving the first or second of the equations (4-5) for ψ or T and replacing the result into the second or first equation respectively -- could not be inverted because they were algorithmically singular matrices. Therefore, the following Gauss-Seidel iteration scheme was used to solve the system of equations (4-5):

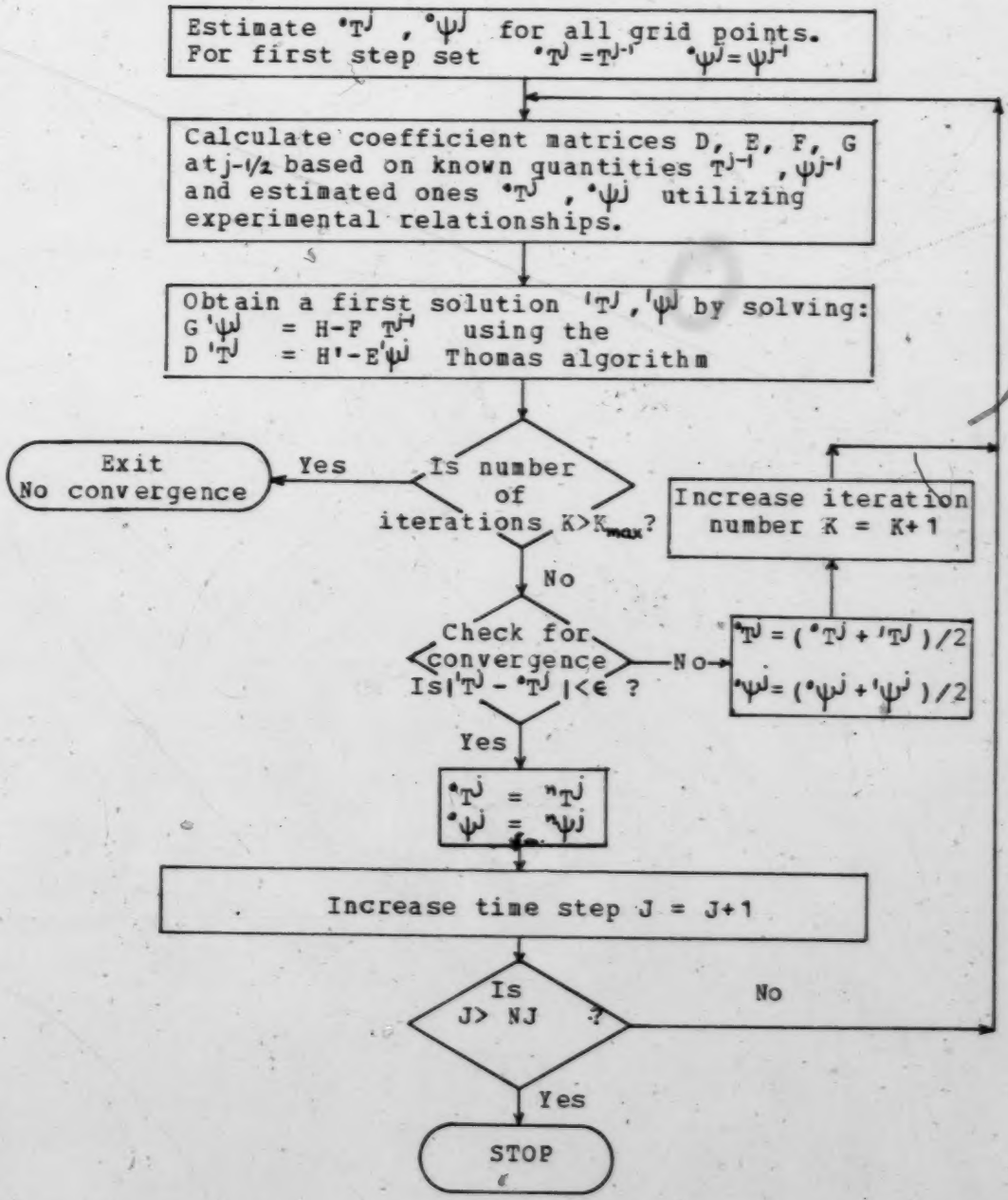
Estimate $^{\circ}T^{j}$, $^{\circ}\psi^{j}$ for all grid points.
For first step set $^{\circ}T^{j} = T^{j-1}$ $^{\circ}\psi^{j} = \psi^{j-1}$
Calculate coefficient matrices D, E, F, G at j-1/2 based on known quantities T^{j-1} , ψ^{j-1} and estimated ones $^{\circ}T^{j}$, $^{\circ}\psi^{j}$ utilizing experimental relationships.
Obtain a first solution $^{1}T^{j}$, $^{1}\psi^{j}$ by solving:
$G\,{}^{1}\psi^{j} = H - F\,T^{j-1}$ using the
$D\,{}^{1}T^{j} = H' - E'\psi^{j}$ Thomas algorithm
Is number of iterations $K > K_{max}$?
Yes
Exit No convergence
Increase iteration number K = K+1
No
Check for convergence Is $|{}^{1}T^{j} - {}^{\circ}T^{j}| < \epsilon$?
No
$^{\circ}T^{j} = (^{\circ}T^{j} + {}^{1}T^{j})/2$
$^{\circ}\psi^{j} = (^{\circ}\psi^{j} + {}^{1}\psi^{j})/2$
Yes
$^{\circ}T^{j} = {}^{n}T^{j}$
$^{\circ}\psi^{j} = {}^{n}\psi^{j}$
Increase time step J = J+1
Is J> NJ ?
No
Yes
STOP

Figure 4-3

$$\begin{bmatrix} G & F \\ E & D \end{bmatrix} \begin{Bmatrix} \psi \\ T \end{Bmatrix} = \begin{Bmatrix} H \\ H' \end{Bmatrix} \xrightarrow[\text{Seidel}]{\text{Gauss}} \qquad (4\text{-}13a)$$

$$\begin{bmatrix} G & 0 \\ E & D \end{bmatrix} \begin{Bmatrix} \psi \\ T \end{Bmatrix}^{j} = \begin{Bmatrix} H \\ H' \end{Bmatrix} - \begin{bmatrix} 0 & F \\ 0 & 0 \end{bmatrix} \begin{Bmatrix} \psi \\ T \end{Bmatrix}^{j-1} \longrightarrow \qquad (4\text{-}13b)$$

$$G\,\psi^{j} = H - F\,T^{j-1} \longrightarrow \psi^{j}$$

Thomas algorithm (4-13c)

$$D\,T^{j} = H' - E\,\psi^{j} \longrightarrow T^{j}$$

As G and D are diagonally dominant tridiagonal matrices, the Thomas algorithm (Carnahan et al., 1969; von Rosenberg, 1969) was used to solve the system of equations (4-13b). This scheme proved to be very fast in converging to a solution. Convergence usually took place within one or two iterations. Thus there was no need to use the successive over-relaxation technique.

4.7 Computer Simulation Program

A listing of the FORTRAN IV computer program used to solve the system of equations (4-5) is presented in Appendix E. All calculations were carried out on the AMDAHL 470V/6 computer of the University of Alberta Computing Services. A brief discussion of some of the features of the computer program follows.

The subsurface profile studied (564 cm deep) was uniformly discretized using 48 nodes (i = 2, ..., 49) of

grid size Δz = 12 cm. The initial water table position was at 300 cm below the surface node i = 2. The general direction of flow was upwards. A time step of 0.5 hr was chosen by a limited trial and error procedure. In most of the early runs, a time step of Δt = 0.2857 hr was used. The entire subsurface profile was assumed to be homogeneous with respect to the thermal conductivity, which in turn was considered a function of water content only. However, with regard to hydraulic conductivity, the saturated domain of the subsurface profile was treated as a heterogeneous medium while the unsaturated domain was treated as homogeneous. In accordance with saturated porous media flow theory (Scott, 1963), saturated hydraulic conductivity between adjacent layers was taken as the harmonic mean of the hydraulic conductivities of the two layers (Fig. 4-4).

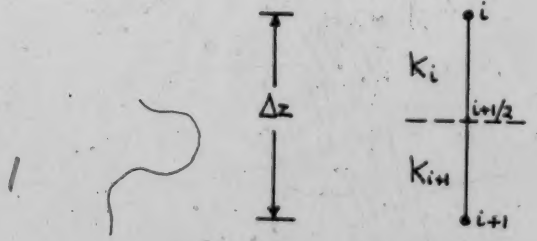

$$K_{i+1/2} = \frac{2\,\Delta z}{\{(\Delta z / K_{i+1}) + (\Delta z / K_i)\}} \qquad (4\text{-}14)$$

Figure 4-4

The saturated zone was divided into three layers (Fig. 4-1) with field-measured hydraulic conductivities of K = 1.256 cm/hr, for the first layer; K = 0.687 cm/hr for the second, and K =0.054 cm/hr for the bottom layer, which indicated the

presence of a loamy lens at that position. Hydraulic conductivities were corrected for the effects of temperature on density and viscosity using the following relationship

$$K(T) = K_{(T_{ref})} \quad (\mu/\rho)_{T_{ref}} \quad (\rho/\mu)_T \qquad (4\text{-}15)$$

where the reference temperature T_{ref} was 10C for the saturated zone and T_{ref} = 20C for the unsaturated zone.

The porous medium was assumed to possess a constant porosity value $\phi = 0.41$ and elastic storage properties that can be effectively represented by the specific storage S_s. The specific storage was assigned a constant value ($S_s = 2 \times 10^{-3}$ cm^{-1}) for the saturated region -- which is an acceptable approximation when the changes in water table elevation occur slowly (McWhorter and Sunada, 1977) -- and zero for the unsaturated zone. In effect, the unsaturated porous medium was assumed to be incompressible.

The top boundary conditions consist of a soil surface temperature specification for the heat flux equation and a prescribed water flux (infiltration or evaporation) for the pressure head equation. The surface temperature may be specified as a sinusoidal wave or as piecewise functions joining measured data. In the case of evaporation condition the user does not have to specify an evaporation flux relation because it is calculated in the program. The evaporation flux is calculated by using the water balance equation (3-21) with the input flux calculated using the non-isothermal flux equation (2-38), and utilizing the water

contents of the current and previous time steps to calculate the time change of moisture content for the top mesh layer.

The bottom boundary water flux was given a range of expected values based on direct or indirect observations of the hydraulic gradient and conductivity of the bottom material. The value assigned to the bottom boundary flux was $w = 0.07$ cm/hr downward. The sign convention followed was negative for upward flow and positive for downward flow. The bottom boundary for the heat flux equation was a zero temperature gradient specification. This gradient was approximated by a forward difference scheme, in contrast to the central difference schemes used generally throughout the computer program to approximate spatial derivatives.

As a convergence criterion, a tolerance of $\epsilon = 0.25$ or 0.3C was used for the computer runs with a $\Delta t = 0.2857$ hr and $\epsilon = 0.5$C for those with a $\Delta t = 0.5$ hr between temperatures calculated during two successive time steps, excluding the surface temperatures. Therefore, if the condition $|T_i^j - T_i^{j-1}| \leq \epsilon$ was satisfied, the computed solution was accepted as valid; otherwise, an iteration cycle was activated (Fig. 4-3). A similar convergence criterion could have been established for the ψ-values. However, judging from the results obtained using only the temperature convergence criterion, such a condition was not considered necessary because the pressure head values may change considerably in a time step, especially during

infiltration into a dry soil. The numerical scheme I used proved to be very fast in converging to the above requirements with only one or two iterations. If the number of iterations exceeded a prescribed number K_{max} without convergence, the procedure was stopped with appropriate messages printed (Fig. 4-3). The computer simulation was also stopped and a warning message printed if the value of the bottom node became negative.

Because of the banded nature of the square matrices D, E, F, G (4-5c) with one upper and one lower diagonal, these matrices were stored row-wise (band storage mode) so that the zero elements were compressed out of the matrices. Thus, the above nxn matrices were reduced to nx3 matrices with the diagonal elements falling into the second column. Equation (4-5) shows an example of the band storage mode used to minimize computer memory requirements.

$$\underset{[nxn]}{\begin{bmatrix} a_{11} & a_{12} & 0 & 0 & 0 & 0 \\ a_{21} & a_{22} & a_{23} & 0 & 0 & 0 \\ 0 & a_{32} & a_{33} & a_{34} & 0 & 0 \\ 0 & 0 & a_{43} & a_{44} & a_{45} & 0 \\ 0 & 0 & 0 & a_{54} & a_{55} & a_{56} \\ 0 & 0 & 0 & 0 & a_{65} & a_{66} \end{bmatrix}} \xrightarrow{\text{stored as}} \underset{[nx3]}{\begin{bmatrix} 0 & a_{11} & a_{12} \\ a_{21} & a_{22} & a_{23} \\ a_{32} & a_{33} & a_{34} \\ a_{43} & a_{44} & a_{45} \\ a_{54} & a_{55} & a_{56} \\ a_{65} & a_{66} & 0 \end{bmatrix}} \quad (4\text{-}16)$$

The simulation program can be controlled by the user in the following ways. By setting the computer input parameter

KODE1 equal to 1 or 0, the bottom boundary condition can be specified as recharge or discharge. By setting KODE5 equal to 0 or 1, the top boundary can be specified as evaporation or infiltration. In a similar way, by putting KODE4 equal to 0 or 1, the user may specify a problem either in an uncoupled (isothermal) or coupled (non-isothermal) transient (unsteady) form. KODE2 = i, where i = 1, 2, ..., NJ (NJ = number of time steps) specifies the number of time steps that may be skipped before the result is printed.

At the beginning of the programming effort, balance equations were used to derive the hydraulic conductivity functions. The water flux was calculated from the measured time change of water content and the known water flux at the bottom of the top mesh layer. A similar balance equation was also used to calculate the heat flux from the measured time change of the soil heat content with the bottom heat flux calculated from the thermal conductivity and temperature gradient. However, these schemes, especially the latter one, resulted in numerical oscillations and inaccuracies. Therefore, the field approach proposed in Chapter 2 was not implemented in the present computer program.

As a consequence of the above development, the transport coefficients involved in the system of equations (4-1) were estimated analytically as shown in Chapter 2. In order to increase the accuracy of such calculations, I used double precision arithmetic throughout the program. Because

of uncertainties surrounding the D_{Tl} coefficient for saturated conditions mentioned in Chapter 2 (p. 29), and in order to simplify the numerical calculations somewhat, the thermal diffusion coefficient D_T was assumed equal to zero under saturated conditions. This assumption does not seem unreasonable in view of the small temperature gradients observed in the saturated zone under study and of its small thickness; also the limited number of relevant data in the saturated zone severely limited direct use of the quantity $\partial\psi/\partial T$ (2-31) by introducing considerable errors.

The ratio ζ of the average temperature gradient in air-filled pores to the overall temperature gradient, which appears in the expression of D_{Tv} coefficient (2-18), has to be specified. The following values were adopted from data provided by Philip and de Vries (1957) and Rose (1968a, b). For $T \leq 25C$, $\zeta = 1.8$, and for $T > 25C$, $\zeta = 1.3$. It should be noted that a conservative point of view was adopted in choosing the ζ values and in incorporating Rose's ξ coefficient -- the liquid-assisted vapor enhancement factor -- into the pore geometry factor f. The computer program provides for both ψ-based and θ-based equations discussed in previous chapters.

Experimentally determined input data to the simulation model include:

-- initial distribution of temperature and pressure head with depth (usually supplied as graphically smoothed

curves);

-- time distribution of surface temperatures. (As mentioned in Chapter 3, the measured soil temperatures at a depth of less than 1 cm were taken as surface temperatures);

-- characteristic function(s) -- ψ vs θ ;

-- hydraulic conductivity function(s) -- K vs θ (this function may be optional because the user may decide to use the water balance equation for calculating K built into the model);

-- thermal conductivity-water content relationship -- λ vs θ;

-- distribution of volumetric percentages of organic matter and mineral matter with depth.

The data from the characteristic and hydraulic conductivity functions, from the thermal conductivity-water content relation, and from a series of table look-up data sets appearing in the program -- such as the relationships μ vs T, ρ vs T, L' vs T, p_v^s vs T, c_ℓ vs T and D_α vs T -- were calculated using the cubic spline interpolation (Ahlberg et al., 1967; Conte and de Boor, 1972). This interpolation method provided a relatively simple, continuous and smooth curve through all points of interest. Thus, values at some unknown points can be evaluated and many common operations, such as differentiation and integration, can be easily performed.

The output of the program consists of a list of some

physical parameters for the system, such as the section length studied, the gas constant, the specific storage value, and others; numerical information, such as the maximum simulation time, the size and number of time and space increments, the maximum number of allowable iterations, and others; a list of top boundary time-temperature distribution and initial depth distribution of ψ, θ and T; the calculated temperature, pressure head and moisture distribution, as well as all transport coefficients and heat and water fluxes.

As the above discussion may suggest, this simulation model is general and flexible. It can handle any type of boundary conditions, heterogeneities, saturated-unsaturated regions, isothermal and non-isothermal environments, transient and steady-state systems.

4.8 Program Verification

The overall error of a simulation result may be considered as the sum of errors introduced by the numerical finite difference analog and/or errors introduced by possible inadequacies of the theoretical framework in describing the particular phenomena. Although the validity of the uncoupled (isothermal) equations is supported by a considerable body of literature, the correspondence of the coupled non-isothermal equations to the physical processes has not been well established. Such uncertainties are mainly

due to the relative scarcity of studies verifying the validity of the non-isothermal coupled models, especially under field conditions. As I will point out in the final chapter, considerable research is still needed to verify several aspects of such systems. However, this study and others (Rose, 1968a, b, c; Jackson et al., 1974, 1975) support its general validity. Therefore, I will assume that errors in the solution are introduced by the numerical algorithm used in the present study and not by the mathematical model.

Because numerical techniques introduce instabilities, truncation and round-off errors in approximating the solution, it is necessary to check the solution with experimental data and/or a theoretical (analytical) solution. Therefore, the uncoupled equations of heat and water with constant coefficients -- for which analytical solutions are available -- were considered for this purpose in order to give an indirect check on the validity of the coupled equations.

A limited number of analytical solutions are available for the complete heat transport equation. However, no truly analytical solutions for the moisture equation are available (Guymon and Luthin, 1974). Kirkham and Powers (1972) summarize some of Philip's (1969) approximate solution techniques of uncoupled moisture problems. Therefore, in order to check the validity of the numerical method, the

transient uncoupled heat equation with constant coefficients was solved using the same computer model. The results were compared with the analytical solutions described, for example, in Carslaw and Jaeger (1959) or in Ingersoll et al., (1954). Specifically, the following heat conduction problem was considered:

$$C\,\partial T/\partial t = \partial(\lambda\,\partial T/\partial z)/\partial z = \lambda(\partial^2 T/\partial z^2) \qquad (4\text{-}17a)$$

$$\partial T/\partial t = (\lambda/C)\,\partial^2 T/\partial z^2 = \alpha\,\partial^2 T/\partial z^2 \qquad (4\text{-}17b)$$

where α is the thermal diffusivity (cm^2/hr) with the following boundary and initial conditions:

$$T = 0C \text{ @ } z = 0$$

$$T = 0C \text{ @ } z = L \qquad (4\text{-}17c)$$

$$T = T_o = 10C \text{ @ } t = 0$$

The analytical solution to the above problem is (Carslaw and Jaeger, 1959):

$$T = (4T_o/\pi)\sum_{n=0}^{\infty}\left(\frac{1}{2n+1}\right)e^{-\alpha(2n+1)^2\pi^2 t/L^2}\sin\frac{(2n+1)\pi z}{L} \qquad (4\text{-}18a)$$

or

$$T = (4T_o/\pi)\left\{e^{-\pi^2\alpha t/L^2}\sin\frac{\pi z}{L} + \frac{1}{3}e^{-9\pi^2\alpha t/L^2}\sin\frac{3\pi z}{L} + \frac{1}{5}e^{-25\pi^2\alpha t/L^2}\sin\frac{5\pi z}{L} + \cdots\right\} \qquad (4\text{-}18b)$$

Using the following representative input data, $\alpha = \lambda/C = 8/0.5 = 16\ cm^2/hr$ and $L = 564$ cm, one finds that for $t = 24$ hr and $z = 36$ cm, for example, the analytical solution -- using the terms shown in (4-18b) -- is $T_{(z=36,\,t=24)} \simeq 8.07C$, while the numerical solution obtained using the present program with a time step $\Delta t = 0.2857$ hr was $T_{(z=36,\,t=24)} = 8.05C$. The agreement between the two is, therefore, excellent (relative error $\simeq 0.25\%$) suggesting that the uncoupled transport equations are solved correctly. Figure

4-5 shows the initial and simulated transient temperature-depth distribution for the conduction problem (4-17) considered here.

The simulation results were also compared with observed field data. Figures 4-6 and 4-7 compare field and simulated results. In all those figures the input depth distribution of temperature or moisture in the early afternoon of August 13th, 1976 at Site 2 are shown with the continuous curves. If one keeps in mind that in the field the unsaturated domain included some discontinuous clay loam lenses but that the simulation model assumed a homogeneous unsaturated zone, the simulated results are in satisfactory agreement with the observed data.

The present modeling study does not represent an exhaustive numerical treatment. Because of the inherent complexity of the numerical problem and the amount of storage and computing time required, the number of cases that could be run economically were somewhat limited. The maximum time for any one simulation trial was one week. The difference equations (4-4) become the original differential equations (4-1) as Δz tends to dz and Δt to dt. Therefore, the accuracy of the finite difference approximation is a function of the fineness of the time and spatial grids used in the solution, subject to computational limitations, such as truncation and round-off errors. However, in order to use the available computer funds most efficiently, rather coarse

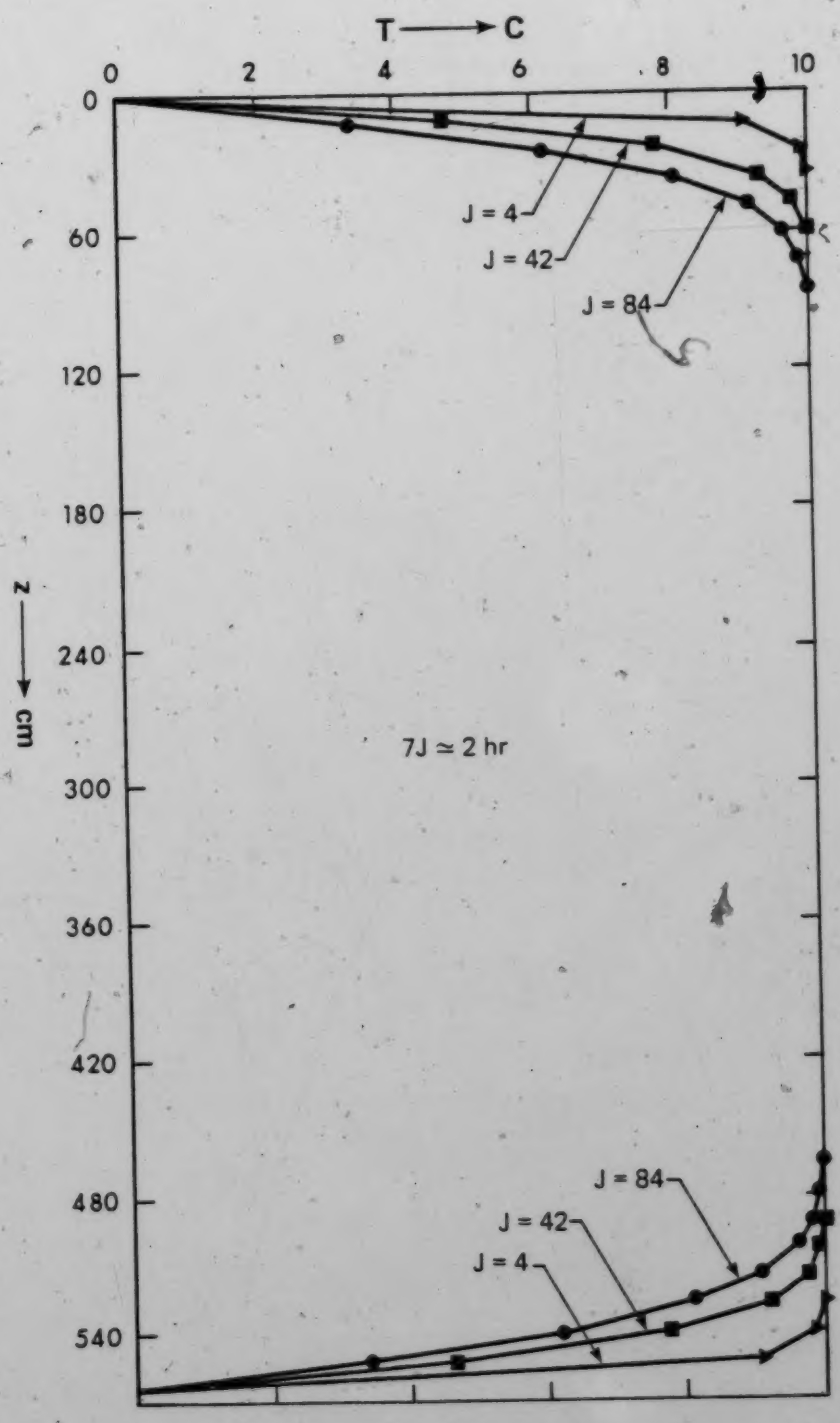

Figure 4-5. Time distribution of temperature for the conduction problem

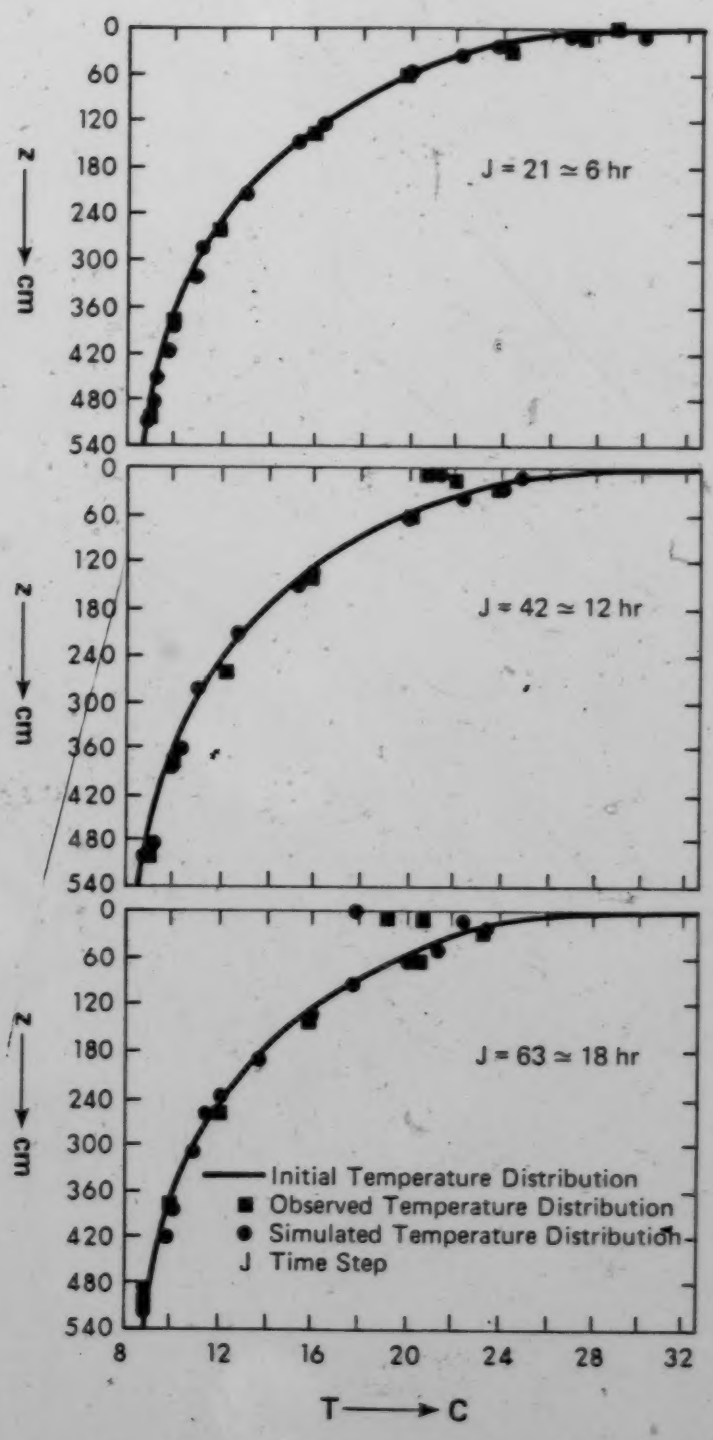

Figure 4-6. Comparison of observed and simulated temperature distributions

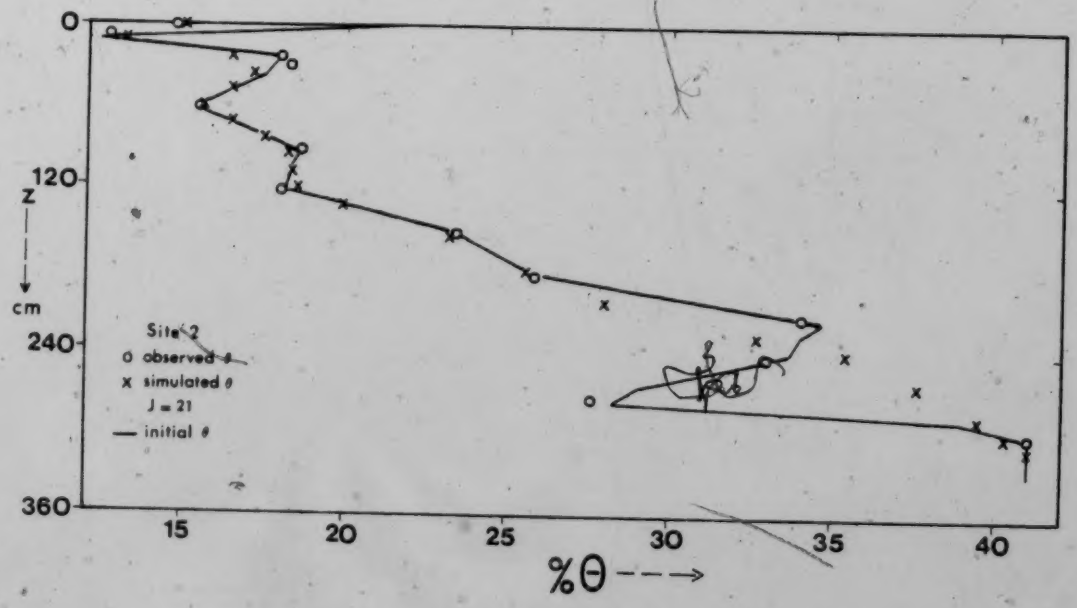

Figure 4-7. Comparison of observed and simulated moisture distributions

grid systems were used to reduce the storage and time requirements. A computer simulation run of 168 hr (one week) with a time step of 0.5 hr used approximately 25 sec of CPU time in the University's fast AMDAHL computer; while, the 24 hr runs with a time step of 0.2875 hr (with some minor later modifications) used approximately 12 to 13 sec.

Owing to the non-linear nature of the present coupled problem, caution should be exercised in using abrupt imposed boundary changes. It may only be possible to handle these by significant reductions in the time step. However, abrupt change may lead to more serious problems such as the divergence of the solution. For better and faster results, the input data sets should be representative, continuously varying and smoothed.

4.9 Results and Discussion

A limited number of simulation problems were solved using the computer simulation program described above. In every case, both the isothermal (uncoupled) and non-isothermal (coupled) models were used in order to evaluate possible coupling effects. Three different initial conditions were used in studying the drying or evaporation problem. These initial conditions are shown in Fig. 4-8; the corresponding computer runs are referred to as Run 1, Run 2 and Run 3. The upper boundary temperature-time distributions used for these simulations are shown in Fig. 4-9. Table 4-1

summarizes the conditions for each run. A list of some physical parameters and numerical information for these simulation runs are shown in Table 4-2.

Using the initial conditions for Run 1 (wet condition with field observed but smoothed data) and for Run 2 (dry condition) indicated above, no appreciable changes in the temperature field occurred by coupling or uncoupling the system of equations (4-1) for short time simulations. However, significant differences were observed in the evaporation and moisture fluxes as indicated in Tables 4-3 and 4-4.

It should be noted in those tables that the evaporation and moisture fluxes computed from the uncoupled equations are higher than the ones computed from the coupled equations, and that the difference is greater when the water contents are at intermediate levels (Run 1). This situation holds true as long as the normal temperature gradients prevail in the soil; that is, when the higher temperatures are at the top and decrease with depth, in opposition to the potential gradients observed at the field sites. Thus, a small flow is set up opposite the potential gradient to slow the drying rate. However, during the diurnal cycle, when temperature gradients are reversed, the opposite holds true, as shown in Tables 4-5 and 4-6.

Figures 4-10 and 4-11 indicate a much faster decrease of K_ψ with decreasing water content than the one of D_T

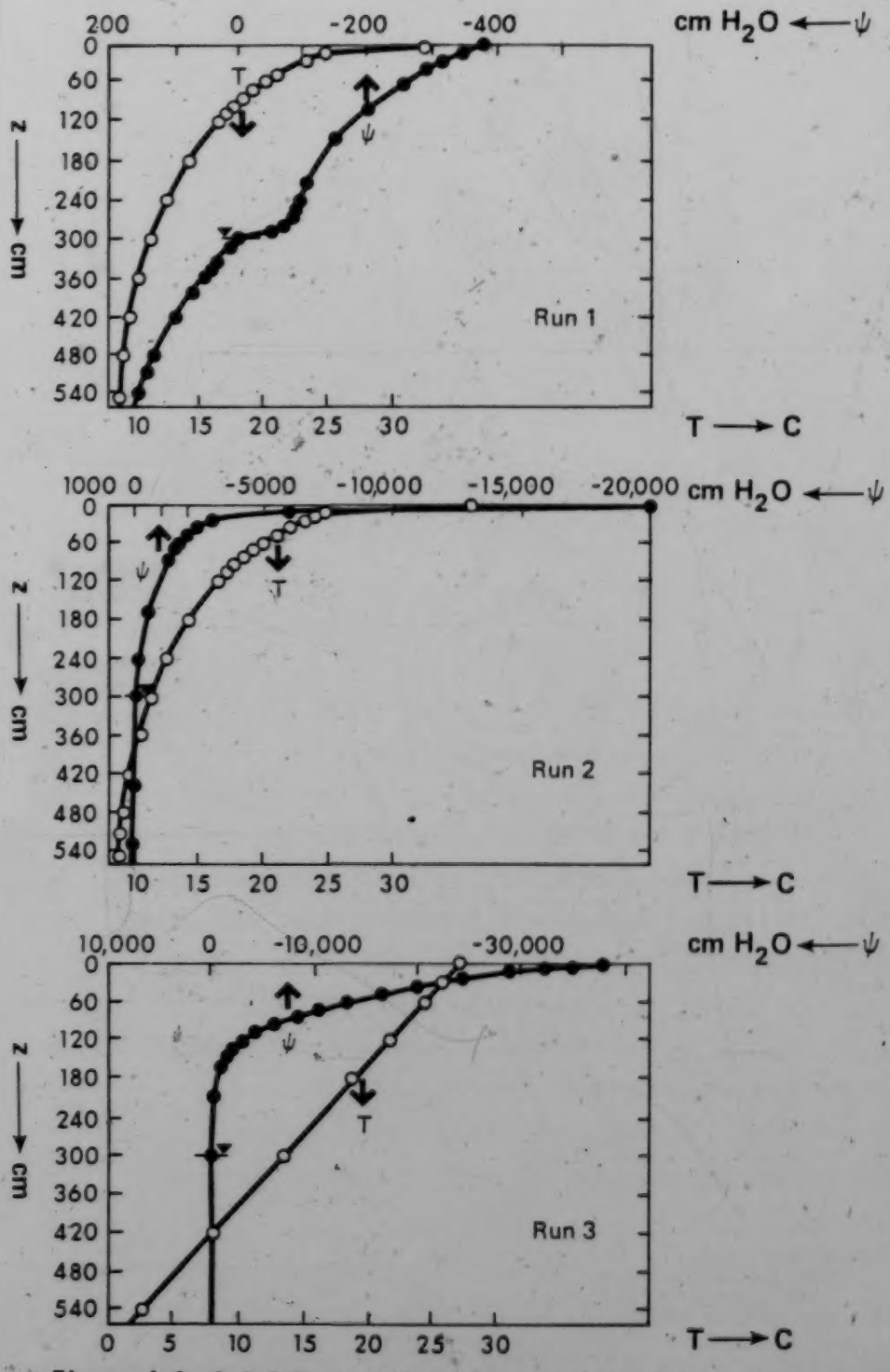

Figure 4-8. Initial conditions for case simulation runs

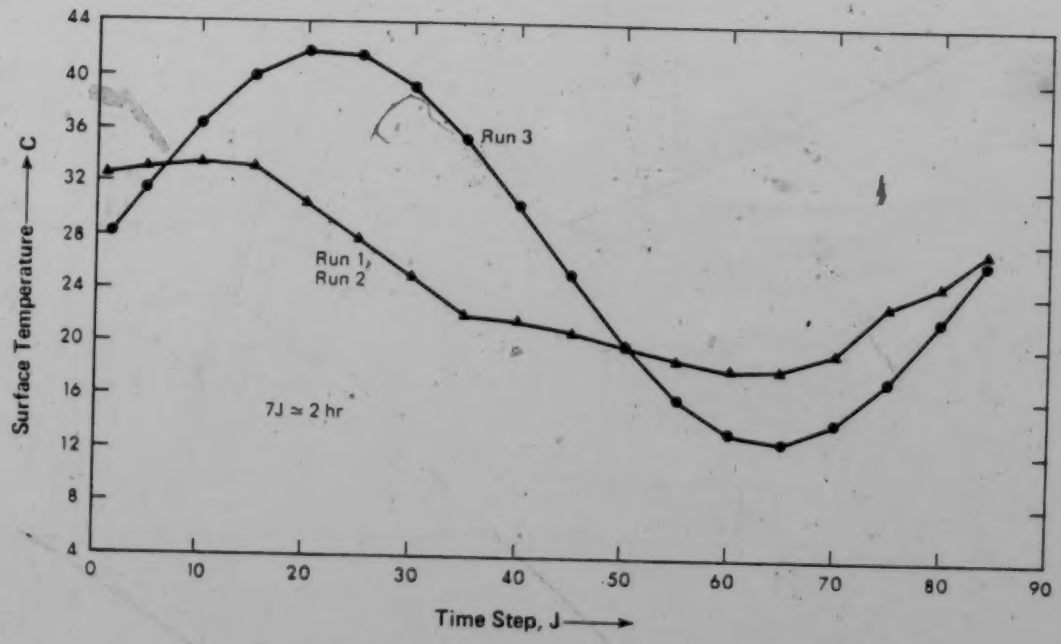

Figure 4-9. Upper boundary time distribution of temperature for case simulation runs

TABLE 4-1

Conditions for case simulation runs

Run	Moisture conditions	$\psi(z)$ data	T(z) data	T(t) data
1	wet	observed-smoothed	observed-smoothed	observed
2	dry	simulated	observed-smoothed	observed
3	very dry	simulated	simulated	simulated

TABLE 4-2

Sample output information from simulation runs

LIST OF PHISICAL PARAMETERS FOR THE SYSTEM

GAS CONSTANT (ERG/DEG.C-MOL)	83143200.0
MOLECULAR WT. OF WATER (GM/MOL)	18.0
SPECIFIC STORAGE(CM**-1)	0.2000000D-02
SECTION LENGTH(CM)	564.0
ACCELERATION OF GRAVITY(CM/SEC**2)	980.665
REFERENCE TEMP.(DEG.C)	10.000
WATER DENSITY AT REF.TEMP.(GM/CC)	0.99973
WATER VISCOSITY AT REF.TEMP.(GM/CM-HR)	47.052

NUMERICAL INFORMATION

MAXIMUM SIMULATION TIME (HR)	24.00000
SIZE OF TIME INCREMENT(HR)	0.2857143
NUMBER OF TIME INCREMENTS	84
NUMBER OF SPACE NODES	49
SIZE OF SPACE INCREMENTS(CM)	12.000
EPSILON	0.3000
MAXIMUM NUMBER OF ITERATIONS	10

TABLE 4-3

Comparison of evaporation fluxes calculated using the coupled and uncoupled equations for Runs 1 and 2. Soil temperatures decreasing with depth.

Initial conditions	Time step J*	Coupled EV**	Uncoupled EV	$\left(\frac{\text{EV uncoupled}}{\text{EV coupled}}\right)$
Run 1	15	-0.7415×10^{-3}	-0.1551×10^{-2}	2.09
	16	-0.7935×10^{-3}	-0.1552×10^{-2}	1.96
	17	-0.8638×10^{-3}	-0.1553×10^{-2}	1.80
	18	-0.9408×10^{-3}	-0.1553×10^{-2}	1.65
	19	-0.1019×10^{-2}	-0.1553×10^{-2}	1.52
	20	-0.1095×10^{-2}	-0.1552×10^{-2}	1.42
	21	-0.1169×10^{-2}	-0.1551×10^{-2}	1.33
Run 2	15	-0.7366×10^{-2}	-0.7752×10^{-2}	1.05
	16	-0.7412×10^{-2}	-0.7776×10^{-2}	1.05
	17	-0.7464×10^{-2}	-0.7798×10^{-2}	1.04
	18	-0.7518×10^{-2}	-0.7817×10^{-2}	1.04
	19	-0.7571×10^{-2}	-0.7833×10^{-2}	1.03
	20	-0.7622×10^{-2}	-0.7847×10^{-2}	1.03
	21	-0.7669×10^{-2}	-0.7857×10^{-2}	1.02

*7J ~ 2 hr
**EV = evaporation flux in cm/hr

TABLE 4-4

Comparison of moisture fluxes calculated using the coupled and uncoupled equations for Runs 1 and 2. Soil temperatures decreasing with depth.

Initial conditions	Node	Depth (cm)	Coupled q_w/ρ @ J=21 (cm/hr)	Uncoupled q_w/ρ @ J=21 (cm/hr)	$\left(\frac{q_w/\rho \mid \text{uncoupled}}{q_w/\rho \mid \text{coupled}}\right)$
Run 1	2	0	-0.1169×10^{-2}	-0.1551×10^{-2}	1.33
	3	12	-0.1099×10^{-2}	-0.1485×10^{-2}	1.35
	4	24	-0.9351×10^{-3}	-0.1303×10^{-2}	1.39
	5	36	-0.8335×10^{-3}	-0.1050×10^{-2}	1.26
	6	48	-0.6808×10^{-3}	-0.8413×10^{-3}	1.24
2	2	0	-0.7669×10^{-2}	-0.7857×10^{-2}	1.02
	3	12	-0.4761×10^{-2}	-0.4899×10^{-2}	1.03
	4	24	-0.1245×10^{-2}	-0.1387×10^{-2}	1.11
	5	36	-0.5071×10^{-3}	-0.5844×10^{-3}	1.15
	6	48	-0.2699×10^{-3}	-0.3208×10^{-3}	1.19

TABLE 4-5

Comparison of evaporation fluxes calculated using the coupled and uncoupled equations for Runs 1 and 2. Soil temperatures increasing with depth.

Initial conditions	Time step J*	Coupled EV**	Uncoupled EV	$\left(\frac{\text{EV uncoupled}}{\text{EV coupled}}\right)$
Run 1	64	-0.1830×10^{-2}	-0.1366×10^{-2}	0.746
	65	-0.1805×10^{-2}	-0.1362×10^{-2}	0.755
	66	-0.1770×10^{-2}	-0.1359×10^{-2}	0.768
	67	-0.1773×10^{-2}	-0.1357×10^{-2}	0.765
	68	-0.1694×10^{-2}	-0.1354×10^{-2}	0.799
	69	-0.1656×10^{-2}	-0.1352×10^{-2}	0.816
	70	-0.1620×10^{-2}	-0.1350×10^{-2}	0.833
Run 2	37	-0.7689×10^{-2}	-0.7619×10^{-2}	0.991
	38	-0.7836×10^{-2}	-0.7585×10^{-2}	0.968
	39	-0.7800×10^{-2}	-0.7550×10^{-2}	0.968
	40	-0.7762×10^{-2}	-0.7514×10^{-2}	0.968
	41	-0.7722×10^{-2}	-0.7477×10^{-2}	0.968
	42	-0.7681×10^{-2}	-0.7440×10^{-2}	0.969

*7J → 2 hr
**EV = evaporation flux in cm/hr

TABLE 4-6

Comparison of moisture fluxes calculated using the coupled and uncoupled equations for Runs 1 and 2. Soil temperatures increasing with depth.

Initial conditions	Node	Depth (cm)	Coupled q_w/ρ (cm/hr)	Uncoupled q_w/ρ (cm/hr)	$\left(\frac{q_w/\rho\|\text{unc.}}{q_w/\rho\|\text{coupled}}\right)$
Run 1 (J* = 70)	2	0	-0.1620×10^{-2}	-0.1350×10^{-2}	0.833
	3	12	-0.1522×10^{-2}	-0.1310×10^{-2}	0.861
	4	24	-0.1306×10^{-2}	-0.1229×10^{-2}	0.941
Run 2 (J* = 42)	2	0	-0.7681×10^{-2}	-0.7440×10^{-2}	0.969
	3	12	-0.4626×10^{-2}	-0.4560×10^{-2}	0.986

*TJ = 2 hr

(p. 160 and thereafter). These figures, in conjunction with the moisture flux equation (2-38)[1], show that the drier the soil becomes the more dominant the second term B in (4-19) becomes. Therefore, under very dry conditions and with the temperature decreasing with depth, the positive (downward) term B in (4-19) exceeds the negative (upward) term A in magnitude. As a consequence, evaporation becomes positive; that is, a condensation effect results. This situation was simulated by imposing the initial and top boundary conditions of Run 3 (Figs. 4-8 and 4-9) consisting of a highly negative ψ distribution with depth, coupled with high surface temperatures and a constant initial temperature gradient of 0.55 C/cm throughout. A sample of simulated results are shown in Tables 4-7 and 4-8.

The transport coefficients used in this model differ from the familiar form of Philip and de Vries' (1957) coefficients in that they are derived from the more general ψ-based equations. As can be seen in Fig. 4-10, the model-calculated $K_{\psi v}$ values (2-17) are extremely small. However, in the range of water contents where the soil relative humidity h is below 100%, the considerable increase of the pressure head gradient $\partial\psi/\partial z$ will cause the product $(K_{\psi v}\, \partial\psi/\partial z)$ appearing in (4-1) to rise to a maximum value

---

[1]In one-dimensional form, this equation becomes

$$q_w/\rho = \underbrace{-\, K_\psi\, \partial\psi/\partial z}_{A} \quad \underbrace{-\, D_T\, \partial T/\partial z}_{B} \quad \underbrace{+\, Ki}_{C} \qquad (4\text{-}19)$$

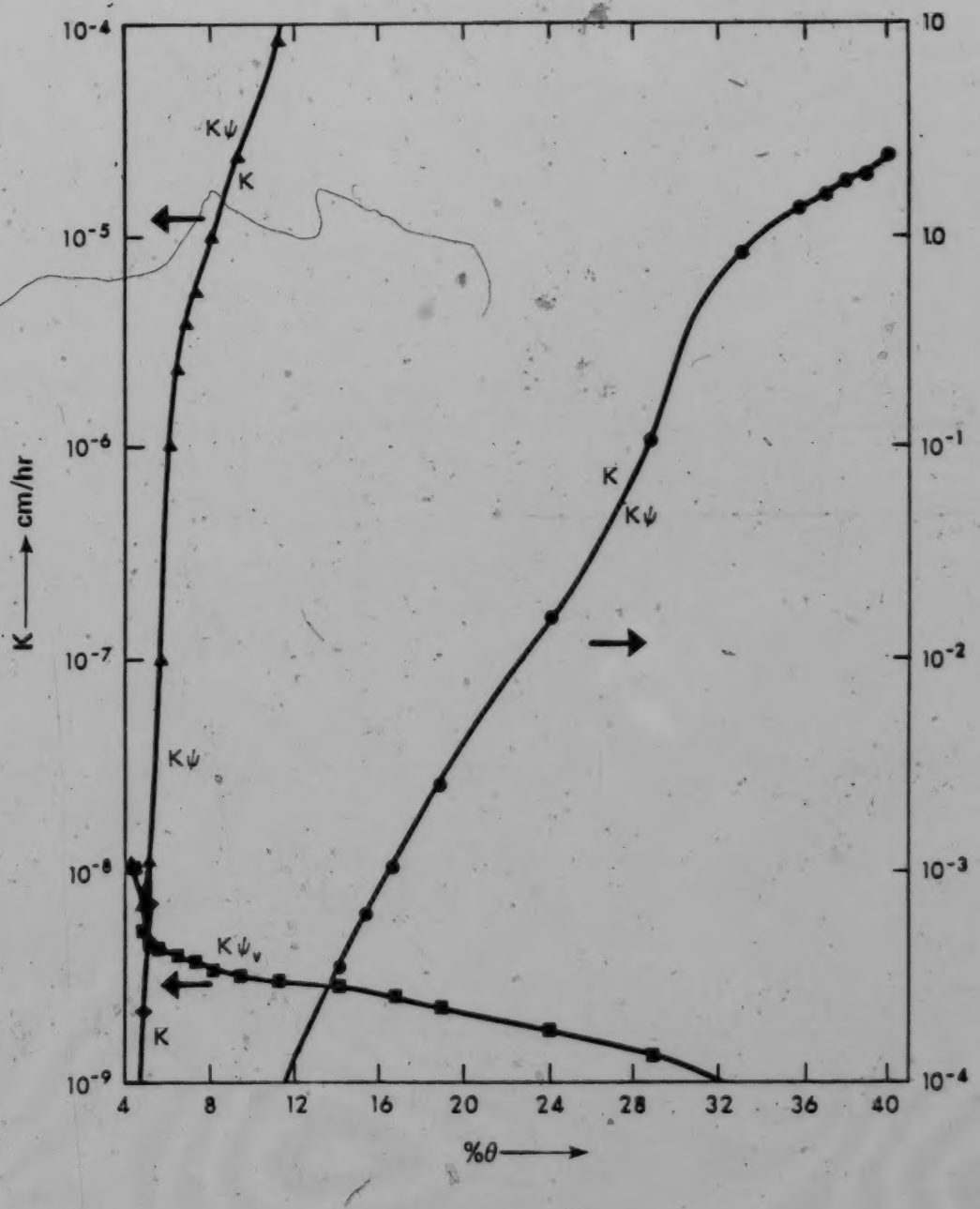

Figure 4-10. Total water (hydraulic) conductivity function K_ψ (θ)

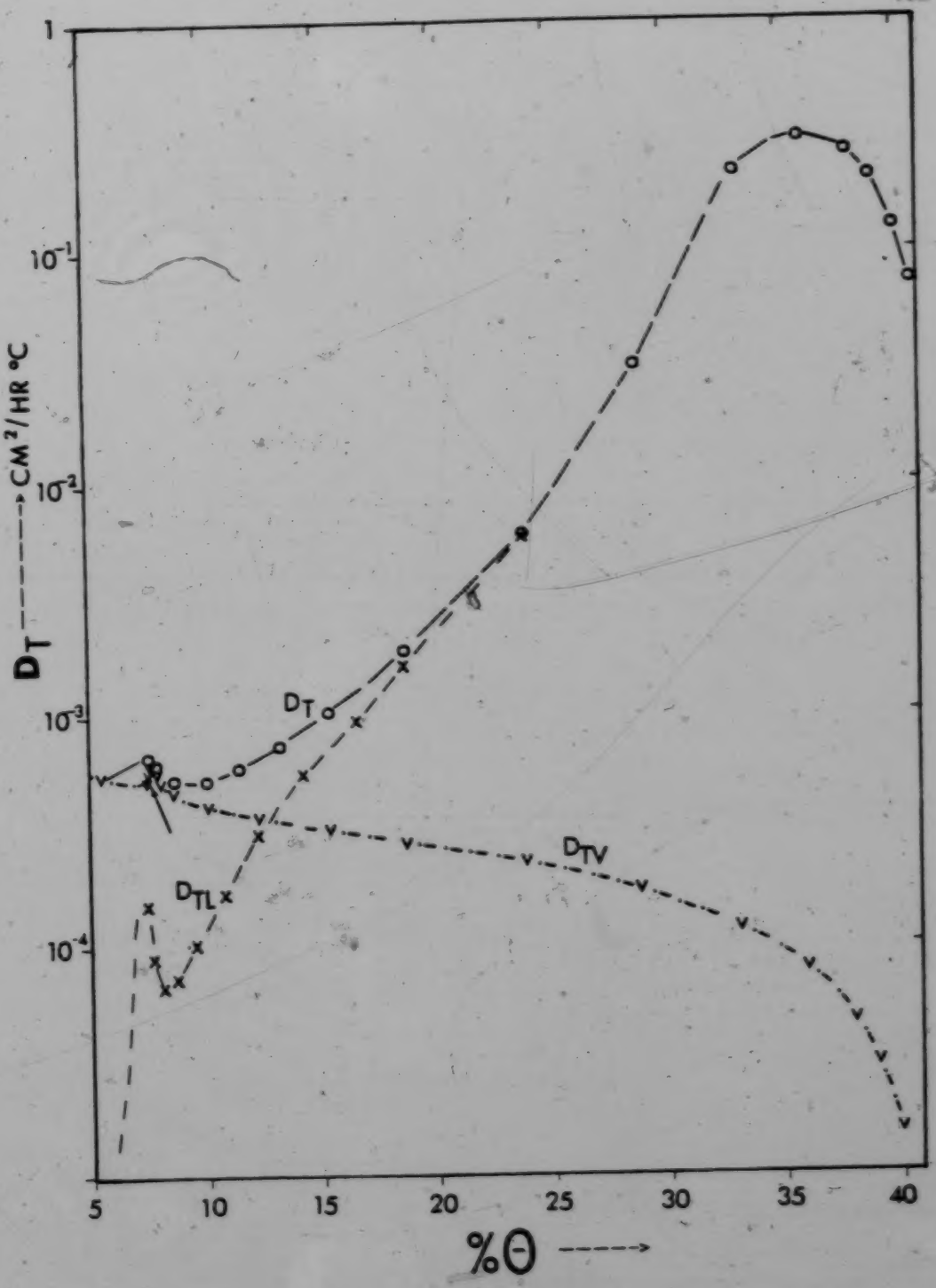

Figure 4-11. Thermal diffusivity function D_T (θ)

TABLE 4-7

Comparison of evaporation fluxes calculated using the coupled and uncoupled equations for Run 3

Time step, J*	Coupled EV**	Uncoupled EV
3	0.3596×10^{-4}	-0.1212×10^{-5}
4	0.4794×10^{-4}	-0.1311×10^{-5}
5	0.4829×10^{-4}	-0.1384×10^{-5}
6	0.3893×10^{-4}	-0.1440×10^{-5}
7	0.2115×10^{-4}	-0.1482×10^{-5}

*7J → 2 hr
**EV = evaporation flux in cm/hr

TABLE 4-8

Comparison of moisture fluxes calculated using the coupled and uncoupled equations for Run 3

Node	Depth (cm)	Coupled q_w^*/ρ @ J = 7	q_v^{**}/ρ @ J=7***	Uncoupled q_w/ρ @ J = 7
2	0	0.2115×10^{-4}	0.2828×10^{-3}	-0.1482×10^{-5}
3	12	0.1536×10^{-3}	0.1545×10^{-3}	-0.9405×10^{-6}
4	24	0.2159×10^{-4}	0.2402×10^{-4}	-0.2474×10^{-5}
5	36	-0.1124×10^{-4}	0.1997×10^{-4}	-0.3152×10^{-4}
6	48	-0.2718×10^{-3}	0.1955×10^{-4}	-0.2941×10^{-3}

*q_w/ρ = moisture flux in cm/hr
**q_v/ρ = vapor flux in cm/hr
***7J ⇒ 2 hr

before eventually falling to zero as θ, and therefore h, approach zero. Notice in Fig. 4-10 that K_{ψ_v} dominates over K at very low moisture contents.

The thermal diffusion coefficients calculated from the model are shown in Fig. 4-11. The D_{Tv} coefficient increases continuously with decreasing moisture content and becomes the dominant thermal diffusion coefficient at low moisture contents, as can be seen in the figure. The break in slope in the D_{Tv} - θ curve (marked by an arrow in the figure) is due to the break-up of the ζ-values used in this program (p. 141). As mentioned before, there is some uncertainty in the determination of $D_{T\ell}$ coefficient, as proposed by the Philip and de Vries surface tension model (p. 29). Values of the $D_{T\ell}$ coefficient computed from (2-37) were compared with the values obtained by the Philip and de Vries model (2-35) and were found 37% to 41% larger than the latter, as shown in Table 4-9. My approximation seems to be a better one in view of the fact that experimentally measured values of D were up to twice (Wilkinson and Klute, 1962) or more as large (Jury and Miller, 1974) as those computed by the Philip and de Vries model. The $D_{T\ell}$ coefficient (Fig. 4-11) increases with increasing water content before starting to rapidly decrease near saturation.

An explanation of this $D_{T\ell}$ coefficient pattern is as follows (Joshua and de Jong, 1973). Most of the observed deviations of water flux in porous media from Darcy's law

TABLE 4-9

Comparison of D_{T1} values computed using the presently proposed model and Philip and de Vries's for Run 1

θ *	${}^1D_{T1}$**	${}^2D_{T1}$** (Ph.& de V.)	${}^1D_{T1} / {}^2D_{T1}$
0.1579	1.023×10^{-3}	6.417×10^{-4}	1.59
0.1631	1.081×10^{-3}	6.711×10^{-4}	1.61
0.1679	1.180×10^{-3}	7.283×10^{-4}	1.62
0.2360	5.868×10^{-3}	3.529×10^{-3}	1.66
0.2945	4.396×10^{-2}	2.625×10^{-2}	1.67
0.3796	2.746×10^{-1}	1.633×10^{-1}	1.68
0.4069	7.900×10^{-2}	4.692×10^{-2}	1.68

*J = 21

**D_{T1}: $cm^2/hr/C$

are attributed to interactions between the water and the porous medium (Swartzendruber, 1969). This interaction is proportional to the area of contact between the porous medium and liquid water and increases as the medium pore sizes decrease. Hence, as the water content in the soil decreases, the proportion of water flow that occurs in the smaller pores increases and thus soil-water interaction increases. In general, coupling phenomena are also pronounced when interaction between the fluid and the porous medium occurs. This phenomenon can be demonstrated by the increase in thermally induced water flow which occurs with increasing soil dryness, a case presented in this thesis. When soil-water flow takes place at high water contents, a large proportion of this flow occurs through the larger pores, thereby minimizing the effect of soil-water interaction. Therefore, the decrease in $D_{T\ell}$ at high water contents may be attributed to low soil-water interaction. However, at very low water contents, when vapor flow becomes of importance, the largest proportion of vapor flow would occur in the large air-filled pores; thus, little coupling between heat and moisture can be expected.

Dirksen (1969) tried to apply the above observations to saturated clay suspensions. He reasoned that by decreasing the water content of these saturated clay suspensions by increasing the compaction pressure, the temperature gradients would become more effective than hydraulic gradients in causing water to move within compacted

sediments. Although he observed an increase in thermally induced flow with increasing compaction pressure, the amount of such flow in his experiments was generally less than that reported for liquid water in unsaturated soils at comparable water contents. This result was attributed to the influence of the vapor phase which is absent under saturated conditions.

The calculated secondary maximum in the $D_{T\ell} - \theta$ relationship (Fig. 4-11) at the low water content range is due to the faster relative increase of $|\ln h|$ with decreasing water content compared to a slower relative decrease of K in that range of water contents (2-37). Data to check the physical significance of this observation are not available.

The transport coefficient D_L (4-1c) appearing in (4-1b) is usually extremely small in magnitude. As can be seen in Fig. 4-12, it increases significantly at low moisture contents. This increase -- combined with a large increase in the pressure head gradient $\partial\psi/\partial z$ -- will cause this latent heat flux component ($D_L \partial\psi/\partial z$) appearing in (4-1b) to reach a maximum value before eventually falling to zero as θ approaches zero.

The temperature field in the simulation runs presented here was not appreciably influenced by coupling or uncoupling because in the range of water contents over which most of the simulations were run, that is, above 5% by

TABLE 4-10

Comparison of conductive and convective heat flux components for Run 3

θ *	| QCD |**	| QCV |***	%(|QCV/QCD|)
0.0610	1.236×10^{-1}	1.551×10^{-4}	0.12
0.0762	1.355×10^{-1}	4.722×10^{-4}	0.35
0.0929	1.632×10^{-1}	6.665×10^{-4}	0.41
0.1124	1.754×10^{-1}	1.194×10^{-3}	0.68
0.1886	5.701×10^{-1}	1.566×10^{-2}	2.75
0.2410	5.966×10^{-1}	2.513×10^{-2}	4.21
0.2882	3.768×10^{-1}	2.524×10^{-2}	6.70
0.3311	3.894×10^{-1}	3.436×10^{-2}	8.82
0.3701	6.896×10^{-1}	3.728×10^{-2}	5.41
0.3904	9.568×10^{-1}	3.533×10^{-2}	3.69

* J = 21

** $|QCD| = |\lambda \partial T/\partial z|$ $(cal/cm^2/hr)$

*** $|QCV| = |c_1 q_w \Delta T|$; $\Delta T = |T_{i+1} - T_i|$
$(cal/cm^2/hr)$

volume, the conductive term of the heat flux equation (2-58) was dominant over the latent and convective terms of the total heat flux. Under very dry conditions, however, the latent heat term of the heat flux equation (2-58) becomes increasingly important. At the same time, the conductive term decreases rapidly. It should be noted that the convective term of the heat flux equation (the third term of 2-58) -- which is usually neglected in non-isothermal studies -- becomes increasingly important at higher water contents, as shown in Table 4-10.

As can be seen in Figs. 4-10, 4-11 and 4-12 shown above, the computed transport coefficients are extremely variable with changing water content. This non-linearity of the system (4-1) prevents characterization by constant coefficients. It should also be noticed that when the volumetric water content becomes less than about 5%, thermally driven moisture is larger than the potential gradient flow (Fig.4-10) for the Taber sites.

The hydraulic conductivity-water content relationship used in any water flow model exerts a significant influence on the simulation results because the calculated water fluxes and several transport coefficients depend on this relationship. For the present study, conductivity functions for two different depths of Site 2 were experimentally determined (Figs.3-25, C-14). Both hydraulic conductivity functions were input to the computer simulation model to

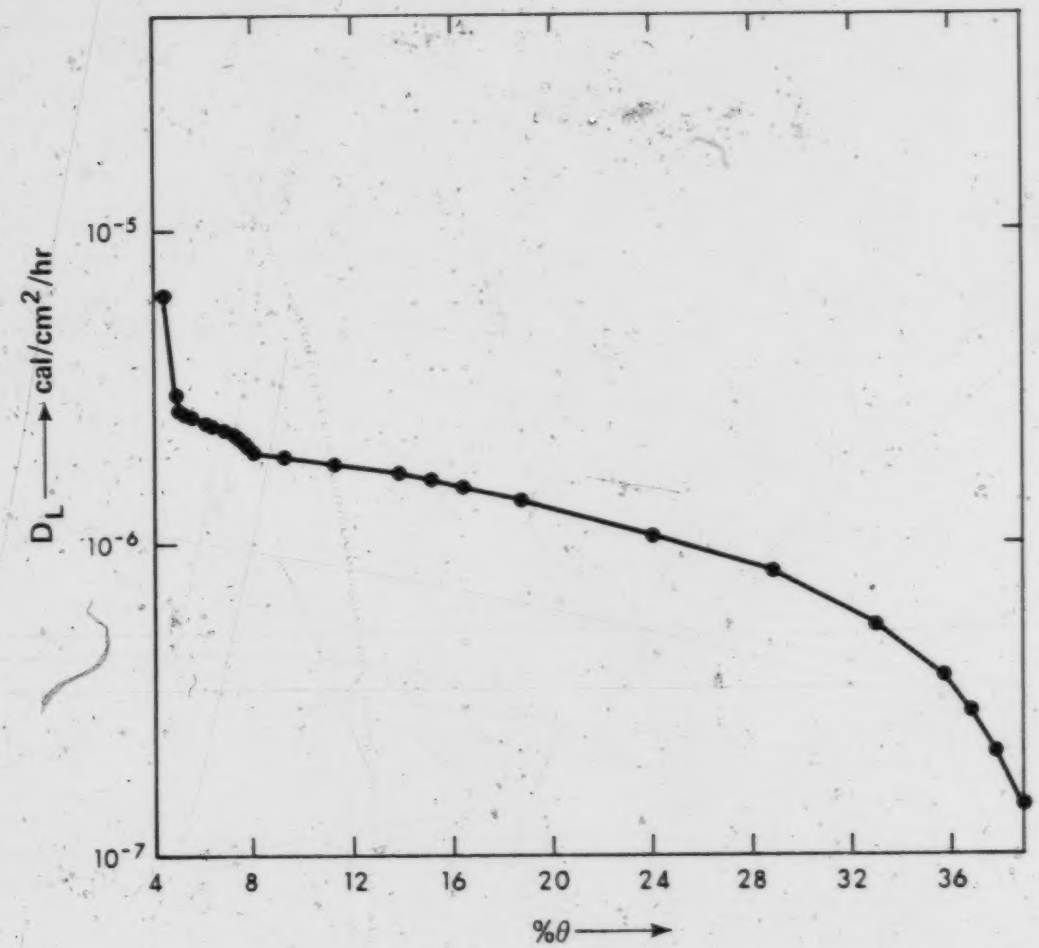

Figure 4-12. D_L (θ) coefficient function

determine which one resulted in a better agreement between observed and simulated results. I found that the hydraulic conductivity function of the surface ~20 cm of soil resulted in a comparatively better match between observed and simulated data and was thus considered more representative of the whole unsaturated profile.

Figure 4-13 shows the sinusoidal input surface temperature-time distribution together with the model calculated temperature distribution at depths of 12 and 24 cm. A decrease in amplitude of the temperature wave and a time lag with increasing depth are apparent in that figure. The calculated evaporation flux-time distribution is also shown. A pattern similar to the temperature distribution is also observed with the heat flux distribution calculated by the model, as shown in Fig. 4-14. The time distribution of the pressure head in the vicinity of the water table for the same drying conditions (Run 2) is shown in Fig. 4-15, where the gradual decrease in the water table depth with time is apparent.

The evaporation rate-time distribution under a diurnally varying environment resulted in a series of diurnal evaporation phases, as shown in Fig. 4-16, which tended to damp down in time as the surface zone desiccation progressed to greater depths. Such a pattern was actually measured in the field by Kimball and Jackson (1971). In simulating this evaporation pattern, a sinusoidal surface

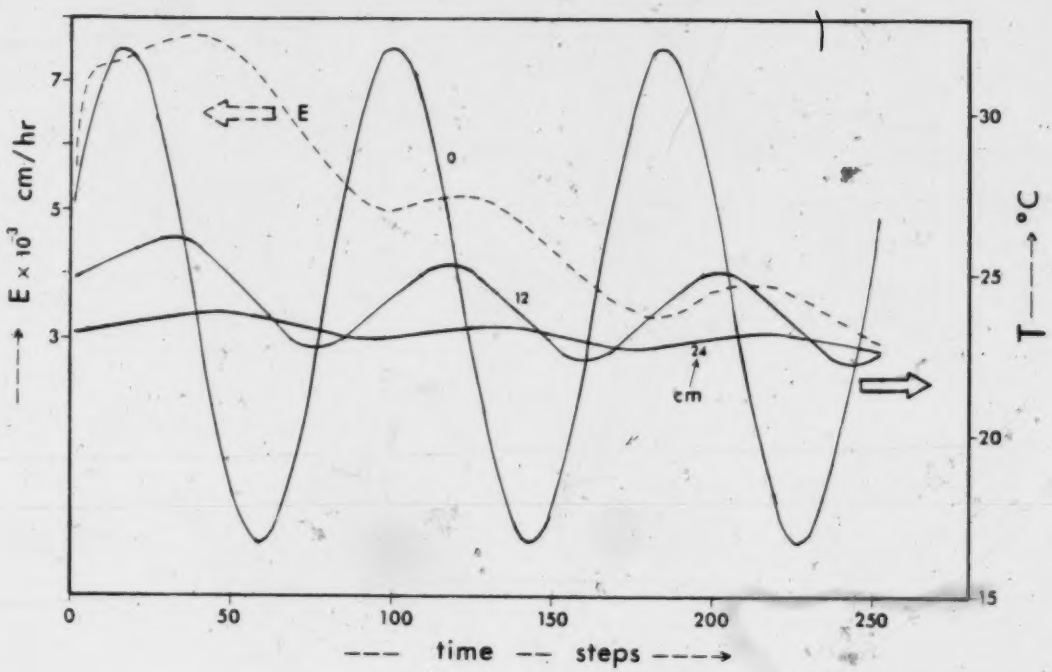

Figure 4-13. Time distribution of evaporation flux and temperatures at various depths

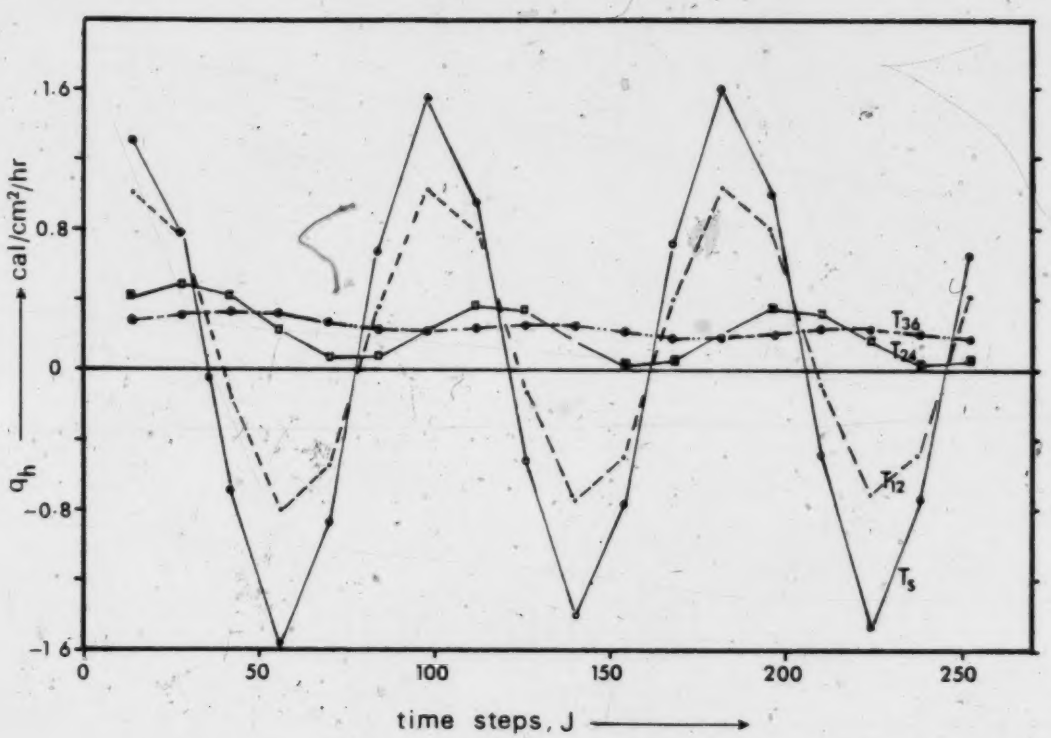

Figure 4-14. Time distribution of heat fluxes at various depths

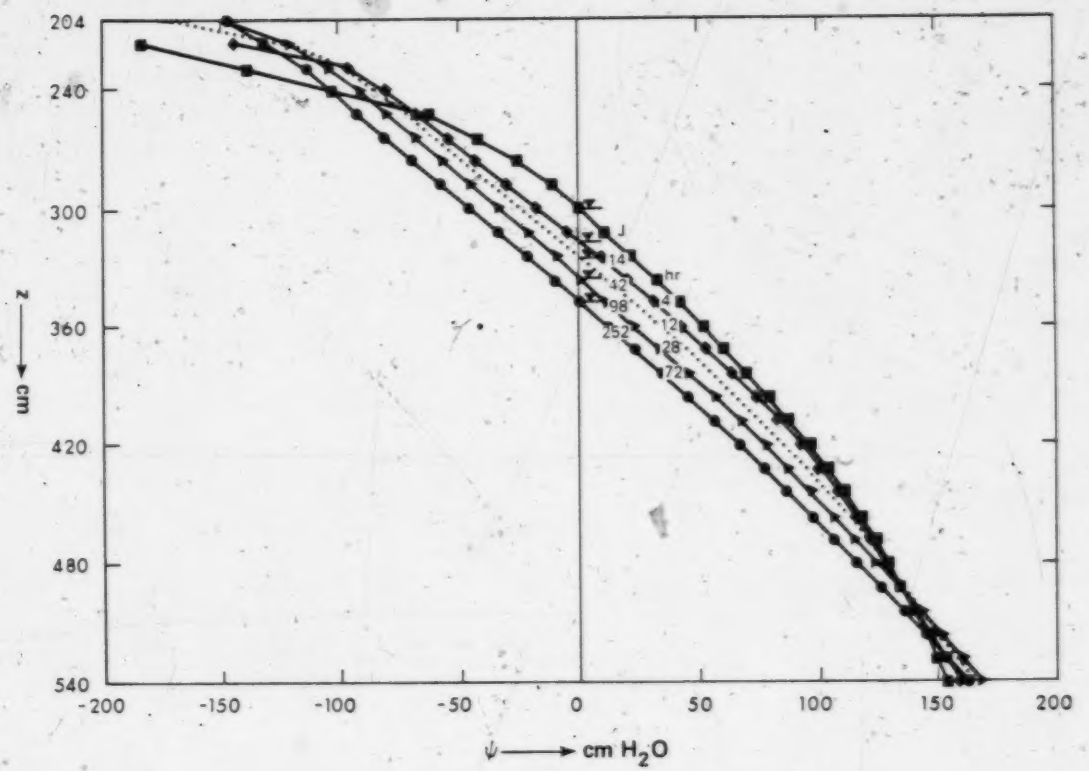

Figure 4-15. Time distribution of pressure head in the vicinity of the water table

temperature distribution similar to the one shown in Fig. 4-13 and the initial conditions for Run 2 (Fig. 4-8) were applied. It should be noticed that after the third day of evaporative drying, a stable evaporation rate-time wave pattern was observed. The time distribution of the water flux at 12 cm depth is also indicated in Figure 4-16. This distribution exhibits a similar diurnal cycle but with smaller fluctuations decreasing progressively in the deeper layers.

Although special emphasis was placed on the drying problem, the infiltration problem could also be handled by the present simulation model. An example of a wetting situation is given in Fig. 4-17, where the time-depth pressure head profiles under a constant infiltration rate of 0.09 cm/hr are shown.

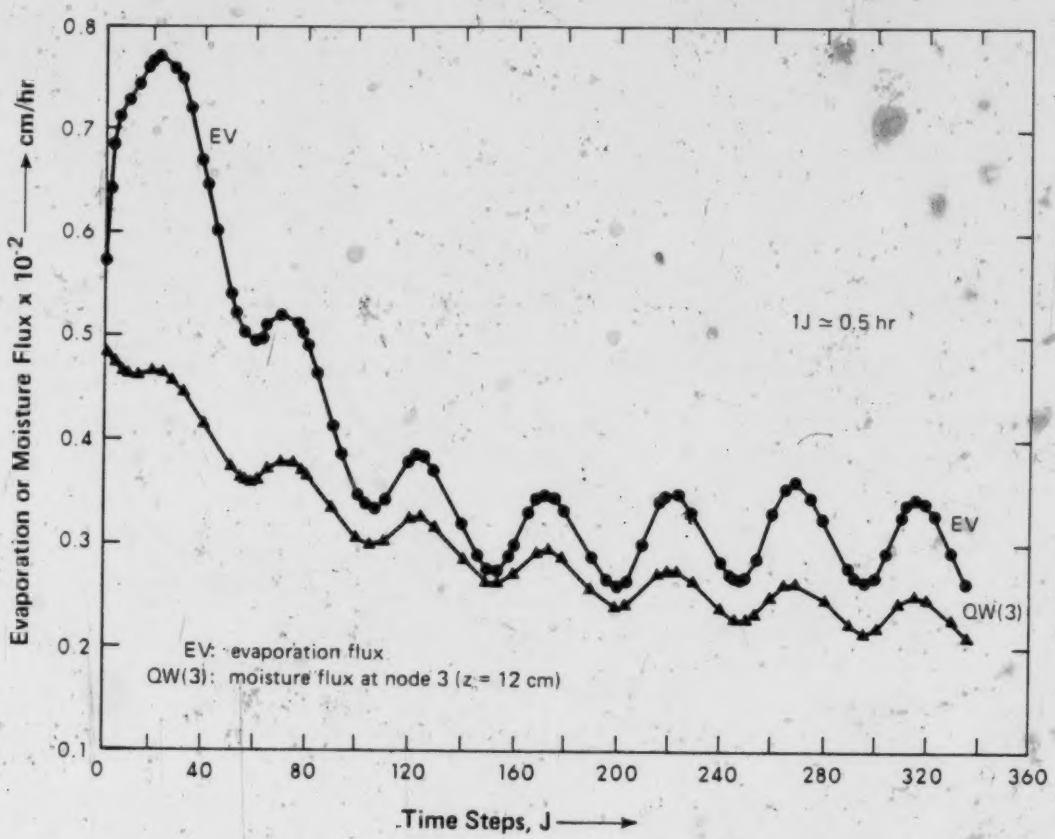

Figure 4-16. Cyclic evaporation distribution

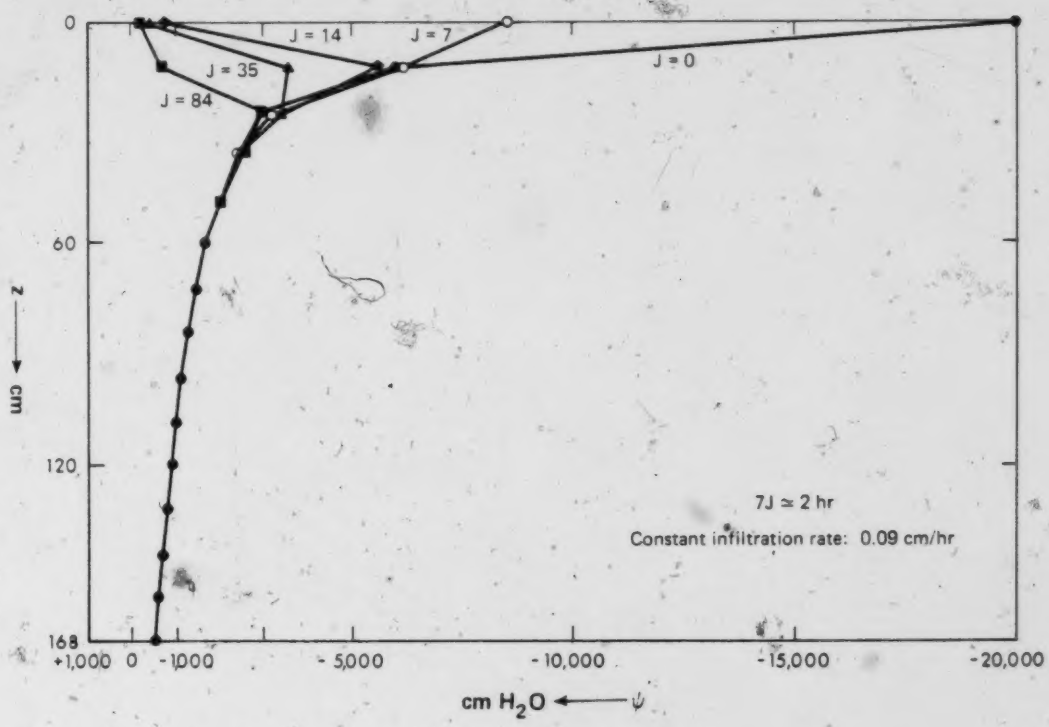

Figure 4-17. Pressure head distribution during infiltration

CHAPTER 5

CONCLUDING COMMENTS AND RECOMMENDATIONS

The present study has demonstrated the feasibility of applying and modeling the non-isothermal flow theory to a field situation. Comprehensive field and laboratory data collected here are generally unavailable in a single study. It is hoped that the present work partly overcomes the deficiency caused by a lack of necessary data for the application and modeling of non-isothermal theories, and for comparisons of theoretical and model results with experimental data. The simplified procedures for field applications of non-isothermal theory developed here (Section 2.8) are as accurate as the available analytical models and are suggested for field applications in suitable environments.

This work showed that the mechanistic Philip and de Vries-type of non-isothermal theory can be modified and extended to saturated conditions. These developments involved the introduction of a new approach for the calculation of liquid thermal diffusion coefficients based on local vapor-liquid equilibration in porous media (2-37); also of procedures for calculating the various transport coefficients based on calculating ratios of these

coefficients and combining these ratios with a detailed heat flux equation (Section 2.8). Several problems involving the application of the proposed field methodology became apparent, such as the inadequacies of the thermocouple psychrometers used in the field, the insensitivity of some instruments to small changes in field parameters, the very small magnitude of various transport coefficients involved in non-isothermal flow studies, and others (Section 3.8).

A comparative study of the mechanistic and irreversible thermodynamics approach to coupled problems indicated that the latter has not yet advanced beyond carefully controlled laboratory conditions. The present study verified, at least in a general sense, the mechanistic non-isothermal theory under field conditions. It is apparent that precise and accurate measurements of heat and water fluxes are essential to test the validity of non-isothermal equations.

This work showed how field equipment can be improved or modified to meet the particular needs of the researcher. For example, in order to meet the challenge of the field experimentation, novel procedures in design and construction of field equipment were developed with respect to thermal conductivity probes, piezometers and the various combinations of data recording devices. Thus, a new design for installing and recovering the thermal conductivity probes was implemented; also, minor modifications in the construction of thermal conductivity probes were carried

out. Another modification which proved to be very useful was the addition of a stainless steel screen to the bottom of the non-slotted piezometers.

This study was the first to demonstrate the possibilities for using a unified unsaturated-saturated approach to non-isothermal flow conditions. As a result, the scope or scale of applicability of the various non-isothermal transport parameters and equations -- which were previously restricted to the uppermost layer of the ground surface or small lab columns -- was extended to accommodate such an approach.

My research showed that it is possible to model the simultaneous flow of water and heat in unsaturated-saturated domains based on an adaptation of the Philip and de Vries model. I developed and tested this modification using measured field and laboratory data. I found the agreement between the transient numerical solution of the coupled equations under varying top boundary conditions and the field observed data satisfactory. The present model predicts soil temperatures, pressure heads and water contents as well as all relevant transport coefficients and fluxes. It is general enough to be applied to related problems of simultaneous heat and water transfer where a predictive capability is needed.

The influence of coupling on diurnal subsurface water and heat transfer can be determined by comparing the

non-isothermal and the isothermal solutions of the water and heat flow equations using the appropriate options built into the present simulation model. The results confirmed that coupling did not noticeably influence the temperature field but did affect the evaporation and subsurface moisture fluxes. Thus, depending on the direction of the temperature and pressure head gradients, the subsurface moisture fluxes might have been underestimated or overestimated significantly (up to ~40% for cases studied here) using an isothermal model. The analysis of transport coefficients for the study area indicated that thermally induced moisture movement becomes dominant at very low moisture contents.

The non-isothermal theory can be used to calculate evaporation from the soil surface based on moisture and temperature profiles. Comparison of evaporation rates calculated using the coupled and uncoupled equations indicated that non-isothermal evaporation rates were higher or lower than the isothermal ones depending on the direction of the temperature and pressure head gradients. The magnitude of such differences was up to a factor of two for the cases studied here, depending on the soil moisture levels. Thus, for example, hourly evaporation estimates using an isothermal model could be overestimated by a factor of two.

A cyclic evaporation pattern was evident under diurnal conditions. As a consequence, the three stages of the

evaporation process (Lemon, 1956) under constant evaporativity (or evaporative demand of the atmosphere) lose their distinctness. At the end of a week-long simulation, such cyclic evaporation-time waves were still apparent.

Because of the predominance of the conductive heat transfer over all other modes of heat transport in the cases studied here and the generally small magnitude of the thermal diffusion coefficient compared to the hydraulic conductivity coefficient under wet soil conditions, the isothermal model may be used adequately to predict pressure head and temperature profiles on a short-term basis (greater than 24 hr). However, for long term simulations under extended drying conditions, the coupled model should be preferred in studying the long range seasonal influences on water transport, especially in view of the fact that measured values of the D_{Tl} coefficient are much larger than model predicted ones (Jury and Miller, 1974).

Much remains to be done in order to consolidate and expand the applicablity of coupled non-isothermal models. Further generalization of results obtained here will require the study of environments differing with respect to the porous materials and the ranges of pressure heads. More experimental information is needed on the thermal dependence of the pressure potential, particularly under saturated conditions. Quantification of such information would assist

in the effort to understand the physical flow processes occurring in geothermal areas. For the same reasons, the simple non-isothermal model extension to saturated conditions that I have proposed needs to be substantiated in suitable environments. More efficient experimental procedures are required in order to determine pore geometry factors (f), ζ or ξ coefficient values appearing in the transport coefficients of non-isothermal models. Comparisons of model-calculated parameters and experimentally measured ones in a broad range of conditions are required to establish their validity. Real world complications involving hysteretic phenomena, solute effects, deformable media and others remain to be considered in non-isothermal studies. Considerable research is still needed in order to develop and/or improve available numerical techniques for the efficient solution of strongly non-linear problems. At present, abrupt changes in model parameters and other conditions cannot be adequately handled in coupled non-linear problems.

The possibilities for a model technique to simulate a real phenomenon rests on the physical representativeness of the characteristic and conductivity functions because all calculated fluxes and coefficients strongly depend on these functions. Improved experimental techniques for the measurement of hydraulic and thermal properties of porous materials as well as of water potential measurements -- especially under high negative pressure heads -- are

required. It is hoped that as specific research perfects experimental measurements, the problem of obtaining reliable field measurements will diminish. In order to expand non-isothermal models from a local to a regional scale, the problem of the determination of hydraulic and thermal properties on a macroscale needs to be solved. Statistical techniques, based on a physical understanding of the processes involved, seem the appropriate method to handle this problem.

Even when all the previously mentioned sophisticated aspects of non-isothermal models are achieved, a model simple enough and accurate enough for practical uses must be the ultimate goal. In my opinion, such a model can be constructed by a combination of physical and statistical strategies: the physical one contributing to a better understanding of each mechanism influencing non-isothermal transfer, and the statistical one simplifying and generalizing the results of the former strategy.

REFERENCES

Ahlberg, J. H., Nilson, E. N. and Walsh, J. L., 1967. The Theory of Splines and Their Applications. Academic Press, New York, N. Y.

Al-Dahir, Z. A., and Morgenstern, N. R., 1969. Intake factors for cylindrical piezometer tips. Soil Sci., 107:17-21.

Anat, A., Duke, H. R. and Corey, A. T., 1965. Steady upward flow from water tables. Hydrology Paper No. 7, Colorado State Univ., Fort Collins, Colo.

van Bavel, C. H. M., 1952. Gaseous diffusion and porosity in porous media. Soil Sci., 73:91-104.

van Bavel, C. H. M., 1969. Three-phase domain in Hydrology. In: Proc. of the Wageningen Symp., Water in the Unsaturated zone, 1:23-30. IASH-UNESCO.

van Bavel, C. H. M., Stirk, G. B. and Brust, K. J., 1968. Hydraulic properties of a clay loam soil and the field measurement of water uptake by roots: I. Interpretation of water content and pressure profiles. Soil Sci. Soc. Amer. Proc., 32:310-317.

Beck, A. E., Anglin, F. M. and Sass J. H., 1971. Analysis of heat flow data - in situ thermal conductivity measurements. Can. J. Earth Sci., 8:1-19.

Beers, Y., 1957. Introduction to the Theory of Error.

Addison-Wesley, Cambridge, Mass.

Bird, R. B., Stewart, W. E. and Lightfoot, E. N., 1960. Transport Phenomena. Wiley, New York, N. Y.

Blackwell, J. H., 1954. A transient-flow method for determination of thermal constants of insulating materials in bulk, Part 1. Theory. J. Appl. Phys., 25:137-144.

Blake, G. R., 1965. Particle density. In: C. A. Black (ed.), Methods of Soil Analysis, Part 1. Agronomy No. 9:371-373. Amer. Soc. of Agron., Madison, Wis.

Bredehoeft, J. D. and Papadopulos, I. S., 1965. Rates of vertical groundwater movement estimated from the earth's thermal profile. Water Resourc. Res., 1:325-328.

Brooks, R. H. and Corey, A. T., 1964. Hydraulic properties of porous media. Hydrology Paper No. 3, Colorado State Univ., Fort Collins, Colo.

Brown R. W. and van Haveren, B. P. (eds.), 1972. Psychrometry in Water Relations Research. Utah Agric. Exp. Sta., Utah State Univ., Logan, Utah.

Brust, K. J., van Bavel, C. H. M. and Stirk, G. B., 1968. Hydraulic properties of a clay loam soil and the field measurement of water uptake by roots. III. Comparison of field and laboratory data on retention and of measured and calculated conductivities. Soil Sci. Soc. Amer. Proc., 32:322-326.

Brutsaert, W., 1975. A theory for local evaporation (or heat

transfer) from rough and smooth surfaces at ground level. Water Resour. Res., 11:543-550.

Carnahan, B., Luther, H. A. and Wilkes, J. O., 1969. Applied Numerical Methods. Wiley, New York, N. Y.

Carslaw, H. S. and Jaeger, J. C., 1959. Conduction of Heat in Solids. Oxford Univ. Press, London, England.

Cary, J. W., 1961. The interaction of heat and water flow in soils. Ann Arbor, Mich., University Microfilms Inc. (Ph. D. thesis, Utah State Univ.).

Cary, J. W., 1963. Onsager's relations and the non-isothermal diffusion of water vapor. J. Phys. Chem., 67:126-129.

Cary, J. W., 1964. An evaporation experiment and its irreversible thermodynamics. Int. J. Heat Mass Transfer, 7:531-538.

Cary, J. W., 1966. Soil moisture transport due to thermal gradients: practical aspects. Soil Sci. Soc. Amer. Proc., 30:428-433.

Cassel, D. K., Nielsen, D. R. and Biggar, J. W., 1969. Soil water movement in response to imposed temperature gradients. Soil Sci. Soc. Amer. Proc., 33:493-500.

Childs, E. C., 1960. The non-steady state of the water table in drained land. J. Geophys. Res., 65:780-782.

Childs, E. C. and Collis-George W., 1950. Permeability of porous materials. Proc. Royal Soc. 201A:392-405.

Conte, S. D. and de Boor, C., 1972. Elementary Numerical Analysis: An Algorithmic Approach. McGraw-Hill, New

York, N. Y.

Cooley, R. L., 1971. A finite difference method for unsteady flow in variably saturated porous media: Application to a single pumping well. Water Resour. Res., 7:1707-1625.

Cooper, H. H., 1966. The equation of groundwater flow in fixed and deforming coordinates. J. Geophys. Res., 71:4785-4790.

Corey, A. T. and Kemper, W. D., 1961. Concept of total potential in water and its limitations. Soil Sci. 91:299-302.

Corey, A. T., Slatyer, R. O. and Kemper, W. D., 1967. Comparative terminologies for water in the soil-plant-atmosphere system. In: R. M. Hagan et al. (eds.), Irrigation of Agricultural Lands. Agronomy No. 11:427-445. Amer. Soc. of Agron., Madison, Wis.

Crank, J., 1956. The Mathematics of Diffusion. Oxford Univ. Press, London, England.

Currie, J. A., 1960. Gaseous diffusion in porous media. II. Dry granular materials. Brit. J. Appl. Phys. 11:318-324.

Currie, J. A., 1961. Gaseous diffusion in porous media. III. Wet granular materials. Brit. J. Appl. Phys. 12:275-281.

Danielson, R. E., 1956. Soil Physics Laboratory Manual. Agronomy Club, Colorado State Univ., Fort Collins, Colo.

Davidson, J. M., Stone, L. R., Nielsen, D. R., LaRue, M. E.,

1969. Field measurement and use of soil-water properties. Water Resourc. Res., 5:1312-1321.

Day, P. R., 1965. Particle fractionation and particle-size analysis. In: C. A. Black (ed.), Methods of Soil Analysis, Part 1:545-567. Agronomy No. 9, Amer. Soc. of Agron., Madison, Wis.

De Wiest, R. J. M., 1966. On the storage coefficient and the equations of ground-water flow. J. Geophys. Res., 71:1117-1122.

Desai, C. S. and Abel, J. F., 1972. Introduction to the Finite-Element Method. Van Nostrand-Reinhold, Princeton, N. J.

Dirksen, C., 1969. Thermo-osmosis through compacted saturated clay membranes. Soil Sci. Amer. Proc., 33:821-826.

Dirksen, C. and Miller, R. D., 1966. Closed-system freezing of unsaturated soil. Soil Sci. Soc. Amer. Proc., 30:168-173.

Doebelin, E. O., 1975. Measurement Systems: Application and Design. McGraw-Hill, New York, N. Y.

Dorn, W. S. and McCracken, D. D., 1972. Numerical Methods with FORTRAN IV Case Studies. Wiley, New York, N. Y.

Douglas, J., Jr. and Jones. B. F., 1963. On predictor-corrector methods for non-linear parabolic differential equations. J. SIAM, 11:195-204.

Eagleson, P. S., 1970. Dynamic Hydrology. McGraw-Hill, New York, N. Y.

Edlefsen, N. E. and Anderson, A. B. C., 1943. The thermodynamics of soil moisture. Hilgardia, 16:31-299.

Enfield, C. G. and Hsieh, J. J. C., 1971. Application of thermocouple psychrometers to soil water transport. Water Resourc. Res., 7:1349-1353.

Emery, A. F. and Carson, W. W., 1971. An evaluation of the use of the finite-element method in the computation of temperature. J. Heat Transfer, Trans. ASME, Ser. C, 93:136-145.

Fitts, D. D., 1962. Non-equilibrium Thermodynamics. McGraw-Hill, New York, N. Y.

Flocker, W. J., Yamaguchi, M. and Nielsen, D. R., 1968. Capillary conductivity and soil-water diffusivity values from vertical soil columns. Agron. J., 60:605-610.

Flühler, H., Ardakani, M. S. and Stolzy, L. H. 1976. Error propagation in determining hydraulic conductivities from successive water content and pressure head profiles. Soil Sci. Soc. Amer. J., 40:830-836.

Forsythe, G. E. and Moler, C. B., 1967. Computer Solution of Linear Algebraic Systems. Prentice-Hall, Englewood Cliffs, N. J.

Forsythe, G. E. and Wasow, W. R., 1960. Finite-Difference Methods for Partial Differential Equations. Wiley, New York, N. Y.

Freeze, R. A., 1969a. The mechanism of natural groundwater recharge and discharge. 1. One-dimensional, vertical,

unsteady, unsaturated flow above a recharging or discharging groundwater flow system. Water Resour. Res., 5:153-171.

Freeze, R. A., 1969b. Regional groundwater flow - Old Wives Lake drainage basin, Saskatchewan. Inland Waters Branch, Dept. of Energy, Mines and Resources, Sci. Series No. 5, Ottawa, Can.

Freeze, R. A., 1971. Three-dimensional, transient, saturated-unsaturated flow in a groundwater basin. Water Resour. Res., 7:347-366.

Fritton, D. D., 1974. Evaluation of experimental procedures by error analysis. J. Agron. Educ., 3:43-48.

Fritton, D. D., Kirkham, D. and Shaw, R. H., 1970. Soil water evaporation, isothermal diffusion, and heat and water transfer. Soil Sci. Soc. Amer. Proc., 34:183-189.

Fritton, D. D., Busscher, W. J. and Alpert, J. E., 1974. An inexpensive but durable thermal conductivity probe for field use. Soil Sci. Soc. Amer. Proc., 38:854-855.

Fuchs, M. and Tanner, C. B., 1968. Surface temperature measurements of bare soils. J. Appl. Meteor., 7:303-305.

Fulford, G., 1969. A survey of recent Soviet research on the drying of solids. Can. J. Chem. Eng., 47:378-391.

Gardner, W.H., 1965. Water content. In: C. A. Black (ed.), Methods of Soil Analysis, Part 1. Agronomy No. 9:82-127. Amer. Soc. of Agron., Madison, Wis.

Gardner, W. R., 1974. The permeability problem. Soil Sci.,

117:243-249.

Gee, G. W., 1966. Water movement in soils as influenced by temperature gradients. Ph. D. thesis, Washington State Univ., Pullman, Wash.

Glansdorff, P. and Prigogine, I., 1971. Thermodynamic Theory of Structure, Stability and Fluctuations. Wiley-Interscience, New York, N. Y.

Groenevelt, P. H. and Bolt, G. H., 1969. Non-equilibrium thermodynamics of the soil-water system. J. Hydrology, 7:358-388.

Groenevelt, P. H. and Kay, B. D., 1974. On the interaction of water and heat transport in frozen and unfrozen soils: II. The liquid phase. Soil Sci. Soc. Amer. Proc., 38:400-404.

de Groot, S. R. and Mazur, P., 1962. Non-equilibrium Thermodynamics. North-Holland, Amsterdam.

Gupta, J. P. and Churchill, S. W., 1972. A model for the migration of moisture during the freezing of wet sand. AIChE Symp. Ser. 69, No. 131, 192-198.

Guymon, G. L. and Luthin, J. N., 1974. A coupled heat and moisture transport model for Arctic soils. Water Resourc. Res., 10:995-1001.

Hadas, A., 1968. Simultaneous flow of water and heat transfer under periodic heat fluctuation. Soil Sci. Soc. Amer. Proc., 32:297-301.

Hadas, A., 1977. Evaluation of theoretically predicted thermal conductivities of soils under field and

laboratory conditions. Soil Sci. Soc. Amer. J., 41:460-466.

Hanks, R. J. and Jacobs, H. S., 1971. Comparison of the calorimetric and flux meter measurements of soil heat flow. Soil Sci. Soc. Amer. Proc., 35:671-674.

Hanks, R. J. and Tanner, C. B., 1972. Calorimetric and flux meter measurements of soil heat flow. Soil Sci. Soc. Amer. Proc., 36:537-538.

Hanley, H. J. M. (ed.), 1969. Transport Phenomena in Fluids. Marcel Dekker, New York, N. Y.

Harlan, R. L., 1973. Analysis of coupled heat-fluid transport in partically frozen soil. Water Resourc. Res., 9:1314-1323.

Harmathy, T. Z., 1969. Simultaneous moisture and heat transfer in porous systems with particular reference to drying. Ind. and Eng. Chem. Fundamentals, 8:92-103.

Hillel, D., 1971. Soil and Water: Physical Principles and Processes. Academic Press, New York, N. Y.

Hillel, D., Krentos, V. D. and Stylianou, Y., 1972. Procedure and test of an internal drainage method for measuring soil hydraulic characteristics in situ. Soil Sci., 144:395-400.

Hubbert, M. K., 1956. Darcy's law and the field equations of the flow of underground fluids. Amer. Inst. Mining Met. Petrol. Eng. Trans., 207:222-239.

Husain, A., Chen, C. S. and Clayton, J. T., 1973. Simultaneous heat and mass diffusion in biological

materials. J. Agric. Engng. Res., 18:343-354.

Hvorslev, M. J., 1951. Time lag and soil permeability in groundwater observations. U. S. Army Corps of Engineers, Waterways Exp. Sta., Vicksburg, Miss., Bull. 36.

Ibrahim, H. I. and Brutsaert, W., 1968. Intermittent infiltration into soil with hysteresis. J. Hyd. Div. ASCE, 94:113-137.

Ingersoll, L. R., Zobel, O. J. and Ingersoll, A. C., 1954. Heat Conduction With Engineering, Geological, and Other Applications. The Univ. of Wisconsin Press, Madison, Wis.

Jackson, R. D., 1963. Temperature and soil-water diffusivity relations. Soil Sci. Soc. Amer. Proc., 27:363-366.

Jackson, R. D., 1964a. Water vapor diffusion in relatively dry soil: I. Theoretical considerations and sorption experiments. Soil Sci. Soc. Amer. Proc., 28:172-176.

Jackson, R. D., 1964b. Water vapor diffusion in relatively dry soil: II. Desorption experiments. Soil Sci. Soc. Amer. Proc., 28:464-466.

Jackson, R. D., 1964c. Water vapor diffusion in relatively dry soil: III. Steady state experiments. Soil Sci. Soc. Amer. Proc., 28:466-470.

Jackson, R. D., 1965. Water vapor diffusion in relatively dry soil: IV. Temperature and pressure effects on sorption diffusion coefficients. Soil Sci. Soc. Amer. Proc., 29:144-148.

Jackson, R. D. and Taylor, S. A., 1965. Heat transfer. In: C. A. Black (ed.), Methods of Soil Analysis, Part 1. Agronomy No. 9:349-360, Amer. Soc. of Agron., Madison, Wis.

Jackson, R. D., Kimball, B. A., Reginato, R. J. and Nakayama, F. S., 1974. Diurnal soil-water evaporation: Comparison of measured and calculated soil-water fluxes. Soil Sci. Soc. Amer. Proc., 38:861-866.

Jackson, R. D., Kimbal, B. A., Reginato, R. J., Idso, S. B. and Nakayama, F. S., 1975. Heat and water transfer in a natural soil environment. In: D. A. de Vries and N. H. Afgan (eds.), Heat and Mass Transfer in the Biosphere: Part I. Transport Processes in Plant Environment, Scripta, Washington, D. C., pp. 67-76.

Jacob, J. C., 1956. Conduction of heat in an infinite region bounded internally by a circular cylinder of a perfect conductor. Austr. J. Phys., 9:167-179.

Janse, A. R. P. and Borel, G., 1965. Measurement of thermal conductivity in situ in mixed materials, e. g. soils. Neth. J. Agric. Sci., 13:57-62.

Joshua, W. D. and de Jong, E., 1973. Soil moisture movement under temperature gradients. Can. J. Soil Sci., 53:49-57.

Jury, W. A., 1973. Simultaneous transport of heat and moisture through medium sand. Ann Arbor, Mich., University Microfilms Inc. (Ph. D. thesis, Univ. of Wisconsin).

Jury, W. A. and Miller, E. E., 1974. Measurement of the transport coefficients for coupled flow of heat and moisture in a medium sand. Soil Sci. Soc. Amer. Proc., 38:551-557.

Katchalsky, A. and Curran, P. F., 1967. Non-equilibrium Thermodynamics in Biophysics. Harvard Univ. Press, Cambridge, Mass.

Kay, B. D. and Groenevelt, P. H., 1974. On the interaction of water and heat transport in frozen and unfrozen soils: I. Basic theory; The vapor phase. Soil Sci. Soc. Amer. Proc., 38:395-400.

Keey, R. B., 1972. Drying: Principles and Practice. Pergamon Press, Oxford, England.

Kersten, M. S., 1949. Thermal properties of soils. Univ. of Minnesota, Engineering Exp. Sta., Bull. 28.

Kimball, B. A. and Jackson, R. D., 1971. Seasonal effects on soil drying after irrigation. Proc. of the Ariz. Sect., AWRA and the Hydrol. Sect., Ariz. Acad. of Sci., 1:85-98.

Kimball, B. A. and Jackson, R. D., 1975. Soil heat flux determination: a null alignment method. Agric. Meteor., 15:1-9.

Kimball, B. A., Jackson, R. D., Reginato, R. J., Nakayama, F. S. and Idso, S. B., 1976. Comparison of field-measured and calculated soil heat fluxes. Soil Sci. Soc. Amer. J., 40:18-25.

King, C. J., 1968. Rates of moisture sorption and desorption

in porous, dried foodstuffs. Food Technol., 22:509-515.

Kirkham, D., 1945. Proposed method for field measurement of permeability of soil below the water table. Soil Sci. Soc. Amer. Proc., 10:58-68.

Kirkham, D., 1955. Measurement of the hydraulic conductivity of soil in place. In: Symp. on Permeability, ASTM STP No. 163:80-97.

Kirkham, D. and Powers, W. L., 1972. Advanced Soil Physics. Wiley-Interscience, New York, N. Y.

Klute, A., 1969. The movement of water in unsaturated soils. In: The progress of hydrology; Int. Seminar for Hydrol. Prof., Proc. 1st., 2:821-888, Univ. of Illinois, Urbana, Ill.

Klute, A., 1973. Soil water flow theory and its application in field situations. In: R. R. Bruce et al. (ed.), Field soil water regime. Special Publ. 5:9-35, Soil Sci. Soc. Amer., Madison, Wis.

Klute, A. and Gardner, W. R., 1962. Tensiometer response time. Soil Sci., 93:204-207.

Kruger, A. J., Daey Ouwens, C., te Velde, K. and de Vries, D. A., 1970. Condensation phenomena in capillaries with diffusion of water vapour in air under influence of a constant temperature gradient. Appl. Sci. Res., 22:390-399.

Laliberte, G. E., Corey, A. T. and Brooks, R. H., 1966. Properties of unsaturated porous media. Hydrology Paper No. 17, Colorado State Univ., Fort Collins, Colo.

Lees, M., 1966. A linear three level difference scheme for quasilinear parabolic equations. Maths of Comp., 20:516-522.

Le Méhauté, B., 1976. An Introduction to Hydrodynamics and Waterwaves. Springer-Verlag, New York, N. Y.

Lemon, E. R., 1956. The potentialities for decreasing soil moisture evaporation loss. Soil Sci. Amer. Proc., 20:120-125.

Lettau, H. H. and Davidson, B. (eds.), 1957. Exploring the Atmosphere's First Mile. Vol. I: Instrumentation and Data Evaluation. Pergamon Press, New York, N. Y.

Long, I. F. and French, B. K., 1967. Measurement of soil moisture in the field by neutron moderation. J. Soil Sci., 18:149-166.

Lopushinsky, W. and Klock, G., 1970. Construction details of ceramic bulb psychrometers. Mimeo. USDA Forest Service, Forest Hydrology Lab., Wenatchee, Wash.

Luikov, A. V., 1966. Heat and Mass Transfer in Capillary-Porous Bodies. Pergamon Press, Oxford, England.

Luikov, A. V. and Mikhailov, Y. A., 1965. Theory of Energy and Mass Transfer. Pergamon Press, Oxford, England.

Luthin, J. N. and Kirkham, D., 1949. A piezometer method for measuring permeability of soil in situ below a water table. Soil Sci., 68:349-357.

Maasland, M., 1957. Soil anisotropy and land drainage. In: J. N. Luthin (ed.), Drainage of Agricultural Lands.

Agronomy No. 7:216-285. Amer. Soc. of Agron., Madison, Wis.

Maclean, A. H., 1974. Soil genesis in relation to groundwater and soil moisture regimes near Vegreville, Alberta. Ph. D. thesis, The Univ. of Alberta, Edmonton, Alta.

Marshall, T. J., 1958. A relation between permeability and size distribution of pores. J. Soil Sci., 9:1-8.

Matthes, R. K. and Bowen, H. D., 1963. Water vapor transfer in soil by thermal gradients and its control. Trans. ASAE, 6:244-248.

Mayo, J. M., 1976. Dept. of Botany, The Univ. of Alberta. Oral communication.

McWhorter, D. B. and Sunada, D. K., 1977. Ground-water Hydrology and Hydraulics. Water Res. Publ., Fort Collins, Colorado.

Mercer, J. W. and Faust, C. R., 1976. The application of finite-element techniques to immiscible flow in porous media. Paper presented at the Int. Conf. on Finite Elements in Wat. Resour., Princeton Univ., Princeton, N. J.

Merrill, S. D. and Rawlins, S. L., 1972. Field measurement of soil water potential with thermocouple psychrometers. Soil Sci., 113:102-109.

Millington, R. J. and Quirk, J. P., 1959. Permeability of porous media. Nature, 183:387-388.

Millington, R. J. and Quirk, J. P., 1960. Transport in

porous media. In: Trans. of 7th Int. Congr. Soil Sci., I:97-106, Madison, Wis.

Mitchell, A. R., 1969. Computational Methods in Partial Differential Equations. Wiley, New York, N. Y.

Moore, R. T. and Caldwell, M. M., 1972. The field use of thermocouple psychrometers in desert soils. In: R. W. Brown and B. P. van Haveren (eds.), Psychrometry in Water Relations Research, Utah Agr. Exp. Sta., Utah State Univ., Logan, Utah.

Mukammal, E. I., 1961. Evaporation pans and atmometers. In: Proc. of Hydrology, Evaporation, Symp. No. 2:84-105, Queen's Printer, Ottawa.

Myers, G. E. Analytical Methods in Conduction Heat Transfer. McGraw-Hill. New York, N. Y.

Nerpin, S. V. and Globus, A. M., 1969. Non-isothermal moisture transfer in unsaturated soils. In: Proc. of the Wageningen Symp., Water in the Unsaturated Zone, 2:761-772. IASH-UNESCO.

Nielsen, D. R., Biggar, J. W. and Erh, K. T., 1973. Spatial variability of field-measured soil-water properties. Hilgardia, 42:215-259.

Nielsen, D. R., Davidson, J. M., Biggar, J. W. and Miller, R. J., 1964. Water movement through Panoche clay loam soil. Hilgardia, 35:491-506.

Nielsen, D. R., Jackson, R. D., Cary, J. W. and Evans, D. D. (eds.), 1972. Soil Water. Amer. Soc. of Agron. and Soil Sci. Soc. Amer., Madison, Wis.

Novak, L. T. and Coulman, G. A., 1974. Simulation of soils drying under natural meteorological conditions. Simulation, 22:11-15.

Penman, H. L., 1940. Gas and vapour movements in the soil. I. The diffusion of vapours through porous solids. J. Agr. Sci., 30:437-462.

Philip, J. R., 1955. The concept of diffusion applied to soil water. Proc. Nat. Acad. Sci. (India) 24A:93-104.

Philip, J. R., 1961. The theory of heat flux meters. J. Geophys. Res. 66:571-579.

Philip, J. R., 1969. Theory of infiltration. In: V. T. Chow (ed.), Advances in Hydroscience, 5:215-296. Acad. Press, New York, N. Y.

Philip, J. R., 1970. Flow in porous media. Ann. Rev. Fluid Mech. 2:177-204.

Philip, J. R. and de Vries, D. A., 1957. Moisture movement in porous materials under temperature gradients. Trans. Amer. Geophys. Union, 38:222-228.

Pinder, G. F. and Gray, W. G., 1977. Finite Element Simulation in Surface and Subsurface Hydrology. Academic Press, New York, N. Y.

Piper, C. S., 1950. Soil and Plant Analysis. Interscience, New York, N. Y.

Portman, D. J., 1954. Determination of the soil heat transfer at O'Neill, Nebraska. Publ. in Climatol., VII:320-325. The John Hopkins Univ. Lab. of Climatol.

Poulovassilis, A., 1962. Hysteresis of pore water, an

application of the concept of independent domains. Soil Sci. 93:405-412.

Poulovassilis, A. and Childs, E. C., 1971. The hysteresis of pore water: The non-independence of domains. Soil Sci., 112:301-312.

Prigogine, I., 1967. Introduction to Thermodynamics of Irreversible Processes. Wiley-Interscience, New York, N. Y.

Prigogine, I. and Nicolis, G., 1977. Self-organization in Nonequilibrium Systems: From Dissipative Structures to Order through Fluctuations. Wiley, New York, N. Y.

Rall, L. B., 1973. Solution of non-linear systems of equations. In: J. G. Gram (ed.), Numerical Solution of Partial Differential Equations. Reidel, Boston, Mass., pp. 55-105.

Remson, I., Hornberger, G. M. and Molz, F. J., 1971. Numerical Methods in Subsurface Hydrology with an Introduction to the Finite Element Method. Wiley-Interscience, New York, N. Y.

Richards, L. A., 1931. Capillary conduction of liquids in porous mediums. Physics, 1:318-333.

Richards, L. A., 1949. Methods of measuring soil moisture tension. Soil Sci., 68:95-112.

Richards, L. A. (eds.), 1954. Diagnosis and improvement of saline and alkali soils. USDA, Agr. Handbook 60.

Richards, L. A., 1965. Physical condition of water in soil. In: C. A. Black (ed.), Methods of Soil Analysis, Part

1: 128-152. Agronomy No. 9., Amer. Soc. of Agron., Madison, Wis.

Richards, L. A., Gardner, W. R. and Ogata, G., 1956. Physical processes determining water loss from soil. Soil Sci. Soc. Amer. Proc., 20:310-314.

Richtmyer, R. D. and Morton, K. W., 1967. Difference Methods for Initial-Value Problems. Wiley-Interscience, New York, N. Y.

Rollins, R. G., Spangler, M. G. and Kirkham, D., 1954. Movement of soil moisture under a thermal gradient. Highway Res. Board Proc., 33:492-508.

van Rooyen, M. and Winterkorn, H. F., 1957. Theoretical and practical aspects of the thermal conductivity of soils and similar granular systems. Highway Res. Board, Bull. 168: 143-205.

Rose, C. W., 1966. Agricultural Physics. Pergamon Press, Oxford, England.

Rose, C. W., 1968a. Water transport in soil with a daily temperature wave: I. Theory and experiment. Aust. J. Soil Res., 6:31-44.

Rose, C. W., 1968b. Water transport in soil with a daily temperature wave: II. Analysis. Aust. J. Soil Res., 6:45-57.

Rose, C. W., 1968c. Evaporation from bare soil under high radiation conditions. Trans. Int. Cong. Soil Sci., 9th, I:57-66, Adelaide, Australia.

Rose, C. W. and Krishnan, A., 1967. A method of determining

hydraulic conductivity characteristics for non-swelling soils in situ, and of calculating evaporation from bare soil. Soil Sci., 103:369-373.

Rose, C. W., Stern, W. R. and Drummond, J. E., 1965. Determination of hydraulic conductivity as a function of depth and water content for soil in situ. Aust. J. Soil Res., 3:1-9.

Rose, D. A., 1963a. Water movement in porous materials: I. Isothermal vapor transfer. Brit. J. Appl. Phys., 14:256-262.

Rose, D. A., 1963b. Water movement in porous materials: II. The separation of the components of water movement. Brit. J. Appl. Phys., 14:491-496.

Rose, D. A., 1965. Water movement in unsaturated porous materials. Bull. RILEM No. 29:119-123.

Rose, D. A., 1971. Water movement in dry soils: II. An analysis of hysteresis. J. Soil Sci., 22:490-507.

von Rosenberg, D. U., 1969. Methods for the Numerical Solution of Partial Differential Equations. Elsevier, New York, N. Y.

Rossen, J. L. and Hayakawa, K., 1977. Simultaneous heat and moisture transfer in dehydrated food: A review of theoretical models. In: C. J. King and J. P. Clark (eds.), Water removal processes: drying and concentration of foods and other materials. AIChE, Symp. Series 1963, 73:71-81.

Royer, J. M. and Vachaud, G., 1975. Field determination of

hysteresis in soil-water characteristics. Soil Sci. Soc. Amer. Proc., 39:221-223.

Rubin, J., 1967. Numerical method for analyzing hysteresis-affected, post-infiltration redistribution of soil moisture. Soil Sci. Soc. Amer. Proc., 31:13-20.

Sagerlind, L. J., 1976. Applied Finite Element Analysis. Wiley, New York, N. Y.

van Schaik, J. C. and Graham, D. P., 1968. Improved outflow barriers for permeability measurements. Can. J. Soil Sci., 49:261-262.

van Schaik, J. C. and Laliberte, G. E., 1969. Soil hydraulic properties affected by saturation technique. Can. J. Soil Sci., 49:95-102.

Schlichting, H., 1968. A Boundary Layer Theory, McGraw-Hill, New York, N. Y.

Scott, R. F., 1963. Principles of Soil Mechanics. Addison-Wesley, Reading, Mass.

Slusarchuk, W. A. and Foulger, P. H., 1973. Development and calibration of a thermal conductivity probe apparatus for use in the field and laboratory. Nat. Res. Council of Can., Div. Build. Res., TP 388, NRCC 13267.

Smith, G. D., 1969. Numerical Solution of Partial Differential Equations. Oxford Univ. Press, London.

Stallman, R. W., 1963. Notes on the use of temperature data for computing groundwater velocity. U.S.G.S., Water Supply Pap. 1544-H:36-46.

Stallman, R. W., 1964. Multiphase fluids in porous media - A

review of theories pertinent to hydrologic studies. U.S.G.S., Prof. Pap. 411-E.

Stallman, R. W., 1967. Flow in the zone of aeration. In: V. T. Chow (ed.), Advances in Hydroscience, 4:151-195. Academic Press, New York, N. Y.

Stigter, C. J., 1969. On measuring properties of soils by thermal methods with special reference to the contact method. Neth. J. Agric. Sci., 17:41-49.

Swatzendruber, D., 1969. The theory of water in unsaturated soils. In: R. J. M. De Wiest (ed.), Flow through Porous Media. Academic Press, New York, N. Y., pp. 215-292.

Swatzendruber, D. and Hillel, D., 1973. The physics of infiltration. In: A. Hadas et al. (eds)., Physical Aspects of Water and Salt in Ecosystems. Springer-Verlag, New York, N. Y., pp.3-15.

Tanner, C. B., 1963. Basic instrumentation and measurement for plant environment and micrometeorology. Soils Bull. 6, Univ. of Wisconsin, Madison, Wis.

Taylor, S. A. and Cary, J. W., 1960. Analysis of the simultaneous flow of water and heat or electricity with the thermodynamics of irreversible processes. Trans. Int. Cong. Soil Sci., 7th, I:80-90, Madison, Wis.

Taylor, S. A. and Cary, J. W., 1965. Soil-water movement in vapour and liquid phases. In: F. E. Eckardt (ed.), Methodology for Plant Eco-physiology. Proc. of the Montpellier Symp., 159-165. UNESCO.

Tokarsky, O., 1974. Hydrogeology of the Lethbridge-Fernie

Area, Alberta. Alberta Research, Rept. 74-1.

Topp, G. C., 1969. Soil water hysteresis measured in a sandy loam and compared with the hysteresis domain model. Soil Sci. Soc. Amer. Proc., 33:645-651.

Topp, G. C., 1971. Soil water hysteresis: the domain theory extended to pore interaction conditions. Soil Sci. Soc. Amer. Proc., 35:219-225.

Topp, G. C. and Miller, E. E., 1966. Hysteretic moisture characteristics and hydraulic conductivities for glass bead media. Soil Sci. Soc. Amer. Proc., 30:156-162.

Vachaud, G., Vauclin, M. and Haverkamp, R., 1975. Towards a comprehensive simulation of transient water table flow problems. In: G. C. Vansteenkiste (ed.), Modeling and Simulation of Water Resources Systems. North-Holland, Amsterdam, pp. 103-116.

Varga, R. S., 1962. Matrix Iterative Analysis. Prentice Hall, Englewood Cliffs, N. J.

de Vries, D. A., 1958. Simultaneous transfer of heat and moisture in porous media. Trans. Amer. Geophys. Union, 39:909-916.

de Vries, D. A., 1963. Thermal properties of soils. In: R. W. van Wijk (ed.), Physics of Plant Environment. North Holland, Amsterdam, pp. 210-235.

de Vries, D. A., 1965. Opening lecture. Bull. RILEM, No. 29:62-65.

de Vries, D. A., 1975. Heat transfer in soils. In: D. A. de Vries and N. H. Afgan (eds.), Heat and Mass Transfer in

the Biosphere: Part I. Transport Processes in Plant Environment. Scripta, Washington, D. C., pp.5-28.

de Vries, D. A. and Kruger, A. J., 1967. On the value of the diffusion coefficient of water vapor in air. C.N.R.S., Colloques Internat. 160:61-72, Paris.

de Vries, D. A. and Peck, A. J., 1958a. On the cylindrical probe method of measuring thermal conductivity with special reference to soils. I. Extension of theory and discussion of probe characteristics. Aust. J. Phys., 11:255-271.

de Vries, D. A. and Peck, A. J., 1958b. On the cylindrical probe method of measuring thermal conductivity with special reference to soils. II. Analysis of moisture effects. Aust. J. Phys. 11:409-423.

Walkley, A. and Black, I. A., 1934. An examination of the Degtjareff method for determining soil organic matter and a proposed modification of the chromic acid titration method. Soil Sci., 37:29-38.

Watson, K. K., Reginato, R. J. and Jackson, R. D., 1975. Soil water hysteresis in a field soil. Soil Sci. Soc. Amer. Proc., 39:242-246.

Wechsler, A. E., 1966. Development of thermal conductivity probes for soils and insulations. CRREL, Tech. Rept. 182.

Wheeler, M. L., Qashu, H. K. and Evans, D. D., 1972. Psychrometric measurements of water potential under desert conditions. In: R. W. Brown and B. P. van

Haveren (eds.), Psychrometry in Water Relations Research. Utah Agr. Exp. Sta., Utah State Univ., Logan, Utah, pp. 171-174.

Whisler, F. D. and Klute, A., 1965. The numerical analysis of infiltration, considering hysteresis, into a vertical soil column at equilibrium under gravity. Soil Sci. Soc. Amer. Proc., 29:489-494.

Whitaker, S., 1977. Simultaneous heat, mass and momentum transfer in porous media: A theory of drying. Adv. in Heat Transf., 13:119-203. Academic Press, New York, N. Y.

Whitner, J. D. and Porterfield, J. G., 1968. Moisture movement in a porous, hygroscopic solid. Trans. ASAE, 11:716-719.

Wiebe, H. H., Campbell, G. S., Gardner, W. H., Rawlins, S. L., Cary, J. W. and Brown, R. W., 1971. Measurement of plant and soil water status. Bull. 484, Utah Agr. Exp. Sta., Utah State Univ., Logan Utah.

Wiegand, C. L. and Taylor, S. A., 1961. Evaporative drying of porous media. Spec. Rept. 15, Utah Agr. Exp. Sta., Utah State Univ., Logan, Utah.

Wierenga, P. J. and de Wit, C. T., 1970. Simulation of heat transfer in soils. Soil Sci. Soc. Amer. Proc., 34:845-848.

van Wijk, W. R. and de Vries, D. A., 1963. Periodic temperature variations in a homogeneous soil. In: W. R. van Wijk (ed.), Physics of Plant Environment.

North-Holland, Amsterdam, pp. 102-143.

Wilkinson, G. E. and Klute, A., 1962. The temperature effect on the equilibrium energy status of water held by porous media. Soil Sci. Soc. Amer. Proc., 26:326-329.

Wilson, R. G., 1971. Methods of measuring soil moisture. Int. Field Year for the Great Lakes, Tech. Manual Ser., No. 1, Can. Nat. Com. for the IHD.

Wooding, R. A. and Morel-Seytoux, H. J., 1976. Multiphase fluid flow through porous media. Ann. Rev. of Fluid Mechanics, 8:233-274.

Woodside, W. and Kuzmak, J. M., 1958. Effect of temperature distribution on moisture flow in porous materials. Trans. Amer. Geophys. Union, 39:670-680.

Young, J. H., 1969. Simultaneous heat and mass transfer in a porous hygroscopic solid. Trans. ASAE, 12:720-725.

Youngs, E. G., 1968. Shape factors for Kirkham's piezometer method for determining the hydraulic conductivity of soil in situ for soils overlying an impermeable floor or infinitely permeable stratum. Soil Sci., 106:235-237.

Zienkiewicz, O. C., 1971. The Finite Element Method in Engineering Science. McGraw-Hill, New York, N. Y.

APPENDIX A

TEMPERATURE AND POTENTIAL EVAPORATION DISTRIBUTIONS

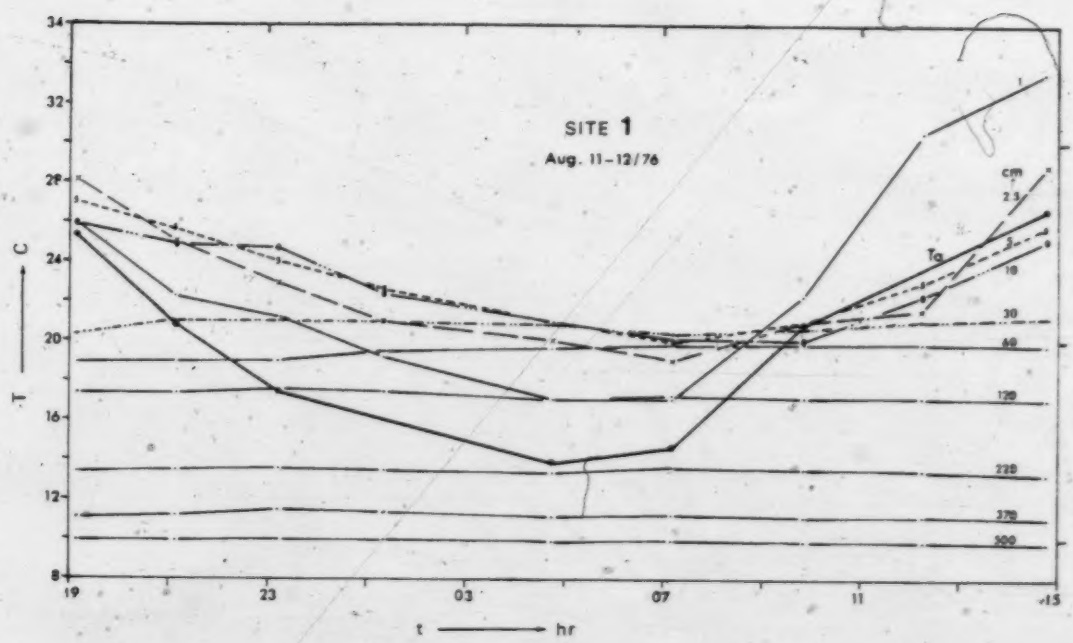

Figure A-1. Time-depth distribution of temperature at Site 1

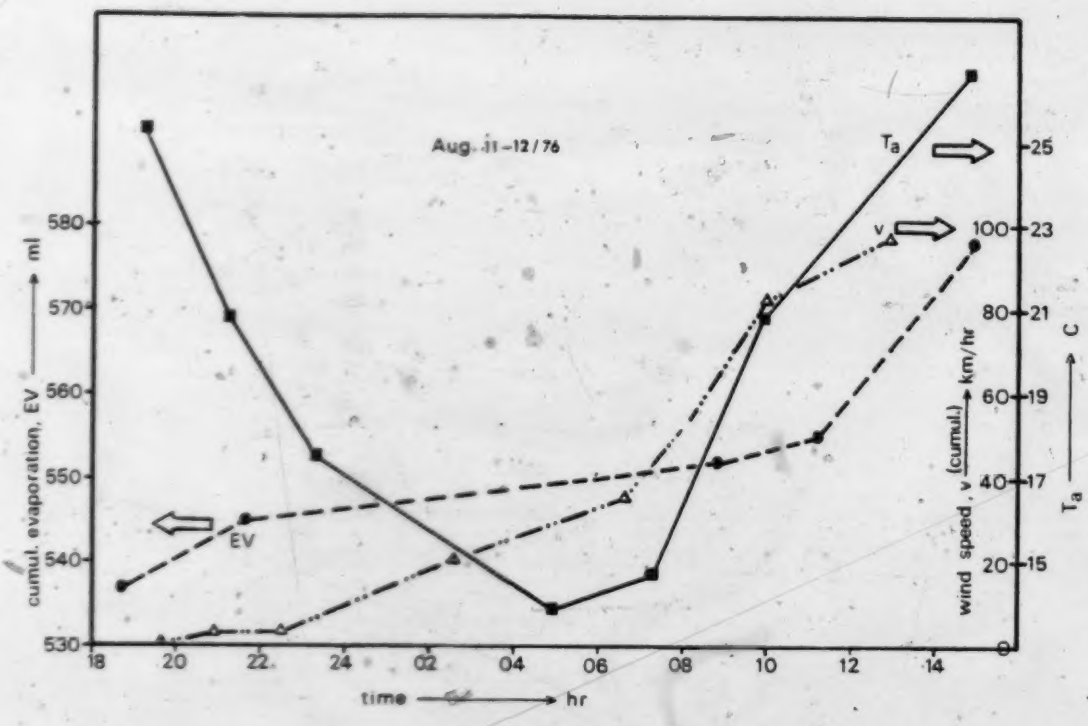

Figure A-2. Potential evaporation fluxes, air temperatures and wind speeds at the Taber sites during August 11-12/76

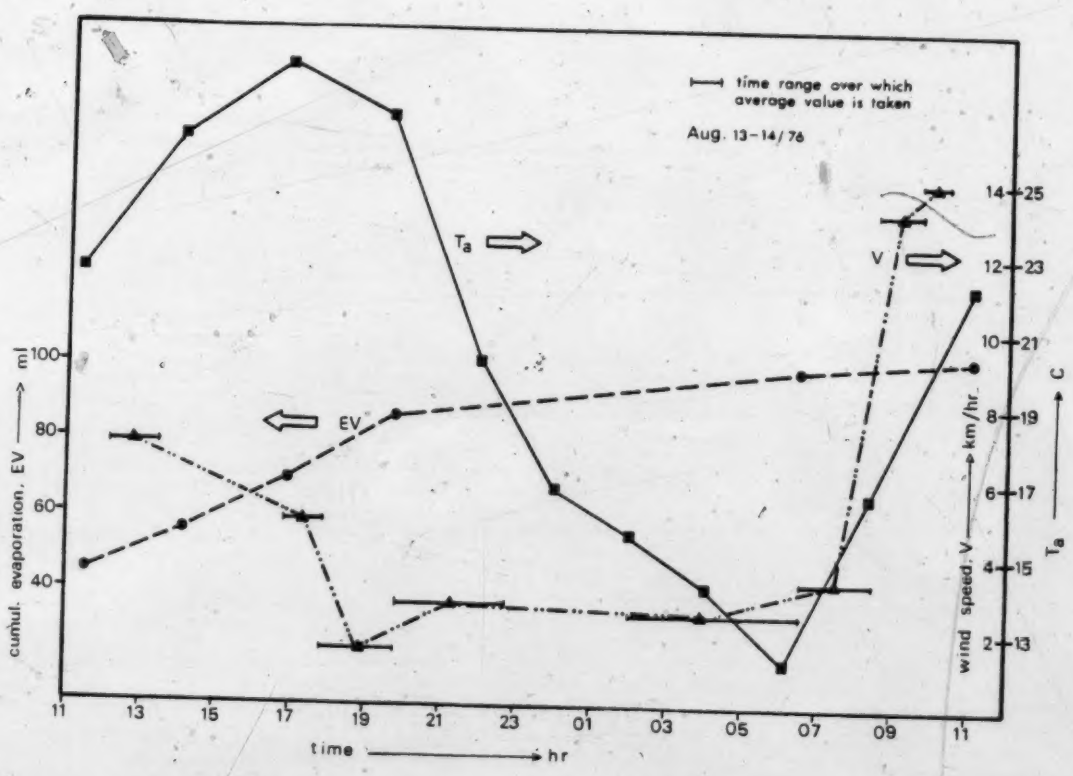
time range over which average value is taken
Aug. 13-14/76
T_a
V
EV
cumul. evaporation, EV → ml
wind speed, V → km/hr.
T_a → C
time → hr
11 13 15 17 19 21 23 01 03 05 07 09 11
40 60 80 100
2 4 6 8 10 12 14
13 15 17 19 21 23 25

Figure A-3. Potential evaporation fluxes, air temperatures and wind speeds at the Taber sites during August 13-14/76

APPENDIX B

WATER CHARACTERISTIC CURVES- SITE 2

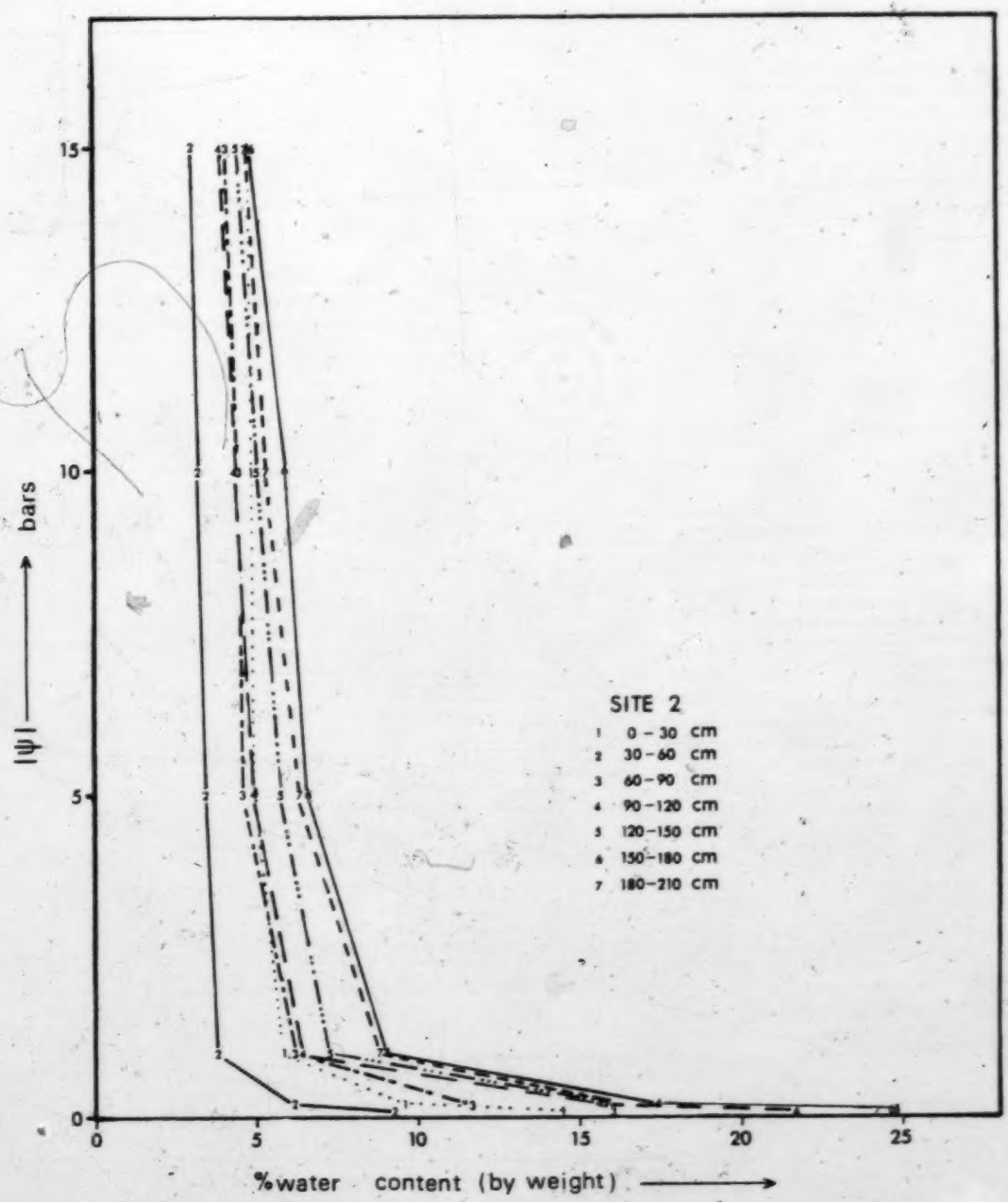

Figure B-1. Laboratory-determined water characteristic curves for Site 2

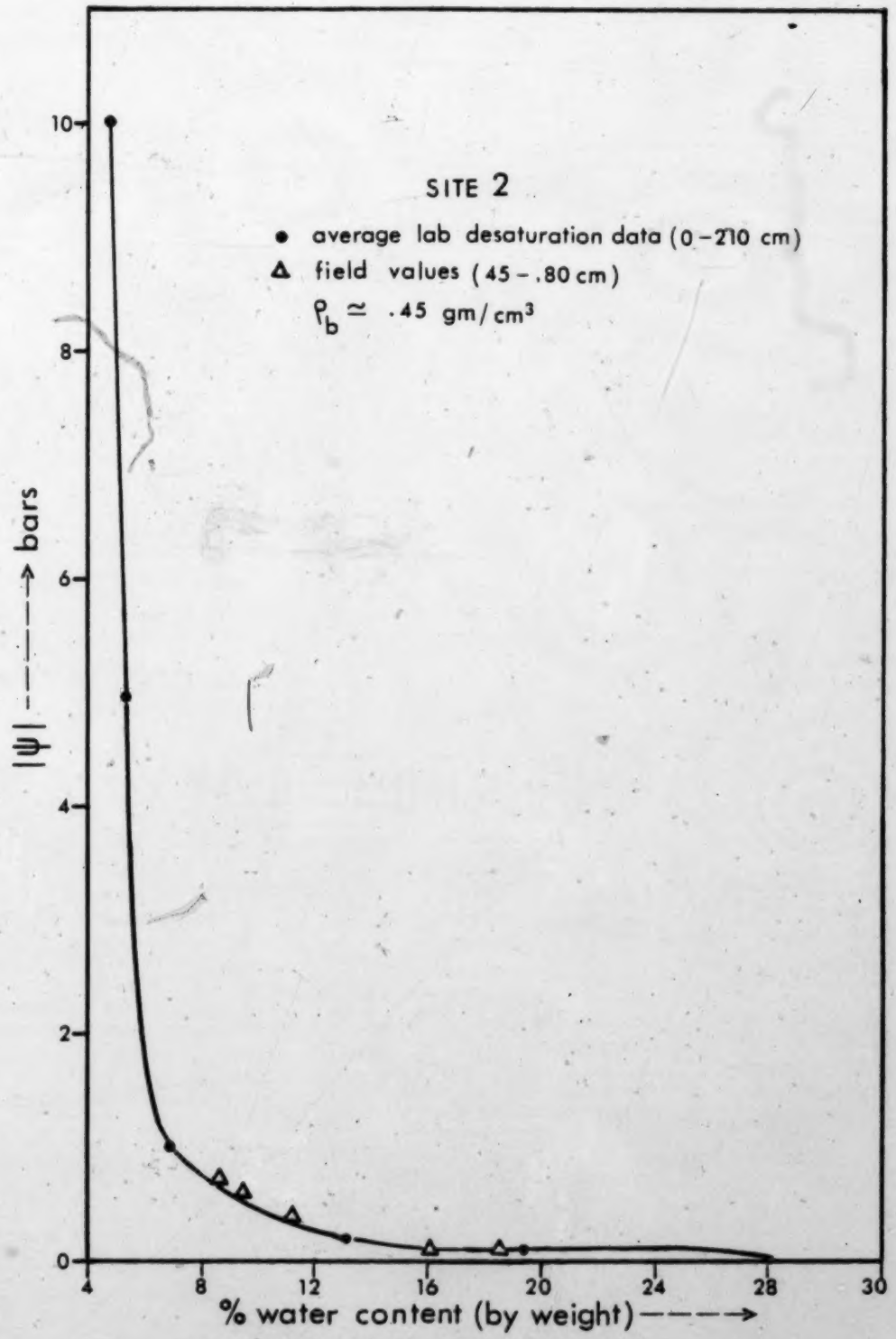

Figure B-2. Comparison of laboratory and field-determined water characteristic data for Site 2

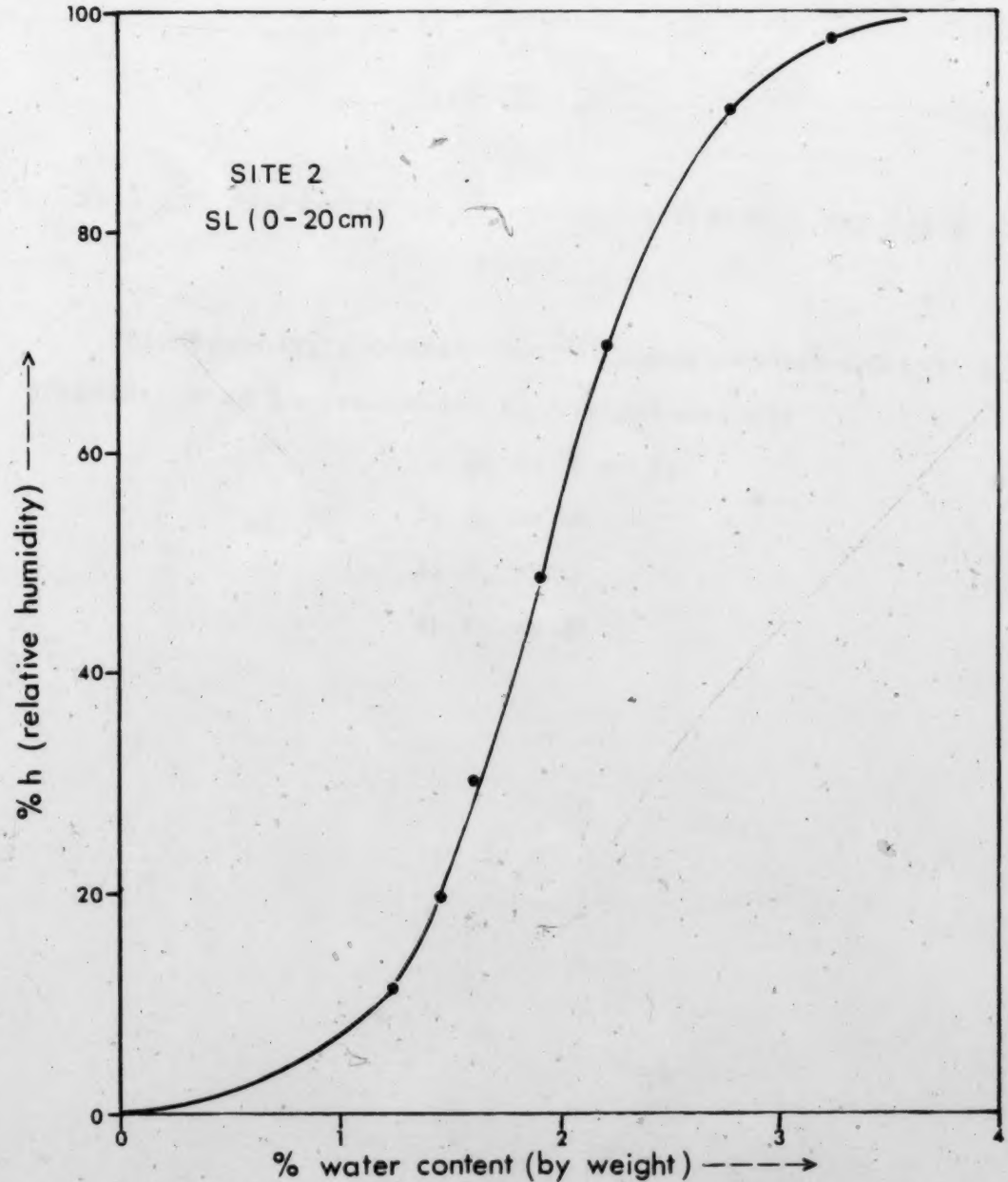

Figure B-3. Vapor equilibration experiments using acid solutions for Site 2 (0-20 cm)

APPENDIX C

HYDRAULIC PROPERTIES OF POROUS MATERIALS FROM THE TABER SITES

This Appendix includes the following relationships in graphical form as determined in the laboratory:

1) ψ vs θ or S_w
2) S_e vs ψ
3) K_r vs ψ
4) K vs θ

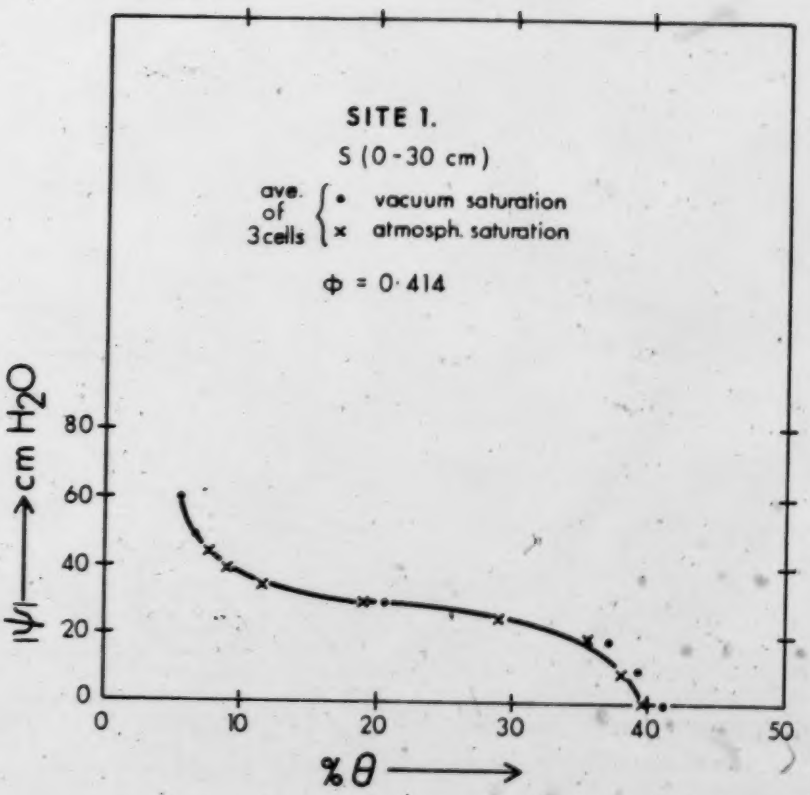

Figure C-1. ψ (θ) relationship for Site 1 (0-30 cm).

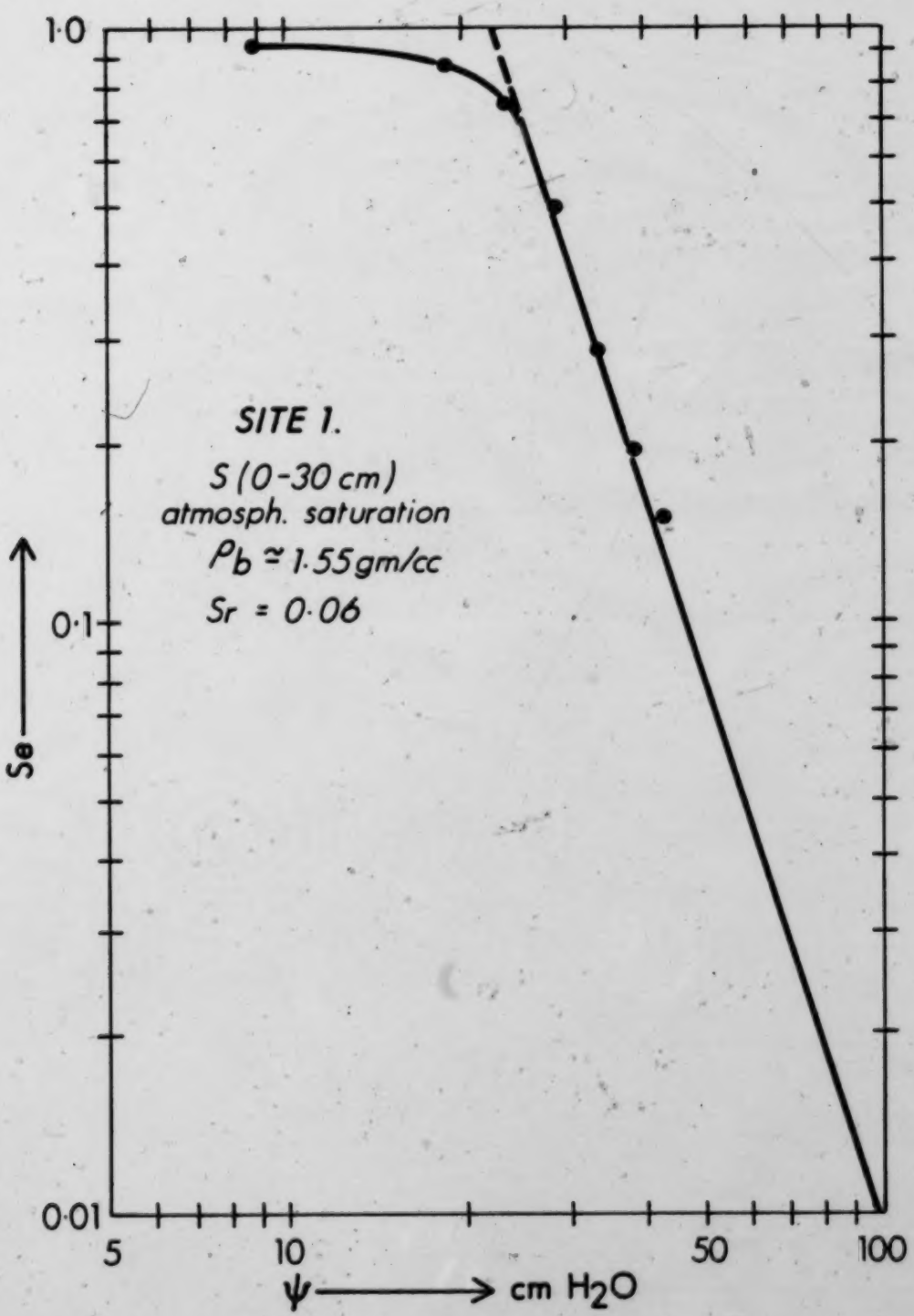

Figure C-2. S_e (ψ) relationship for Site 1 (0-30 cm)

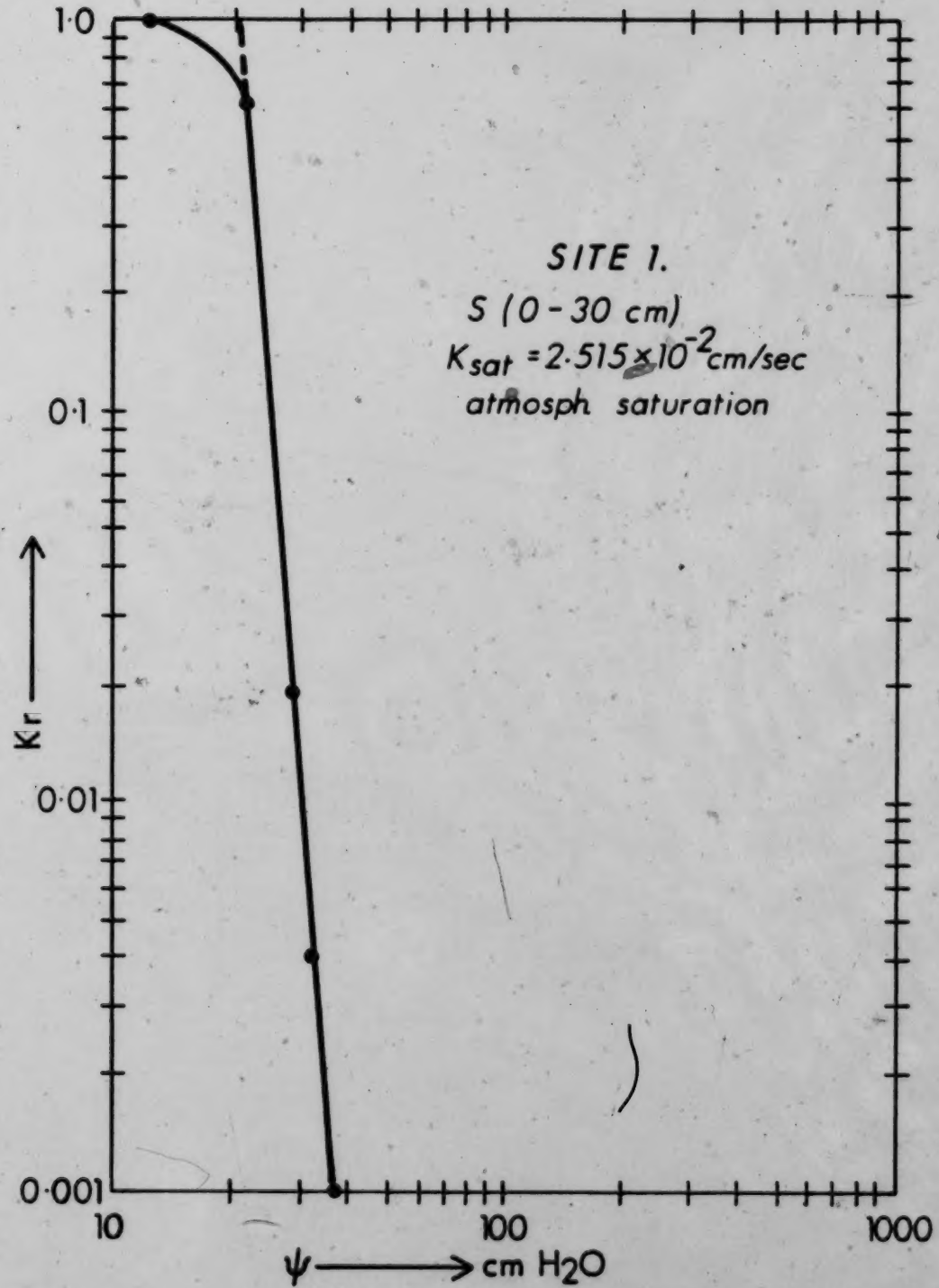

Figure C-3. K_r (ψ) relationship for Site 1 (0-30 cm)

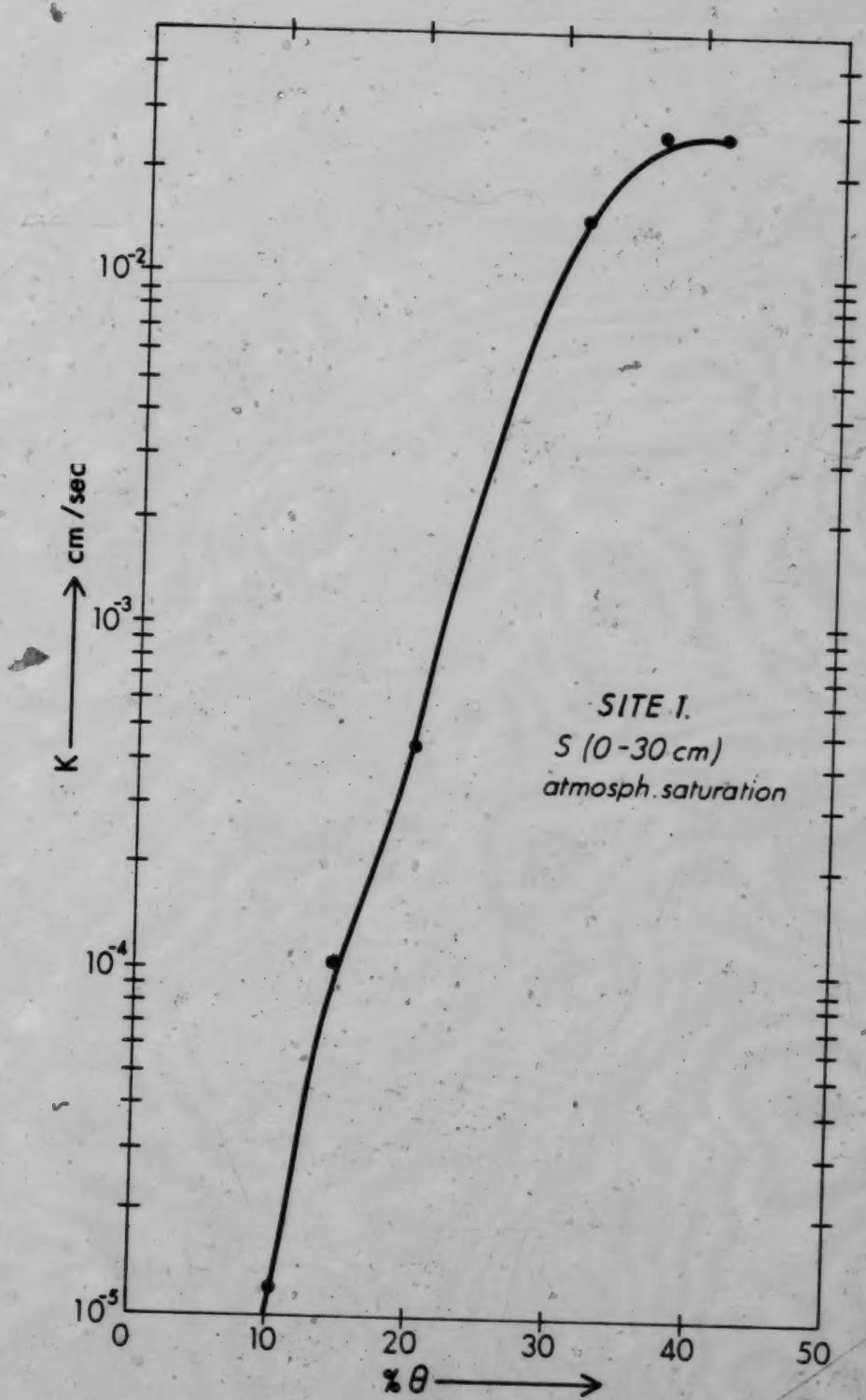

Figure C-4. K (θ) relationship for Site 1 (0-30 cm)

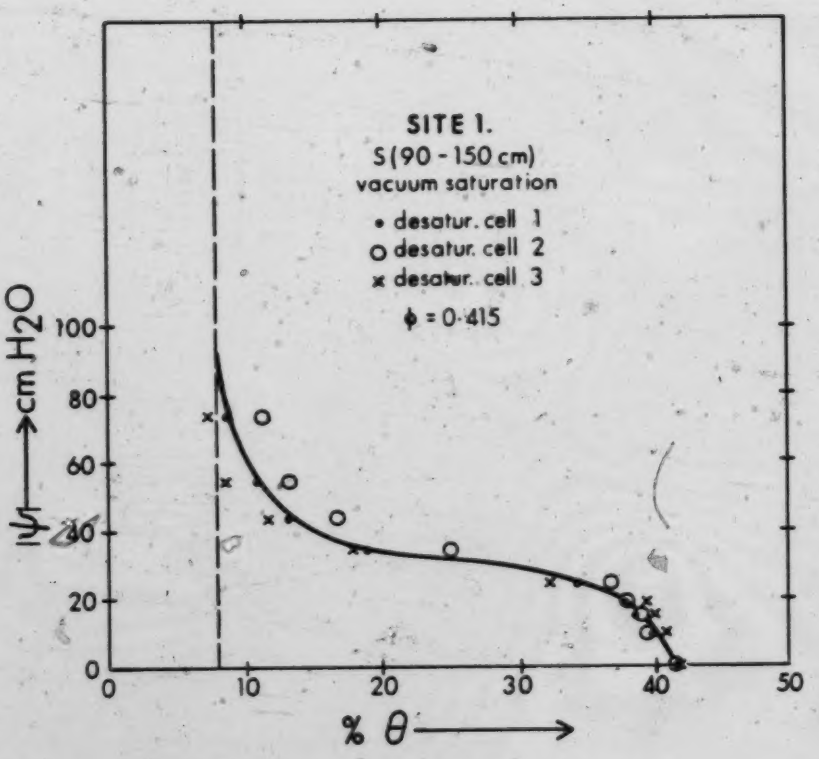

Figure C-5. ψ (θ) relationship for Site 1 (90-150 cm)

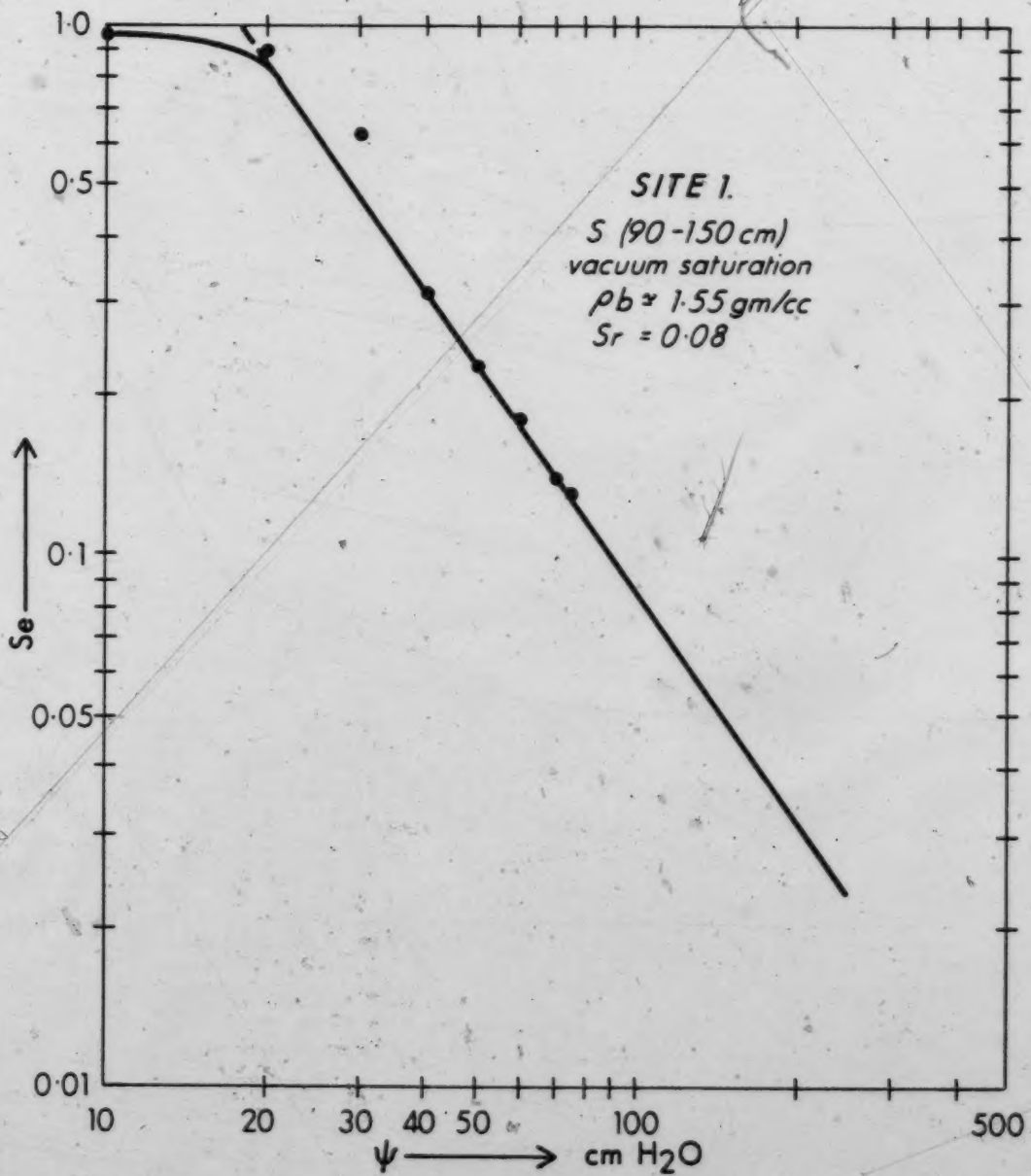

Figure C-6. S_e (ψ) relationship for Site 1 (90-150 cm)

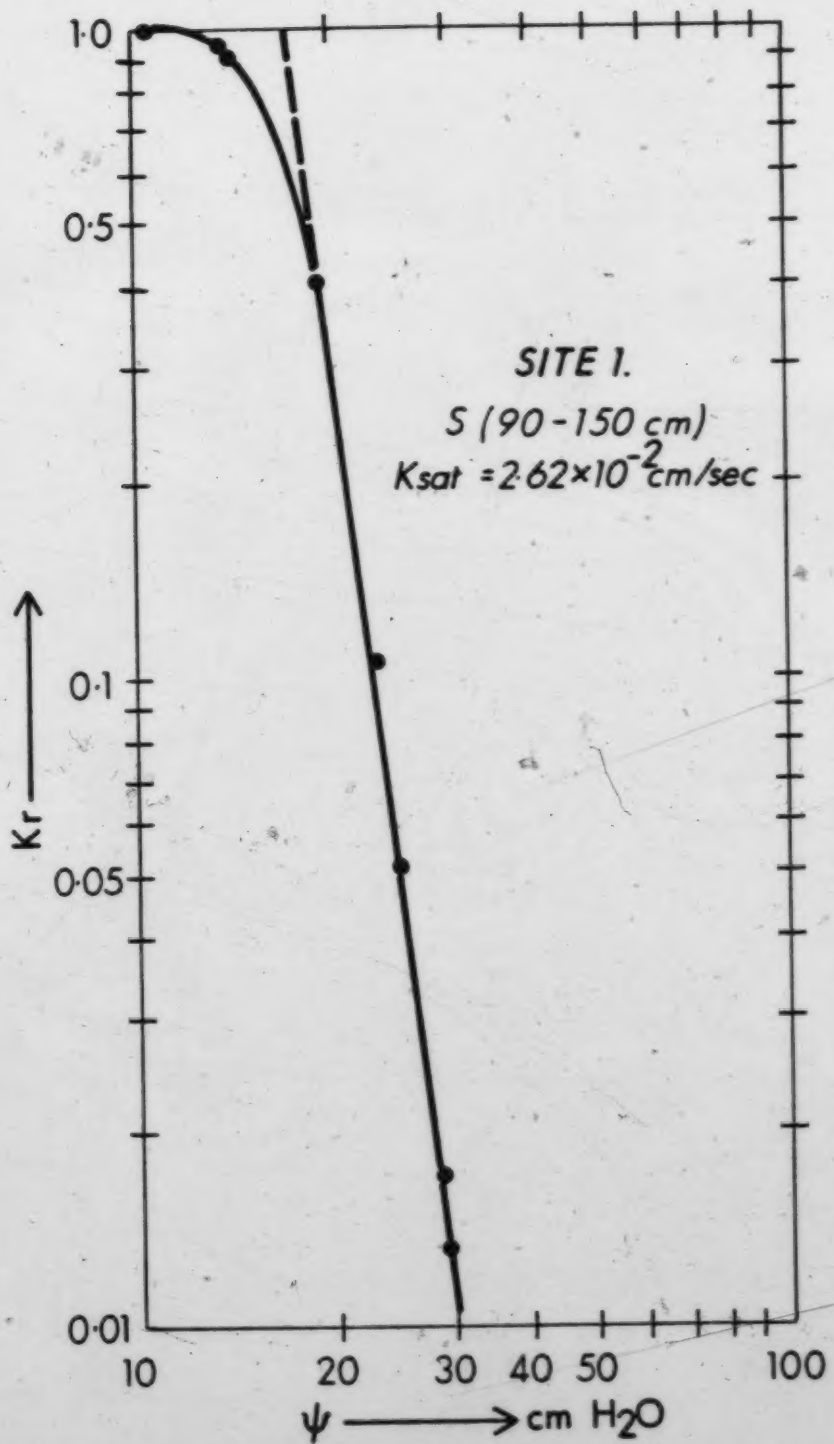

Figure C-7. K_r (ψ) relationship for Site 1 (90- 150 cm)

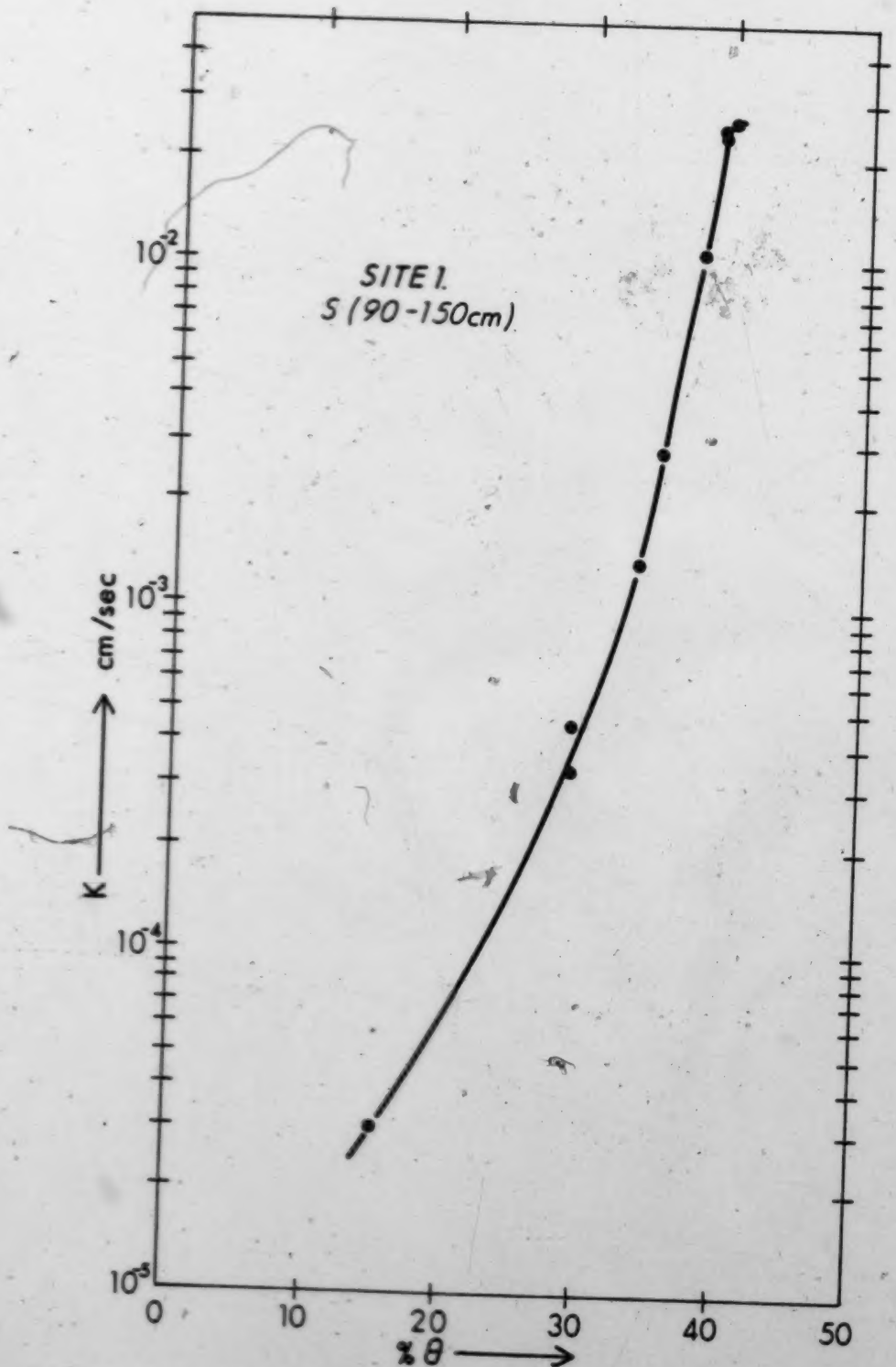

Figure C-8. K (θ) relationship for Site 1 (90- 150 cm)

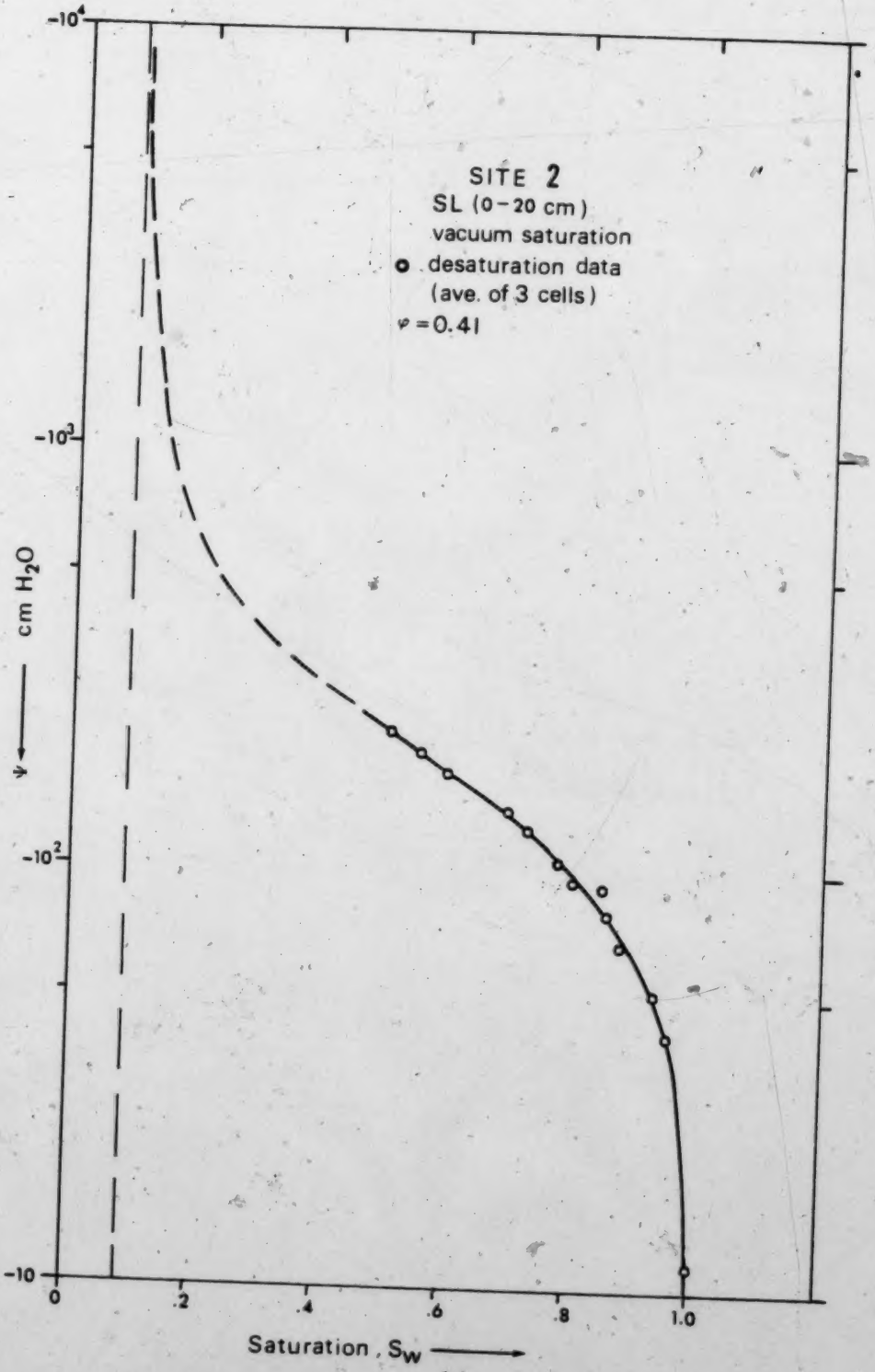

Figure C-9. ψ (S_w) relationship for Site 2 (0-20 cm)

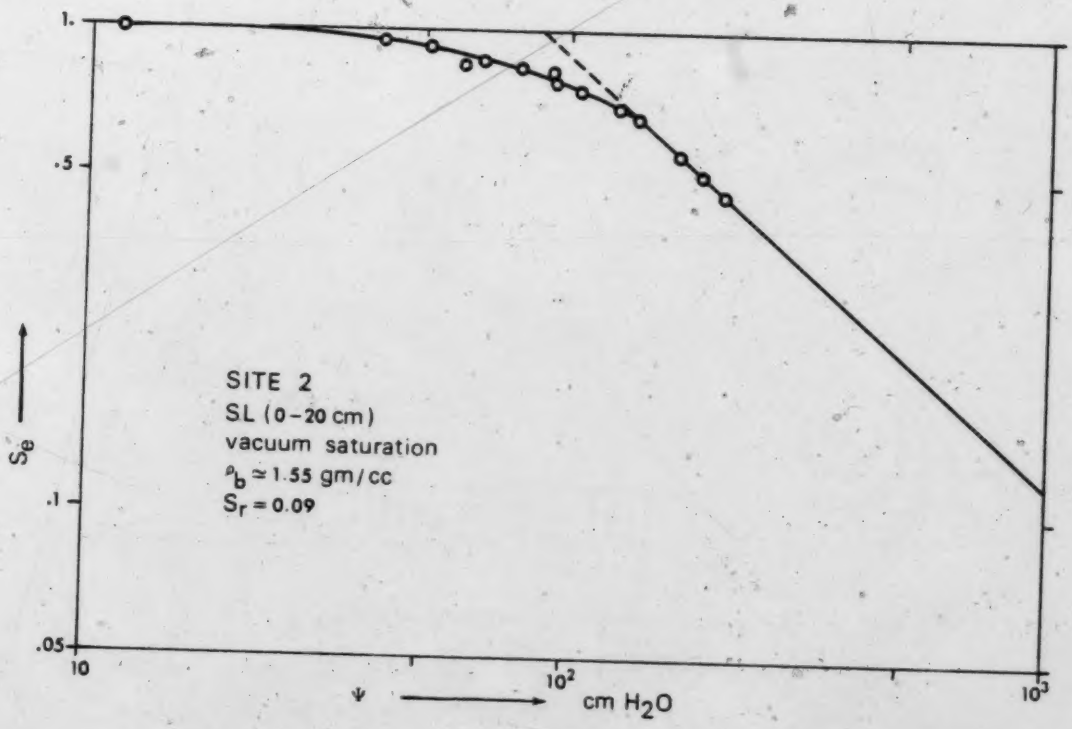

Figure C-10. S_e (ψ) relationship for Site 2 (0-20 cm)

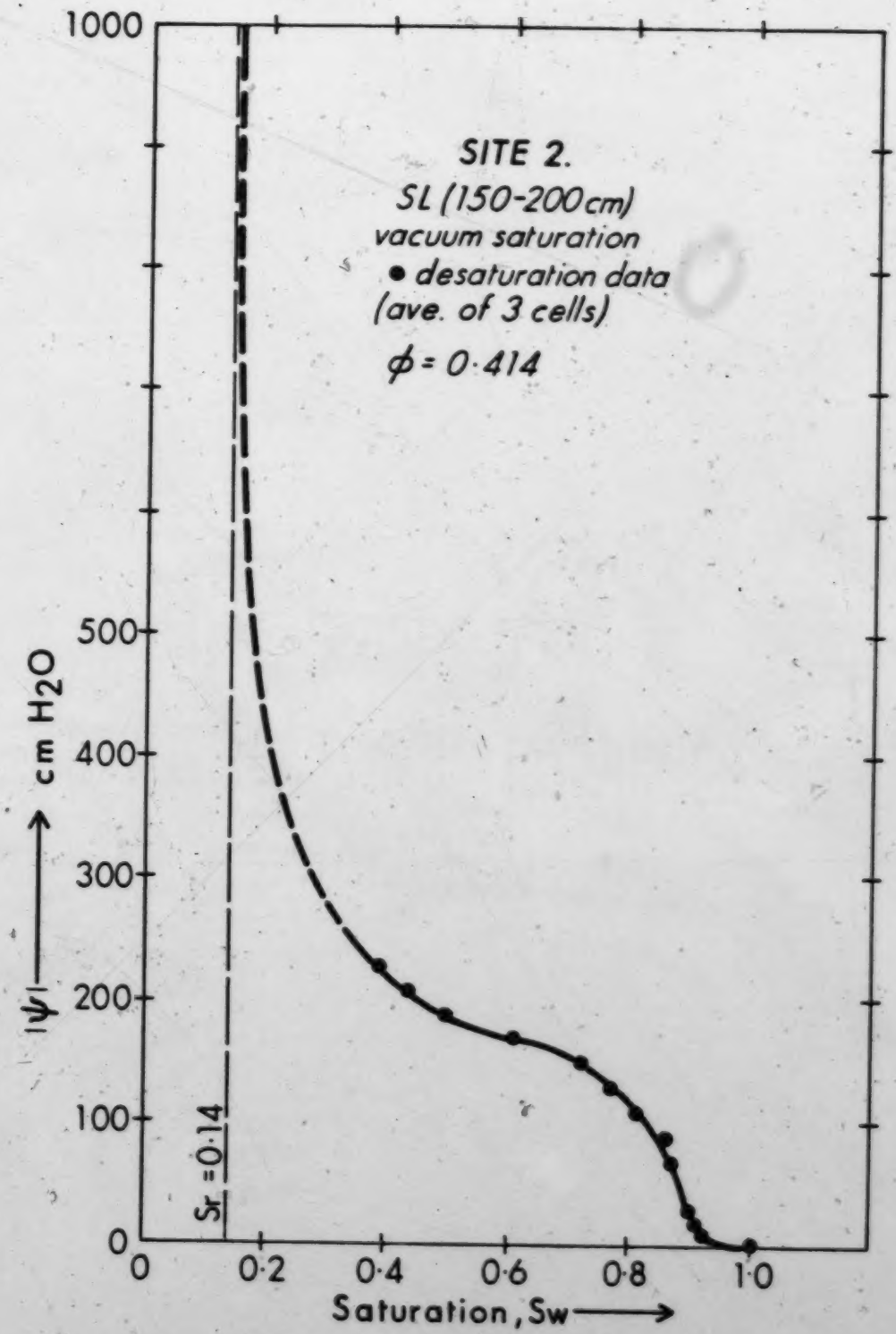

Figure C-11. ψ (S_w) relationship for Site 2 (150-200 cm)

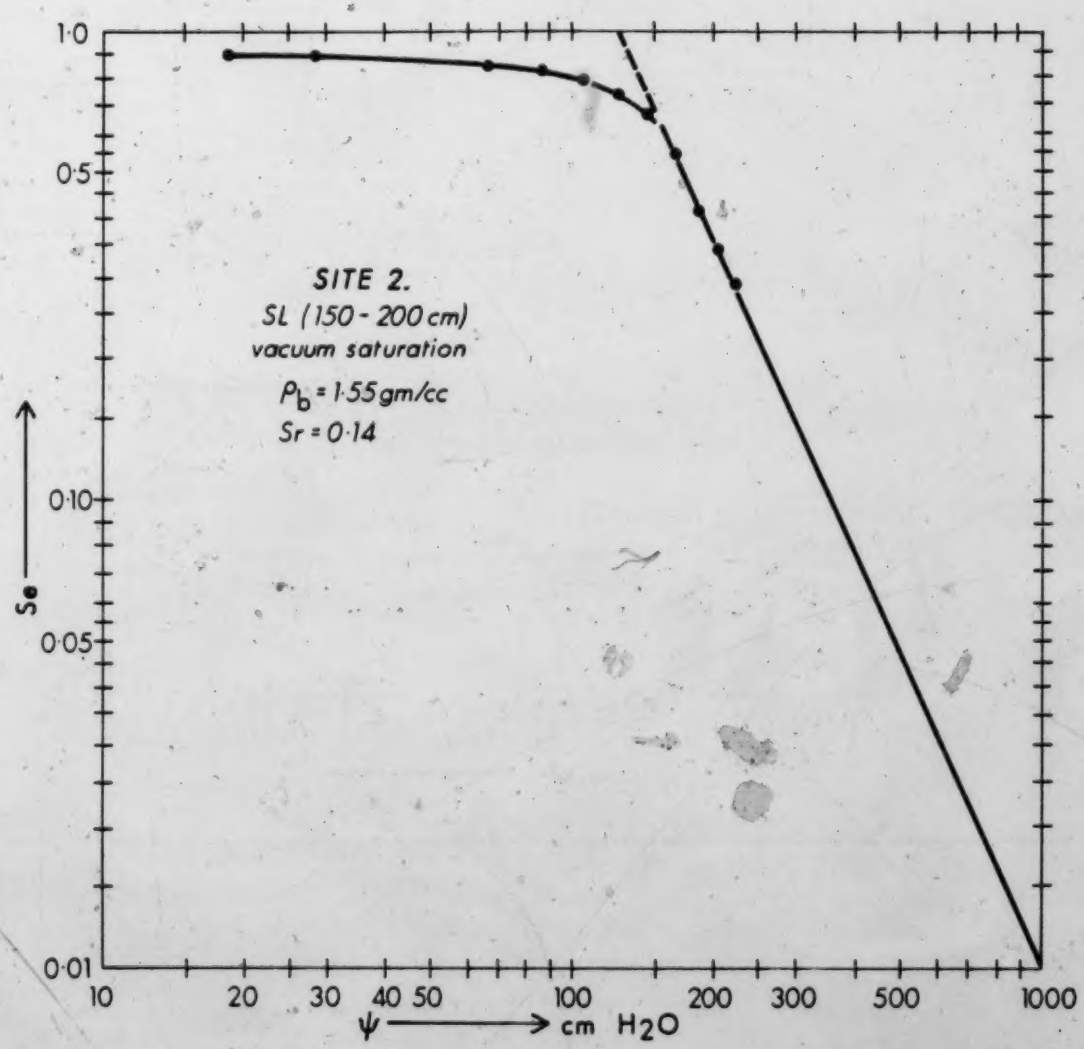

Figure C-12. S_e (ψ) relationship for Site 2 (150-200 cm)

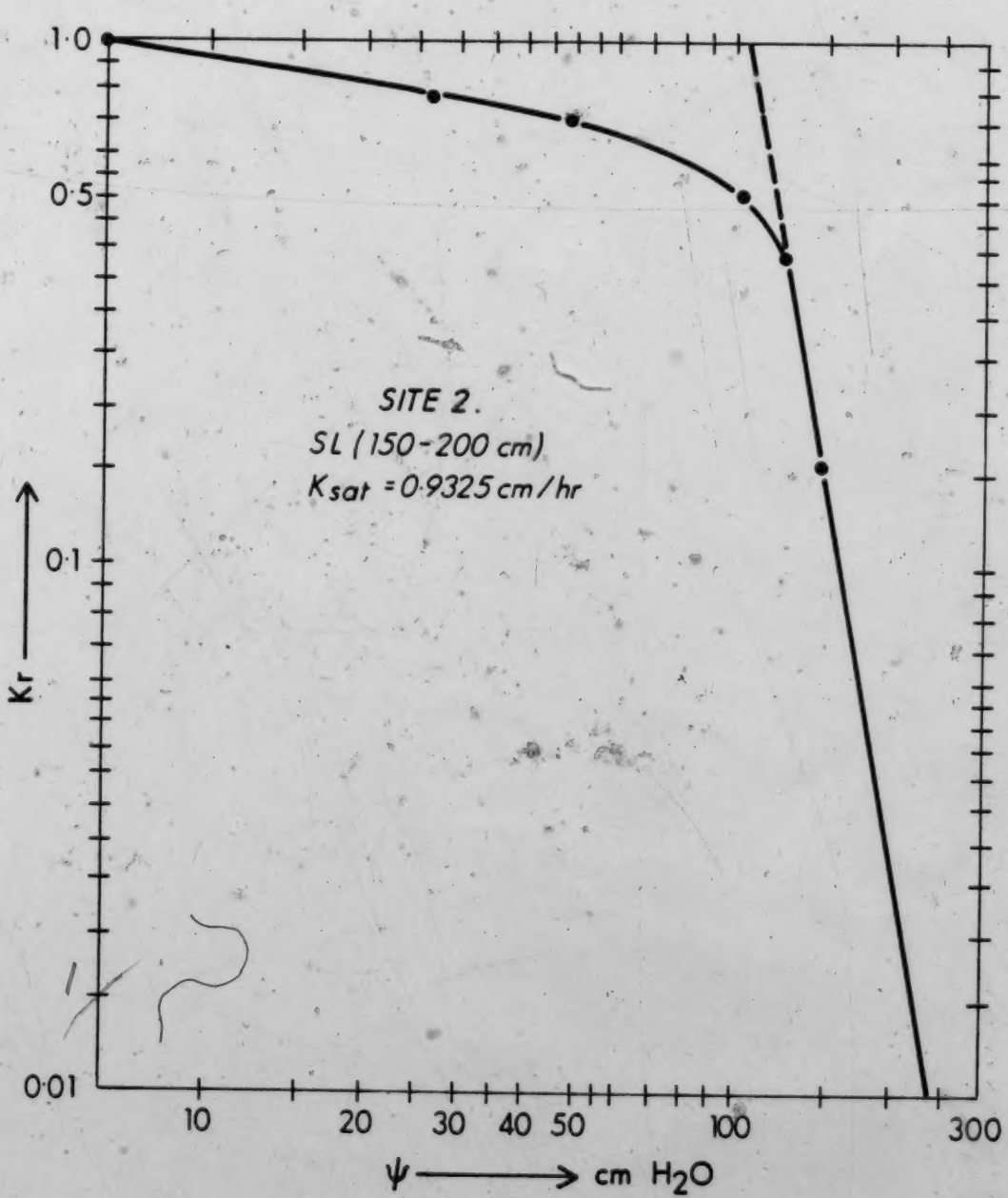

Figure C-13. K_r (ψ) relationship for Site 2 (150-200 cm)

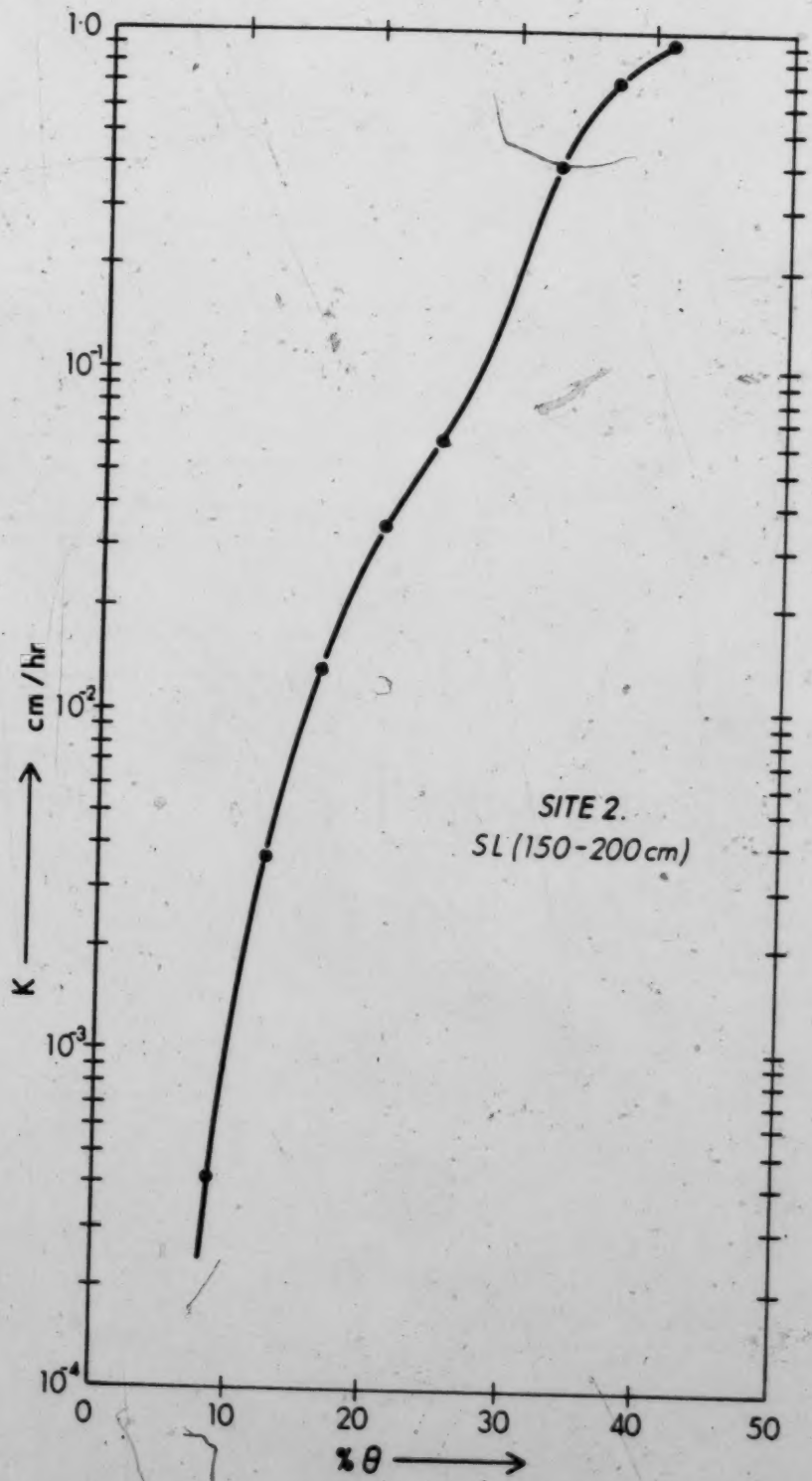

Figure C-14. K (θ) relationship for Site 2 (150-200 cm)

APPENDIX D

DERIVATION OF THE FINITE DIFFERENCE EQUATIONS OF THE ONE-DIMENSIONAL COUPLED NON-ISOTHERMAL FLOW USING A CRANK-NICHOLSON APPROXIMATION METHOD

The set of equations to be solved is (4-1) subject to the initial and the boundary conditions (4-2) and (4-3) respectively. The spatial and time domains are discretized using the grid of Fig. 4-2. The following modification of the Crank-Nicholson method of finite differencing (Richtmyer and Morton, 1967) is used to approximate the partial derivatives appearing in the above equations:

$$\partial(k\,\partial n/\partial z)/\partial z \rightarrow 0.5[K_{i+1/2}^{j-1/2}(n_{i+1}^{j}+n_{i+1}^{j-1}-n_{i}^{j}-n_{i}^{j-1})/(\Delta z)^2] + 0.5[K_{i-1/2}^{j-1/2}(n_{i}^{j}+n_{i}^{j-1}-n_{i-1}^{j}-n_{i-1}^{j-1})/(\Delta z)^2] \quad (D-1)$$

$$\partial n/\partial t \rightarrow (n_{i}^{j}-n_{i}^{j-1})/\Delta t \quad (D-2)$$

$$\partial k/\partial z \rightarrow (K_{i+1/2}^{j-1/2}-K_{i-1/2}^{j-1/2})/\Delta z \quad (D-3)$$

where the terms $K_{i+1/2}^{j-1/2}$, $K_{i-1/2}^{j-1/2}$ are arbitrarily given by (4-4r) and (4-4s) respectively.

Using the above approximations to equations (4-1) they become

$$F_i^{j-1/2}\,(\psi_i^j-\psi_i^{j-1})/\Delta t = (1/\Delta z)\,[\,K_{\psi\,i+1/2}^{j-1/2}\,(\psi_{i+1}^j+\psi_{i+1}^{j-1}-\psi_i^j-\psi_i^{j-1})/(2\Delta z)$$
$$-K_{\psi\,i-1/2}^{j-1/2}\,(\psi_i^j+\psi_i^{j-1}-\psi_{i-1}^j-\psi_{i-1}^{j-1})/(2\Delta z)$$
$$+D_{T\,i+1/2}^{j-1/2}\,(T_{i+1}^j+T_{i+1}^{j-1}-T_i^j-T_i^{j-1})/(2\Delta z)$$
$$-D_{T\,i-1/2}^{j-1/2}\,(T_i^j+T_i^{j-1}-T_{i-1}^j-T_{i-1}^{j-1})/(2\Delta z)-(K_{i+1/2}^{j-1/2}-K_{i-1/2}^{j-1/2})\,] \qquad \text{(D-4)}$$

$$C_i^{j-1/2}\,(T_i^j-T_i^{j-1})/\Delta t = (1/\Delta z)\,[\,\lambda_{i+1/2}^{j-1/2}\,(T_{i+1}^j-T_{i+1}^{j-1}-T_i^j-T_i^{j-1})/(2\Delta z)$$
$$-\lambda_{i-1/2}^{j-1/2}\,(T_i^j+T_i^{j-1}-T_{i-1}^j-T_{i-1}^{j-1})/(2\Delta z)$$
$$+D_{L\,i+1/2}^{j-1/2}\,(\psi_{i+1}^j+\psi_{i+1}^{j-1}-\psi_i^j-\psi_i^{j-1})/(2\Delta z)$$
$$-D_{L\,i-1/2}^{j-1/2}\,(\psi_i^j+\psi_i^{j-1}-\psi_{i-1}^j-\psi_{i-1}^{j-1})/(2\Delta z)$$
$$-C_{l_i}^{j-1/2}\,q_{w_i}^{j-1/2}\,(T_{i+1/2}^{j-1/2}-T_{i-1/2}^{j-1/2})\,] \qquad \text{(D-5)}$$

where the terms of the form $k_i^{j-1/2}$ are given by (4-4t). Rearranging terms and making use of (4-4f), the above equations become

$$-K_{\psi\,i-1/2}^{j-1/2}\,\psi_{i-1}^j+(2F_i^{j-1/2}/r+K_{\psi\,i+1/2}^{j-1/2}+K_{\psi\,i-1/2}^{j-1/2})\,\psi_i^j-K_{\psi\,i+1/2}^{j-1/2}\,\psi_{i+1}^j$$
$$-D_{T\,i-1/2}^{j-1/2}\,T_{i-1}^j+(D_{T\,i+1/2}^{j-1/2}+D_{T\,i-1/2}^{j-1/2})\,T_i^j-D_{T\,i+1/2}^{j-1/2}\,T_{i+1}^j=$$
$$K_{\psi\,i+1/2}^{j-1/2}\,(\psi_{i+1}^{j-1}-\psi_i^{j-1})+K_{\psi\,i-1/2}^{j-1/2}\,(\psi_{i-1}^{j-1}-\psi_i^{j-1})+D_{T\,i+1/2}^{j-1/2}\,(T_{i+1}^{j-1}-T_i^{j-1})$$
$$+D_{T\,i-1/2}^{j-1/2}\,(T_{i-1}^{j-1}-T_i^{j-1})+2\Delta z\,(K_{i+1/2}^{j-1/2}-K_{i-1/2}^{j-1/2})+(2F_i^{j-1/2}/r)\,\psi_i^{j-1} \qquad \text{(D-6)}$$

$$-(\lambda_{i-1/2}^{j-1/2}+C_{l_i}^{j-1/2}\,q_{w_i}^{j-1/2}\,\Delta z/2)\,T_{i-1}^j+(2C_i^{j-1/2}/r+\lambda_{i+1/2}^{j-1/2}+\lambda_{i-1/2}^{j-1/2})\,T_i^j$$
$$-(\lambda_{i+1/2}^{j-1/2}-C_{l_i}^{j-1/2}\,q_{w_i}^{j-1/2}\,\Delta z/2)\,T_{i+1}^j-D_{L\,i-1/2}^{j-1/2}\,\psi_{i-1}^j$$
$$+(D_{L\,i+1/2}^{j-1/2}+D_{L\,i-1/2}^{j-1/2})\,\psi_i^j+D_{L\,i+1/2}^{j-1/2}\,\psi_{i+1}^j=$$
$$\lambda_{i+1/2}^{j-1/2}\,(T_{i+1}^{j-1}-T_i^{j-1})+\lambda_{i-1/2}^{j-1/2}\,(T_{i-1}^{j-1}-T_i^{j-1})$$
$$+D_{L\,i+1/2}^{j-1/2}\,(\psi_{i+1}^{j-1}-\psi_i^{j-1})+D_{L\,i-1/2}^{j-1/2}\,(\psi_{i-1}^{j-1}-\psi_i^{j-1})$$
$$+C_{l_i}^{j-1/2}\,q_{w_i}^{j-1/2}\,(\Delta z/2)\,(T_{i-1}^{j-1}-T_{i+1}^{j-1})+(2C_i^{j-1/2}/r)\,T_i^{j-1} \qquad \text{(D-7)}$$

Using (4-4c) to (4-4g), the above equations become (4-4a) and (4-4b).

Boundary Conditions

The top boundary condition for the pressure head equation is

$$q_w/\rho = \pm E = -K_\psi \, \partial\psi/\partial z - D_T \, \partial T/\partial z + Ki \qquad \text{(D-8)}$$

which, after discretization becomes

$$E_i = -K^{j-1/2}_{\psi_{i-1/2}} \underline{(\psi^j_i + \psi^{j-1}_i - \psi^j_{i-1} - \psi^{j-1}_{i-1})/(2\Delta z)}$$

$$\underline{-D^{j-1/2}_{T_{i-1/2}} (T^j_i + T^{j-1}_i - T^j_{i-1} - T^{j-1}_{i-1})/(2\Delta z) + K^{j-1/2}_{i-1/2}} \qquad \text{(D-9)}$$

where i=2 (top node) and the (i-1/2) subcripts are approximated by i. Examination of (D-4) indicates that the underlined terms actually constitute (D-9). Therefore, replacing the terms which are identical to (D-9) by term E in (D-4) results in

$$F^{j-1/2}_i (\psi^j_i - \psi^{j-1}_i)/\Delta t = (1/\Delta z)[K^{j-1/2}_{\psi_{i+1/2}} (\psi^j_{i+1} + \psi^{j-1}_{i+1} - \psi^j_i - \psi^{j-1}_i)/(2\Delta z)$$
$$+ D^{j-1/2}_{T_{i+1/2}} (T^j_{i+1} + T^{j-1}_{i+1} - T^j_i - T^{j-1}_i)/(2\Delta z) + E_i - K^{j-1/2}_{i+1/2}] \qquad \text{(D-10)}$$

which after some rearrangement becomes

$$(2F^{j-1/2}_i/\tau + K^{j-1/2}_{\psi_{i+1/2}}) \psi^j_i - K^{j-1/2}_{\psi_{i+1/2}} \psi^j_{i+1} + D^{j-1/2}_{T_{i+1/2}} T^j_i - D^{j-1/2}_{T_{i+1/2}} T^j_{i+1} =$$
$$(2F^{j-1/2}_i/\tau - K_{\psi_{i+1/2}}) \psi^{j-1}_i + K^{j-1/2}_{\psi_{i+1/2}} \psi^{j-1}_{i+1} - D^{j-1/2}_{T_{i+1/2}} T^{j-1}_i + D^{j-1/2}_{T_{i+1/2}} T^{j-1}_{i+1}$$
$$+ 2\Delta z \, (E_i - K^{j-1/2}_{i+1/2}) \qquad \text{(D-11)}$$

or, using (4-4c) to (4-4i)

$$(B_2 - A_2)\psi^j_2 - C_2 \psi^j_3 + (\overline{B}_2 - \overline{A}_2) T^j_2 - \overline{C}_2 T^j_3 = H(2) \qquad \text{(D-12)}$$

where H(2) is the right-hand-side of (D-11).

If (D-9) is solved for the terms underlined, with i=3 (assuming that $E|_{i=2} = E|_{i=3}$) and the result replaced in the heat flow equation (D-5), the following result is obtained:

$$C_i^{j-1/2}(T_i^j - T_i^{j-1})/\Delta t = (1/\Delta z)[\lambda_{i+1/2}^{j-1/2}(T_{i+1}^j + T_{i+1}^{j-1} - T_i^j - T_i^{j-1})/(2\Delta z)$$
$$- \lambda_{i-1/2}^{j-1/2}(T_i^j + T_i^{j-1} - T_{i-1}^j - T_{i-1}^{j-1})/(2\Delta z)$$
$$+ D_{L\,i+1/2}^{j-1/2}(\psi_{i+1}^j + \psi_{i+1}^{j-1} - \psi_i^j - \psi_i^{j-1})/(2\Delta z) - D_{L\,i-1/2}^{j-1/2} K_{i-1/2}^{j-1/2}/K\psi_{i-1/2}^{j-1/2}$$
$$+ D_{L\,i-1/2}^{j-1/2}(D_{T\,i-1/2}^{j-1/2}/K\psi_{i-1/2}^{j-1/2})(T_i^j + T_i^{j-1} - T_{i-1}^j - T_{i-1}^{j-1})/(2\Delta z)$$
$$+ D_{L\,i-1/2}^{j-1/2} E_i/K\psi_{i-1/2}^{j-1/2}] \qquad \text{(D-13)}$$

where $(i-1) = 2$ (top node). After some rearrangement, the above equation becomes

$$(2C_i^{j-1/2}/r + \lambda_{i+1/2}^{j-1/2} + \lambda_{i-1/2}^{j-1/2} - D_{L\,i-1/2}^{j-1/2} D_{T\,i-1/2}^{j-1/2}/K\psi_{i-1/2}^{j-1/2})T_i^j$$
$$- (\lambda_{i+1/2}^{j-1/2} - c_{l_i}^{j-1/2} q_{w_i}^{j-1/2}\Delta z/2)T_{i+1}^j + D_{L\,i+1/2}^{j-1/2}\psi_i^j - D_{L\,i+1/2}\psi_{i+1}^j =$$
$$(2C_i^{j-1/2}/r)T_i^{j-1} + \lambda_{i+1/2}^{j-1/2}(T_{i+1} - T_i^{j-1}) + \lambda_{i-1/2}^{j-1/2}(T_i^{j-1} - T_{i+1}^{j-1})$$
$$+ (D_{L\,i-1/2}^{j-1/2} D_{T\,i-1/2}^{j-1/2}/K\psi_{i-1/2}^{j-1/2})(T_i^{j-1} - T_{i-1}^{j-1})$$
$$+ D_{L\,i+1/2}^{j-1/2}(\psi_{i+1}^{j-1} - \psi_i^{j-1}) + (2\Delta z\, D_{L\,i+1/2}^{j-1/2}/K\psi_{i+1/2}^{j-1/2})(E_i - K_{i-1/2}^{j-1/2})$$
$$- c_{l_i}^{j-1/2} q_{w_i}^{j-1/2}\Delta z/2\,(T_{i+1}^{j-1} - T_{i-1}^{j-1})$$
$$+ (\lambda_{i+1/2}^{j-1/2} - D_{L\,i-1/2}^{j-1/2} D_{T\,i-1/2}^{j-1/2}/K\psi_{i-1/2}^{j-1/2} + c_{l_i}^{j-1/2} q_{w_i}^{j-1/2}\Delta z/2)T_{i-1}^{j-1} \qquad \text{(D-14)}$$

where $T_{i-1}^j = T_z^j$ is the specified surface temperature, or using (4-4c) to (4-4p)

$$[B_3' - (\bar{A}_3'\bar{A}_3/A_3)]T_3^j - C_3'T_4^j + (\bar{B}_3' - \bar{A}_3')\psi_3^j - \bar{C}_3'\psi_4^j = H'(3) \qquad \text{(D-15)}$$

where $H'(3)$ is the right-hand-side of (D-14).

With regard to the bottom boundary conditions, the water flux equation (2-38) -- after discretization using forward differences -- becomes

$$-K_L(\psi_{L+1} - \psi_L)/\Delta z - D_{T\ell}(T_{L+1} - T_L)/\Delta z + K_L = \pm w \qquad \text{(D-16)}$$

where w is the specified bottom boundary water flux. Solving (D-16) for ψ_{L+1} results in

$$\psi_{L+1} = \psi_L - \Delta z(1 - w/K_L) - (D_T/K)_L(T_{L+1} - T_L) \qquad \text{(D-17)}$$

while from the bottom boundary condition (D-18) for the heat flow equation

$$(\partial T/\partial z)|_{z=L} \rightarrow (T_{L+1} - T_L)/\Delta z = 0 \qquad \text{(D-18)}$$

one obtains

$$T_{L+1} = T_L \qquad \text{(D-19)}$$

APPENDIX E

DOCUMENTED COMPUTER PROGRAMS

E1 Introduction

The present computer program simulates the one-dimensional simultaneous flow of water and heat in the subsurface (4-1). It consists of a main program and 21 subroutines or function routines. Most transport parameters and coefficients are written in separate subroutines in order to facilitate changes by simply inserting the appropriate program segment. The program was initially run in WATFIV for debugging purposes and subsequently in FORTRAN G for shorter execution time. Double precision arithmetic was used throughout for the various calculations involved in the model. The amount of computer storage required was dependent on the size of the finite difference scheme to be solved. The present program is set up for 50 nodes. In order to alter the size of the system, the dimension statements must be changed.

The main program is the control program which directs the sequence of operations for solving the system of coupled partial differential equations (4-1). It calls all appropriate subroutines; it controls the input and output

data, and boundary and initial conditions; it checks the time increments, the number of iterations and convergence constraints.

E2 Subroutines

Subroutine DTCOEF calculates the thermal diffusion coefficients $D_{T\ell}$ and D_T ; the non-isothermal water flux $q_{w/\rho}$; the heat flux due to the movement of water q_{cv} and the total heat flux q_h.

Subroutine DPSICF calculates the total water conductivity K_ψ .

Subroutine HYCOND adjusts the measured saturated hydraulic conductivity for temperature using (4-15). It also provides for the calculation of the unsaturated hydraulic conductivity function from the non-isothermal water flux equation (4-1d).

Subroutine EVAPO calculates the evaporation rate from a water conservation equation; that is, from the time change of the water content of the top finite difference mesh element and the known water flux at the bottom of that element. This water flux is estimated from the non-isothermal flux equation (4-1d) employing the specified hydraulic conductivity function (K vs θ) for the top element.

Subroutine HCAPT calculates the volumetric heat

capacity of the subsurface layers as functions of their mineral matter, organic matter and water fractions (3-15).

Subroutine HFLUX calculates the water vapor conductivity K_{ψ_v} ; the conductive q_{cd} and latent q_{lh} heat fluxes; the vapor thermal diffusion coefficient D_{Tv} and the vapor flux q_v/ρ.

Subroutine FCOEF calculates the specific water capacity (2-47).

Subroutine DLCOEF calculates the coupling coefficient for heat transfer D_L (4-1c).

Subroutine TRIDAG (Carnahan et al., 1969) solves a system of linear simultaneous equations with a tridiagonal matrix; such a system results form the implicit finite difference scheme used here. The equations are numbered from IF through L and their subdiagonal, diagonal and superdiagonal coefficients are stored in the arrays AZ, BZ and CZ. The computed solution vector is stored in the array VZ.

Subroutines SPLINE and CALCCF and function PCUBIC form the piecewise-cubic interpolation program (Conte and de Boor, 1972). This cubic spline program is called extensively to interpolate input data for a number of parameters required in the program. Subroutine SPLINE uses Gauss elimination adapted to take advantage of the tridiagonal character of the resulting coefficient matrix (Conte and de

Boor, 1972) to calculate the spline coefficients C(2,i), i = 2, ... , N, given the numbers C(1,i) = $f(x_i)$, i = 1, ... , N+1, C(2,1) = $f'(x_i)$ and C(2, N+1) = $f'(x_{N+1})$, where $f(x_i)$ comprises the input data corresponding to x_i and C(2,1) and C(2,N+1) are reasonable approximations to the end slopes of $f(x_i)$. Subroutine CALCCF calculates the spline coefficients C(3,i) and C(4,i), where i = 1, ... , N. Function PCUBIC evaluates the cubic spline equation (E-1)

$$f(x_i) \neg C(1,i)+C(2,i)(x-x_i)+C(3,i)(x-x_i)^2+C(4,i)(x-x_i)^3 \quad \text{(E-1)}$$

for any particular point once the spline coefficients C(j,i), j=1,...4, i=1,...N are known.

Subroutine KSPLEN interpolates the specified hydraulic conductivity function (K vs θ) data using cubic splines and adjusts the conductivity values for temperature.

Subroutines DENS, VISCO, VAPSPL, CLQCF and DAWCF calculate water density ρ, viscosity μ, latent heat of vaporization of water L', saturated vapor pressure p_v^s, specific heat of liquid water c_l, and molecular diffusion coefficient of water vapor in air D_a, respectively, as functions of temperature. All the above subroutines call the cubic spline interpolation program to interpolate the input data.

Subroutines THESP2 and THCOND calculate the volumetric water content and thermal conductivity as functions of the negative pressure head and water content, respectively. Both subroutines interpolate the input data using the cubic

spline interpolation program mentioned above.

E3 List of Variables[1]

CC, CCO	volumetric heat capacity of porous material (C) at current and previous time steps
CLQ, CLQO	specific heat of liquid water (c_ℓ) at current and previous time steps
CSATi, i=1,...,4	saturated hydraulic conductivity (K_{sat}) of layer i
DAW	molecular diffusion coefficient of water vapor in air (D_a)
DELT	time increment (Δt)
DELZ	depth increment (Δz)
DPSI, DPSIO	total water conductivity (K_ψ) of current and previous time steps
DPSIV, DPSIVO	vapor conductivity (K_{ψ_v}) of current and previous time steps
DT, DTO	thermal water diffusivity (D_T) of current and previous time steps
DTHETA	water diffusivity (D_θ)
DTHV	vapor diffusivity (D_v)
DTL	liquid thermal diffusivity ($D_{T\ell}$),
DTV, DTVO	thermal vapor diffusivity (D_{Tv}) of current, and previous time steps
EPS	a small positive number (ϵ)
FF, FO	specific water capacity ($\partial\theta/\partial\psi$) or

[1]Units: [length] = cm; [time] = hr; [mass] = gm; [temperature] = C; [heat] = cal.

	specific storage (S_s)
GR	acceleration of gravity (g)
HVAP	latent heat of vaporization of water (L')
J	time step index
K, KO	hydraulic conductivity (K) or current and previous time steps
KMAX	maximum number of iterations per time step
KODE1	specifies the top boundary condition of evaporation or infiltration
KODE2	specifies after how many time steps the output is to be printed
KODE4	specifies if the coupled or uncoupled equations are to be used
KODE5	specifies the bottom boundary condition of recharge or discharge
KOUNT	count index
KSAT	saturated hydraulic conductivity (K_{sat})
L	total number of space nodes
LAMDA, LAMDAO	apparent thermal conductivity (λ) of current and previous time steps
MI	dynamic viscosity of water (μ)
MITREF	dynamic viscosity of water at reference temperature [$\mu(T_o)$]
MO	node below which the mineral and

	organic matter fractions remain constant
MW	molecular weight of water vapor (M)
Ni	number of specified input data of various parameters
N1	number of $\rho(T)$ input data
N2	" " $\mu(T)$ " "
N3	" " $L'(T)$ " "
N5	" " $K(\theta)$ " "
N7	" " $p_v^s(T)$ " "
N8	" " $c_l(T)$ " "
N9	" " $D_a(T)$ " "
N11	" " $\lambda(\theta)$ " "
N66	" " $\psi(\theta)$ " "
NJ	number of time increments
NR, NI, NII	depths at which the saturated hydraulic conductivity changes
NSTOP	upper limit on the number of time increments
Pi, i=1,2,3,5,7, 8,9,11,66	end slope of input data $f(x_i)$
Pi(1,I), I=1,Ni	input data correspomding to Ni (see Ni)
PSIO, PSI, PSII	pressure head (ψ) of previous, current and next time steps
PSI66	input pressure head data in the water characteristic function

QH	total heat flux (q_h)
QCD	conductive heat flux (q_{cd})
QCV	convective heat flux (q_{cv})
QS	latent heat flux (q_{lh})
QW, QWO	water flux (q_w/ρ) of current and previous time steps
QVAP	vapor flux (q_v/ρ)
R	universal gas constant (R)
RO	liquid water density (ρ)
ROTREF	liquid water density at the reference temperature [$\rho(T_o)$]
SL	total length of subsurface profile studied (L)
SRH	soil relative humidity (h)
SS	specific storage (S_s)
SVP	saturated vapor pressure (p_v^s)
TO, T, TI	porous medium temperature (T) of previous current and next time steps
Ti(I), I=1,Ni	input temperature data corresponding to Ni (see Ni)
THETAO, THETA, THETAI	moisture content (θ) of previous, current and next time steps
THETA5	input moisture content data in the $K(\theta)$ relationship
THET11	input moisture content data in the $\lambda(\theta)$ relationship
TINCR	incremental time step

TREF	reference temperature (T_o)
TS	ground surface temperature
W	specified water flux at bottom boundary
XM	volumetric mineral matter fraction (x_{mm})
XMAXST	maximum simulation time
XO	volumetric organic matter fraction (x_o)
Z	incremental depth (z).

E4 Program Listing

```
      IMPLICIT REAL*8(A-H,O-Z)
      COMMON/DSWBE/ PSI(50),THETA(50),T(50),QW(50),QH(50),DELTAT(50),
     1LAMDA(50),CLQ(50),SVP(50),RO(50),NI(50),P2(4,50),T2(50),
     2T1(50),P1(4,50),T3(50),P3(4,50),THET11(50),P11(4,50),HVAP(50),
     3THETA5(50),P5(4,50),T9(50),P9(4,50),FF(50),
     4PSI66(50),P66(4,50),T7(50),P7(4,50),T8(50),
     5P8(4,50),SRH(50),K(50),QWO(50),DAW(50),DT(50),
     6THETAO(50),NJ,L,L1,KL,NW,DELZ
C
      COMMON/NN/ N1,N2,N3,N5,N7,N8,N9,N11,N66
      DIMENSION PSIO(50),TO(50), LAMDAO(50),APR(50),DTL(50),
     1CPR(50),BPR(50),CC(50),CCO(50),DL(50),DLO(50),QVAP(50),
     2CBARPR(50),BBARPR(50),DTO(50),ABAR(50),CBAR(50),
     3A(50),C(50),B(50),DPSI(50),DPSIO(50),KPLUS(50),DTHETA(50),
     4XO(50),KSAT(50),DTV(50),DTVO(50),DTHV(50),DPSIV(50),
     5D(50,3), E(50,3), F(50,3),G(50,3),CTT(50),FTT(50),
     6H(50),HPR(50),U(50),V(50),TS(600),QS(50),XI(50),
     7DELTRP(50),KMINUS(50),TI(50),PSII(50),THETAI(50),
     8XM(50),IO(50),ABARPR(50),BBAR(50),QCD(50),P(4,50),
     9DPSIVO(50),FO(50),CQ(50),QWB(50),CLQO(50),
     >DI(50),DII(50),DIII(50),GI(50),GII(50),GIII(50)
C
      REAL*8 K,NW,LAMDA,KSAT,NI,NITREF,HVAP,KMINUS,KPLUS,LAMDAO,KO
C---READ IN AND PRINT PHYSICAL PARAMETERS FOR THE SYSTEM
      READ(5,501) R,NW,SS,SL,GR,TREF,ROTREF,NITREF
      WRITE(6,200)  R,NW,SS,SL,GR,TREF,ROTREF,NITREF
  200 FORMAT(1H1,'LIST OF PHISICAL PARAMETERS FOR THE SYSTEM',//
     11HO,'GAS CONSTANT (ERG/DEG.C-MOL)      ',
     2 ,F10.1,/1HO,'MOLECULAR WT. OF WATER ( GM/MOL  )',F10.1,/
     31HO,'SPECIFIC STORAGE(CM**-1)',5X,E15.7,/
     41HO,'SECTION LENGTH( CM )',14X,F10.1,/
     61HO,'ACCELERATION OF GRAVITY(CM/SEC**2)',F10.3,/
     71HO,'REFERENCE TEMP. (DEG.C)',12X,F10.3,/
     81HO,'WATER DENSITY AT REF.TEMP.(GM/CC)',F11.5,/
     91HO,'WATER VISCOSITY AT REF.TEMP.(GM/CM-HR)',F6.3,////)
  501 FORMAT(2F10.1,D10.5,F10.1,2F10.3,/2F10.5)
C---READ IN AND PRINT NUMERICAL INFORMATION
      READ(5,502)NSTOP,L,NJ,KMAXST,EPS,KMAX,DELZ
  502 FORMAT(3I6,F8.2,F7.5,I4,F10.3)
      XNJ=NJ
      L1=L-1
      DELT=KMAXST/XNJ
      RATIO=DELT/DELZ
      RATIOR=RATIO/DELZ
      WRITE(6,230) KMAXST,DELT,NJ,L,DELZ,EPS,KMAX
  230 FORMAT(1H1,'NUMERICAL INFORMATION',//1HO,'MAXIMUM SIMULATION TIME
     1(HR)',1X,G15.7,/1HO,'SIZE OF TIME INCREMENT(HR)',3X,G15.7,/1HO,
     2'NUMBER OF TIME INCREMENTS',I15,/1HO,
     3'NUMBER OF SPACE NODES'      ,I19,/1HO,
     4'SIZE OF SPACE INCREMENTS( CM )', F10.3,/1HO,'EPSILON',23X,F10.4,
     5/1HO,'MAXIMUM NUMBER OF ITERATIONS',2X,I10,////)
C---READ IN AND PRINT BOUNDARY CONDITIONS
      TINCR=0.0D0
      DO 81 I=1,NJ
      TS(I)=24.4D0+7.7D0*DSIN(6.2830D0*TINCR/24.0D0+0.3927D0)
   81 TINCR=TINCR+DELT
      IF(NJ.LE.1000) GO TO 93
C--- PICEWICE LINEAR SURFACE TEMPERATURE DISTRIBUTION
      TS(1)=32.5D0
      DO 82 I=2,7
```

```
      82 TS(I)=TS(I-1)+0.13666D0
         DO 83 I=8,14
      83 TS(I)=TS(I-1)+0.05571D0
         DO 84 I=15,21
      84 TS(I)=TS(I-1)-0.53D0
         DO 85 I=22,28
      85 TS(I)=TS(I-1)-0.59286D0
         DO 86 I=29,35
      86 TS(I)=TS(I-1)-0.49571D0
         DO 88 I=36,42
      88 TS(I)=TS(I-1)-0.13143D0
         DO 89 I=43,56
      89 TS(I)=TS(I-1)-0.19692D0
         DO 90 I=57,63
      90 TS(I)=TS(I-1)-0.13333D0
         DO 91 I=64,70
      91 TS(I)=TS(I-1)+0.22833D0
         DO 92 I=71,77
      92 TS(I)=TS(I-1)+0.755D0
      93 READ(5,121) KODE1,KODE2,KODE3,KODE5
     121 FORMAT (4I3)
C---BOTTOM BOUNDARY WATER FLUX
         IF(KODE1) 5,5,10
       5 QW(L)=0.0D0
         GO TO 122
      10 QW(L)= 0.07D0
     122 IJK=NJ/2
         DO 94 J=1,IJK
         JJ=J+IJK
      94 WRITE(6,141) J,TS(J),TS(JJ),JJ
     141 FORMAT(1H ,I3,3X,'SURFACE TEMPERATURE(DEG.C)',G15.7,3X,G15.7,
        12X,I3)
         W=QW(L)
C---READ IN AND PRINT OUT INITIAL CONDITIONS
         READ(5,503) (PSI(I),I=2,L)
         READ(5,503) (T(I),I=2,L)
     503 FORMAT( 6F10.3)
         T(2)=TS(1)
     241 WRITE(6,240)
     240 FORMAT(1H1,'LISTING OF INITIAL CONDITIONS',//1H0,10X,'INCREMENT',
        110X,'POSITION',17X,'PSI',5X,'MOISTURE CONTENT(THETA)',5X,
        2'TEMPERATURE',/1H ,41X,'(CM)',12X,'(CM H2O)',10X,'(DIM.)',
        313X,'(DEG.C)',///)
C
         KL=L+1
         READ(5,281) N1,N2,N3,N5,N7,N8,N9,N11
     281 FORMAT (8I5)
         READ(5,2222) (T1(I),P1(1,I),I=1,N1),P1(2,1),P1(2,N1)
         READ(5,2222) (THET11(I),P11(1,I),I=1,N11),P11(2,1),P11(2,N11)
         READ(5,282) N66,NO
     282 FORMAT(2I5)
C--- CHARACTERISTIC CURVES
         READ(5,3333) (PSI66(I),P66(1,I),I=1,N66),P66(2,1),P66(2,N66)
    3333 FORMAT(D15.7,F10.4)
         READ(5,154) NR,NI,NII,CSAT1,CSAT2,CSAT3,CSAT4
     154 FORMAT(3I5,4P10.5)
         DO 1 I=2,NR
       1 KSAT(I)=CSAT1
         NN1=NR+1
         DO 2 I=NN1,NI
```

```
      2 KSAT(I)=CSAT2
        NN2=NI+1
        DO 3 I=NN2,L1
      3 KSAT(I)=CSAT3
      4 KSAT(L)=CSAT4
        CALL THESP2 (PSI,KL,THETA,N66,PSI66,P66,L)
C---
        DO 6 I=2,L
        IF(I.GT.MO) GO TO 7
        READ(5,1111) XN(I),XO(I)
        GO TO 6
      7 XN(I)=XN(MO)
        XO(I)=XO(MO)
      6 CONTINUE
 1111 FORMAT(F10.3,F10.5)
        READ(5,2222)  (T9(I),P9(1,I),I=1,N9),P9(2,1),P9(2,N9)
        READ(5,2222)  (T8(I),P8(1,I),I=1,N8),P8(2,1),P8(2,N8)
        READ(5,2222)  (T7(I),P7(1,I),I=1,N7),P7(2,1),P7(2,N7)
        READ(5,2222)  (T3(I),P3(1,I),I=1,N3),P3(2,1),P3(2,N3)
 2222 FORMAT(2F10.5)
        READ(5,2222)  (T2(I),P2(1,I),I=1,N2),P2(2,1),P2(2,N2)
        READ(5,2225)  (THETA5(I),P5(1,I),I=1,N5),P5(2,1),P5(2,N5)
 2225 FORMAT(F10.5,D10.6)
        DO 250 I=2,L
        Z=I-2
        Z=DELZ*Z
  211 WRITE(6,260) I,Z,PSI(I),THETA(I),T(I)
  250 CONTINUE
  260 FORMAT(I20,6X,F20.8,4X,3F20.8)
        T(KL)=T(L)
        PSI(KL)=PSI(L)-DELZ*(1.0D0+B/KSAT(L))
        KODE4=KODE2
C---BEGIN TIME ITERATIONS
   40 DO 270 J=1,NJ
        IF(NJ.GT.NSTOP) GO TO 999
        KOUNT=0
        IF(J.EQ.1) GO TO 6981
        GO TO 699
 6981 DO 697 I=2,L
        THETAO(I)=THETA(I)
        TO(I)=T(I)
        PSIO(I)=PSI(I)
  697 CONTINUE
C---CALCULATE TRANSPORT COEFFICIENTS
  699 CALL dCAPT(XN,XO,L,THETA,CC,KL)
        IF(J.GE.43) GO TO 999
        CALL THESP2 (PSI,KL,THETA,N66,PSI66,P66,L)
        DO 5325 I=2,L
        IF(J.EQ.1)  CCO(I)=CC(I)
        DELTAT(I)=DABS(T(I+1)-T(I))
        CTT(I)=(CC(I)+CCO(I))/2.0D0
        DELTRF(I)=DABS(T(I)-TREF)
        IF(KODE3.EQ.0)  DL(I)=0.0D0
        IF(KODE3.EQ.0)  GLQ(I)=0.0D0
  359 IF (PSI(I).GE.0.0D0) GO TO 361
        EN=MW*GR*PSI(I)
        ED=R*(T(I)+273.16D0)
        RE=EN/ED
        SRH(I)=DEXP(RE)
        GO TO 5325
```

```
181       361 SRH(I)=1.0D0
182      5325 CONTINUE
183       698 CALL VAPSPL(T,L,HVAP,N3,T3,P3,KL)
184           CALL DSNS(T,L,RO,N1,T1,P1,KL)
185           CALL THCOND(L,LAMDA,PSI,THETA,KL,THET11,P11,N11)
186           CALL VISCO(T,L,HI,N2,T2,P2,KL)
187           CALL SVPSPL(T,L,SVP,N7,T7,P7,KL)
188           CALL DAWCP(T,L,DAW,N9,T9,P9,KL)
189           CALL PCOEF(L,PSI,THETA,SS,FF,KL)
190           IF(KODE3.EQ.0) GO TO 605
191           CALL CLQCP(T,L,CLQ,N8,T8,P8,KL)
192       605 CALL KSPLEN(THETA,K,N5,THETA5,P5,L,PSI,T,HI,RO,
193          1T1,T2,P1,P2,N1,N2,KL,KSAT)
194           CALL HFLUX(DTHV,DTV,QVAP,DPSIV,QS,QCD,KODE3)
195           CALL EVAPO(EV,DELT,DTV,DPSIV,DTL,J,KOUNT,KODE3,KODE5)
196       606 CALL HYCOND(J,KSAT,NITREF,ROTREF,DTHV,DPSIV,
197          1DELTRF,DTV,EV)
198           CALL DPSICP(DTHV,DPSI,KSAT,DTHETA,DPSIV)
199           CALL DTCOEF(DTV,DTL,DPSI,EV,NR,HI,QCD,QS,KODE3)
200           IF(KODE3.EQ.0) GO TO 696
201           CALL DLCOEF(DTHV,DL,DPSIV)
202       696 IF(KOUNT.EQ.0) GO TO 777
203       778 KOUNT=KOUNT+1
204           IF(KODE2.EQ.1) GO TO 6011
205           IF(J-KODE4.NE.0) GO TO 341
206      6011 WRITE(6,6768)
207      6768 FORMAT(1H0,10X,'THETA',14X,'K',12X,'QH ',11X,'CC ',13X,'QW',
208          112X,'DTL',12X,'PSI',12X,'T')
209           DO 6769 I=2,L
210      6769 WRITE(6,6770)I,THETA(I),K(I),QH(I),CC(I),QW(I),DTL(I),PSI(I),
211          1T(I)
212      6770 FORMAT(1H ,I2,2X,8G15.6)
213           WRITE(6,6767)
214      6767 FORMAT(1H0,10X,'THETA',12X,'DT',12X,'DTV',12X,'DL',10X,
215          1'LAMDA ',11X,'DPSIV',11X,'DPSI',10X,'QVAP')
216           DO 5163 I=2,30
217      5163 WRITE(6,5164)I,THETA(I),DT(I),DTV(I),DL(I),LAMDA(I),DPSIV(I),
218          1DPSI(I),QVAP(I)
219      5164 FORMAT(1H ,I2,2X,8G15.6)
220       341 DO 340 I=2,L
221           FFF(I)=(FF(I)+FO(I))/2.0D0
222           CQ(I)=(CLQ(I)+CLQO(I))/2.0D0
223           QWW(I)=(QW(I)+QWO(I))/2.0D0
224       340 CONTINUE
225           DO 720 I=3,L1
226           APR(I)=(LAMDA(I)+LAMDA(I-1)+LAMDAO(I-1)+LAMDAO(I))/4.0D0
227          1+CQ(I)*RO(I)*QWW(I)*DELZ/2.0D0
228       718 CPR(I)=(LAMDAO(I)+LAMDAO(I+1)+LAMDA(I+1)+LAMDA(I))/4.0D0
229          1-CQ(I)*RO(I)*QWW(I)*DELZ/2.0D0
230       716 BPR(I)=((CC(I)+CCO(I))/RATIOR)+APR(I)+CPR(I)
231       720 CONTINUE
232           APR(2)=(LAMDA(2)+LAMDAO(2))/2.0D0+CQ(2)*RO(2)*QWW(2)*DELZ/2.0D0
233           CPR(2)=(LAMDAO(2)+LAMDA(2)+LAMDAO(3)+LAMDA(3))/4.0D0
234          1-CQ(2)*RO(2)*QWW(2)*DELZ/2.0D0
235           BPR(2)=((CC(2)+CCO(2))/RATIOR)+APR(2)+CPR(2)
236           APR(L)=(LAMDA(L)+LAMDA(L1)+LAMDAO(L1)+LAMDAO(L))/4.0D0
237          1+CQ(L)*RO(L)*QWW(L)*DELZ/2.0D0
238           CPR(L)=(LAMDA(L)+LAMDAO(L))/2.0D0-CQ(L)*RO(L)*QWW(L)*DELZ/2.0D0
239           BPR(L)=((CC(L)+CCO(L))/RATIOR)+APR(L)+CPR(L)
240           DO 740 I=3,L1
```

```
241         ABARPR(I)=(DL(I)+DL(I-1)+DLO(I-1)+DLO(I))/4.0D0
242       738 CBARPR(I)=(DLO(I)+DLO(I+1)+DL(I+1)+DL(I))/4.0D0
243       736 BBARPR(I)=ABARPR(I)+CBARPR(I)
244       740 CONTINUE
245           ABARPR(2)=(DLO(2)+DL(2))/2.0D0
246           CBARPR(2)=(DLO(2)+DL(2)+DLO(3)+DL(3))/4.0D0
247           BBARPR(2)=ABARPR(2)+CBARPR(2)
248           ABARPR(L)=(DL(L)+DL(L1)+DLO(L1)+DLO(L))/4.0D0
249           CBARPR(L)=(DLO(L)+DL(L))/2.0D0
250           BBARPR(L)=ABARPR(L)+CBARPR(L)
251       782 DO 760 I=3,L1
252           ABAR(I)=(DT(I)+DT(I-1)+DTO(I-1)+DTO(I))/4.0D0
253       758 CBAR(I)=(DTO(I)+DTO(I+1)+DT(I+1)+DT(I))/4.0D0
254       756 BBAR(I)=ABAR(I)+CBAR(I)
255       760 CONTINUE
256           ABAR(2)=(DT(2)+DTO(2))/2.0D0
257           CBAR(2)=(DTO(2)+DT(2)+DTO(3)+DT(3))/4.0D0
258           BBAR(2)=ABAR(2)+CBAR(2)
259           ABAR(L)=(DT(L)+DT(L1)+DTO(L1)+DTO(L))/4.0D0
260           CBAR(L)=(DTO(L)+DT(L))/2.0D0
261           BBAR(L)=ABAR(L)+CBAR(L)
262           DO 780 I=3,L1
263           A(I)=(DPSI(I)+DPSI(I-1)+DPSIO(I-1)+DPSIO(I))/4.0D0
264       768 C(I)=(DPSIO(I)+DPSIO(I+1)+DPSI(I+1)+DPSI(I))/4.0D0
265       766 B(I)=((FF(I)+FO(I))/RATIOR)+A(I)+C(I)
266       780 CONTINUE
267           A(2)=(DPSI(2)+DPSIO(2))/2.0D0
268           C(2)=(DPSIO(2)+DPSI(2)+DPSIO(3)+DPSI(3))/4.0D0
269           B(2)=((FF(2)+FO(2))/RATIOR)+A(2)+C(2)
270           A(L)=(DPSI(L)+DPSI(L1)+DPSIO(L1)+DPSIO(L))/4.0D0
271           C(L)=(DPSIO(L)+DPSI(L))/2.0D0
272           B(L)=((FF(L)+FO(L))/RATIOR)+A(L)+C(L)
273           DO 800 I=3,L1
274           IF(I.GE.NR) GO TO 775
275           KMINUS(I)=(K(I)+K(I-1)+KO(I-1)+KO(I))/4.0D0
276       788 KPLUS(I)=(KO(I)+KO(I+1)+K(I+1)+K(I))/4.0D0
277           GO TO 800
278       775 KMINUS(I)=4.0D0/(1.0D0/K(I)+1.0D0/K(I-1)+1.0D0/KO(I-1)+1.0D0/
279          1KO(I))
280           KPLUS(I)=4.0D0/(1.0D0/KO(I)+1.0D0/KO(I+1)+1.0D0/K(I+1)+1.0D0/
281          1K(I))
282       800 CONTINUE
283           KMINUS(2)=(K(2)+KO(2))/2.0D0
284           KPLUS(2)=(KO(2)+K(2)+KO(3)+K(3))/4.0D0
285           KMINUS(L)=4.0D0/(1.0D0/K(L)+1.0D0/K(L1)+1.0D0/KO(L1)+1.0D0/
286          1KO(L))
287           KPLUS(L)=2.0D0/(1.0D0/K(L)+1.0D0/KO(L))
288       C---FORMULATE SUBMATRICES D,E,F,G
289         811 D(3,1)=0.0D0
290           D(3,2)=BPR(3)-ABARPR(3)*ABAR(3)/A(3)
291           D(3,3)=-CPR(3)
292           DO 300 I=4,L1
293           D(I,1)=-APR(I)
294           D(I,2)=BPR(I)
295           D(I,3)=-CPR(I)
296       300 CONTINUE
297           D(L,1)=-APR(L)
298           D(L,2)=BPR(L)
299           D(L,3)=0.0D0
300           G(2,1)=0.0D0
```

```
      G(2,2)=B(2)-A(2)
      G(2,3)=-C(2)
      DO 330 I=3,L1
      G(I,1)=-A(I)
      G(I,2)=B(I)
      G(I,3)=-C(I)
  330 CONTINUE
      G(L,1)=-A(L)
      G(L,2)=B(L)
      G(L,3)=0.0D0
      E(3,1)=0.0D0
      E(3,2)=CBARPR(3)
      E(3,3)=-CBARPR(3)
      DO 310 I=4,L1
      E(I,1)=-ABARPR(I)
      E(I,2)=BBARPR(I)
      E(I,3)=-CBARPR(I)
  310 CONTINUE
      E(L,1)=-ABARPR(L)
      E(L,2)=BBARPR(L)
      E(L,3)=0.0D0
      F(2,1)=0.0D0
      F(2,2)=CBAR(2)
      F(2,3)=-CBAR(2)
      DO 320 I=3,L1
      F(I,1)=-ABAR(I)
      F(I,2)=BBAR(I)
      F(I,3)=-CBAR(I)
  320 CONTINUE
      F(L,1)=-ABAR(L)
      F(L,2)=BBAR(L)
      F(L,3)=0.0D0
C---APPLY TOP B.C.
      TI(2)=TS(J)
C---APPLY BOTTOM B.C.
  322 TI(KL)=T(L)
   30 PSI(KL)=PSI(L)-DELZ*(1.0D0+W/K(L))-DT(L)*(T(KL)-T(L))/K(L)
      PSII(KL)=PSI(KL)
      IF(PSI(L).LT.0.0D0) GO TO 887
C
   35 DO 350 I=3,L
      H(I)=-(C(I)*(PSI(I)-PSI(I+1))+A(I)*(PSI(I)-PSI(I-1))
     1+CBAR(I)*(T(I)-T(I+1))+ABAR(I)*(T(I)-T(I-1))
     2-(KMINUS(I)-KPLUS(I))*2.0D0*DELZ-(2.0DJ*PTT(I)/RATIOR)*PSI(I))
C
      HPR(I)=-(CPR(I)*(T(I)-T(I+1))+APR(I)*(T(I)-T(I-1))+
     1CBARPR(I)*(PSI(I)-PSI(I+1))+ABARPR(I)*(PSI(I)-PSI(I-1))
     2+CQ(I)*RO(I)*QWW(I)*DELZ*(T(I+1)-T(I-1))/2.0D0
     3-(2.0D0*CTT(I)/RATIOR)*T(I))
  350 CONTINUE
      H(2)=((2.0D0*PTT(2)/RATIOR)-C(2))*PSI(2)+C(2)*PSI(3)+2.0D0*
     1DELZ*(EV-KPLUS(2))+CBAR(2)*(T(3)-T(2))
      HPR(3)=2.0D0*CTT(3)*T(3)/RATIOR+(APR(3)+CQ(3)*RO(3)*QWW(3)*
     1DELZ/2.0D0-(ABARPR(3)*ABAR(3))
     2/A(3))*TI(2)+CPR(3)*(T(4)-T(3))+APR(3)*(T(2)-T(3))+ABARPR(3)*
     3ABAR(3)/A(3)*(T(3)-T(2))+CBARPR(3)*(PSI(4)-PSI(3))+2.0D0*
     4DELZ*ABARPR(3)/A(3)*(EV-KMINUS(3))-CQ(3)*RO(3)*QWW(3)*DELZ*
     5(T(4)-T(2))/2.0D0
      I=L
  352 H(I)=H(I)+C(I)*PSI(I+1)+CBAR(I)*T(I+1)
```

```
      HPR(I)=HPR(I)+CPR(I)*T(I+1)+CBARPR(I)*PSI(I+1)
C---FORM RHS : HPR-(E)*(PSI)=G ; H-(F)*(T)=V
      DO 9875 I=2,L
      IF(I.EQ.2) GO TO 9874
      V(I)=H(I)-F(I,1)*T(I-1)-F(I,2)*T(I)-F(I,3)*T(I+1)
      GO TO 9873
 9874 V(2)=H(2)-F(2,2)*T(2)-F(2,3)*T(3)
 9873 GI(I)=G(I,1)
      GII(I)=G(I,2)
      GIII(I)=G(I,3)
 9875 CONTINUE
      CALL TRIDAG(2,L,GI,GII,GIII,V,PSII)
      DO 9870 I=3,L
      U(I)=HPR(I)-E(I,1)*PSII(I-1)-E(I,2)*PSII(I)-E(I,3)*PSII(I+1)
      DI(I)=D(I,1)
      DII(I)=D(I,2)
      DIII(I)=D(I,3)
 9870 CONTINUE
      CALL TRIDAG(3,L,DI,DII,DIII,U,TI)
      CALL THESP2 (PSII,KL,THETAI,M66,PSI66,P66,L)
      IF(KOUNT.GT.KMAX) GO TO 888
      DO 77 I=3,L
      IF(DABS(TI(I)-T(I)).LE.EPS) GO TO 77
      GO TO 9
   77 CONTINUE
      DO 710 I=2,L
      TO(I)=T(I)
      T(I)=TI(I)
      IF(I.EQ.1) GO TO 710
      PSIO(I)=PSI(I)
      PSI(I)=PSII(I)
      THETAO(I)=THETA(I)
      THETA(I)=THETAI(I)
      CCO(I)=CC(I)
  710 CONTINUE
      GO TO 271
    9 DO 711 I=2,L
      TO(I)=T(I)
      T(I)=(TI(I)+TO(I))/2.000
      IF(I.EQ.1) GO TO 711
      PSIO(I)=PSI(I)
      PSI(I)=(PSII(I)+PSIO(I))/2.000
      THETAO(I)=THETA(I)
      THETA(I)=(THETAI(I)+THETAO(I))/2.000
      CCO(I)=CC(I)
  711 CONTINUE
      GO TO 699
  777 DO 17 I=2,L
      CCO(I)=CC(I)
      DPSIO(I)=DPSI(I)
      FO(I)=FF(I)
      LAMDAO(I)=LAMDA(I)
      KO(I)=K(I)
      CLQO(I)=CLQ(I)
      QWO(I)=QW(I)
      DLO(I)=DL(I)
      DTO(I)=DT(I)
   17 CONTINUE
      GO TO 778
C---PRINT OUT CALCULATED VALUES
```

```
      271 IF(KODE2.EQ.1) GO TO 6016
          IF(J-KODE4.NE.0) GO TO 270
          KODE4=KODE2+J
     6016 WRITE(6,5019) J,KOUNT,(TI(I),I=2,L)
          WRITE(6,5020) J,(PSII(I),I=2,L)
     5019 FORMAT(1HO,'J=',I3,3X,'KOUNT=',I3,/(1HO,'T',6G15.7))
     5020 FORMAT(1HO,'J=',I3,/(1HO,'PSI',6G15.7))
     6015 WRITE(6,700)
      700 FORMAT(1HO,'================================================')
      270 CONTINUE
          WRITE(6,702) J
      702 FORMAT(1HO,'NORMAL TERMINATION,J=',I5,2X,'ITERATIONS')
          GO TO 999
      887 WRITE(6,87)
       87 FORMAT(1HO,'WARNING--PROFILE DRIED TO THE BOTTOM')
          GO TO 999
      888 WRITE(6,889)
      889 FORMAT(1HO,'LIMITS EXCEEDED; NO CONVERGENCE')
      999 STOP
          END
C
C---SUBROUTINES
C
          SUBROUTINE DTCOEF(DTV,DTL,DPSI,EV,NN,NI,QCD,QS,KODE3)
C
          IMPLICIT REAL*8(A-H,O-Z)
          COMMON/D5WHE/ PSI(50),THETA(50),T(50),QW(50),QH(50),DELTAT(50),
         1LAMDA(50),CLQ(50),SVP(50),RO(50),RI(50),P2(4,50),T2(50),
         2T1(50),P1(4,50),T3(50),P3(4,50),THET11(50),P11(4,50),HVAP(50),
         3THETA5(50),P5(4,50),T9(50),P9(4,50),FF(50),
         4PSI66(50),P66(4,50),T7(50),P7(4,50),T8(50),
         5P8(4,50),SRH(50),K(50),QWO(50),DAW(50),DT(50),
         6THETAO(50),NJ,L,L1,KL,NW,DELZ
          COMMON/NN/ N1,N2,N3,N5,N7,N8,N9,N11,N66
C
          DIMENSION DTV(L),DTL(L),DPSI(L),
         1QCV(50),QCD(L),QS(L)
          REAL*8 K,NW,LAMDA,KSAT,NI,NITREF,HVAP
          DATA R/831432.0D+2/,GR/980.665D0/
          DO 333 I=2,L
       33 IF(PSI(I).GE.0.0D0) GO TO 303
          DTL(I)=K(I)*R*DLOG(SRH(I))/(NW*GR)
       30 DTL(I)=DABS(DTL(I))
          IF(KODE3.EQ.0) DTL(I)=0.0D0
          DT(I)=DTL(I)+DTV(I)
          IF(KODE3.EQ.0) DT(I)=0.0D0
          IF(I.LE.3) GO TO 331
          QW(I)=-DPSI(I)*(PSI(I+1)-PSI(I-1))/(2.0D0*DELZ)-DT(I)*
         1(T(I+1)-T(I-1))/(2.0D0*DELZ)+K(I)
          GO TO 333
      303 DT(I)=0.0D0
          DTL(I)=DT(I)
          IF(I.LE.3) GO TO 331
          IF(I.EQ.L) GO TO 333
      298 QW(I)=-(2.0D0/(1.0D0/K(I-1)+1.0D0/K(I+1)))*((PSI(I+1)-PSI(I-1))
         1/(2.0D0*DELZ)-1.0D0)
          GO TO 333
      331 QW(2)=EV
      333 CONTINUE
          DO 100 I=2,L
```

```
481           QCV(I)=RO(I)*CLQ(I)*DELTAT(I)*QW(I)
482           IF(KODE3.EQ.0)  QCV(I)=0.0D0
483           QH(I)=QCD(I)+QS(I)+QCV(I)
484       100 CONTINUE
485       440 RETURN
486           END
487     C
488           SUBROUTINE DPSICP(DTHV,DPSI,KSAT,DTHETA,DPSIV)
489     C
490           IMPLICIT REAL*8(A-H,O-Z)
491           COMMON/D5WHE/ PSI(50),THETA(50),T(50),QW(50),QH(50),DELTAT(50),
492          1LAMDA(50),CLQ(50),SVP(50),RO(50),HI(50),P2(4,50),T2(50),
493          2T1(50),P1(4,50),T3(50),P3(4,50),THET11(50),P11(4,50),HVAP(50),
494          3THETA5(50),P5(4,50),T9(50),P9(4,50),FF(50),
495          4PSI66(50),P66(4,50),T7(50),P7(4,50),T8(50),
496          5P8(4,50),SRH(50),K(50),QWO(50),DAW(50),DT(50),
497          6THETAO(50),NJ,L,L1,KL,NW,DELZ
498           COMMON/NN/ N1,N2,N3,N5,N7,N8,N9,N11,N66
499     C
500           DIMENSION DTHV(L),DPSI(L),KSAT(L),DTHETA(L),DPSIV(L)
501           REAL*8 K,NW,LAMDA,KSAT,HI,HITREF,HVAP
502           DATA R/831432.0D+2/,GR/980.665D0/
503           DO 455 I=2,L
504           IF(PSI(I).GE.0.0D0)  GO TO 45
505           DPSI(I)=K(I)+DPSIV(I)
506           IF(FF(I).EQ.0.0D0)  GO TO 453
507           DTHETA(I)=DPSI(I)/FF(I)
508           GO TO 454
509        45 DPSI(I)=K(I)
510       453 DTHETA(I)=0.0D0
511       454 DPSI(I)=DABS(DPSI(I))
512       455 CONTINUE
513           RETURN
514           END
515     C
516           SUBROUTINE HYCOND(J,KSAT,HITREF,ROTREF,DTHV,DPSIV,
517          1DELTRP,DTV,EV)
518     C
519           IMPLICIT REAL*8(A-H,O-Z)
520           COMMON/D5WHE/ PSI(50),THETA(50),T(50),QW(50),QH(50),DELTAT(50),
521          1LAMDA(50),CLQ(50),SVP(50),RO(50),HI(50),P2(4,50),T2(50),
522          2T1(50),P1(4,50),T3(50),P3(4,50),THET11(50),P11(4,50),HVAP(50),
523          3THETA5(50),P5(4,50),T9(50),P9(4,50),FF(50),
524          4PSI66(50),P66(4,50),T7(50),P7(4,50),T8(50),
525          5P8(4,50),SRH(50),K(50),QWO(50),DAW(50),DT(50),
526          6THETAO(50),NJ,L,L1,KL,NW,DELZ
527           COMMON/NN/ N1,N2,N3,N5,N7,N8,N9,N11,N66
528     C
529           DIMENSION DTHV(L),DPSIV(L),
530          1DELTRP(L),KSAT(L),DTV(L),BL(50)
531           REAL*8 HI,HITREF,K,KSAT,NW,LAMDA,HVAP
532           DATA R/831432.0D+2/,GR/980.665D0/
533           DO 111 I=2,L
534           IF(PSI(I).LT.0.0D0)  GO TO 111
535           IF(DELTRP(I).GE.1.0D0)  GO TO 102
536       101 K(I)=KSAT(I)
537           GO TO 111
538       102 K(I)=KSAT(I)*(HITREF/ROTREF)*RO(I)/HI(I)
539       111 CONTINUE
540
```

```
      IF(J.LE.1000) GO TO 113
C---CALCULATION OF UNSAT K USING NON-ISOTHERMAL WATER FLUX EQN
      DO 112 I=2,L1
      IF (PSI(I).LT.0.0D0) GO TO 103
      GO TO 112
  103 IF(I.EQ.3) GO TO 112
      BL(I)=R*DLOG(SRH(I))/(MW*GR)
      IF(I.EQ.2) GO TO 99
      K(I)=(-QW(I)-DPSIV(I)*(PSI(I+1)-PSI(I-1))/(2.0D0*DELZ)
     1-DTV(I)*(T(I+1)-T(I-1))/(2.0D0*DELZ))
     2/(BL(I)*(T(I+1)-T(I-1))/(2.0D0*DELZ)+
     3(PSI(I+1)-PSI(I-1))/(2.0D0*DELZ)-1.0D0)
      GO TO 98
   99 K(I)=(-QW(I)-DPSIV(I)*(PSI(I+1)-
     1PSI(I))/DELZ-DTV(I)*(T(I+1)-T(I))/DELZ)/(BL(I)*(T(I+1)-T(I))/
     2DELZ+(PSI(I+1)-PSI(I))/DELZ-1.0D0)
   98 K(I)=DABS(K(I))
  112 CONTINUE
  113 RETURN
      END
C
      SUBROUTINE EVAPO(EV,DELT,DTV,DPSIV,DTL,J,KOUNT,KODE3,KODE5)
C
      IMPLICIT REAL*8(A-H,O-Z)
      COMMON/DSMNE/ PSI(50),THETA(50),T(50),QW(50),QN(50),DELTAT(50),
     1LAMDA(50),CLQ(50),SVP(50),BO(50),BI(50),P2(4,50),T2(50),
     2T1(50),P1(4,50),T3(50),P3(4,50),THET11(50),P11(4,50),EVAP(50),
     3THETA5(50),P5(4,50),T9(50),P9(4,50),PP(50),
     4PSI66(50),P66(4,50),T7(50),P7(4,50),T8(50),
     5P8(4,50),SRH(50),K(50),QWO(50),DAW(50),DT(50),
     6THETAO(50),NJ,L,L1,KL,MW,DELZ
      COMMON/MN/ N1,N2,N3,N5,N7,N8,N9,N11,N66
C
      DIMENSION DTV(L),DPSIV(L),DTL(L)
      REAL*8 MW,K,LAMDA,HVAP,MI
      DATA R/8.31432.0D+2/,GR/980.665D0/
      DT(3)=DTV(3)*DABS(K(3)*R*DLOG(SRH(3))/(MW*GR))
      IF(KODE3.EQ.0) DT(3)=0.0D0
   48 QW(3)=-(K(3)*DPSIV(3))*(PSI(4)-PSI(2))/(2.0D0*DELZ)
     1-DT(3)*(T(4)-T(2))/(2.0D0*DELZ)*K(3)
      IF(KODE5.GT.0) GO TO 40
  444 EV=DABS(QW(3))-(THETA(2)-THETAO(2)+THETA(3)-THETAO(3))/2.0D0
     1*DELZ/DELT
      IF(QW(3).GT.0.0D0) EV=-QW(3)-(THETA(2)-THETAO(2)+THETA(3)
     1-THETAO(3))/2.0D0*DELZ/DELT
   45 WRITE(6,47) J,KOUNT,EV,QW(3),K(3),THETA(2),THETA(3)
   47 FORMAT(1HO,'J=',I3,2X,'KOUNT',I3,2X,'EV=',G15.7,2X,'QW(3)=',
     1G15.7,2X,'K(3)=',G15.7,2X,'THETA(2,3)',2G15.7)
      EV=-EV
      GO TO 41
   40 EV=0.09D0
   41 RETURN
      END
C
      SUBROUTINE HCAPT (XM,XO,L,THETA,CC,KL)
      IMPLICIT REAL*8(A-H,O-Z)
      DIMENSION XM(KL),XO(KL),THETA(KL),CC(KL)
      DO 213 I=2,L
      CC(I)=0.46D0*XM(I)+0.60D0*XO(I)+THETA(I)
  213 CONTINUE
```

```
      RETURN
      END
C
      SUBROUTINE HFLUX(DTHV,DTV,QVAP,DPSIV,QS,QCD,KODE3)
      IMPLICIT REAL*8(A-H,O-Z)
      COMMON/D5HE/ PSI(50),THETA(50),T(50),QW(50),QN(50),DELTAT(50),
     1LAMDA(50),CLQ(50),SVP(50),RO(50),HI(50),P2(4,50),T2(50),
     2T1(50),P1(4,50),T3(50),P3(4,50),THET11(50),P11(4,50),HVAP(50),
     3THETA5(50),P5(4,50),T9(50),P9(4,50),FF(50),
     4PSI66(50),P66(4,50),T7(50),P7(4,50),T8(50),
     5P8(4,50),SRH(50),K(50),QWO(50),DAW(50),DT(50),
     6THETAO(50),NJ,L,L1,KL,NW,DELZ
C
      COMMON/NN/ N1,N2,N3,N5,N7,N8,N9,N11,N66
      DIMENSION DTHV(L),DTV(L),QVAP(L),QCD(L),QS(L),QCV(50),
     1DPSIV(L)
      REAL*8 LAMDA,HVAP,NW,K,NI
      DATA R/831432.0D+2/,GR/980.665D0/
      POR=0.41D0
      DO 100 I=2,L
      IF(PSI(I).GE.0.0D0) GO TO 99
      ZETA=1.8D0
      IF(THETA(I).LE.0.09D0) GO TO 95
      RK=(POR-THETA(I))/(POR-0.09D0)
      FF=(2.0D0/3.0D0)*(POR-THETA(I)+RK*THETA(I))
      GO TO 96
   95 FF=2.0D0*POR/3.0D0
   96 RT=NW*GR/(R*(T(I)+273.16D0))
      RTS=RT*RT
      DPSIV(I)=FF*DAW(I)*SVP(I)*RTS*SRH(I)
   97 IF(KODE3.EQ.0) DPSIV(I)=0.0D0
      GO TO 98
   99 DPSIV(I)=0.0D0
      QS(I)=0.0D0
   98 IF(I.EQ.2) GO TO 30
      QCD(I)=-LAMDA(I)*(T(I+1)-T(I-1))/(2.0D0*DELZ)
      QS(I)=-DPSIV(I)*RO(I)*HVAP(I)*(PSI(I+1)-PSI(I-1))/(2.0D0*DELZ)
      SP=(SVP(I+1)-SVP(I-1))/(T(I+1)-T(I-1))
      GO TO 40
   30 QCD(2)=-LAMDA(I)*(T(I+1)-T(I))/DELZ
      QS(2)=-DPSIV(I)*RO(I)*HVAP(I)*(PSI(I+1)-PSI(I))/DELZ
      SP=(SVP(I+1)-SVP(I))/(T(I+1)-T(I))
   40 IF(PSI(I).GE.0.0D0) GO TO 331
      IF(FF(I).EQ.0.0D0) GO TO 45
      DTHV(I)=DPSIV(I)/FF(I)
   45 IF(T(I).GE.25.0D0) ZETA=1.3D0
   56 DTV(I)=ZETA*FF*RT*DAW(I)*SRH(I)*SP
      IF(KODE3.EQ.0) DTV(I)=0.0D0
      IF(I.EQ.2) GO TO 300
      QVAP(I)=-DPSIV(I)*(PSI(I+1)-PSI(I-1))/(2.0D0*DELZ)
     1-DTV(I)*(T(I+1)-T(I-1))/(2.0D0*DELZ)
      GO TO 100
  300 QVAP(2)=-DPSIV(2)*(PSI(3)-PSI(2))/DELZ-DTV(2)*(T(3)-T(2))/DELZ
      GO TO 100
  331 DTV(I)=0.0D0
      DTHV(I)=0.0D0
      QVAP(I)=0.0D0
  100 CONTINUE
  321 RETURN
      END
```

```
661   C
662         SUBROUTINE PCOEF(L,PSI,THETA,SS,FF,KL)
663         IMPLICIT REAL*8(A-H,O-Z)
664         DIMENSION PSI(KL),THETA(KL),FF(L)
665         DO 45 I=2,L
666         IF(PSI(I).GE.0.0D0) GO TO 35
667         IF(I.EQ.2) GO TO 33
668         IF(PSI(I+1).GE.0.0D0) GO TO 34
669         IF(PSI(I+1).EQ.PSI(I-1)) GO TO 32
670         FF(I)=(THETA(I+1)-THETA(I-1))/(PSI(I+1)-PSI(I-1))
671         GO TO 45
672        33 IF(PSI(2).EQ.PSI(3)) GO TO 32
673         FF(I)=(THETA(I+1)-THETA(I))/(PSI(I+1)-PSI(I))
674         GO TO 45
675        34 FF(I)=(THETA(I+1)-THETA(I))/(-PSI(I))
676         GO TO 45
677        32 FF(I)=0.0D0
678         GO TO 45
679        35 FF(I)=SS
680        45 CONTINUE
681         RETURN
682         END
683   C
684         SUBROUTINE DLCOEF(DTHV,DL,DPSIV)
685   C
686         IMPLICIT REAL*8(A-H,O-Z)
687         COMMON/DSWHZ/ PSI(50),THETA(50),T(50),QW(50),QH(50),DELTAT(50),
688        1LAMDA(50),CLQ(50),SVP(50),RO(50),HI(50),P2(4,50),T2(50),
689        2T1(50),P1(4,50),T3(50),P3(4,50),THET11(50),P11(4,50),HVAP(50),
690        3THETA5(50),P5(4,50),T9(50),P9(4,50),FF(50),
691        4PSI66(50),P66(4,50),T7(50),P7(4,50),T8(50),
692        5P8(4,50),SRH(50),K(50),QWO(50),DAW(50),DT(50),
693        6THETAO(50),NJ,L,L1,KL,NW,DELZ
694         COMMON/NN/ N1,N2,N3,N5,N7,N8,N9,N11,N66
695   C
696         DIMENSION DTHV(L),DL(L),DPSIV(L)
697         REAL*8 NW,HVAP,KSAT,K,LAMDA,HI,HITEEP
698         DATA R/831432.0D+2/,GR/980.665D0/
699         DO 65 I=2,L
700         IF(PSI(I).GE.0.0D0) GO TO 75
701         DL(I)=RO(I)*HVAP(I)*DPSIV(I)
702         GO TO 65
703        75 DL(I)=0.0D0
704        65 CONTINUE
705         RETURN
706         END
707   C
708         SUBROUTINE DENS(T,L,RO,N1,T1,P1,KL)
709         IMPLICIT REAL*8(A-H,O-Z)
710         DIMENSION RO(KL),T(KL),T1(N1),P1(4,N1)
711         NR=N1-1
712         CALL SPLINE(NR,T1,P1,N1)
713         CALL CALCCF(NR,T1,P1,N1)
714         DO 63 I=2,L
715         X=T(I)
716        63 RO(I)=PCUBIC(X,NR,T1,P1,N1)
717         RETURN
718         END
719   C
720         SUBROUTINE VISCO (T,L,MI,N2,T2,P2,KL)
```

```
      IMPLICIT REAL*8(A-H,O-Z)
      DIMENSION T2(N2),P2(4,N2),MI(KL),T(KL)
      REAL*8 MI
      NR=N2-1
      CALL SPLINE(NR,T2,P2,N2)
      CALL CALCCP(NR,T2,P2,N2)
      DO 63 I=2,L
      X=T(I)
   63 MI(I)=PCUBIC(X,NR,T2,P2,N2)
      RETURN
      END
C
      SUBROUTINE VAPSPL(T,L,HVAP,N3,T3,P3,KL)
      IMPLICIT REAL*8(A-H,O-Z)
      DIMENSION T3(N3),P3(4,N3),HVAP(KL),T(KL)
      REAL*8 HVAP
      NR=N3-1
      CALL SPLINE(NR,T3,P3,N3)
      CALL CALCCP(NR,T3,P3,N3)
      DO 63 I=2,L
      X=T(I)
   63 HVAP(I)=PCUBIC(X,NR,T3,P3,N3)
      RETURN
      END
C
      SUBROUTINE THESP2 (PSI,KL,THETA,N66,PSI66,P66,L)
      IMPLICIT REAL*8(A-H,O-Z)
      DIMENSION THETA(KL),PSI(KL),P66(4,N66),PSI66(N66)
      NR=N66-1
      CALL SPLINE(NR,PSI66,P66,N66)
      CALL CALCCP(NR,PSI66,P66,N66)
      DO 64 I=2,L
      IF(PSI(I).GE.0.0D0) GO TO 62
      IF(PSI(I).LE.-1.0D5) GO TO 63
      X=PSI(I)
  663 THETA(I)=PCUBIC(X,NR,PSI66,P66,N66)
      GO TO 64
   62 THETA(I)=0.41D0
      GO TO 64
   63 THETA(I)=0.037D0
   64 CONTINUE
      RETURN
      END
C
      SUBROUTINE SVPSPL(T,L,SVP,N7,T7,P7,KL)
      IMPLICIT REAL*8(A-H,O-Z)
      DIMENSION T7(N7),P7(4,N7),SVP(KL),T(KL)
      NR=N7-1
      CALL SPLINE(NR,T7,P7,N7)
      CALL CALCCP(NR,T7,P7,N7)
      DO 63 I=2,KL
      X=T(I)
   63 SVP(I)=PCUBIC(X,NR,T7,P7,N7)
      RETURN
      END
C
      SUBROUTINE CLQCP(T,L,CLQ,N8,T8,P8,KL)
      IMPLICIT REAL*8(A-H,O-Z)
      DIMENSION T8(N8),P8(4,N8) ,CLQ(KL),T(KL)
      NR=N8-1
```

```
781           CALL SPLINE(NR,T8,P8,N8)
782           CALL CALCCF(NR,T8,P8,N8)
783           DO 63 I=2,L
784           X=T(I)
785        63 CLQ(I)=PCUBIC(X,NR,T8,P8,N8)
786           RETURN
787           END
788     C
789           SUBROUTINE SPLINE(NR,XI,P,NSIZE)
790           IMPLICIT REAL*8(A-H,O-Z)
791           DIMENSION XI(NSIZE),P(4,NSIZE),D(50),DIAG(50)
792           DIAG(1)=1.0D0
793           D(1)=0.0D0
794           NP1=NR+1
795           DO 10 M=2,NP1
796           D(M)=XI(M)-XI(M-1)
797        10 DIAG(M)=(P(1,M)-P(1,M-1))/D(M)
798           DO 20 M=2,NR
799           P(2,M)=3.0D0*(D(M)*DIAG(M+1)+D(M+1)*DIAG(M))
800        20 DIAG(M)=2.0D0*(D(M)+D(M+1))
801           DO 30 M=2,NR
802           G=-D(M+1)/DIAG(M-1)
803           DIAG(M)=DIAG(M)+G*D(M-1)
804        30 P(2,M)=P(2,M)+G*P(2,M-1)
805           NJ=NP1
806           DO 40 M=2,NR
807           NJ=NJ-1
808        40 P(2,NJ)=(P(2,NJ)-D(NJ)*P(2,NJ+1))/DIAG(NJ)
809           RETURN
810           END
811     C
812           SUBROUTINE CALCCF(NR,XI,P,NSIZE)
813           IMPLICIT REAL*8(A-H,O-Z)
814           DIMENSION XI(NSIZE),P(4,NSIZE)
815           DO 10 I=1,NR
816           DX=XI(I+1)-XI(I)
817           DIVDF1=(P(1,I+1)-P(1,I))/DX
818           DIVDF3=P(2,I)+P(2,I+1)-2.0D0*DIVDF1
819           P(3,I)=(DIVDF1-P(2,I)-DIVDF3)/DX
820           P(4,I)=DIVDF3/DX/DX
821        10 CONTINUE
822           RETURN
823           END
824     C
825           FUNCTION PCUBIC(XBAR,NR,XI,P,NSIZE)
826           IMPLICIT REAL*8(A-H,O-Z)
827           DIMENSION XI(NSIZE),P(4,NSIZE)
828           I=1
829           DX=XBAR-XI(I)
830           IF (DX) 10,30,20
831        10 IF (I.EQ.1) GO TO 30
832           I=I-1
833           DX=XBAR-XI(I)
834           IF (DX) 10,30,30
835        19 I=I+1
836           DX=DDX
837        20 IF (I.EQ.NR) GO TO 30
838           DDX=XBAR-XI(I+1)
839           IF (DDX) 30,19,19
840        30 PCUBIC=P(1,I)+DX*(P(2,I)+DX*(P(3,I)+DX*P(4,I)))
```

```
      RETURN
      END
C
      SUBROUTINE TRIDAG(I1,L,AZ,BZ,CZ,DR,VZ)
      IMPLICIT REAL*8(A-H,O-Z)
      DIMENSION AZ(50),BZ(50),CZ(50),DR(50),VZ(50),BETA(50),GAMMA(50)
      BETA(I1)=BZ(I1)
      GAMMA(I1)=DR(I1)/BETA(I1)
      I1P1=I1+1
      DO 1 I=I1P1,L
      BETA(I)=BZ(I)-AZ(I)*CZ(I-1)/BETA(I-1)
    1 GAMMA(I)=(DR(I)-AZ(I)*GAMMA(I-1))/BETA(I)
      VZ(L)=GAMMA(L)
      LAST=L-I1
      DO 2 K=1,LAST
      I=L-K
      VZ(I)=GAMMA(I)-CZ(I)*VZ(I+1)/BETA(I)
    2 CONTINUE
      RETURN
      END
C
      SUBROUTINE THCOND(L,LAMDA,PSI,THETA,KL,THET11,P11,N11)
      IMPLICIT REAL*8(A-H,O-Z)
      DIMENSION LAMDA(KL),PSI(KL),THETA(KL),THET11(N11),P11(4,N11)
      REAL*8 LAMDA
      NR=N11-1
      CALL SPLINE(NR,THET11,P11,N11)
      CALL CALCCP(NR,THET11,P11,N11)
      DO 63 I=2,L
      X=THETA(I)
   63 LAMDA(I)=PCUBIC(X,NR,THET11,P11,N11)
      RETURN
      END
C
      SUBROUTINE DAWCP(T,L,DAW,N9,T9,P9,KL)
      IMPLICIT REAL*8(A-H,O-Z)
      DIMENSION T9(N9),P9(4,N9),DAW(KL),T(KL)
      NR=N9-1
      CALL SPLINE(NR,T9,P9,N9)
      CALL CALCCP(NR,T9,P9,N9)
      DO 63 I=2,L
      X=T(I)
   63 DAW(I)=PCUBIC(X,NR,T9,P9,N9)
      RETURN
      END
C
      SUBROUTINE KSPLEN(THETA,K,N5,THETA5,P5,L,PSI,T,HI,RO,
     1T1,T2,P1,P2,N1,N2,KL,KSAT)
      IMPLICIT REAL*8(A-H,O-Z)
      DIMENSION THETA5(N5),P5(4,N5),THETA(KL),K(KL),PSI(KL),HI(KL),
     1T1(N1),T2(N2),P1(4,N1),P2(4,N2),T(KL),RO(KL),KSAT(KL)
      REAL*8 K,HI,KSAT
      NR=N5-1
      CALL DENS(T,L,RO,N1,T1,P1,KL)
      CALL VISCO(T,L,HI,N2,T2,P2,KL)
   59 CALL SPLINE(NR,THETA5,P5,N5)
      CALL CALCCP(NR,THETA5,P5,N5)
      DO 63 I=2,L
   62 IF(PSI(I).GE.0.0D0) GO TO 64
      X=THETA(I)
      K(I)=PCUBIC(X,NR,THETA5,P5,N5)
C---   TEMPERATURE ADJUSTMENT OF K-UNSAT BASED ON TREF=20C
   60 IF(DABS(T(I)-20.0D0).GE.1.0D0) K(I)=K(I)*36.1367D0*RO(I)/HI(I)
      GO TO 63
   64 K(I)=KSAT(I)
   63 CONTINUE
   65 RETURN
      END
```

E5 Sample Input Data and Output Results

A sample input data to the present simulation program follows; also a sample output data using these input data.

Input data for the simulation program. The line numbers below refer to the Program Listing of Section E4.

```
 1
 2
 3
 4
 5
 6  .3143200.0       10.0    2.00-03      560.0     980.665     10.0 ]  --Line 625: READ(5,501)B,RH,SS,SL,GR,TREF,ROTREF,ALTREF
 7    0.99973  67.052
 8      80   40     80    20.00  .30000  10       12.0                --Line 630: READ(5,502)NSTOP,L,NJ,KRAYST,EPS,KRAY,DELX
 9       7    1    0                                                   --Line 680: READ(5,121)KODE1,KODE2,KODE3,KODE5
10 -20000.0   -6000.0   -3000.0   -2400.0   -2000.0   -1640.0 ]
11  -1400.0   -1250.0   -1095.0    -960.0    -840.0    -730.0
12   -630.0    -538.0    -450.0    -378.0    -305.0    -240.0
13   -185.0    -140.0    -100.0     -65.0     -45.0     -26.0  --Line 695: READ(5,503) (PSI(I),I=2,L)
14    -11.0       3.0      10.0      21.0      32.0      42.0
15     52.0      61.0      70.0      79.0      87.0      96.0
16    101.0     111.0     117.0     126.0     130.0     135.0 ]
17    141.0     146.0     150.0     154.0     157.0     160.0
18     27.35     24.90     23.20     22.00     21.00     20.00 ]
19     19.20     18.50     17.70     17.10     16.60     16.10
20     15.50     15.00     14.60     14.20     13.80     13.50
21     13.20     12.80     12.50     12.20     11.90     11.70  --Line 696: READ(5,503) (T(I),I=2,L)
22     11.50     11.25     11.10     10.80     10.70     10.50
23     10.30     10.20     10.00      9.90      9.75      9.60
24      9.50      9.40      9.30      9.20      9.10      9.00
25      8.90      8.80      8.75      8.73      8.72      8.71 ]
26   10    10   10    36   10   10   10   11                          --Line 8100: READ(5,201)N1,N2,N3,N5,N7,N8,N9,N11
27    0.          .99967 ]
28    5.          .99959
29   10.          .99973
30   15.          .99913
31   20.          .99823
32   25.          .99707                                              --Line 8108: READ(5,2222) (T1(I),P1(1,I),I=1,N1),P1(2,1),P1(2,N1)
33   30.          .99568
34   35.          .99406
35   40.          .99222
36   45.          .99021
37    0.         0.
38     .030      1.00 ]
39     .080      2.23
40     .055      2.50
41     .085      3.13
42     .110      3.78
43     .145      5.00
44     .180      6.66                                                --Line 8109: READ(5,2222) (THET11(I),P11(1,I),I=1,N11),P11(2,1),P11(2,N11)
45     .230      9.36
46     .265     11.52
47     .300     14.00
48     .410     22.32 ]
49  49.18       0.
50  27   31                                                           --Line 8110: READ(5,202)N66,NO
51  -180.0000D03     .0370 ]
52   -68.0000D03     .0380
53   -54.0000D03     .0390
54   -43.3300D03     .0400
55   -35.7250D03     .0450
56   -31.1310D03     .0475
57   -27.8650D03     .0478
58   -20.9240D03     .0550
59   -15.3100D03     .0622
60   -10.2070D03     .0698
```

```
                -5.1030D03      .0760
                -3.0620D03      .0775
                -2.1940D03      .0800
                -1.7350D03      .0825
                -1.1230D03      .0950
                -0.8883D03      .1050
                -0.6532D03      .1213
                -0.5103D03      .1350
                -0.3470D03      .1575
                -0.2295D03      .1850
                -0.1429D03      .2275
                -0.1021D03      .2800
                -0.0919D03      .3050
                -0.0817D03      .3375
                -0.0612D03      .3675
                -0.0204D03      .4000
                 0.             .4100
                 0.             0.
      27    37    46    3.00000   1.25640   0.66724   0.05544
               .575          .01777
               .573          .01200
               .537          .00940
               .508          .00740
               .516          .00650
               .535          .00600
               .538          .00560
               .540          .00530
               .541          .00510
               .542          .00500
               .543          .00492
               .544          .00490
               .546          .00488
               .547          .00483
               .548          .00481
               .549          .00480
               .550          .00477
               .551          .00474
               .552          .00470
               .553          .00467
               .555          .00463
               .556          .00461
               .557          .00459
               .558          .00457
               .559          .00453
               .560          .00450
               .561          .00447
               .563          .00443
               .564          .00441
               .565          .00440
        0.          802.6
        5.          828.0
       10.          850.8
       15.          885.6
       20.          910.8
       25.          939.6
       30.          960.4
       35.          997.2
       40.         1029.6
       45.         1050.4
      5.04           5.76
```

..Line #113: READ(5,3333) (PSI66(I),P66(1,I),I=1,866),P66(2,1),P66(2,866)

..Line #115: READ(5,154)NB,N1,NII,CSAT1,CSAT2,CSAT3,CSAT4

..Line #130: READ(5,1111)X0(I),X0(I)

..Line #136: READ(5,2222) (T9(I),P9(1,I),I=1,89),P9(2,1),P9(2,89)

```
121        0.          1.00736
122        5.          1.00368
123       10.          1.00129
124       15.           .99976
125       20.           .99883
126       25.           .99828
127       30.           .99802
128       35.           .99795
129       40.           .99804
130       45.           .99826
131        0.          0.
132        0.          6.22841
133        5.          8.89140
134       10.         12.51463
135       15.         17.38036
136       20.         23.83451
137       25.         32.29627
138       30.         43.26825
139       35.         57.30710
140       40.         75.22936
141       45.         97.74119
142      0.45          5.03
143        0.        597.3
144        5.        594.5
145       10.        591.7
146       15.        588.9
147       20.        586.0
148       25.        583.2
149       30.        580.4
150       35,        577.6
151       40.        574.7
152       45.        571.9
153      -0.56        -0.57
154        0.         60.332
155        5.         58.684
156       10.         47.052
157       15.         41.004
158       20.         36.072
159       25.         32.040
160       30.         28.692
161       35.         25.884
162       40.         23.512
163       45.         21.467
164     -2.246        -0.383
165      .03567     3.000-12
166      .03690     5.100-12
167      .03800     9.220-12
168      .04000     2.510-11
169      .04200     6.710-11
170      .04400     2.010-10
171      .04510     3.300-10
172      .04600     6.370-10
173      .04800     1.680-09
174      .04961     3.600-09
175      .05200     1.260-08
176      .05371     3.000-08
177      .05600     9.220-08
178      .05822     2.520-07
179      .06000     6.200-07
180      .06200     1.260-06
181      .06800     3.080-06
182      .07544     6.300-06
183      .09061     1.940-05
184      .11192     6.110-05
185      .12751     1.920-04
186      .13981     3.400-04
187      .14924     5.400-04
188      .17507     1.560-03
189      .19065     3.000-03
190      .21771     7.590-03
191      .23206     1.260-02
192      .25707     3.300-02
193      .27798     7.800-02
194      .29520     1.650-01
195      .31857     5.250-01
196      .32800     8.220-01
197      .33784     1.200+00
198      .35600     1.510+00
199      .36941     1.800+00
200      .39196     2.280+00
201      .40467     2.520+00
202      .41060     3.000+00
203        0.          0.
```

..Line 0137: READ(5,2222) (T6(I),P6(1,I),I=1,86),P6(2,1),P6(2,86)

..Line 0138: READ(5,2222) (T7(I),P7(1,I),I=1,67),P7(2,1),P7(2,87)

..Line 0139: READ(5,2222) (T3(I),P3(1,I),I=1,83),P3(2,1),P3(2,83)

..Line 0141: READ(5,2222) (T2(I),P2(1,I),I=1,82),P2(2,1),P2(2,82)

..Line 0142: READ(5,2225) (THETA5(I),P5(1,I),I=1,85),P5(2,1),P5(2,85)

J		
1	SURFACE TEMPERATURE (DEG.C)	27.34667
2	SURFACE TEMPERATURE (DEG.C)	27.87003
3	SURFACE TEMPERATURE (DEG.C)	28.37000
4	SURFACE TEMPERATURE (DEG.C)	28.85573
5	SURFACE TEMPERATURE (DEG.C)	29.31255
6	SURFACE TEMPERATURE (DEG.C)	29.76190
7	SURFACE TEMPERATURE (DEG.C)	30.19138

LISTING OF INITIAL CONDITIONS

INCREMENT	POSITION (CM)	PSI (CM H2O)	MOISTURE CONTENT (THETA) (DIM.)	TEMPERATURE (DEG.C)
2	0.00000000	-20000.00000000	0.05023918	27.34666496
3	12.00000000	-6000.00000000	0.07541908	28.90000000
4	24.00000000	-3000.00000000	0.07761752	23.20000000
5	36.00000000	-2000.00000000	0.07912898	22.00000000
6	48.00000000	-2000.00000000	0.08071805	21.00000000
7	60.00000000	-1440.00000000	0.08354827	20.00000000
8	72.00000000	-1440.00000000	0.08679540	19.20000000
9	84.00000000	-1250.00000000	0.09111715	18.50000000
10	96.00000000	-1095.00000000	0.09595952	17.70000000
11	108.00000000	-960.00000000	0.10137728	17.10000000
12	120.00000000	-840.00000000	0.10777394	16.60000000
13	132.00000000	-730.00000000	0.11522549	16.10000000
14	144.00000000	-630.00000000	0.12317400	15.50000000
15	156.00000000	-538.00000000	0.13200078	15.00000000
16	168.00000000	-454.00000000	0.14224839	14.50000000
17	180.00000000	-373.00000000	0.15252347	14.20000000
18	192.00000000	-305.00000000	0.16493883	13.80000000
19	204.00000000	-240.00000000	0.18037600	13.50000000
20	216.00000000	-185.00000000	0.20026544	13.20000000
21	228.00000000	-140.00000000	0.22999572	12.80000000
22	240.00000000	-100.00000000	0.28874210	12.50000000
23	252.00000000	-65.00000000	0.36935206	12.20000000
24	264.00000000	-45.00000000	0.38063157	11.90000000
25	276.00000000	-26.00000000	0.39572426	11.70000000
26	288.00000000	-11.00000000	0.40647344	11.50000000
27	300.00000000	0.00000000	0.41000000	11.25000000
28	312.00000000	13.00000000	0.41000000	11.10000000
29	324.00000000	21.00000000	0.41000000	10.80000000
30	336.00000000	32.00000000	0.41000000	10.70000000
31	348.00000000	42.00000000	0.41000000	10.50000000
32	360.00000000	52.00000000	0.41000000	10.30000000
33	372.00000000	61.00000000	0.41000000	10.20000000
34	384.00000000	70.00000000	0.41000000	10.00000000
35	396.00000000	79.00000000	0.41000000	9.90000000
36	408.00000000	87.00000000	0.41000000	9.75000000
37	420.00000000	96.00000000	0.41000000	9.60000000
38	432.00000000	103.00000000	0.41000000	9.50000000
39	444.00000000	111.00000000	0.41000000	9.40000000
40	456.00000000	117.00000000	0.41000000	9.30000000
41	468.00000000	124.00000000	0.41000000	9.20000000
42	480.00000000	130.00000000	0.41000000	9.10000000
43	492.00000000	135.00000000	0.41000000	9.00000000
44	504.00000000	141.00000000	0.41000000	8.90000000
45	516.00000000	146.00000000	0.41000000	8.80000000
46	528.00000000	150.00000000	0.41000000	8.75000000
47	540.00000000	154.00000000	0.41000000	8.71000000
48	552.00000000	157.00000000	0.41000000	8.72000000
49	564.00000000	160.00000000	0.41000000	8.71000000

J= 1 KOUNT 0 EV= 0.48569270-02 QW(3)= -0.48569270-02 E(3)= 0.70507450-05 THETA(2,3) 0.56239160-01 0.75410000-01

J= 2 KOUNT 0 EV= 0.48960340-02 QW(3)= -0.48960000-02 E(3)= 0.70298620-05 THETA(2,3) 0.56220580-01 0.75370400-01

J= 2 KOUNT 1 EV= 0.57290810-02 QW(3)= -0.48175620-02 E(3)= 0.70170220-05 THETA(2,3) 0.56197200-01 0.75350380-01

J= 3 KOUNT 0 EV= 0.68731210-02 QW(3)= -0.47923480-02 E(3)= 0.69948520-05 THETA(2,3) 0.56157530-01 0.75310010-01

J= 4 KOUNT 0 EV= 0.68267260-02 QW(3)= -0.47627630-02 E(3)= 0.69735030-05 THETA(2,3) 0.56099930-01 0.75269230-01

J= 5 KOUNT 0 EV= 0.69980510-02 QW(3)= -0.47366030-02 E(3)= 0.69533520-05 THETA(2,3) 0.56033180-01 0.75228290-01

J= 6 KOUNT 0 EV= 0.71256960-02 QW(3)= -0.47159230-02 E(3)= 0.69340550-05 THETA(2,3) 0.55961640-01 0.75187160-01

J= 7 KOUNT 0 EV= 0.71823630-02 QW(3)= -0.47014500-02 E(3)= 0.69153920-05 THETA(2,3) 0.55887110-01 0.75145860-01

	THETA	R	QH	CC	QW	BTL	PSI	T
2	0.550871D-01	0.1099170-06	0.971469	0.330567	-0.7182360-02	0.735347D-05	-20268.2	29.7619
3	0.7514650-01	0.6915340-05	0.779929	0.365925	-0.4741450-02	0.1453680-03	-6268.51	25.0808
4	0.7723390-01	0.7463480-05	0.371266	0.329654	-0.1178870-02	0.8514460-04	-3195.85	23.2648
5	0.7930110-01	0.9035210-05	0.283369	0.317101	-0.3836040-03	0.7372320-04	-2408.57	22.0282
6	0.8071930-01	0.9945130D-05	0.253348	0.321679	-0.2567770-03	0.6686120-04	-1949.73	21.0007
7	0.8353200-01	0.1186400-04	0.231103	0.333232	-0.2241980-03	0.6041780-04	-1641.31	20.0200
8	0.8671780-01	0.1492330-04	0.202093	0.337196	-0.1955550-03	0.5382040-04	-1433.59	19.2087
9	0.9134010-01	0.1979820-04	0.202852	0.342540	-0.2321950-03	0.4853050-04	-1289.89	18.6478
10	0.9596940-01	0.2709940-04	0.196561	0.347029	-0.2708220-03	0.4319880-03	-1094.72	17.7188
11	0.101393	0.3849310-04	0.165127	0.351713	-0.3459250-03	0.1272630-03	-959.665	17.1091
12	0.107800	0.5769920-04	0.158511	0.359980	-0.4713690-03	0.1671840-03	-839.568	16.5957
13	0.115261	0.8988160-04	0.178605	0.367901	-0.6699250-03	0.2286970-03	-729.522	16.0832
14	0.123325	0.1385030-03	0.188381	0.376885	-0.9820860-03	0.3019370-03	-629.417	15.5063
15	0.132091	0.2100770-03	0.171589	0.386111	-0.1342960-02	0.3932580-03	-537.142	15.0073
16	0.142359	0.3435530-03	0.166702	0.396639	-0.1924110-02	0.5366110-03	-449.456	14.5941
17	0.152730	0.5354000-03	0.175876	0.407670	-0.2689560-02	0.7018180-03	-376.670	14.1919
18	0.165316	0.8703420-03	0.175406	0.420714	-0.4136050-02	0.9201580-03	-303.388	13.8036
19	0.181015	0.1319720-02	0.209388	0.436875	-0.7591180-02	0.1825590-02	-237.619	13.4795
20	0.206684	0.2437480-02	0.355941	0.463004	-0.1951500-01	0.2621120-02	-172.718	13.0731
21	0.274808	0.5625280-01	0.406605	0.531588	-0.140805	0.2069760-01	-105.060	12.3780
22	0.327725	0.661289	0.145550	0.585425	-6.319286	0.197369	-84.9162	12.2219
23	0.360003	1.28429	0.185483	0.616163	-0.309311	0.312568	-69.4316	12.1229
24	0.372470	1.53580	0.208196	0.631090	-0.273246	0.296635	-55.0628	11.9215
25	0.383793	1.79228	0.300101	0.662873	-0.274928	0.258476	-41.0857	11.7320
26	0.394693	1.79736	0.348016	0.658233	-0.246230	0.172747	-27.3310	11.5261
27	0.404769	2.01504	0.369666	0.668767	-0.254030	0.9786930-01	-13.7590	11.2476
28	0.409997	2.37434	0.368670	0.670657	-0.101576	0.2286480-02	-0.273708	11.0663
29	0.410000	1.25440	0.368095	0.671180	-0.9580270-01	0.000000	11.2682	10.8955
30	0.410000	1.25440	0.302938	0.671840	-0.5615380-01	0.000000	28.3906	10.6841
31	0.410000	1.25440	0.332109	0.672300	0.4886830-01	0.000000	36.1408	10.5093
32	0.410000	1.25440	0.311512	0.672300	0.124094	0.000000	47.4651	10.1360
33	0.410000	1.25440	0.306863	0.672300	0.183481	0.000000	57.9551	10.1935
34	0.410000	1.25440	0.298978	0.672300	0.227428	0.000000	67.9609	10.0170
35	0.410000	1.25440	0.288946	0.672300	0.259302	0.000000	77.6107	9.90449
36	0.410000	1.25440	0.296089	0.672300	0.281603	0.000000	87.0077	9.76560
37	0.410000	1.25440	0.261768	0.672300	0.297701	0.000000	96.2314	9.62790
38	0.410000	0.687240	0.240873	0.672300	0.309436	0.000000	103.852	9.51575
39	0.410000	0.687240	0.222263	0.672300	0.317611	0.000000	109.942	9.41149
40	0.410000	0.687240	0.218590	0.672300	0.326678	0.000000	116.361	9.31109
41	0.410000	0.687240	0.218558	0.672300	0.336486	0.000000	122.574	9.21148
42	0.410000	0.687240	0.219254	0.672300	0.345967	0.000000	128.618	9.11209
43	0.410000	0.687240	0.217578	0.672300	0.349823	0.000000	134.492	9.01274
44	0.410000	0.665888	0.205000	0.672300	0.355286	0.000000	140.197	8.91496
45	0.410000	0.644183	0.156915	0.672300	0.363009	0.000000	145.869	8.82625
46	0.410000	0.663000	0.9213650-01	0.672300	0.321243	0.000000	151.407	8.76742
47	0.410000	0.662909	0.4712090-01	0.672300	0.288129	0.000000	158.285	8.73757
48	0.410000	0.662105	0.2391180-01	0.672300	0.8669940-01	0.000000	165.370	8.72199
49	0.410000	0.5339650-01	0.1117510-01	0.672300	0.7000000-01	0.000000	161.142	8.71322

	THETA	DT	DTV	DL	LAMDA	DPSIV	DPSI	QVAR
2	0.556871D-01	0.525356D-03	0.514005D-03	0.115483D-05	2.57582	0.565741D-08	0.115374D-06	0.196569D-01
3	0.751455D-01	0.619773D-03	0.599405D-03	0.244036D-05	2.92718	0.419693D-08	0.691954D-05	0.130456D-03
4	0.772339D-01	0.668191D-03	0.583046D-03	0.220880D-05	2.96817	0.378339D-08	0.790119D-05	0.726760D-04
5	0.793011D-01	0.613219D-03	0.539696D-03	0.205004D-05	3.00970	0.351297D-08	0.903872D-05	0.507370D-04
6	0.807193D-01	0.573867D-03	0.507306D-03	0.192964D-05	3.03880	0.330265D-08	0.983860D-05	0.422329D-04
7	0.835320D-01	0.547842D-03	0.481424D-03	0.182044D-05	3.09812	0.311213D-08	0.118671D-04	0.358738D-04
8	0.867178D-01	0.532691D-03	0.458671D-03	0.173444D-05	3.16816	0.296226D-08	0.149953D-04	0.292469D-04
9	0.911401D-01	0.523114D-03	0.439483D-03	0.165989D-05	3.27074	0.283252D-08	0.197971D-04	0.227812D-04
10	0.959694D-01	0.522538D-03	0.420549D-03	0.157918D-05	3.38996	0.269235D-08	0.238021D-04	0.241269D-04
11	0.101393	0.530823D-03	0.403560D-03	0.151525D-05	3.54294	0.258150D-08	0.304956D-04	0.188567D-04
12	0.107800	0.555636D-03	0.388453D-03	0.146009D-05	3.71848	0.248605D-08	0.577017D-04	0.165796D-04
13	0.115261	0.600216D-03	0.373519D-03	0.140822D-05	3.94318	0.238949D-08	0.890839D-04	0.169344D-04
14	0.123325	0.661212D-03	0.359236D-03	0.136459D-05	4.21131	0.228311D-08	0.133506D-03	0.160897D-04
15	0.132091	0.738216D-03	0.344982D-03	0.126886D-05	4.52836	0.218712D-08	0.210976D-03	0.130456D-04
16	0.142359	0.867521D-03	0.330912D-03	0.123526D-05	4.91097	0.209844D-08	0.341556D-03	0.112256D-04
17	0.152730	0.101941D-02	0.317587D-03	0.118340D-05	5.37158	0.201013D-08	0.535802D-03	0.104483D-04
18	0.165314	0.122357D-02	0.303414D-03	0.112742D-05	5.98616	0.191444D-08	0.870344D-03	0.900823D-05
19	0.181015	0.171186D-02	0.288266D-03	0.106750D-05	6.71069	0.181124D-08	0.171972D-02	0.873481D-05
20	0.206684	0.288032D-02	0.259207D-03	0.970845D-06	8.04651	0.164652D-08	0.431174D-02	0.118761D-04
21	0.274800	0.204887D-01	0.191087D-03	0.697429D-06	12.1626	0.118194D-08	0.562528D-01	0.674880D-05
22	0.327725	0.197487	0.123697D-03	0.457500D-06	16.6671	0.775337D-09	0.663289	0.131375D-05
23	0.360083	0.312646	0.780741D-04	0.290061D-06	19.7937	0.491436D-09	1.28429	0.976770D-06
24	0.372470	0.296695	0.591403D-04	0.218859D-06	20.8010	0.370724D-09	1.53580	0.967732D-06
25	0.383793	0.258518	0.414517D-04	0.153415D-06	21.5370	0.259816D-09	1.79228	0.666088D-06
26	0.394693	0.172771	0.242642D-04	0.877857D-07	22.0390	0.152024D-09	1.79936	0.447116D-06
27	0.404767	0.9747768-01	0.830174D-05	0.306548D-07	22.2657	0.518513D-10	2.01504	0.158292D-06
28	0.409997	0.2286648-02	0.412874D-06	0.152913D-10	22.3200	0.257939D-13	2.37434	0.760192D-10
29	0.410000	0.000000	0.000000	0.000000	22.3200	0.000000	1.25640	0.000000
30	0.410000	0.000000	0.000000	0.000000	22.3200	0.000000	1.25640	0.000000

J= 7 KOUNT= 1

T	30.19138	25.08456	23.27542	22.02816	21.00129	20.02280
T	19.20997	18.48643	17.72123	17.11037	16.59504	16.08102
T	15.50693	15.00798	14.59323	14.19066	13.80318	13.47110
T	13.02376	12.34317	12.20500	12.11389	11.92110	11.72905
T	11.52238	11.28787	11.06530	10.84871	10.68292	10.50991
T	10.33895	10.19423	10.04019	9.906021	9.767770	9.631374
T	9.518461	9.413491	9.312887	9.213277	9.113923	9.014682
T	8.917334	8.829532	8.778420	8.738912	8.722516	8.713602

J= 7

PSI	-20321.44	-6308.045	-3224.733	-2410.435	-1999.709	-1641.509
PSI	-1439.530	-1249.874	-1094.676	-959.6134	-839.5010	-729.4481
PSI	-629.3264	-537.0113	-449.3678	-376.4640	-303.1277	-237.0162
PSI	-168.5050	-103.5251	-84.53443	-69.46569	-55.29346	-41.54995
PSI	-28.07565	-16.92229	-2.654657	10.26002	23.17795	35.32232
PSI	46.65839	57.33435	67.49839	77.27640	86.77073	96.05809
PSI	103.3233	109.6719	116.2482	122.4603	128.5166	134.4536
PSI	140.2553	146.0563	152.1327	158.6867	165.8600	161.6926